Mechanisms and Behavioral Relevance of Aminergic Modulation of Motoneurons in *Drosophila melanogaster*

Dissertation zur Erlangung des Grades

Doktor der Naturwissenschaften

Am Fachbereich Biologie der

Johannes Gutenberg-Universität Mainz

Natalie Schützler

Mainz, 2017

Tag der mündlichen Prüfung: 20.12.2017

Table of Contents

Abbreviations

AP	-	action potential
Ca^{2+}	-	calcium
$CaCl_2$	-	calcium chloride
CNS	-	central nervous system
DI	-	de-ionized (water)
EPSP / IPSP	-	excitatory / inhibitory postsynaptic potential
F.-T.	-	Friedman-Test
GFP	-	green fluorescent protein
GPCR	-	G protein-coupled receptor
ID	-	inner diameter
K^+	-	potassium
KCl	-	potassium chloride
KGluc	-	potassium gluconate
La^{3+}	-	lanthanum
$MgCl_2$	-	magnesium chloride
MN	-	motoneuron
Na^+	-	sodium
nAChR	-	nicotinic acetylcholine receptors
NaCl	-	sodium chloride
n. mean / median	-	normalized mean / median
NMJ	-	neuromuscular junction
OA / OAR	-	octopamine / octopamine receptor
OD	-	outer diameter
PBS	-	phosphate buffered saline
PFA	-	paraformaldehyde
Q1 / Q3	-	25 % quartile / 75 % quartile
RNAi	-	RNA interference
RPP	-	ramp pulse protocol
SPP	-	square pulse protocol
TA / TAR	-	tyramine / tyramine receptor
TßH	-	tyrosine-ß-hydroxylase
Tdc2	-	tyramine-decarboxylase 2
TrpA1	-	transient receptor potential ankyrin 1
TTX	-	tetrodotoxin
VGCC	-	voltage-gated calcium channel
VNC / VNS	-	ventral nerve cord / ventral nervous system
VUM	-	ventral unpaired median
w. r. m.	-	with repeated measures, one-way ANOVA
YH	-	yohimbine

Summary

Biogenic amines are modulators of numerous behaviors in both vertebrates and invertebrates, including memory, learning, motivation, arousal, states of hunger, depression, aggression, and locomotion. By acting as neuromodulators, biogenic amines like dopamine, epinephrine, norepinephrine, or serotonin regulate neuronal firing patterns and functions through the modulation of either intrinsic membrane properties or synaptic transmission. In human spinal motoneurons, intrinsic motoneuron excitability is regulated by the serotonergic and noradrenergic modulation of persistent inward currents, including L-type Ca^{2+} channels (Ca_v1), that amplify synaptic input to maximize motor force production during motor output.

Analog to the findings in vertebrates, aminergic modulation of motor behavior was demonstrated in invertebrates. Here, the most prominent biogenic amines are octopamine and its precursor molecule tyramine, the invertebrate counterparts of the adrenergic system. In *Drosophila*, opposing effects of octopamine and tyramine have been reported for flight and larval crawling behavior, as well as for muscle properties. However, the underlying cellular and molecular basis remain poorly understood.

This thesis addresses the hypothesis that motoneurons are a primary, direct target of tyraminergic modulation in the context of adaptive control of locomotor behavior. I combined electrophysiological and imaging techniques to identify the cellular targets and molecular mechanisms of tyraminergic modulation of the identified larval motoneuron MNISN-Is. My results show that, first, motoneurons are innervated by aminergic neurons. Second, motoneuron excitability is reduced by the direct action of tyramine in a dose-dependent manner. Third, the modulatory effect is mediated by an α_2-adrenerg-like tyramine-specific receptor, the octopamine-tyramine receptor (CG7485). Fourth, tyramine affects the Ca^{2+} influx into motoneuron dendrites by inhibiting the function of L-type like DmCa1D Ca^{2+} channels (Ca_v1 homolog), which was demonstrated by both genetic knockdown and acute pharmacological blockade of the channel. And fifth, behavioral studies on mid-L3 larvae with a motoneuron-specific knockdown of the identified tyramine receptor indicate that the aminergic modulation of motoneurons is sufficient to explain the effects of TA on larval crawling behavior.

In sum, my thesis points to conserved mechanisms from flies to humans, of controlling locomotor output by aminergic modulation of L-type Ca^{2+} channels in motoneurons. Moreover, the results underscore the notion that motoneurons are not merely passive integrators of synaptic input from the central pattern generating networks, but instead, conditional membrane properties of motoneurons play fundamentally important roles in shaping motor output in an adaptive manner.

1 Introduction

1.1 Neuromodulation

Neuromodulation has been defined as a regulatory mechanism within neuronal networks, in which presynaptic neurons alter the synaptic or cellular properties of postsynaptic neurons through modulator substances (Florey, 1967; Kupfermann, 1979). The term neuromodulation has later been described more generally as a communication between neurons through the release of chemicals, which can act more diverse than just excitatory or inhibitory (Katz, 1999). The release of such modulatory substances onto target neurons can efficiently alter the dynamics of cell-to-cell communication through modification of synaptic signaling, intrinsic membrane properties like the membrane potential, and firing patterns (Marder, 2012; Marder & Thirumalai, 2002). These alterations in postsynaptic neurons can occur through amplification of postsynaptic input by altering ion channel conductance properties in dendrites (Heckman et al., 2008; Marder & Thirumalai, 2002) or by inhibition of action potential initiation by alteration of ion currents in the axon membrane of postsynaptic neurons (Bender et al., 2010; Marder & Thirumalai, 2002) (see introduction section 1.2.1). However, neuromodulation is not simply communication between neighboring neurons, but rather a mechanism to adapt neurons to a huge variety of demands. In short-term periods, it is a way to adjust behavior appropriately to environmental or social situations, such as mating rituals, threats, hunting or fighting. Eliciting, e.g., fight or flight reactions is not a matter of organismic decision. Within seconds, muscles in legs or wings have to be primed to give a maximum of force output in a short time (Evans & Siegler, 1982). In long-term periods, neuromodulation is a mechanism to specialize and adapt neurons for various demands like learning, memory or in persistently stressful situations even depression (Harris-Warrick & Marder, 1991).

One key factor for neuromodulation is the neuromodulator. Different modulators can have different or even opposing effects on the same target neurons. Common neuromodulators are hormones, neurotransmitters or substances which can act as both, such as the biogenic amines epinephrine and norepinephrine.

1.2 Biogenic Amines

1.2.1 Aminergic Modulation

Some of the most commonly known neuromodulators are the biogenic amines epinephrine, norepinephrine, dopamine, and serotonin. Less known but particularly important in invertebrates are the biogenic amines octopamine and tyramine. They all play major roles in modulating vertebrate and invertebrate memory (Scheiner et al., 2006), learning (Hammer & Menzel, 1998), motivation (Bromberg-Martin et al., 2010), arousal (Adamo et al., 1995; Andretic et al., 2005), states of hunger (Koon et al., 2011), metabolism (Mentel et al., 2003; Roeder, 2005), depression (Ries et al., 2017), and aggression (Stevenson et al., 2005).

The diverse and vigorous effects of aminergic modulation of motoneurons and therefore motor behavior are highly conserved. In zebrafish, it was shown that dopaminergic diencephalospinal neurons (DDN), which densely innervate the spinal cord, have a modulatory effect on larval swimming behavior. Without the dopaminergic input from these neurons, swimming behavior cannot be maintained (Jay et al., 2015). Serotonin is known to increase the firing frequency and decrease the afterhyperpolarization in spinal cord motoneurons in lamprey (Wallén et al., 1989). Swimming behavior of *Xenopus* tadpoles can be increased or reduced by application of either serotonin or norepinephrine (McDearmid et al., 1997). To modulate vertebrate fight or flight responses, dendritically generated persistent inward currents (PICs), which are created by L-type Ca^{2+} currents and persistent Na^{+} currents (R. H. Lee & Heckman, 1999; Li et al., 2003; Li et al., 2004) in motoneurons, are highly modulated by supraspinal release of serotonin and norepinephrine from aminergic neurons. As a consequence of this modulation, the synaptic input is amplified and prolonged which in turn allows the generation of high output forces from comparably low input stimuli (Alvarez et al., 1998; Heckman et al., 2008; Heckman et al., 2003). In invertebrates, the motor behavior is similarly modulated by octopamine and tyramine (Brembs et al., 2007; Ormerod et al., 2013; Saraswati et al., 2004; Zumstein et al., 2004).

1.2.2 Octopamine and Tyramine as Invertebrate Counterparts of the Adrenergic System

In vertebrates and invertebrates, levels of biogenic amines are differently distributed. Some of the more abundant amines in vertebrates, like epinephrine and norepinephrine, are only trace amines in invertebrates, where the adrenergic counterparts are octopamine (OA) and its precursor molecule tyramine (TA) (Adamo et al., 1995; Roeder, 1999). Vice versa, OA, and TA are only trace amines in human central nervous systems (Khan & Nawaz, 2016).

Octopamine is one of the most ubiquitous transmitters in insects, which besides modulating locomotion, is strongly involved in the modulation of metabolism (Mentel et al., 2003), egg laying (Orchard & Lange, 1985), learning and memory (Hammer & Menzel, 1998; Schwaerzel et al., 2003), arousal (Adamo et al., 1995), and even modulation of the immune system (Adamo, 2010). It is also thought to be highly involved in fight or flight responses, acting directly homolog to norepinephrine in vertebrates (Roeder, 1999; Roeder et al., 2003). For a long time, only octopamine was thought to be a modulatory active neurotransmitter. This conclusion was due to the fact that OA is the product of a two-step synthesis pathway with TA being the precursor molecule of OA (introduction section 1.2.3). Before its role as a neurotransmitter was shown, TA was only a necessary part of the OA synthesis. However, TA has proven to be not only a precursor of OA, but also an independent neurotransmitter with specific release sites, receptors, and reuptake mechanisms (Alkema et al., 2005; Bayliss et al., 2013; Lange, 2009; Nagaya et al., 2002).

In *Drosophila* flight, OA, as well as TA, are necessary in a specific ratio for wild-type-like flight initiation and maintenance (Brembs et al., 2007). Octopamine and tyramine also modulate muscle contraction properties in an antagonistic manner in *Drosophila* larval crawling muscles (Nagaya et al., 2002; Ormerod et al., 2013). Interestingly, *Drosophila* larvae with a severe lack of OA and an eight-fold increase in TA show a strongly reduced and odd crawling behavior. The animals crawl only a fraction of the wild-type track length. Instead, they turn their heads excessively often (Fox et al., 2006; Saraswati et al., 2004). In both studies with adult flies and larvae $T\beta H^{nM18}$, a mutant for the OA-producing enzyme tyrosine beta-hydroxylase (TßH) was tested, which led to the odd OA - TA ratio (Monastirioti et al., 1996). OA was fed to mutant animals in the attempt to rescue their severe phenotypes. This alone was sufficient to partially rescue the phenotype and create wild-type like behavior. Surprisingly, blocking only tyramine receptors by feeding yohimbine (YH), an α_2-adrenergic receptor antagonist, to affected animals, also rescued the phenotype significantly (Brembs et al., 2007; Saraswati et al., 2004). In electrophysiological recordings of excitatory junction potentials (EJPs) from *Drosophila* larval muscles, treatment with OA raised the EJP amplitude, whereas TA decreased it. But this effect was not mediated by the same receptor. The mutation of one receptor gene, $TyrR^{hono}$, abolished the reducing effects of TA, but not the increasing effects of OA (Nagaya et al., 2002; Ormerod et al., 2013).

However, effects of OA and TA on only neuromuscular synapses do not seem to be sufficient to change locomotion behavior in such a drastically way, as it is described in behavioral studies (Brembs et al., 2007; Saraswati et al., 2004). It is the aim of this study to unravel the basics of

tyraminergic modulation of motor behavior on single cell level, utilizing the model organism *Drosophila melanogaster*.

1.2.3 Synthesis and Degradation of Tyramine

In several studies in *Drosophila* and other invertebrates, it was shown that TA is not only a precursor molecule of OA but also a physiologically relevant modulator itself (Brembs et al., 2007; Fox et al., 2006; Lange, 2009; Nagaya et al., 2002; Saraswati et al., 2004). To be accepted as a neurotransmitter, several prerequisites must be met. The molecule has to be synthesized by specific enzymes and released from vesicles of the same neuron, it has to act on target receptors, and it has to be cleared from the site of action by a reuptake mechanism (Bear et al., 2007). Tyramine fulfills these criteria. In *Drosophila* larvae, the synthesis of both OA and TA takes place in the ventral unpaired median (VUM) neurons. Both TA and OA derive from the α-amino acid tyrosine, which is also a key molecule for the synthesis of dopamine (Figure 1).

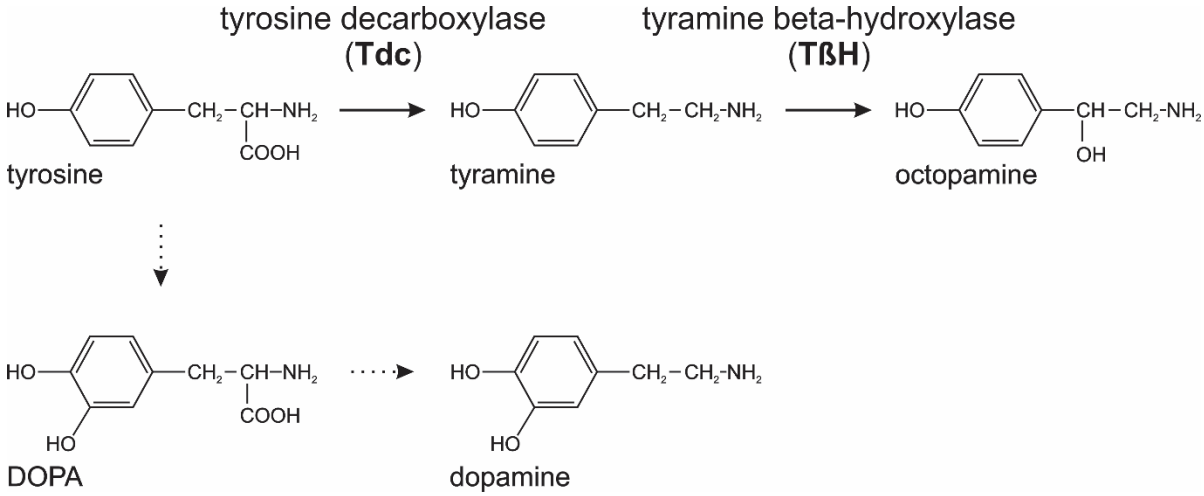

Figure 1: Synthesis pathway of tyramine and octopamine.
The starting point of the shown synthesis pathway is the α-amino acid tyrosine. Tyrosine is decarboxylated by the tyrosine decarboxylase (Tdc), which results in TA. In a second step, TA is converted into OA by the tyramine beta-hydroxylase (TßH) (Livingstone & Tempel, 1983; Neckameyer & White, 1993). In a different pathway, tyrosine may be hydroxylated to form dopamine (Lange, 2009; Roeder, 2005).

In the first step, tyrosine is decarboxylated to TA by the enzyme tyrosine decarboxylase (Tdc) (Livingstone & Tempel, 1983). In the second step, TA is hydroxylated at its sidechain by TßH to form OA (Monastirioti et al., 1996; Neckameyer & White, 1993). In *Drosophila*, two genes exist for Tdc, *Tdc1* and *Tdc2*. The expression patterns do not overlap, while Tdc1 is mainly expressed in non-neuronal tissue, Tdc2 can be found within the central nervous system (Vömel & Wegener, 2008). Three VUM somata are located to the midline of each segment on the

ventral side of the *Drosophila* larval ventral nerve cord (VNC). The axons are directed to the dorsal side, where they bifurcate and bilaterally leave the VNC to innervate multiple body wall muscles. VUM neurons also form synapses onto other neurons in the VNC, where they release OA and TA (Landgraf et al., 1997; Monastirioti et al., 1995; Selcho et al., 2012). In *Drosophila* as well as in *C. elegans*, cells were identified which only release TA, but not OA (Alkema et al., 2005; Nagaya et al., 2002).

An octopamine independent and tyramine-specific reuptake mechanism could be found in locust glia cells (Downer et al., 1993). Another octopamine/tyramine-specific reuptake transporter was found in the caterpillar of the cabbage looper, where it is co-expressed with TßH in octopaminergic neurons (Malutan et al., 2002). In *Drosophila*, no such transporter was yet identified. However, it is suggested that in *Drosophila*, tyramine is specifically degraded by a dehydrogenase/reductase in astrocyte-like glia (de Visser, 2016; Ryglewski et al., 2017). Furthermore, tyramine-specific receptors have been identified in the nervous system of *Drosophila*.

1.2.4 Tyramine Receptors

So far, four types of insect octopamine receptors (OAR) and three types of insect tyramine receptors (TAR) have been described, which all belong to a common superfamily of G protein-coupled receptors (GPCR). The founding protein of this group is rhodopsin, and all receptors in its family are similarly built (Palczewski et al., 2000) (Figure 2). The N-terminal end (NH_2) is located extracellularly, and the C-terminal end (COOH) is located intracellularly. In between, seven α-helical transmembrane domains (TMD) span through the lipid bilayer, linked by three extracellular loops alternating with three intracellular loops. A fourth intracellular loop connects the seventh TMD with the membrane, and functions as an anchor (Baldwin, 1994; Ji et al., 1998; Palczewski et al., 2000). The size of the seven TMDs is highly conserved with 20 - 27 amino acids each, whereas the N-terminal, C-terminal, and loop segments are variable in length, which might correlate with their respective functions (Ji et al., 1998).

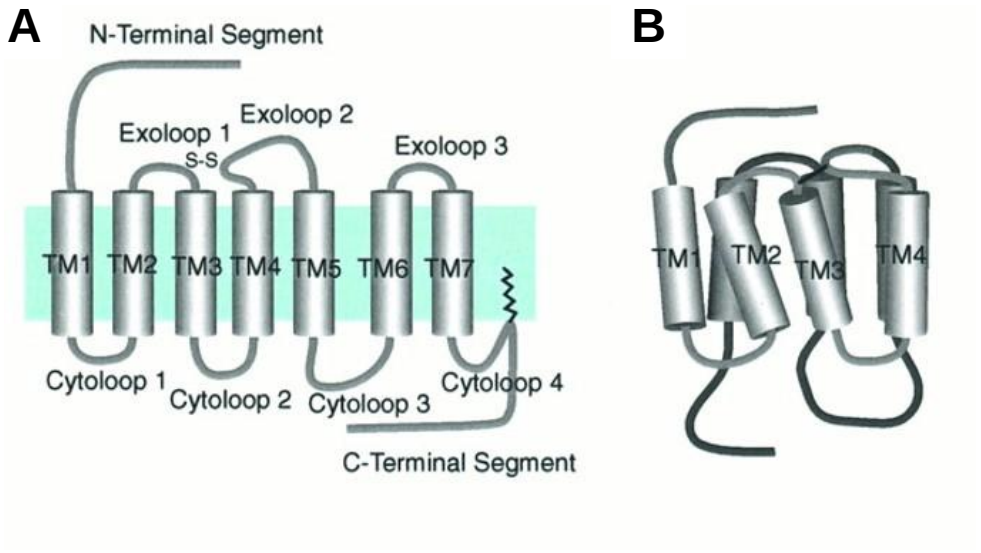

Figure 2: Structure of G protein-coupled receptors as suggested by Ji et al.
Most G protein-coupled receptors are composed in the same way. **A** The N-terminal part is located on the extracellular side of the membrane; its length varies due to different receptor types and tasks. They all share seven α-helical transmembrane domains (TMDs), which are embedded in the membrane. The TMDs are linked by three intracellular loops (cytoloop), alternating with three extracellular loops (exoloop). A fourth intracellular loop connects the TMDs with the lipid bilayer membrane. The C-terminal end is located intracellularly. **B** The TMDs are arranged in a circular way so that TMD 1 is located next to TMD7. Figure from Ji et al., 1998.

Ligand binding can take place either at the N-terminal segment or in a binding pocket formed inside the core of the TMDs, depending on the kind and size of the ligand. For biogenic amine receptors, the ligands bind inside the core and involve the TMDs three, five, and six in binding and activation of the receptor (Gether & Kobilka, 1998; Ji et al., 1998).

Typically, the activation of the GPCR leads to an activation of the respective GTP-binding protein (G protein), which is a heterotrimeric complex consisting of the α-subunit, and the permanently conjoint βγ-subunit (Oldham & Hamm, 2008). The Gα-subunit detaches from the compound as soon as the receptor is activated and GTP is provided to the complex (Iiri et al., 1998). The Gα-subunits must be further distinguished by their respective function and the subsequent cascade they elicit upon activation. In general, there are four classes of α-subunits, $G\alpha_s$, $G\alpha_i$, $G\alpha_q$, and $G\alpha_{12}$, with each one initiating a different cascade and with a total of 17 members (Simon et al., 1991). Both subunits $G\alpha_s$, and $G\alpha_i$ interact with the adenylyl cyclase (AC), but in opposing manner. $G\alpha_s$ interaction increases AC activity, and more ATP is converted into cyclic AMP (cAMP), which in turn raises the intracellular cAMP level, $[cAMP]_i$ (Blenau & Baumann, 2001; Simon et al., 1991). cAMP activates the cAMP-dependent protein kinase A (PKA), which phosphorylates molecules like ligand- or voltage-gated ion channels. (Blenau & Baumann, 2001; Ismailov & Benos, 1995). L-type Ca^{2+} channels, for example, undergo conformational changes and are more likely to open upon membrane depolarization if the channel is phosphorylated (Reuter, 1983). In contrast, activation of a $G\alpha_i$-subunit results in

the reduction of AC activity, and therefore in reduced $[cAMP]_i$ (Blenau & Baumann, 2001; Reale et al., 1997; Robb et al., 1994; Simon et al., 1991). The third class, $G\alpha_q$-subunits, causes the intracellular Ca^{2+} level, $[Ca^{2+}]_i$, to increase upon activation. The cascade involves the activation of phospholipase C, the diffusion of the second messenger IP_3, and the release of Ca^{2+} from intracellular stores (Blenau & Baumann, 2001; Robb et al., 1994). The last subunit class, $G\alpha_{12}$, is involved in various processes like embryonic development, cell growth, angiogenesis and many other (Suzuki et al., 2009).

In *Drosophila*, octopamine receptors (OAR) and tyramine receptors (TAR) are expressed in larval muscles, and also throughout larval and adult central nervous systems (El-Kholy et al., 2015; Han et al., 1998). Since this thesis aims to find the basis of tyraminergic modulation of locomotion, TARs, especially in the nervous system, need to be analyzed. TARs do not have a consistent nomenclature in publications, which is why the same receptors might be found under different names.

The first tyramine receptor, CG 7485, was cloned in 1990 by two independent groups (Arakawa et al., 1990; Saudou et al., 1990). One of them found this receptor to be an octopamine receptor. TA, however, was not included in their replacement essays (Arakawa et al., 1990). The other group and later studies showed that the receptor had a much higher binding affinity to TA than to OA (Reale et al., 1997; Robb et al., 1994; Saudou et al., 1990). However, this receptor is called octopamine-tyramine receptor (Oct-TyrR). The activation of this receptor leads to a decrease of $[cAMP]_i$ in transfected CHO cells and in *Xenopus* oocytes, which indicates the coupling to a $G\alpha_i$-subunit (Blenau & Baumann, 2003; Reale et al., 1997; Robb et al., 1994). A second pathway leading to an increased $[CA^{2+}]_i$ was suggested, but not confirmed to be caused by a $G\alpha_q$-subunit (Reale et al., 1997; Robb et al., 1994). According to FlyAtlas, Oct-TyrR is expressed most prominently in the adult brain, thoracicoabdominal ganglion, and the larval central nervous system (CNS) (Chintapalli et al., 2007; www.flyatlas.org). For this receptor, a mutation called *honoka* has been created by insertion of a *P*-element 100 base pairs upstream of the *oct-tyrR* gene. Mutant animals show a defective olfactory behavior (Kutsukake et al., 2000), and neuromuscular recordings of mutant animals showed that EPSPs are not affected by tyraminergic modulation anymore (Nagaya et al., 2002). Due to the strong expression of Oct-TyrR in the nervous system, the *honoka* mutant is a promising candidate to investigate tyraminergic modulation of motoneurons.

The second TAR, CG 7431, has been cloned and expressed in CHO cells. The receptor was specific for the activation by TA. It showed no cross-reactions to other tested substances, including OA (Cazzamali et al., 2005). The receptor is hereafter simply called tyramine

receptor, TyrR. Activation of the receptor elicits the release of Ca^{2+} from intracellular stores, indicating a coupling to a $G\alpha_q$-subunit. $[cAMP]_i$ is not altered by activation of TyrR (Bayliss et al., 2013; Cazzamali et al., 2005). According to FlyAtlas, TyrR is mainly expressed in adult midgut and larval tubules. Lower expression levels were also found in the adult brain, thracicoabdominal ganglion, larval midgut and only small amounts in larval CNS (Chintapalli et al., 2007; www.flyatlas.org).

The third receptor, CG 16766, was also the last one to be further characterized. Cazzamali et al. (2005) suggested CG 16766 to also be a TAR, based on sequence similarities to TyrR (CG 7431). CG 16766 was cloned and expressed in CHO cells. Exposure of the transfected cells to TA led to the release of Ca^{2+} from internal stores. Furthermore, it is the only one of the three TARs that is insensitive to the receptor antagonist yohimbine (Bayliss et al., 2013). Since the receptor is most specific to TA, it has been called tyramine receptor II, TyrR II. According to the microarray-based FlyAtlas, TyrR II is prominently expressed in the crop of adult flies (Chintapalli et al., 2007; www.flyatlas.org).

1.3 Crawling Behavior in *Drosophila* Larvae

Drosophila larvae spend most of their time with seeking for food, which is why they display a variety of different locomotor behaviors tuned for this task (C. H. Green et al., 1983). Larval crawling is characterized by periodic rhythmic contractions of the segmented body wall muscles, which run from posterior to anterior in forward locomotion, and from anterior to posterior in backward locomotion (Fox et al., 2006; C. H. Green et al., 1983; Heckscher et al., 2012). The abdominal segments A2 - A7 each have an identical composition of 30 muscles (Figure 3). The abdominal segment A1 holds fewer muscles than the other abdominal segments. The thoracic segments T2 and T3 have more muscles, which are necessary for controlling the mouthparts. The terminating segments T1 and A8 are specially built with completely different muscle patterns, which is not further relevant to this thesis (Bate, 1990; Hooper, 1986). Crawling behavior can easily be studied in *Drosophila* larvae (C. H. Green et al., 1983; Saraswati et al., 2004). And such behavioral studies showed that high concentrations of TA, either due to genetic manipulation or by feeding TA, elicit odd crawling behavior in L3 larvae (Fox et al., 2006; Saraswati et al., 2004).

1.4 MNISN-Is, a *Drosophila* Larval Motoneuron

In each hemisegment of an L3 larval ventral nervous system (VNS), 32 motoneurons (MN) are localized, which innervate the 30 muscles (Figure 3). Most of the MNs are well described in their morphological properties (Landgraf et al., 1997; Schmid et al., 1999). Each MN forms synapses either on one specific muscle or on a specific group of muscles. The large type I boutons formed by MNs are subdivided into two types, type Is and type Ib. Type Is boutons, where s refers to as 'small', are 2-4 µm in diameter. They are glutamatergic and form long and arborized terminals on most of the muscles. Type Ib boutons, where b refers to as 'big', are, with a diameter of 3-6 µM, slightly larger than Is boutons. The terminals formed by Ib boutons are shorter and less complex than Is boutons, are also glutamatergic, and can be found in all muscles (Guan et al., 1996; Hoang & Chiba, 2001; Johansen et al., 1989; Johansen et al., 1989a). Besides type I boutons, muscles are also innervated by type II and type III boutons. Type II boutons are very small, about 1-2 µm, form bead cord-like terminals, can be found on most muscles, and contain octopamine and tyramine (Hoang & Chiba, 2001; Koon et al., 2011; Monastirioti et al., 1995). Type III boutons are 2-3 µm in diameter, contain insulin, and can only be found on muscle 12 (Gorczyca et al., 1993; Hoang & Chiba, 2001).

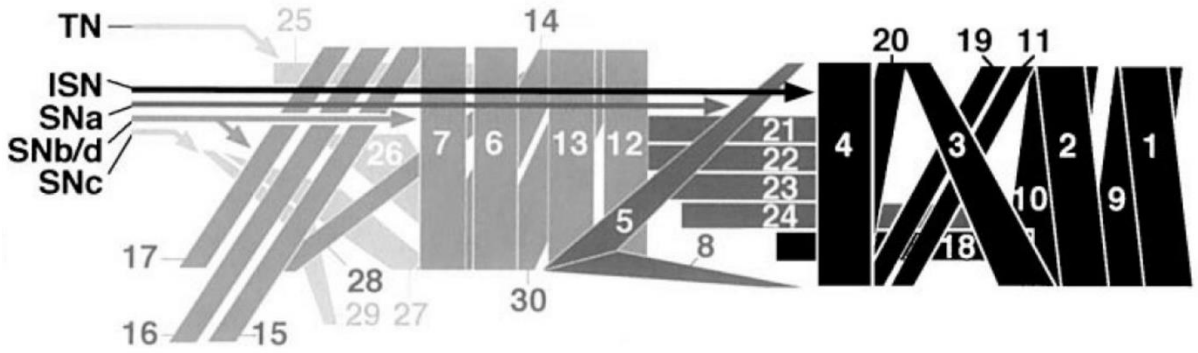

Figure 3: Representative scheme of the larval muscle arrangement in the abdominal hemisegment A2 as suggested by Hoang & Chiba.
One hemisegment is shown, which represents all abdominal hemisegments A2 - A7. The ventral midline has to be seen on the left side of the scheme, whereas the most dorsal part has to be seen on the right end of the scheme. Innervation of the 30 muscles is color-coded and labeled with the respective nerve branches (ISN = intersegmental nerve branch, SN = segmental nerve branch, TN = transverse nerve). ISN includes the MNs MN1-Ib (aCC) and MNISN-Is (RP2). Figure from Hoang & Chiba, 2001.

To minimize variability, one specific and individually identified motoneuron, MNISN-Is, was selected to test for tyraminergic modulation. This neuron has a well described and characteristic morphology, localization, and firing pattern (Choi et al., 2004; Landgraf et al., 1997; Schmid et al., 1999). It is located dorsally in each hemisegment of the VNC, which makes it easily accessible. Due to its embryonic origin and appearance, this MN is also called RP2, which refers to as Raw Prawn (Broadie et al., 1993). It derives from the embryonic neuroblast NB 4-

2 and is part of the intersegmental nerve (ISN) in larvae (Figure 3). MNISN-Is forms type Is boutons on the nine ipsilateral innervated muscle fibers 1, 2, 3, 4, 9, 10, 18, 19, and 20.

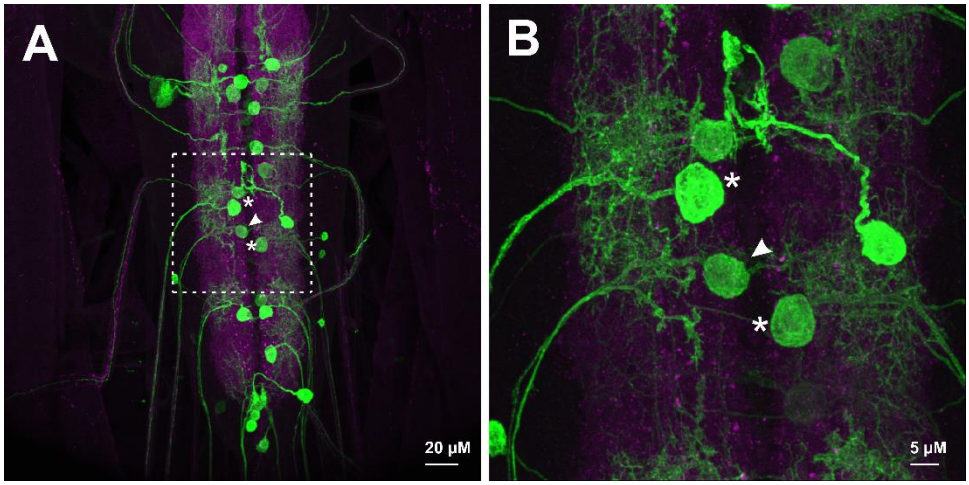

Figure 4: Localization and appearance of MNISN-Is in the larval VNC.
A Maximum projection of an immunohistochemical staining of a larval VNC. Due to its genotype, individual MN1-Ib and MNISN-Is motoneurons are GFP-labeled in a mosaic-like pattern (green) (methods section 2.3). The synaptic marker anti-brp labels the neuropil (magenta). Single MN1-Ib (arrowhead) and MNISN-Is (asterisks) neurons can be identified by their characteristic structure. **B** Magnification of the dashed square of A.

A widespread dendritic tree branches off of the primary neurite near the soma, which gives the neuron a characteristic appearance (Choi et al., 2004; Goodman et al., 1984; Hoang & Chiba, 2001; Kim et al., 2009; Landgraf et al., 1997; Schmid et al., 1999) (Figure 4). Also, the electrophysiological properties of MNISN-Is are well described. In whole-cell current-clamp recordings from the soma, the resting membrane potential is around -60 mV and the firing threshold is at around -30 mV. If the threshold is exceeded upon somatic current injection, the cell responds with firing delayed action potentials (AP) (Choi et al., 2004) (Figure 5 E, arrow). The origin of the MNISN-Is-specific delay to the first action potential is not yet fully understood. It is abolished by the transient potassium current blocker 4-aminopyridine, by knocking out Shal channels, and by giving a subthreshold prepulse prior to somatic current injections exceeding the firing threshold (Choi et al., 2004; Ping et al., 2011; Schaefer et al., 2010), suggesting that transient A-type Shal potassium channels (K_v4) are required for this effect. A similar phenomenon was found in *Aplysia*. In electrophysiological recordings of inking motoneurons, a 4-aminopyridine-sensitive, fast transient outward potassium (K^+) current was found to induce a delay to the first AP in response to a threshold-exceeding current injection (Byrne et al., 1979).

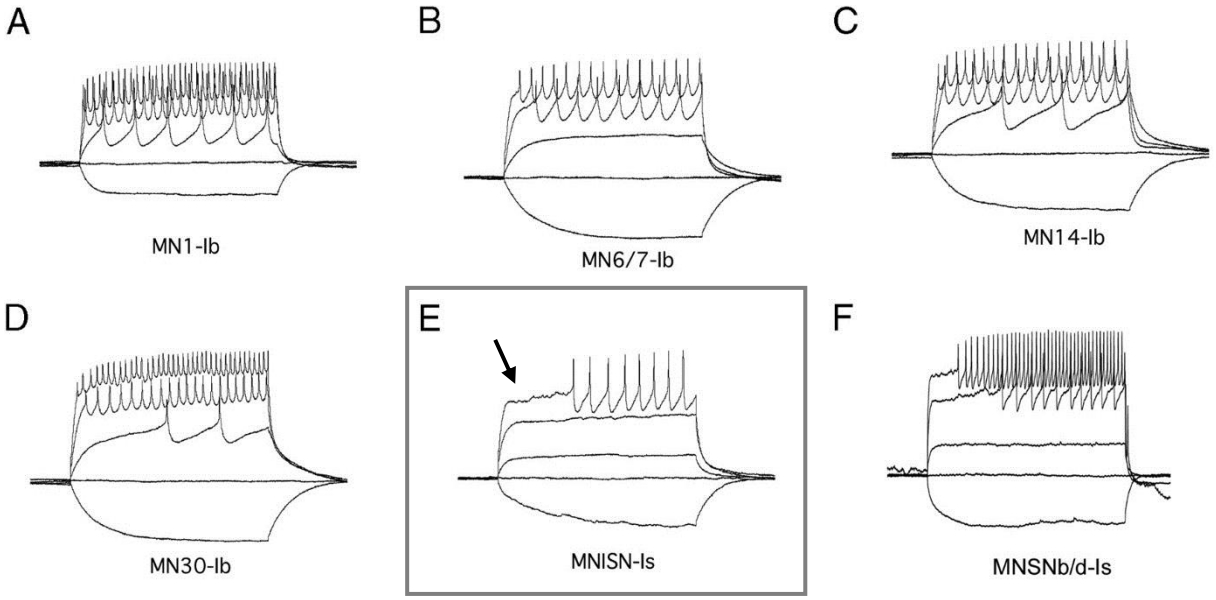

Figure 5: Firing pattern of different motoneurons in *Drosophila* L3 larvae by Choi et al.
Whole-cell current-clamp recording of six identified dorsomedial motoneurons. Each cell shows typical firing patterns. Most remarkable is recording **E**, which shows MNISN-Is. Upon somatic current injection, the cell fires delayed action potentials (arrow). Figure from Choi et al., 2004.

In F-type motoneurons of neonatal mice, a delayed action potential firing was found to be mediated by two independent components: a transient A-type K^+ current, and a slow-inactivating K^+ current. The A-type current inhibits a fast depolarization of the membrane in the first place, while the slow-inactivating component allows a slow depolarization of the membrane until the firing threshold is reached, which further delays the action potential (Leroy et al., 2015). Besides transient A-type Shal currents, MNISN-Is of *Drosophila* larvae also show a delayed rectifier K^+ current encoded by *shab* (K_v2) (Tsunoda & Salkoff, 1995), and a calcium (Ca^{2+}) activated sustained K^+ current encoded by *slo* (Kadas et al., 2015). A combined action of these components could underlie the characteristic firing properties of MNISN-Is.

Furthermore, motoneurons of *Drosophila* are equipped with voltage-gated Ca^{2+} channels (VGCC), which contribute to the shape of MN firing. The L-type Ca^{2+} channel DmCa1D (Ca_v1) is present in larval muscles and in all compartments of larval motoneurons (synapse, axon, and dendrites) (Kadas et al., 2017; Klein, 2016; Zheng et al., 1995). Dendritically localized DmCa1D channels increase motoneuron excitability and amplify synaptic input by prolonging postsynaptic responses to cholinergic input (Kadas et al., 2017). The same conserved mechanism can be found in vertebrate spinal motoneurons, where L-type Ca^{2+} channels contribute to PICs, which amplify a given synaptic input to maximize motoneuron output (Heckman et al., 2003).

As already described, both vertebrate and invertebrate motor behavior is highly modulated by biogenic amines. Since the modulation of only muscle properties seems unlikely to be solely

responsible for altered behavior, targets for aminergic modulation are suggested to be localized in the motoneurons. However, the molecular basis and the cellular targets in the CNS remain unknown and shall be the subject of this thesis.

1.5 Hypothesis

Aminergic modulation of motor behavior occurs in numerous vertebrate and invertebrate species (Brembs et al., 2007; Jay et al., 2015; McDearmid et al., 1997; Saraswati et al., 2004; Wallén et al., 1989). However, the underlying molecular and cellular mechanisms are incompletely understood. In vertebrate spinal motoneurons, biogenic amines such as serotonin and norepinephrine released from descending brainstem fibers amplify synaptic input via modulation of persistent inward currents (Heckman et al., 2008; Heckman et al., 2003). In *Drosophila*, the biogenic amines octopamine and tyramine modulate flight motor behavior in adult flies (Brembs et al., 2007), and crawling behavior in larvae (Fox et al., 2006; Saraswati et al., 2004). Bath-application of tyramine onto larval preparations decreases firing amplitudes of excitatory junction potentials of muscles, whereas treatment with octopamine increases firing amplitudes (Nagaya et al., 2002). However, these effects on the neuromuscular junction can unlikely explain the observed effects of octopamine and tyramine on behavior. There are several potential sites of action by which the biogenic amines octopamine and tyramine may affect locomotor behavior. First, the amines might regulate the motivation to locomote by acting on higher brain centers (Marella et al., 2012; Schwaerzel et al., 2003). Second, modulation of brain activity might affect general arousal and therefore regulate states of activity and locomotion (Andretic et al., 2005; van Swinderen et al., 2004). Third, aminergic modulation of sensory neurons might increase sensitivity and responsiveness to sensory stimuli (Harris-Warrick & Marder, 1991). Fourth, metabolism might be affected by biogenic amines (Brembs et al., 2007; Mentel et al., 2003). Fifth, octopamine and tyramine might alter neuromuscular transmission or muscle properties (Nagaya et al., 2002). Finally, the amines might regulate the intensity of locomotion by direct actions on motoneurons, as seen in vertebrates (Heckman et al., 2008; Heckman et al., 2003). Based on the substantial effects of biogenic amines on vertebrate spinal motoneurons, I hypothesize that direct modulation of motoneuron firing properties by biogenic amines is also a key feature for regulating locomotor behavior in invertebrates.

1.5.1 Aim of the Study

Based on my hypothesis, I tested the following predictions experimentally:

1. MNISN-Is is innervated by tyraminergic neurons within the CNS.

   To test this, an immunohistochemical triple-staining of identified tyraminergic neurons (VUM) (Landgraf et al., 1997; Monastirioti et al., 1995; Selcho et al., 2012), MNISN-Is motoneurons, and synaptic active zones was carried out and analyzed for spots of co-labeling.

2. Tyramine reduces the intrinsic excitability of MNISN-Is.
   a. To test this, tyramine was bath-applied during current-clamp recordings of MNISN-Is. Two firing properties were analyzed for changes upon application of tyramine.
   b. To show the effect of endogenously released tyramine, larvae were genetically manipulated, so that the tyraminergic VUM neurons could be activated by increasing the bath-temperature during recordings.
3. Knockdown or knockout of the octopamine-tyramine receptor (Oct-TyrR) reduces or prevents the effect of tyramine.
   a. To prove the role of Oct-TyrR, the firing properties of MNISN-Is upon bath-application of tyramine were analyzed in larvae with a motoneuron-specific knockdown of the receptor.
   b. Furthermore, the firing properties of MNISN-Is upon bath-application of tyramine were analyzed in larvae with a mutation for the receptor (*TyrR*^{hono}) (Kutsukake et al, 2000).
4. Tyramine modulates the properties of single ion channels in MNISN-Is.
   a. To show a possible role of Shal potassium channels (Choi et al., 2004; Ping et al., 2011), I analyzed the firing properties of MNISN-Is in larvae which were genetically manipulated to express a motoneuron-specific UAS-*shal*-RNAi.
   b. To show a possible role of dendritically localized DmCa1D calcium channels (Kadas et al., 2017; Worrell & Levine, 2008), I analyzed the firing properties of MNISN-Is in larvae which were genetically manipulated to express a motoneuron-specific UAS-*DmCa1D*-RNAi. Furthermore, calcium imaging experiments were carried out in controls and DmCa1D knockdowns. DmCa1D channels were also acutely blocked by La^{3+} in both current-clamp recordings and calcium imaging experiments.

5. Aminergic modulation of motoneurons is sufficient to alter larval crawling behavior.
    a. To confirm this, mid-L3 larvae were fed with TA and analyzed for altered crawling behavior.
    b. To show the role of tyraminergic modulation of motoneurons, larvae with both a mutation of the Oct-TyrR (*TyrR*^{hono}) and a knockdown of the Oct-TyrR were fed with TA and analyzed for altered crawling behavior.

    The experimental assays for larval crawling-analysis were established by me, and the experiments were conducted by a student, who confirmed this prediction in her bachelor thesis (Girwert, 2017).

2 Material and Methods

All specifications and origins of chemicals used in this thesis are listed in the appendix (Table 6).

2.1 *Drosophila melanogaster*

2.1.1 Fly Lines

For all experiments, animals were either taken directly from the stocks (Table 1) or crossed from the stocks to receive offspring with the desired genotype.

Table 1: List of all fly stocks used in this thesis.
Ordering numbers refer to Bloomington *Drosophila* Stock Center (**BL**), Vienna *Drosophila* Resource Center (**VDRC**), or Kyoto Stock Center (**Kyoto**)

	Ordering # / Origin	**FlyBase Genotype**
Controls	**BL** 3605	w^{1118} ; + ; + ; +
	BL 64349	Canton-S
GAL4 lines	S. Sanyal BIOGEN-Idec, Cambridge, USA	w^{*}; RN2-GAL4, UAS-mCD8::GFP / CyO ; Act<Stop>GAL4, UAS-FLP ; +
	S. Sanyal BIOGEN-Idec, Cambridge, USA – modified by S. Ryglewski, DuchLab	w^{*}; RN2-GAL4 / CyO ; Act<Stop>GAL4, UAS-FLP ; +
	S. Sanyal BIOGEN-Idec, Cambridge, USA – modified by S. Ryglewski, DuchLab	w^{*}; RN2-GAL4, UAS-GCaMP6s / CyO ; Act<Stop>GAL4, UAS-FLP ; +
	S. Sanyal BIOGEN-Idec, Cambridge, USA	+ ; OK37-1-GAL4 ; + ; +
	BL 9313	w^{*} ; P{Tdc2-GAL4.C}2 ; + ; +
Balancer line	**BL** 9493 / Aylin Klein	+ ; CyO / In(2LR)bw^{V1}, ds^{33k} dp^{ov1} b^{1} bw^{V1} ; CxD / TM6B, Tb^{1} ; +
DmCa1D-RNAi	**BL** 33413	y^{1} sc^{*} v^{1} ; + ; P{TRiP.HMS00294}attP2 ; +
TyrR-RNAi	**VDRC** v102643	+ ; P{KK103572}VIE-260B ; + ; +
	BL 25857	y^{1} v^{1}; + ; P{TRiP.JF01878}attP2 ; +
TyrR II-RNAi	**VDRC** v110525	+ ; P{KK110990}VIE-260B ; + ; +
Oct-Tyr- RNAi	**VDRC** v26877	w^{1118} ; P{GD13188}v26877 ; + ; +
	BL 28332	y^{1} v^{1} ; + ; P{TRiP.JF02967}attP2 ; +
Oct-TyrR mutant	**Kyoto** 109038	w^{1118} ; + ;P{lwB}Oct-$TyrR^{hono}$; +

Shal-RNAi	**VDRC** v103363	+ ; P{KK100264}VIE-260B ; + ; +
UAS-dcr2	**BL** 24651	w^{1118} ; + ; P{UAS-Dcr-2.D}10 ; +
UAS-TrpA1	L. Griffith Lab, Brandeis University	w ; UAS-TrpA1 ; + ; +
shi^1	**BL** 7068	w^{1118} shi^1 ; + ; + ; +
GCaMP6m	**BL** 42748	w^{1118} ; P{20XUAS-IVS-GCaMP6m}attP40 ; + ; +
	BL 42750	w^{1118} ; + ; PBac{20XUAS-IVS-GCaMP6m}VK00005 ; +
TßH null mutant	(Monastirioti et al., 1996)	$TßH^{nM18}$ / FM7c ; + ; + ; +

2.1.2 Fly Keeping and Crossing

All fly lines and crosses were reared in plastic vials (ø 2 cm) with mite-proof foam stoppers on standard cornmeal-agarose food (Table 2). The vials were kept at 25 °C with a 12 h light/dark cycle, except noted otherwise (Ryglewski & Duch, 2009). Temperature sensitive flies were kept in an incubator at 18 °C with a 12 h light/dark cycle.

Table 2: Recipe for one liter of cornmeal-agarose based fly food.

Water (DI)	1 liter	• The water is heated to 90 °C • Glucose is added and dissolved. Cornmeal, yeast, and agarose are added and stirred until the heat is at 90 °C again • Cook for 1 h 15 min under stirring • Cook another 1 h at 85 °C under stirring • Let cool to 66 °C
Glucose	116.94 g	
Cornmeal	55.32 g	
Yeast	29.24 g	
Agarose	10.65 g	
Tegosept (10%)	12.26 ml	• Add tegosept and ascorbic acid • Fill the still warm food into plastic vials
Ascorbic acid	0.56 g	

All flies kept at 25 °C were put on new food once a week. Flies kept at 18 °C were put on new food bi-weekly. For crosses, female virgins of the desired genotype were collected daily as pupae over a period of one week and then crossed with males two to one. New crosses were set up once a week, and one-week-old crosses were put on new food the day after if no flies of the F1 generation had hatched. In this way, the parental generation was kept three weeks maximum.

2.1.3 A Special Line: *RN2*-GAL4 […] UAS-*FLP*

The *RN2*-GAL4 driver line (Line 1) drives expression in all MN1-Ib (aCC) and MNISN-Is (RP2) motoneurons, as well as in some interneurons, under the control of the *even-skipped* promoter (Fujioka et al., 2003). On the second chromosome, there is also a GFP fusion protein, UAS-*mCD8::GFP*, which is always activated by the *RN2*-GAL4 (Fujioka et al., 2003; T. Lee & Luo, 1999). This GFP is integrated into the cell membrane.

Line 1

$$w^{*}\ ;\ \frac{\mathrm{RN2-GAL4, UAS-mCD8::GFP}}{\mathrm{CyO}}\ ;\ \frac{\mathrm{Act<Stop>GAL4, UAS-FLP}}{\mathrm{Act<Stop>GAL4, UAS-FLP}}\ ;\ +$$

In this line, the third chromosome holds a second, stronger GAL4 driver, *act*-GAL4. The *actin* promoter is separated from the GAL4 by a stop-codon, which is flanked by two FRT sites. (Golic & Lindquist, 1989; Hartwig et al., 2008). The weak *RN2* driver can activate the recombinase gene, *FLP*, randomly in some MN1-Ib and MNISN-Is motoneurons in embryonic stages. In these cells, the stop-codons are cut out, and then *act*-GAL4 is the main driving force for expression of GFP, RNAi or other constructs under UAS control. With this technique, single motoneurons are GFP labeled and simultaneously affected by RNAi, if used, in a mosaic-like pattern while the GFP negative cells are not affected by UAS-constructs.

2.2 Electrophysiology

2.2.1 Saline

All dissections, as well as electrophysiological recordings, were, if not noted otherwise, carried out in standard saline (Table 3) (Ryglewski & Duch, 2009). To test the effects of tyramine (TA) on neuronal excitability, TA was added to standard saline in different concentrations. Also, other chemicals like ion channel blockers or toxins were either added to standard saline or directly applied to the bath or the VNC. Fresh-made saline was used and stored at room temperature (25 °C) for two consecutive days and was then disposed. All glassware used to make and store any solutions used for electrophysiology were free of any soap and always cleaned by hand with pure DI water.

If beside standard saline other salines containing chemicals were used, one stock solution was made and then separated to have the same pH and osmolarity in all solutions. The chemicals were then added to one part of the stock solution. Which chemicals specifically were used is noted in the respective chapter of the results.

Table 3: Recipe for standard saline

Ingredient	Concentration	
NaCl	128 mM	• All ingredients are put into a measuring cylinder • The cylinder is filled up to the desired volume with Millipore water • Stir on a stirring plate • pH is adjusted to 7.24 – 7.25 with NaOH • Osmolarity should be at 300 - 310 mOsm
$MgCl_2$	4 mM	
KCl	2 mM	
$CaCl_2$	1.8 mM	
HEPES	5 mM	
Sucrose	35 mM	
Water (Millipore)	add to desired	
NaOH		

2.2.2 Experimental Procedures

For all experiments, wandering L3 larvae of the desired genotype were fixed with short-cut minutien pins in a Sylgard-silicone-filled petri dish lid (ø 4 cm). To keep the bath-volume constant, a silicone ring (OD: 1.7 mm, ID: 0.9 mm, height: 1 mm) was placed on the dish; the dissection was carried out inside the ring. The pinned-down larvae were covered in standard saline (Table 3) and dissected by opening the cuticle on the dorsal side in a straight line from the tip of the abdomen to the mouth hooks with sharp spring scissors (Fine Science Tools, USA). With another four pins the cuticle was stretched out and pinned down anteriorly and posteriorly. All internal organs and glands were carefully removed (Jan & Jan, 1976), until only the ventral nervous system (VNS) with its nerves, the mouthparts, and the muscles were left and exposed. The preparation was rinsed with standard saline several times until the bath was free from particles.

For all electrophysiological experiments, the setup was used with an upright Axioscope 2 FS plus microscope (Zeiss, Germany), an Axopatch 200B amplifier (Molecular Devices, USA), a Digidata 1322A (Molecular Devices) using a sampling rate of 20 kHz, an HS-2A headstage (Molecular Devices) with appropriate pipette holder (1-HL-U, Molecular Devices), an MP-225 micromanipulator (Sutter Instrument, USA) and the software pCLAMP (v 10.2, Molecular Devices) for data acquisition and analysis.

The ganglionic sheath was removed from the VNC under the microscope at 400x magnification (40x objective with water immersion lens, LUMPlanFl 40x / 0.80 w, Olympus) by carefully applying protease (1 %, in saline) and sucking in the dissolved parts of the sheath. For the focal application of protease, a patch pipette was pulled from borosilicate glass capillaries (no filament, OD: 1.5 mm, ID: 1.0 mm) in two steps in a vertical electrode puller (PC-10, Narishige;

No. 1 heater: 62.0, No. 2 heater: 42.8). The tip of the pipette was broken off with fine forceps under visual control and thereafter filled with protease.

MNISN-Is neurons could be identified by their unique morphology and location. As reported in the corresponding results section, motoneurons were either identified by expressing GFP or if GFP was not available, by a thorough investigation of the location and morphology of the soma with its associated axon (Choi et al., 2004; Srinivasan et al., 2012b; Worrell & Levine, 2008). After two to four MNISN-Is somata were cleaned thoroughly, the bath solution was continuously exchanged by a BPS-8 perfusion system (ALA Scientific Instruments, USA). The preparation was washed at least 2 min with standard saline before patching a neuron, if not noted otherwise. A patch pipette, also pulled from borosilicate capillaries (no filament, OD: 1.5 mm, ID: 1.0 mm) as described above but with its tip intact, was filled bubble-free with internal patch solution (Table 4) (Ryglewski et al., 2012). With this solution, the pipette resistance was 6 – 8 MΩ.

Table 4: Recipe for 20 ml internal patch solution

Ingredient	**Concentration**
KGluc	140 mM
$MgCl_2$	2 mM
EGTA	1.1 mM
HEPES	10 mM
MgATP	2 mM
Water (Millipore)	fill to 20 ml
KOH	
Glucose	

- All ingredients but $MgCl_2$ are put into a 50-ml beaker
- $MgCl_2$ is directly added to 20 ml Millipore water
- Add water and $MgCl_2$ into the beaker
- Stir on a stirring plate
- pH is adjusted to 7.24 – 7.25 with KOH
- Osmolarity is adjusted to 300 - 305 mOsm with glucose
- The solution is aliquoted in 1-ml portions and stored at -28 °C until use

For all experiments, MNISN-Is motoneurons were chosen from either the thoracic segment T3 or from the abdominal segments A1 to A3. The patch pipette was brought to the soma under continuous application of positive pressure, to keep the pipette tip clean from any particles. When the tip of the pipette nearly touched the soma, and a slight concavity could be seen, the pressure was released to obtain a gigaseal, i.e., the pipette resistance reached ≥ 1 GΩ instantly (Hamill et al., 1981; Mollemann, 2003). To achieve the whole-cell patch configuration, negative pressure was applied to the membrane until it broke. Only cells with a membrane potential more negative than -30 mV and with seals ≥ 1 GΩ were accepted for further experiments.

In the whole-cell configuration, currents could be measured in voltage-clamp mode with a clamped potential at -70 mV and a square pulse protocol reaching from -90 mV to 0 mV in 10 mV increments with each step lasting for 200 ms. Membrane potential changes and action potentials (AP) were measured in current-clamp mode, using a square pulse protocol and a ramp pulse protocol. Membrane potentials were adjusted to -60 to -75 mV. The square pulse protocol consisted of 2-s steps, injecting currents from 0 pA to 120 pA in 20 pA increments to the soma. The ramp pulse protocol injected gradually increasing currents. The ramps were 2 s long. A first ramp injected current to a maximum of 150 pA, and a second ramp injected current to a maximum of 300 pA. Between the starts of each square and each ramp current injection within the protocols, 10 s were left free of any changes for recovery. After the first recording in voltage-clamp mode was acquired to check for the healthiness of the cells, the settings were switched to current-clamp mode, and one square pulse protocol, as well as one ramp pulse protocol, was run. To verify the stability of the patched cell, it was washed another 2 min with standard saline and was recorded a second time in current-clamp mode. Only if these second recordings in square and ramp pulse protocols showed similar results to the first ones, the application of standard saline was stopped, and a different saline which contained TA, drugs, blockers, or similar was perfused into the bath for at least 2 min. Again, square and ramp pulse protocols were run twice 2 min apart. If TA was used for the respective experiment, its reversibility was verified by switching the perfusion system back to standard saline, and, again, recording twice after another 2 min. Each experiment, consisting of recordings in standard saline, saline with TA, and again standard saline, was done in a different animal since the effect of TA should only be measured in cells naive to TA.
As parameters for motoneuron excitability, the delay to the first action potential and the firing frequency were analyzed in all recordings.

If other protocols or solutions were used, those are described in the corresponding results chapter (results section 3).

2.3 Immunohistochemistry

L3 larvae were dissected as described above (methods section 2.2) in standard saline in a Sylgard-silicone-filled petri dish (Ø 4 cm). After the dissection, the preparation was rinsed thoroughly to get rid of all remains of tissue. For fixation, the preparation was completely covered with 4 % PFA (Table 5) and incubated for 40 min at room temperature (RT).

Subsequently, the preparation was rinsed with PBS at least three times and then washed with PBS three times 20 min at RT.

Table 5: Recipe for 10 ml PFA (4 %)

Ingredient	Quantity	
PFA	0.4 g	• PFA is completely dissolved in PBS at 56 °C on a heat plate with stirrer for 1 h • PFA (4 %) can be used for two consecutive days
PBS	10 ml	

The preparation was washed with 0.5 % Triton X (in PBS) six times 30 min at RT to perforate the tissues for better antibody penetration. For the triple-staining (results section 3.1, 3.2), all three primary antibodies, α-brp (mouse, 1:400), α-GFP (chicken, 1:200), and α-Tdc2 (rabbit, 1:200), were diluted together in 1 ml 0.3 % Triton X (in PBS). The antibodies were incubated overnight at 4 °C on a platform rocker. Primary antibodies are reusable two to three times and were put back into an Eppendorf tube and stored in the fridge. The preparations were washed at least eight times 30 min in PBS at RT before the secondary antibodies were applied. The secondary antibodies, α-chicken (goat, 1:400, Alexa Fluor® 488), α-mouse (goat, 1:400, Cy5), and α-rabbit (donkey, 1:400, Alexa Fluor® 568), were diluted together in 1 ml PBS and incubated overnight at 4 °C on a platform rocker. From this time point on, the preparations had to be protected from light. Again, the incubation was followed by washing the preparations in PBS for six times 30 min at RT. An increasing EtOH-series was carried out for dehydration of the samples. Each concentration, 50 %, 70 %, 90 %, and 100 %, was incubated for 10 min at RT. For embedding, a metal slide (100 µm) with a hole (Ø 1 cm) was used, so that the samples had enough vertical space to the coverslip. One cover slip (20 x 20 mm) was glued to the lower side of the metal slide with super glue. The hole of the metal slide was filled with methyl salicylate, in which the samples were put after complete dehydration. For covering, a second coverslip (18 x 18 mm) was put on top of the metal slide. After all air bubbles were thoroughly filled with methyl salicylate, the coverslip of the upper side was sealed with clear nail polish. Samples could be stored at 4 °C for several days.

The samples were scanned with a TCS SP8 confocal microscope (Leica) and the Leica Application Suite AF (LAS AF, Leica) software. Images (1024 x 1024 pixel) were scanned with a 40x oil immersion objective (HC PL APO 40x/1.30 Oil CS2, Leica), with Type F immersion oil (Leica Microsystems). The fluorophores of the Alexa Fluor® 488 antibody were excited with an argon laser at 488 nm and detected at 500 - 550 nm. The fluorophores of the Alexa Fluor® 568 antibody were excited with a diode laser at 561 nm and detected at 570 - 620

nm. The fluorophores of the Cy5 antibody were excited at 633 nm and detected at 645 - 700 nm. For further analysis, the LAS AF Lite (Leica, version 2.6) software was used.

2.4 Calcium Imaging with GCaMP6

2.4.1 Structure of GCaMP

GCaMP6 is a highly enhanced protein-based genetically encoded calcium indicator (GECI) with the three subtypes 6f, 6m, and 6s (referring to as fast, medium, and slow) (Akerboom et al., 2012; Chen et al., 2013; Tian et al., 2009). The difference between these subtypes lies in their Ca^{2+} binding kinetics, with GCaMP6s being the most sensitive indicator with the slowest kinetics (Chen et al., 2013). All GCaMPs consist of a circularly permuted single green fluorescent protein (cpGFP), which folds into a stable 11-strand *ß*-barrel with its original N and C termini connected (Baird et al., 1999; Heinemann, 1995). A cpGFP chromophore is located inside the *ß*-barrel (Baird et al., 1999). In addition, the cpGFP is connected to a protein complex consisting of the Ca^{2+} sensor and binding protein calmodulin (CaM), and the CaM-binding peptide M13 (Crivici & Ikura, 1995; Miyawaki et al., 1997), which is close to the chromophore of the cpGFP. If there is only a little or no Ca^{2+} available, the chromophore is protonated, and only a weak fluorescence could be measured. If in contrast, the CaM-M13 complex is saturated with four Ca^{2+} ions, a conformational change of this complex leads to a deprotonation and a rapid increase in fluorescence (Akerboom et al., 2009).

2.4.2 Experimental Procedures

In this thesis, mainly GCaMP6m was used for detecting Ca^{2+} influx into the dendrites of MNISN-Is motoneurons upon activation of the nicotinic acetylcholine receptors (nAChR). In control larvae, GCaMP6m was expressed, for example, under the control of OK37-1 (Line 2) by utilizing the GAL4/UAS system (Duffy, 2002).

Line 2

$$w^{*};\ \frac{OK37-1-GAL4}{P\{20XUAS-IVS-GCaMP6m\}attP40}\ ;\ \frac{+}{+}\ ;\ \frac{+}{+}$$

Due to the availability of fly strains and the affected chromosomes of the used RNAi knockdowns and mutants, GCaMP6m was expressed either on the second or third chromosome, and GCaMP6s had to be utilized for a few experiments. Precise genotypes are listed in the

respective experiment in the results section (chapter 3.10). Animals were dissected as described for electrophysiological experiments (methods section 2.2). Also, the nervous system was cleaned thoroughly from the ganglionic sheath with protease (1 % in saline) to expose as much of the dendrites as possible. Due to the base fluorescence of GCaMP at its inactivated state, motoneurons and corresponding dendritic trees could easily be identified. After the removal of the ganglionic sheath, the preparation was washed with standard saline for at least 2 min, then the perfusion of saline was stopped. Tetrodotoxin (TTX, 400 nM) was applied directly to the bath and could incubate for 3 min. TTX blocked all voltage-activated Na^+ currents and prevented the remaining muscles from twitching, and inhibited presynaptic input (Catterall, 1980). Following the incubation, the perfusion was switched on with standard saline. The setup was used with an upright Axioscope 2 FS plus microscope (Zeiss, Germany), an HS-2A headstage (Molecular Devices) with appropriate pipette holder (1-HL-U, Molecular Devices) for cleaning the VNC, an MP-225 micromanipulator (Sutter Instrument, USA) which was also only used for cleaning the VNC, a simple micromanipulator without electrical regulation for the puffing pipette, a Picospritzer III (Parker Hannifin, USA) used with 40 psi and external command from an isolated pulse stimulator (model 2100, A-M Systems), an ORCA-100 CCD camera (model C4742-95, Hamamatsu), and the software simple PCI (v 5.2.1.1609, Hamamatsu) for data acquisition and analysis. Pipettes were pulled from borosilicate glass capillaries (with filament, OD: 1.0 mm, ID: 0.5 mm) in a horizontal Flaming/Brown micropipette puller (model P-97, Sutter Instruments) with the following specifications: pressure = 500, heat = 475, which is depending on the condition of the heating filament, pull = /, velocity = 30, time = 250. The resulting pipette was filled bubble-free with nicotine (20 µM in ddest H_2O, from a 20 mM stock in EtOH). The tip was brought close to the dendritic tree of an MNISN-Is motoneuron. With a pulse duration of 4 to 12 ms, which was depending on the accessibility to the dendrites and whether the pipette tip was clean, nicotine was puffed onto the dendrites in single pulses. Within each experiment, the same pulse duration was kept. A puff of the receptor agonist nicotine onto the dendrites activated the nicotinic acetylcholine receptors (nAChR), which are unspecific channels for mono- and divalent ions (Dani, 2015). Ca^{2+}, as well as Na+, could flow into the dendrites, which raised the membrane potential. This depolarization, in turn, could activate voltage-gated calcium channels (VGCC). Both the Ca^{2+} influx through nAChRs and through VGCCs contributed to the increase in fluorescence of GCaMP, which bound the Ca^{2+}.

The immediate changes in fluorescence were filmed for further analysis. One experiment consisted of two consecutive sets of four nicotine puffs with a puffing interval of 15 seconds in

a standard saline bath, two sets of four nicotine puffs in a bath with saline containing TA (10 µM), and another two sets of four nicotine puffs in a standard saline bath. Each set of four nicotine puffs with the subsequent changes in fluorescence were recorded as single videos to keep the single video size as small as possible. Between two videos with experiments in the same bath solution, a pause of one minute was made. Between two videos with experiments in different bath solutions, an incubation time of at least 2 min was given.

For analysis, the maximum intensity of fluorescence upon each puff of nicotine was measured from the dendrites and compared with the brightness of the respective backgrounds over the period of each video. The data of the individual videos from each experiment were then merged. Pauses of one minute were manually inserted to distinguish between the single videos and runs, even if the actual pauses were longer.

2.5 Endogenous Release of TA via TrpA1

2.5.1 Structure of TrpA1

At least 20 genes exist for transient receptor potential (Trp) channels, which can be divided into seven subfamilies (Clapham et al., 2003; Montell et al., 2002; Ramsey et al., 2006). These channels are nonselective ion channels, that can be activated differentially, by either other receptors, by ligands, or directly by deformation or heat (Moqrich, 2005; Ramsey et al., 2006; Todaka et al., 2004). The transient receptor potential ankyrin 1 (TrpA1) channel is one of the known temperature sensors and is related to TRPV channels, which are heat sensitive. As other Trp channels, each TrpA1 channel consists of tetramers with six α-helical transmembrane domains, S1 to S6, in each subunit. Segments S5 and S6 are connected by a pore loop, composed of two short α-helices, reaching down into the pore. Furthermore, 15 to 18 ankyrin repeats are located on the N-terminus, which has led to its name. Each repeat consists of 33 amino acids, which form two α-helices (Jaquemar et al., 1999). TrpA1 can be activated by the reactive chemicals of onions or wasabi and associated spices, as well as by heat (Clapham, 2015; Laursen et al., 2015) in *Drosophila* and by cold (Laursen et al., 2015; Story et al., 2003; Viswanath et al., 2003) in mice and human.

Activation of this receptor leads to a depolarization of the cell membrane, caused by cation influx through the channel along their gradient (Ramsey et al., 2006).

2.5.2 Experimental Procedures

In this study, TrpA1 was utilized to activate specific tyraminergic cells by temperature shifts. To only address tyraminergic cells, a fly line was crossed which expressed the TrpA1 channel under the control of Tdc2 (Line 3, Table 1) by utilizing the GAL4/UAS system (Duffy, 2002).

Line 3

$$w^{*}; \frac{P\{Tdc2-GAL4.C\}2}{UAS-TrpA1}; +; +$$

The aim of this experiment was the release of TA from tyraminergic cells onto the motoneuron dendrites by activation of the endogenous TrpA1 channels by an increase in temperature. The activation of TrpA1 leads to an increase of the membrane potential, which in turn leads to vesicle release from the synapses. All patch-clamp experiments were conducted as described in the methods section 2.2. The set-up was used as described with the addition of a temperature controller (TC-10, Cornerstone), to heat or cool the bath solution as needed. Prior to the experiments with TrpA1 activated cells, a control experiment was done with Canton S larvae to test whether a mere shift of the temperature to 30 °C led to different firing properties in the cell. For all experiments, the animals were dissected in ice-cold saline. The ganglionic sheath was removed, and single MNISN-Is cells were patched. The temperature controller was adjusted to 20 °C for the first recordings. After two recordings at 20 °C, the temperature controller was set to 30 °C. After about four minutes the next two sets of recordings were carried out at a bath temperature of 30 °C. The temperature was set back to 20 °C, and the next recordings were carried out when the temperature was at 20 °C, which took about five minutes. After both the experiments with Canton S and *Tdc2*-GAL4 x UAS-*TrpA1* larvae were done as described, a third line was tested.

Line 4

$$\frac{T\beta H^{nM18}}{Y}; \frac{P\{Tdc2-GAL4.C\}2}{UAS-TrpA1}; +; +$$

Since tyraminergic cells do not only contain TA but also OA, it was likely that after a depolarization of these cells, OA was released together with TA. By using male larvae with a mutation of TßH, *TßH*^{nM18}, together with *Tdc2*-GAL4 x UAS-*TrpA1*, the release of OA could be prevented (Line 4, Table 1).

2.6 Testing Tyramine Receptor RNAis

For all three known *Drosophila* tyramine receptors (TARs) (introduction section 1.2.4), RNAi lines can be obtained from the Bloomington *Drosophila* Stock Center and from the Vienna *Drosophila* Resource Center. Various UAS-RNAi constructs were utilized to determine which one of the three receptors mediates the tyraminergic effects in MNISN-Is (Dietzl et al., 2007; Duffy, 2002). For the Tyramine Receptor (TyrR, CG 7431) (Bayliss et al., 2013; Cazzamali et al., 2005), two RNAi lines were tested, a TRiP (Transgenic RNAi Project) (Perkins et al., 2015) line from Bloomington (BL 25857), and a KK line from Vienna (v102643) (E. W. Green et al., 2014) (Table 1). For the Tyramine Receptor II (TyrR II, CG 16766) (Bayliss et al., 2013) one KK RNAi line, obtained from the Vienna *Drosophila* Resource Center, was used (v110525). For the third known tyramine receptor, the Oct-TyrR (CG 7485) (Arakawa et al., 1990; Bayliss et al., 2013; Saudou et al., 1990), two RNAi lines were used. They were obtained from each one of the two fly stock centers, a TRiP line from the Bloomington *Drosophila* Stock Center (BL 28332), and a GD line from the Vienna *Drosophila* Resource Center (v26877) (E. W. Green et al., 2014). Every RNAi line was individually crossed to the *RN2*-GAL4, *mCD8::GFP* driver line. The resulting lines were Line 5 and Line 6 for TyrR,

Line 5

$$w^{*}\ y^{*}\ v^{*}\ ;\ \frac{RN2-GAL4,UAS-mCD8::GFP}{+}\ ;\ \frac{Act<Stop>GAL4,UAS-FLP}{P\{TRiP.JF01878\}attP2}\ ;\ +$$

Line 6

$$w^{*}\ ;\ \frac{RN2-GAL4,UAS-mCD8::GFP}{P\{KK103572\}VIE-260B}\ ;\ \frac{Act<Stop>GAL4,UAS-FLP}{+}\ ;\ +$$

Line 7 for TyrR II,

Line 7

$$w^{*}\ ;\ \frac{RN2-GAL4,UAS-mCD8::GFP}{P\{KK110990\}VIE-260B}\ ;\ \frac{Act<Stop>GAL4,UAS-FLP}{+}\ ;\ +$$

and Line 8 and Line 9 for Oct-TyrR,

Line 8

$$w^{*}\ y^{*}\ v^{*};\ \frac{RN2-GAL4,UAS-mCD8::GFP}{+}\ ;\ \frac{Act<Stop>GAL4,UAS-FLP}{P\{TRiP.JF02967\}attP2}\ ;\ +$$

Line 9

$$w^{*};\ \frac{RN2-GAL4,UAS-mCD8::GFP}{P\{GD13188\}v26877}\ ;\ \frac{Act<Stop>GAL4,UAS-FLP}{+}\ ;\ +$$

For all experiments, L3 larvae from the progeny of these crosses were used. Due to the genotype of the RN2 driver-line, a mosaic pattern of randomly GFP-labeled motoneurons could be seen in the VNCs of all animals. Only MNISN-Is cells with a clear GFP-labeling were used for current-clamp recordings. All experiments were conducted as described in the methods section 2.2.2.

2.7 Statistical Analysis

Raw data were analyzed in the respective programs, depending on whether the data was acquired from Ca^{2+} imaging or from patch-clamping experiments. Summaries and tables were made in Microsoft Excel 2010 and 2013. All statistical analyses were done in IBM SPSS Statistics (versions 22 & 23). All parameters were separated into three 'runs', which most frequently were (1) before application of TA, (2) with TA, and (3) after washing TA out. If other groups were used due to different experimental set-ups or different solutions, it is noted in the corresponding results section. For comparison and analysis, all data were normalized to the first values of the first run of the respective experiment, which is always noted.

For all statistical tests, an alpha level of $\alpha = 0.05$ was chosen, thus statistical tests with a *p*-value smaller than 0.05 were assumed to be significant (Field, 2013; Hubbard & Armstrong, 2006). Before any other statistical tests were applied, a Shapiro Wilk test for normal distribution was carried out on all groups within one parameter. As the null hypothesis, it was assumed that a normal distribution was given. If the resulting *p*-value was smaller than 0.05, the null hypothesis was rejected and tests for not normally distributed data were used. If the *p*-value was higher than 0.05, a normal distribution was assumed, and tests for normally distributed data could be utilized. Since the three runs within the parameters marked three time points within one set of experiments, the runs were treated as related samples. For not normally distributed data, a

Friedman-Test was executed. This non-parametric test is a sign rank test, and it is used to compare three or more related groups where no normal distribution is required. It is similar to the parametric repeated measures ANOVA, where the normal distribution of the data is required (Field, 2013). If this test resulted in a *p*-value smaller than 0.05, a significant difference between at least two of the groups could be assumed. A follow-up analysis was automatically executed to compare all groups pairwise (Field, 2013). From this pairwise analysis, only corrected *p*-values were used for further comparison and presentation, to reduce the risk of a type I error. If only two related groups had to be compared, a Wilcoxon signed-rank test was utilized.
If the data were normally distributed, a parametric repeated measures ANOVA was applied. A pairwise comparison was automatically executed if the *p*-value of the ANOVA was smaller than 0.05. Again, only Bonferroni-corrected *p*-values were allowed (Field, 2013; Rasch et al., 2010). A paired T-Test was used if only two related groups with normal distribution had to be compared.
For comparison of non-related groups, a Kruskal-Wallis ANOVA with subsequent Mann-Whitney U-Tests was used for groups without normal distribution, and a one-way ANOVA with subsequent T-Tests was utilized if the data were normally distributed (Field, 2013).

All results are either shown as boxplots (Figure 6), even if the respective data were normally distributed or as median and single data points if the group size was smaller than eight. If not stated otherwise, the data are given as mean and standard deviation of the measured values. To describe variance of the normalized values, the normalized medians are given with their second and third quartiles.

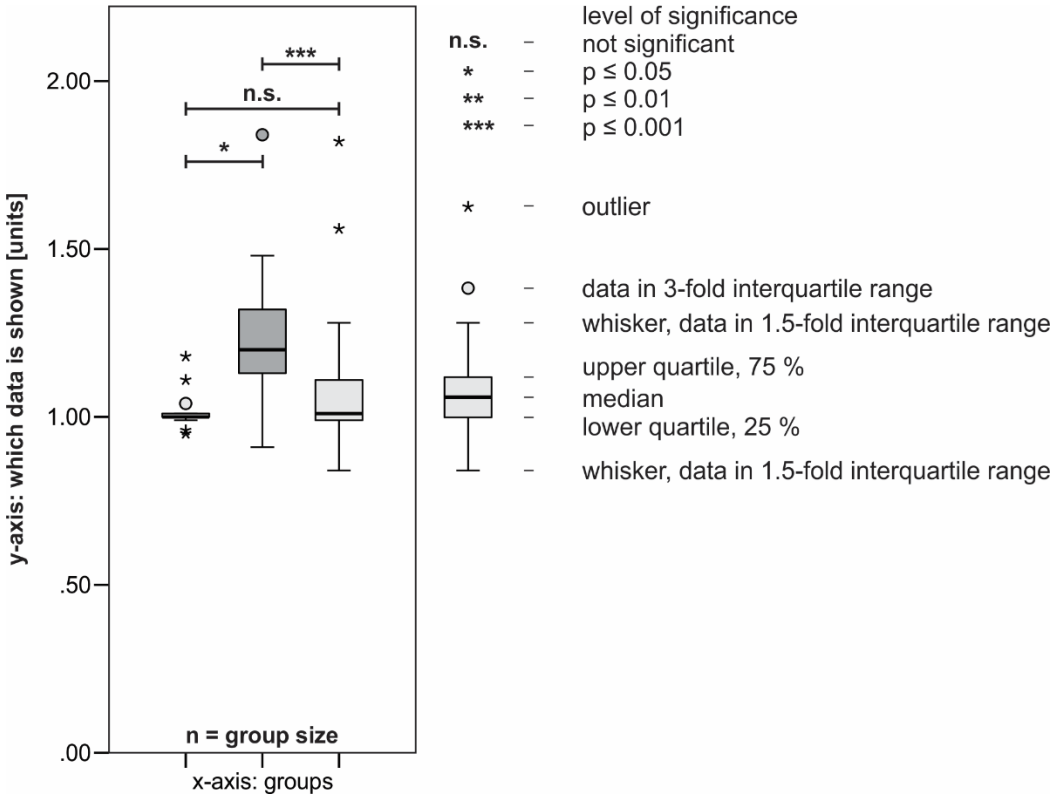

Figure 6: Boxplot as used in this thesis.
All statistics and boxplots were generated with IBM SPSS Statistics (versions 22 & 23).

2.8 Feeding and Crawling Assay

In a bachelor thesis, having the hypotheses of this Ph.D. thesis underlying, the impact of TA on larval locomotion was investigated. For experiments, flies were put on fresh food in plastic vials (Table 2), where they were allowed to lay eggs for 2 h, after which they were removed from the food. 72 h later, mid-L3 larvae could be gathered. For some genotypes, it took more time until the mid-L3 larvae were developed. The animals were randomly split into two groups, one control group, and one test group. For both groups, a small petri dish (Ø 4 cm) was filled with instant food containing brilliant blue (Formula 4-24, Carolina Biologicals, 750 mg / 1 ml H_2O). For better feeding results, a little bit of dry yeast was mixed into the water before using it for the food. The control group received mere instant food, for the test group, TA was also mixed into the water of the food (30 mg/ml). Larvae were allowed to feed for 2 h at 25 °C. Due to the brilliant blue, only larvae with a visible blue staining in their guts were collected and used for experiments (Saraswati et al., 2004).

Single larvae were put onto a smell- and taste-free agarose gel (0.7 %) in a big petri dish (Ø 14.5 cm). Their crawling tracks were filmed with an acA2000-165um camera (Basler) with an NMV-6x11.5 zoom macro lens (Navitar) and the Pylon Viewer software (Basler, version

5.0.0.6150) at a sampling rate of 4 fps for 2 min. The recording was started 30 s after the larva was put on the gel or as soon as it showed first crawling movements (Saraswati et al., 2004; J. W. Wang et al., 1997). Canton S was used as wild-type control, *TyrR*^{hono} was used, and an *Oct-TyrR*-RNAi was utilized (Line 10, Table 1) (Girwert, 2017).

Line 10

$$+\,;\ \frac{\mathrm{OK37-1-GAL4}}{\mathrm{UAS-dcr2}}\ ;\ \frac{\mathrm{P\{TRiP.JF02967\}attP2}}{+}\ ;\ +$$

All videos were analyzed with the open source software Tracker (www.opensourcephysics.org, version 4.9.8). For each frame of each video, relative X and Y values in a pre-defined coordinate system could be measured for the centroids of the larvae. With these values, the crawling speed and the total track length could be calculated, which were then compared between the different test groups, and genotypes.

3 Results

3.1 Tyraminergic Axons are Located Close to the Dendrites of Motoneurons

To see whether the anatomical prerequisites for a tyraminergic modulation of neuronal excitability by an endogenous release of TA onto MNISN-Is motoneurons (MN) are given, an immunohistochemical staining was done. Larvae of the RN2 control genotype were dissected and treated as described (Line 11, methods section 2.3). In this genotype, some MNs expressed UAS-*mCD8::GFP*, which resulted in a mosaic pattern of GFP-labeled neurons.

Line 11

$$w^{1118}\ ;\ \frac{\mathrm{RN2-GAL4,UAS-mCD8::GFP}}{+}\ ;\ \frac{\mathrm{Act<Stop>GAL4,UAS-FLP}}{+}$$

All MNISN-Is MNs are located to the dorsal side of the ventral nerve cord (VNC). The axons do not cross the midline of the nervous system and innervate dorsal muscles on the ipsilateral side. Their dendrites spread off the axon in close proximity to the respective somata. The cells which are thought to release TA onto the MN dendrites are the ventral unpaired median neurons (VUM), which are located to the ventral side of the VNC. Their axons grow towards the dorsal side of the VNC, where they form a T-crossing with two neurites heading towards body-wall muscles on both sides of the larva (Figure 7) (Sink & Whitington, 1991).

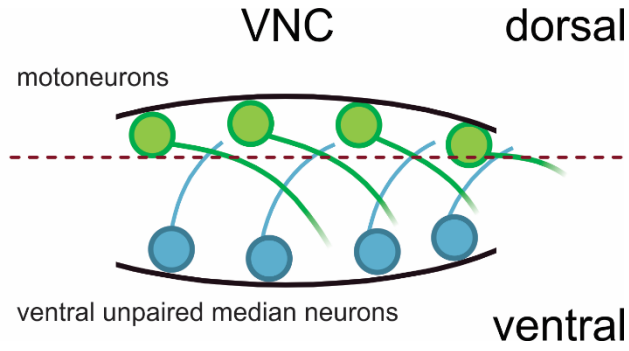

Figure 7: Schematic picture of the VNC as seen from laterally.
In this scheme, the relative positions of motoneurons and ventral unpaired median neurons are shown as if looked from a lateral angle. VUM neurons are on the ventral side (blue), MNs are located to the dorsal side (green) of the VNC. Axons of the VUM cells are projecting upwards to the dorsal side, where they separate and go out to the muscles (not shown). MN dendrites are located in close proximity to the respective somata. The axons grow ipsilaterally out to the muscles (not shown). The dashed line is a possible section, where VUM axons and MN dendrites could form synaptic contacts.

In *Drosophila* larvae, ablation of the VUM neurons leads to strongly reduced crawling behavior (Selcho et al., 2012). OA, which is released by VUM neurons, modulates motor output like force production in leg muscles in adult flies (Harvey et al., 2008; Zumstein et al., 2004). But

whether the processes of VUM neurons innervate the MNs or if they only project onto muscles and organs, remains unclear (Cole et al., 2005; Monastirioti et a., 1996; Sink & Whitington, 1991; Vömel & Wegener, 2008). However, aminergic modulation at the input site of MNs, i.e., the dendrites, is a known mechanism for amplification of synaptic input. One prominent example are persistent inward currents, which are mainly generated in dendrites of motoneurons and are highly modulated by serotonin (Clements et al., 1986; Heckman et al., 2008).

Single *Drosophila* larval MNISN-Is motoneurons were labeled by targeted expression of mCD8::GFP and subsequent immunostaining against GFP (Figure 8, green). The tyraminergic ventral unpaired median neurons were labeled with an antibody against tyrosine decarboxylase, Tdc2 (Figure 8, cyan). Tdc2 is the enzyme necessary for the synthesis of TA from tyrosine. An antibody against the synaptic marker Bruchpilot, brp, was used to show possible synaptic connections at sites of neurite overlap between VUM axons and MN dendrites (Figure 8, magenta).

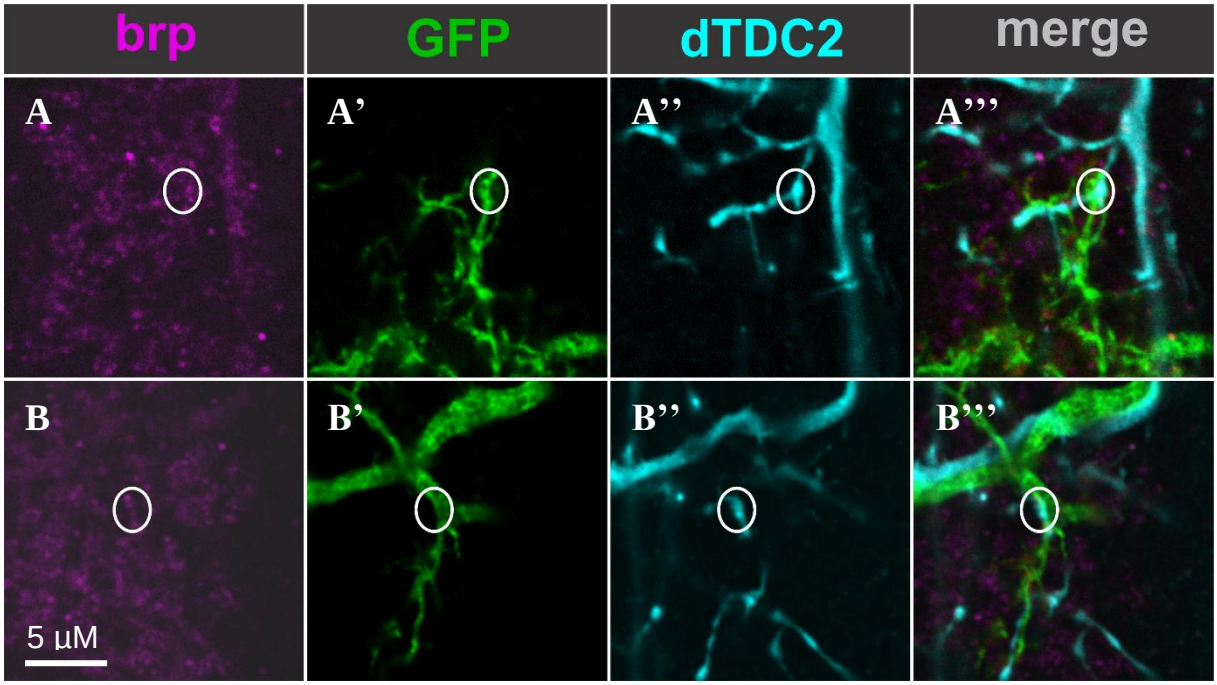

Figure 8: Immunohistochemical staining of motoneuron dendrites, tyraminergic VUM axons, and synaptic active zones. **A, B** The first column shows the active zone marker brp (magenta). Single spots indicate active zones, i.e., synaptic connections in the neuropil. **A', B'** GFP is shown in the second column, labeling dendritic trees of MNISN-Is neurons (green). **A'', B''** In the third column axonal arborizations of tyraminergic VUM neurons are labeled by anti-Tdc2 (cyan). **A''', B'''** In the last column, all three channels are merged into one slide. A and B show single sections from two different animals. In the merge, an overlap of all three labels could be assumed (circle). N = 4

Antibodies against brp are commonly used to label single active zones since brp is essential for the formation of T-bars in synapses, and for synaptic vesicle release (Kittel et al., 2006; Wagh

et al., 2006). In single sections of this triple-staining, several spots could be found where all three labels, MN dendrites, VUM axons, and synapses, were co-localized on the level of confocal laser scanning microscopy (CLSM) resolution (single voxel size 81 * 81 * 450 nM, true resolution in tissue might be lower) (Figure 8). If there is physical contact between the neurites on the level of light microscopy, at least the anatomical prerequisite for synaptic communication would be given.

3.2 Axonal Connections between Motoneurons and Tyraminergic Neurons

Modulation of dendritic ion channels does not exclusively determine action potential shape. In hippocampal CA3 pyramidal neurons, the AP shape can be broadened by application of glutamate to the axon, which in turn leads to an increased Ca^{2+} influx at the synapse and higher vesicle release rates. AP initiation can also be modulated. Dopamine, for example, inhibits AP initiation by downregulating T-type Ca^{2+} channel activity at the axon initial segment of cartwheel cells in the dorsal cochlear nucleus (Bender et al., 2010; Sasaki et al., 2011). The axons of VUM neurons project onto several ventral, transverse, and dorsal *Drosophila* larval muscles (Sink & Whitington, 1991). To also show a co-localization of VUM axons and axons of motoneurons in the same nerves, the triple-immunostaining (results section 3.1) was analyzed for overlap of the labels in nerves of the VNC.

Figure 9 shows single sections of nerves directing towards body wall muscles. GFP (green) labels axons of several motoneurons, and Tdc2 (cyan) labels axons of tyraminergic VUM neurons. The synaptic marker brp (magenta) could also be found in these sections, but it seemed to only label the Tdc2 positive tyraminergic VUM neurites and not the axons of motoneurons, which run in parallel to the tyraminergic axons. The axons might have synaptic contact, but brp might as well just be transported to the axon terminals of the VUM neurons. Synaptic connections between the axons of motoneurons and the axons of VUM neurons could not finally be assumed.

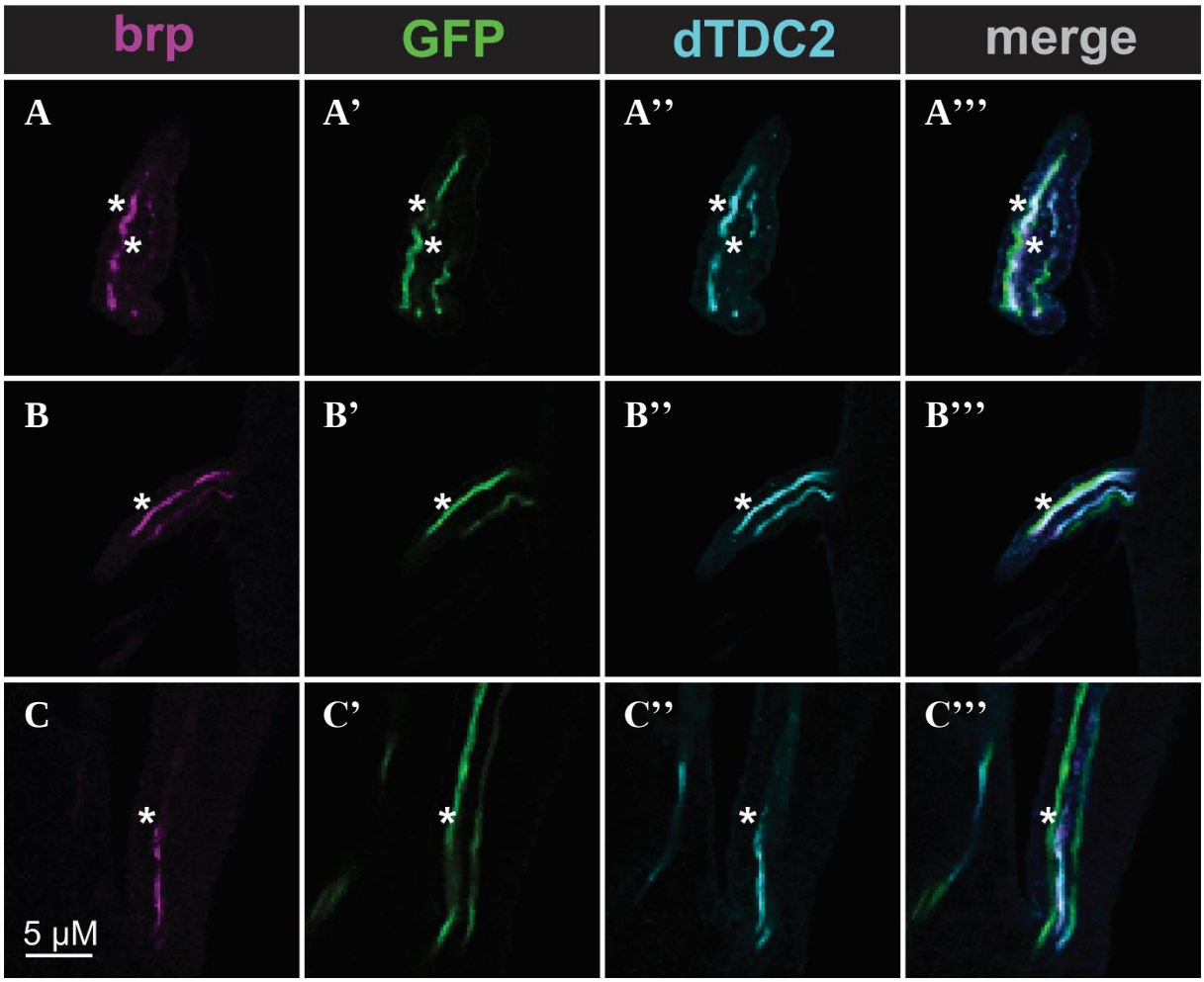

Figure 9: Immunohistochemical triple-staining of nerves.
A, B, C Staining against the synaptic marker brp (magenta). The marker could be seen in tyraminergic neurites. **A', B', C'** Staining against GFP (green). Axons of MNISN-Is and MN1-Ib are labeled. **A'', B'', C''** Staining against Tdc2 (cyan). Tyraminergic axons of VUM neurons are labeled. It is co-labeled with brp. **A''', B''', C'''** Overlay of all three labels.
Only single sections of nerves are shown. A and B show two sections of the same nerve, C shows one section of a different animal. Asterisks are used for better evaluation of distances between axons. N = 4

3.3 Tyramine Reduces Intrinsic Motoneuron Excitability

Whole-cell patch-clamp experiments were conducted to show tyraminergic modulation in MNISN-Is of the control strains Canton S (n = 10) and a cross of w^{1118} with *RN2*-GAL4, UAS-*mCD8::GFP* (n = 11) (Line 11). Current-clamp recordings were used to evaluate MN excitability by analyzing the properties of evoked firing in the well-described MNISN-Is (Choi et al., 2004; Hoang & Chiba, 2001; Kadas et al., 2015; Schaefer et al., 2010). The two parameters for analysis were the delay to first action potential and the firing frequency. TA was bath-applied in a concentration of 10 µM during the recordings to reveal its modulatory effects.

The membrane potential was clamped to -60 to -75 mV for all recordings if possible. The value might vary slightly because of intrinsic cell activity. In the shown example in standard saline, a somatic current injection of 80 pA increased the membrane potential from -60.21 mV to -21.30 mV, where a delayed firing of action potentials can be seen (Figure 10 A).

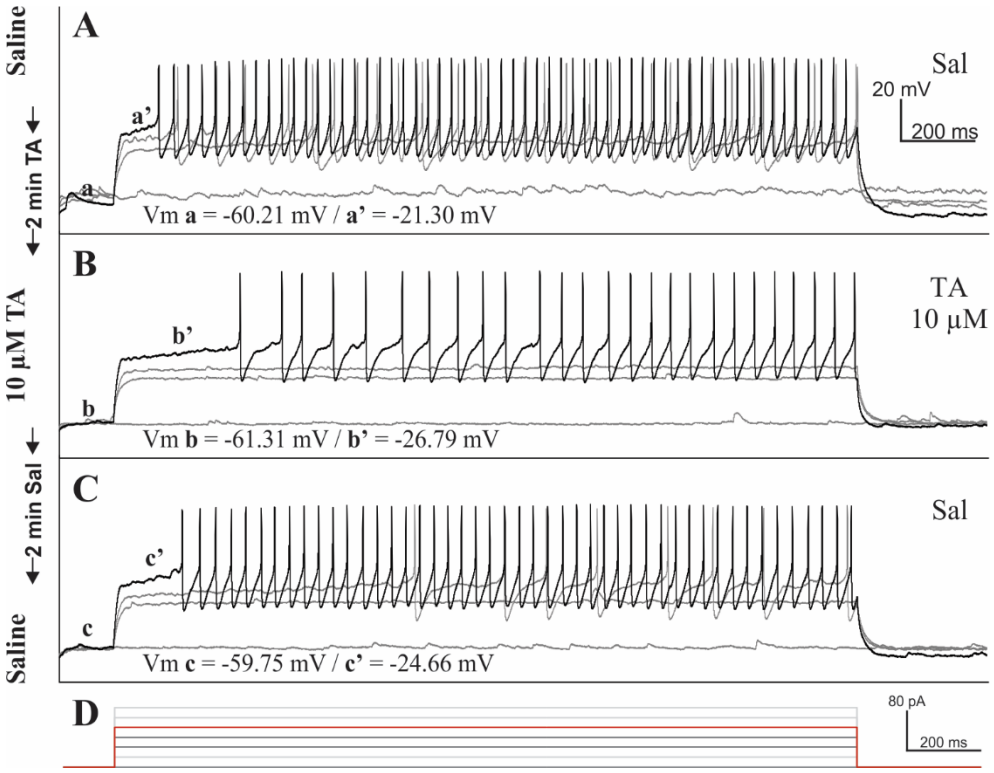

Figure 10: Firing pattern of MNISN-Is in square pulse protocols.
Sweeps with 0, 40, 60, and 80 pA somatic current injection are shown **A** Response to current injection in standard saline. An injected current of 40 pA elicited first APs at a membrane potential of -28.96 mv. An injection of 80 pA increased the membrane potential from -60.21 mV to -21.30 mV. **B** Weaker depolarization of the membrane after bath-application of 10 µM TA. The first step in which APs could be found was at 80 pA, with a depolarization to -26.79 mV. **C** TA could be washed out with standard saline. After 2 min, a current injection of 60 pA evoked first APs, which depolarized the membrane to -27.65 mV. Injection of 80 pA raised the membrane potential to -24.66 mV. **D** Current injection steps with 20 pA increments. The steps shown in A-C are marked in dark grey and red.

The first step in which action potential (AP) firing occurred in standard saline, was at 40 pA, which depolarized the cell to -28.96 mV. After 10 µM TA was bath-applied and incubated for two minutes, the somatic current injection of 80 pA depolarized the membrane from its resting potential (-61.31 mV) to -26.79 mV. In TA, this was the first step in which AP firing occurred (Figure 10 B). After washing TA out with standard saline, the cell fired APs one step earlier, with 60 pA of injected current to the soma. In the subsequent step, at 80 pA, the membrane potential was raised from -59.75 mV to -24.66 mV (Figure 10 C).

Ramp pulse protocols were used to mimic increasing synaptic input (Kadas et al., 2015). Cells were also clamped to a membrane potential between -60 mV and -75 mV if possible. Two

somatic ramp currents were injected, one with a maximum of 150 pA, the second with a maximum of 300 pA (Figure 11). In the first ramp of the example, the shown cell started firing APs at a membrane potential of -23.44 mV. This threshold was just slightly varied after application of TA. First APs were evoked at a membrane potential of -20.45 mV. After TA was washed out, the cell fired at -19.23 mV.

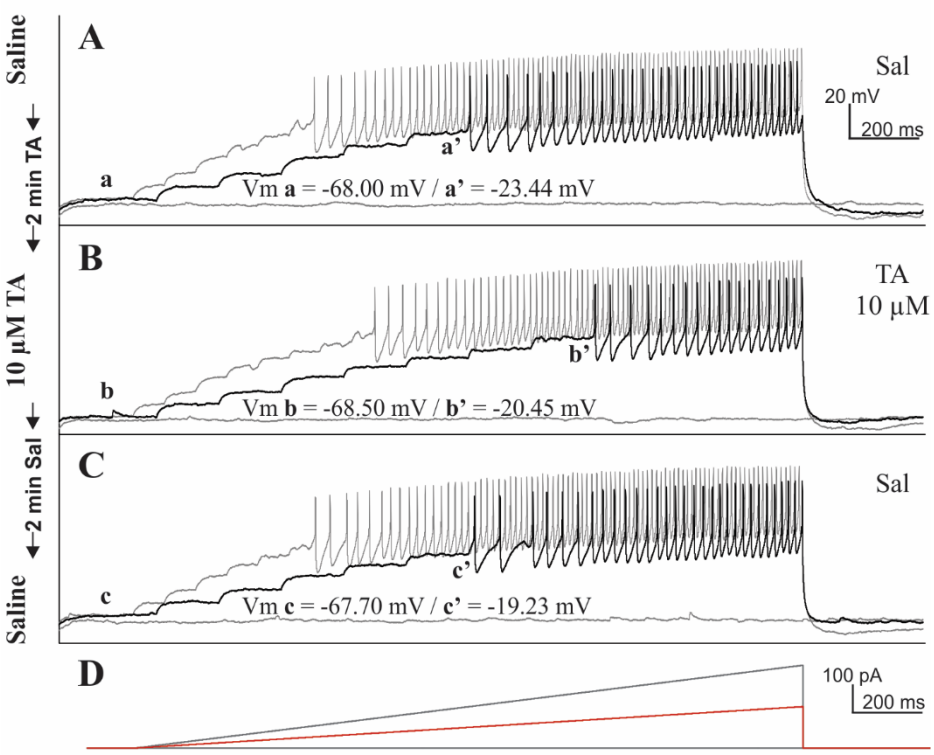

Figure 11: Firing pattern of MNISN-Is in ramp pulse protocols.
MNISN-Is response upon ramp current injection. The membrane potential was clamped to about -68 mV in all three runs. **A** APs were fired as soon as the membrane was depolarized to -23.44 mV in standard saline. **B** After TA was bath-applied, the cell began firing at -20.45 mV. **C** Washing TA out did not alter the threshold. The cell fired APs with reaching a threshold of -19.23 mV. **D** Ramps of injected currents with maxima of 150 and 300 pA.

For analysis of the two parameters delay to the first AP and the firing frequency in square pulse protocols, only those steps were used in which AP firing occurred in all three conditions, in standard saline, in 10 µM TA, and in standard saline after washing TA out. In the example (Figure 10), this would be sweep five, with 80 pA. In ramp pulse protocols, always the first ramp was analyzed. For clarity, only the analyzed traces are shown in future figures if not necessary otherwise.

For each condition (in standard saline, in 10µM TA, and again in standard saline), two runs at two-minute intervals were made from square, and ramp pulse protocols as described (methods section 2.2.2). The two runs of each condition were compared and statistically analyzed for significant differences (Figure 12).

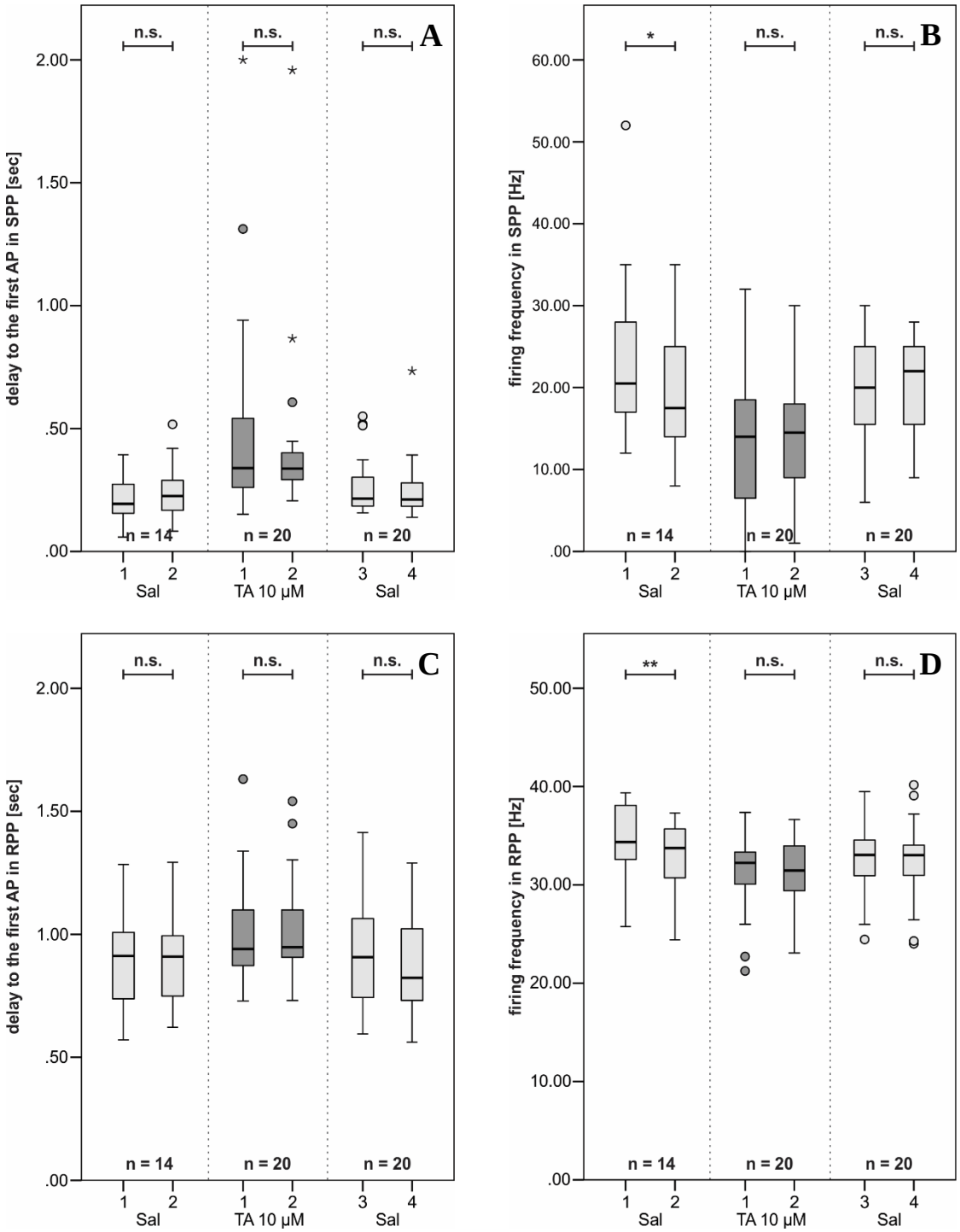

Figure 12: Comparison of run one and two in recordings with and without TA

For each bath solution (standard saline, 10 µM TA, and again standard saline), two recordings were made two minutes apart to check for differences caused by time and to check for increased modulatory effects due to longer incubation times. **A** For the delay in square pulse protocols, Wilcoxon signed-rank tests showed no significant differences between the two runs in standard saline ($p = 0.594$; $n = 14$), between the two runs in 10 µM TA ($p = 0.502$; $n = 20$), and between the two runs in standard saline after washing TA out ($p = 0.173$; $n = 20$). **B** For the corresponding firing frequency, Wilcoxon signed-rank tests showed a significant difference between the two runs in standard saline ($p = 0.022$; $n = 14$), but not between the two runs in 10 µM TA ($p = 0.747$; $n = 20$), and between the two runs after washing TA out ($p = 0.175$; $n = 20$). **C** For ramp pulse protocols, the delays to the first AP were tested with paired samples T-Tests, which revealed no significant differences between the three pairs of runs (standard saline, $p = 0.362$; $n = 14$; 10 µM TA, $p = 464$; $n = 20$; after washing TA out, $p = 0.144$; $n = 20$). **D** The corresponding firing frequencies of the runs were tested with Wilcoxon signed-rank tests, which showed a significant difference between the two runs in standard saline ($p = 0.009$; $n = 14$), but not in TA ($p = 0.881$; $n = 20$), and after the washing-out of TA ($p = 0.575$; $n = 20$).

In the comparison of the delays to the first AP of all runs in square pulse protocols, Wilcoxon signed-rank tests did not show significant differences between the two runs in standard saline ($p = 0.594$; $n = 14$), in 10 µM TA ($p = 0.502$; $n = 20$), or in standard saline after washing TA out ($p = 0.173$; $n = 20$). To test the respective firing frequencies, Wilcoxon signed-rank tests were carried out, which showed a statistically significant difference between the two runs in standard saline ($p = 0.022$; $n = 14$), but not between the runs in 10 µM TA ($p = 0.747$; $n = 20 / 20$), and the two runs in standard saline after washing out TA ($p = 0.175$; $n = 20 / 20$) (Figure 12 A, B). To test for differences in the delay to the first AP between the runs in ramp pulse protocols, paired samples T-Tests were conducted, which showed no significant differences between the runs in standard saline ($p = 362$; $n = 14$), in 10 µM TA ($p = 0.464$; $n = 20$) and in standard saline after washing TA out ($p = 0.144$; $n = 20$). The firing frequencies of the corresponding runs were, again, compared by Wilcoxon signed-rank tests. A significant difference could be found between the runs in standard saline before application of TA ($p = 0.009$; $n = 14$), but not between the runs in 10 µM TA ($p = 0.881$; $n = 20$), or in standard saline after the removal of TA ($p = 0.575$; $n = 20$). These results show that the modulatory effects after a two-minute application of TA were not further intensified by a longer incubation time. Since no significant differences were found but in the firing frequencies in standard saline, data of the same conditions were pooled (Figure 12), resulting in one pooled run for each condition in the further analysis, referring to as run one, two, and three.

MNISN-Is motoneurons showed the characteristic delay to the first action potential in all recordings with square pulse protocols (Choi et al., 2004; Schaefer et al., 2010) (Figure 13 A). In standard saline, this delay was on average 201.45 ± 84.76 ms (mean; standard deviation; $n = 21$). It was measured from the beginning of the depolarization to the onset of the first AP. For all square pulse protocols, the firing frequency was taken from one second of the middle of the recording. The firing frequency was on average 24.14 ± 9.1 Hz ($n = 21$) in standard saline. Two minutes after the bath-application of standard saline containing 10 µM TA, the delay was increased to 468.29 ± 338.53 ms ($n = 21$), and the firing frequency was reduced to 14.1 ± 7.7 Hz ($n = 21$) (Figure 13 B). Both effects were reversible, as shown by a two-minute washing in standard saline. The delay was reduced to 254 ± 107.68 ms ($n = 21$), and the firing frequency was increased to 20.67 ± 7.09 Hz ($n = 21$) (Figure 13 C). For statistical analysis, data were normalized to the first value of the first run in standard saline and tested for significant differences between the three pooled runs (in standard saline, in 10 µM TA, and again in standard saline) with a one-way ANOVA with repeated measures if data were normally distributed. Data were tested with a Friedman-Test if they were not normally distributed

(methods section 2.7). Since the data of the delay to the first AP were not normally distributed, a Friedman-Test was conducted, which showed a significant difference between the three runs ($p < 0.001$; $n = 21$). The pairwise follow-up comparison revealed that the increase of 112 % in the delay after bath-applying 10 µM TA for 2 min was significant (normalized (n.) median = 2.12; $n = 21$) ($p < 0.001$; $n = 21$), and that the reduction of 80 % after washing TA out for 2 min was also significant ($p = 0.002$; $n = 21$). The delay to the first AP of the first run (n. median = 1.00; $n = 21$) was not significantly different from the delay of the third run, after removing TA (n. median = 1.32; $n = 21$) ($p = 0.368$; $n = 21$) (Figure 14 A).

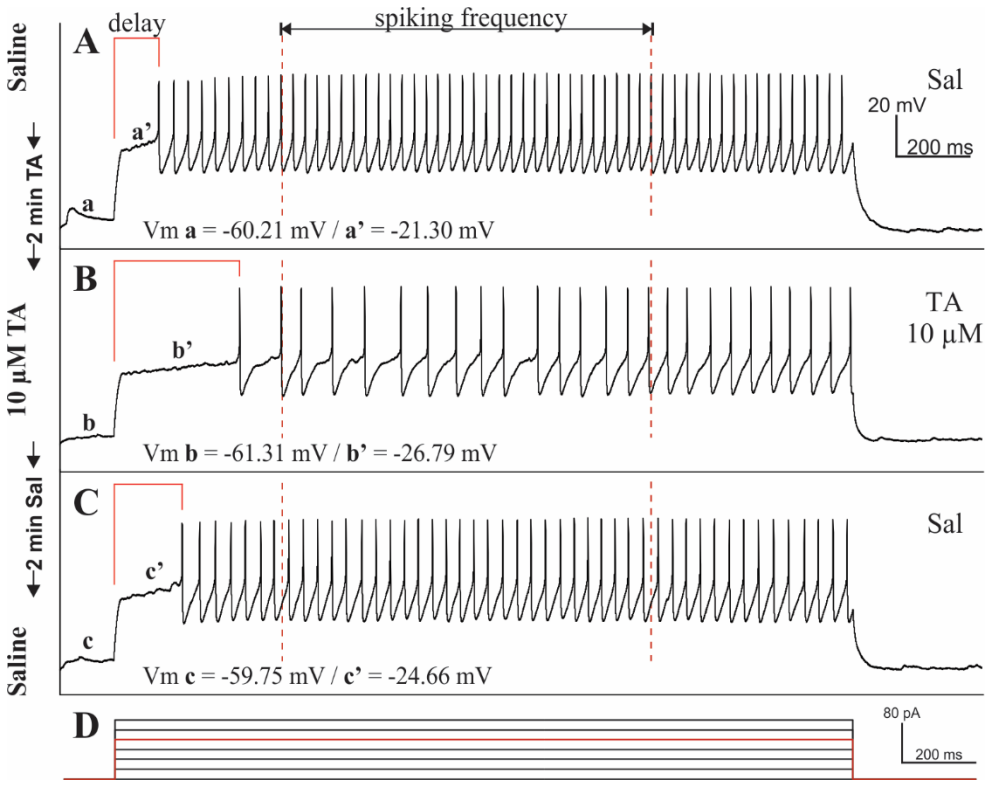

Figure 13: Firing pattern of MNISN-Is in square pulse protocols.
Typical firing pattern of MNISN-Is motoneurons upon a two-second somatic square pulse current injection of 80 pA. **A-C** Red lines indicate where the delay was measured. Red dashed lines indicate where the firing frequency was measured. **A** Response to current injection in standard saline with a characteristic delay to the first AP. **B** Increased delay to the first AP after 2 min of washing in 10 µM TA. The delay increased while the firing frequency decreased. **C** Washing the preparation in standard saline for 2 min removed the effects of TA on the delay and the firing frequency. **D** Current injection steps in 20 pA increments. The step shown in A-C is marked in red.

The data for analysis of the firing frequency were normally distributed in the three runs, which is why a one-way ANOVA with repeated measures was conducted. The ANOVA revealed a significant difference between the runs ($p < 0.001$; $n = 21$). Pairwise follow-up comparisons showed that the 40 % reduction of the firing frequency by TA was significant (n. median = 0.56) (pairwise follow-up comparison, $p < 0.001$; $n = 21$). The effect was reversible since the firing frequency was a significant 27 % increased after the preparation was washed with

standard saline for two minutes (n. median = 0.83) (pairwise follow-up comparison, $p < 0.001$; n = 21). The frequency of the third run was not significantly different from the first one (n. median = 1.00) (pairwise follow-up comparison, $p = 0.262$; n = 21) (Figure 14 B).

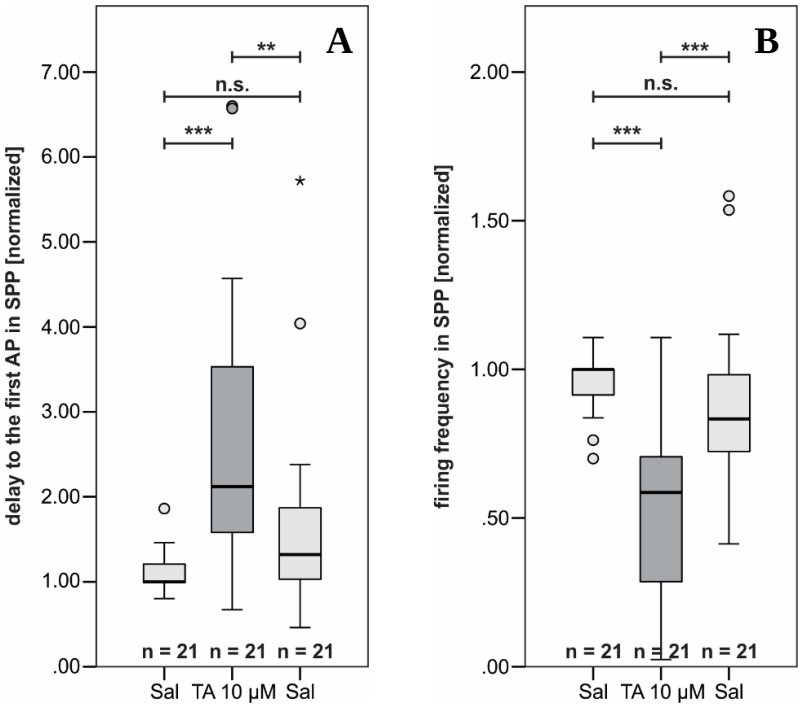

Figure 14: Statistical analysis of the delay to the first AP and the firing frequency in square pulse protocols.
A Analysis of the delay to the first AP of the three runs (F.T., $p < 0.001$; n = 21). Upon application of 10 µM TA, the delay to the first AP was significantly increased (pairwise follow-up comparison, $p < 0.001$; n = 21), and significantly reduced after the removal of TA (pairwise follow-up comparison, $p = 0.002$; n = 21). **B** Analysis of the firing frequency of the three runs (one-way ANOVA w. r. m., $p < 0.001$; n = 21). The firing frequency was significantly reduced after the application of 10 µM TA (pairwise follow-up comparison, $p < 0.001$; n = 21), and significantly increased after washing out TA (pairwise follow-up comparison, $p < 0.001$; n = 21).

Besides the square pulse protocols, ramp pulse protocols (RPP) were analyzed for differences between the delays to the first AP and the firing frequencies of the three runs. The delay was measured from the beginning of the depolarization to the onset of the first AP in the first ramp of each recording (Figure 15). On average, the delay to the first AP was 844.18 ± 172.39 ms in standard saline (n = 21). The firing frequency was calculated from all APs of the analyzed ramp (Figure 15). In standard saline, the mean firing frequency was 34.45 ± 3.75 Hz (n = 21). In the ramp pulse protocols, similar effects could be seen upon application of TA as in the square pulse protocols. Upon application of TA, the delay to the first AP was increased to 1029 ± 218 ms (n = 21), whereas the firing frequency was reduced to 31.04 ± 3.66 Hz (n = 21). After TA was washed out for two minutes, both the delay and the firing frequency were back close to the starting values, with a delay of 864.87 ± 19.54 ms (n = 21) and a firing frequency of 32.45 ±

3.65 Hz (n = 21) in the third run (Figure 15).

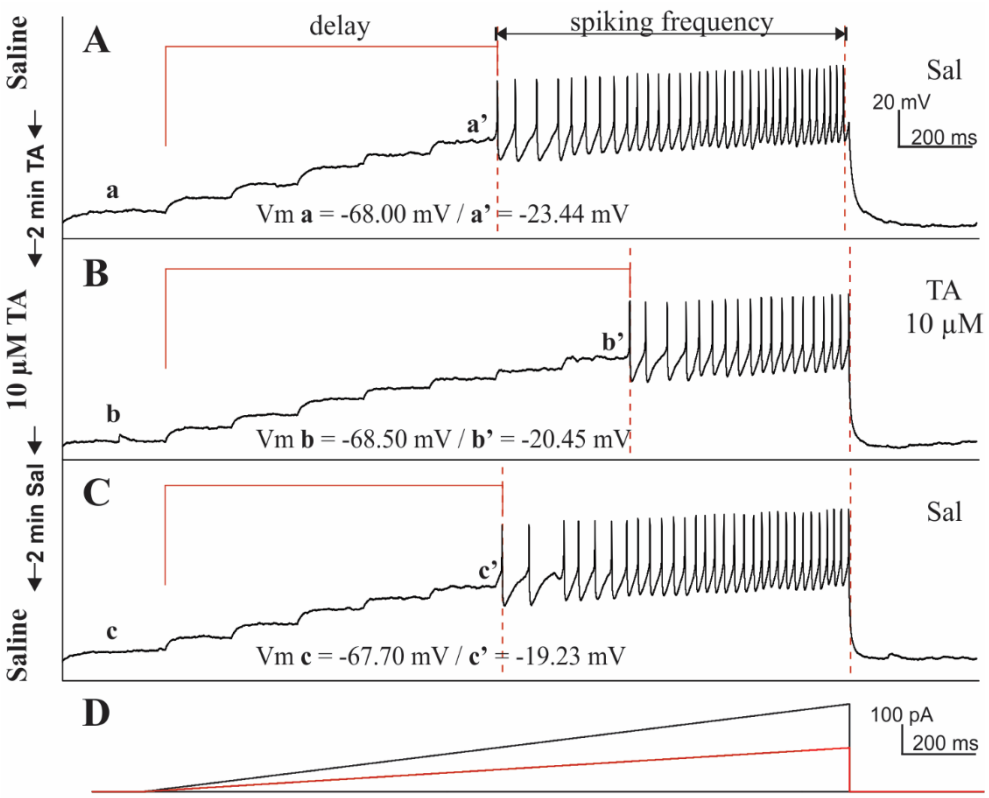

Figure 15: Firing pattern of MNISN-Is upon stimulation with a ramp pulse.
Typical firing pattern of MNISN-Is motoneurons upon a two-second somatic ramp current injection up to 150 pA. **A-C** The red lines indicate where the delay to the first AP was measured. The red dashed lines indicate where the firing frequency was measured. **A** Response to current injection in standard saline. **B** Increased delay to the first AP after two-minute bath-application of 10 µM TA. The delay increased while the firing frequency decreased. **C** Washing TA out with standard saline for 2 min removed the effects of TA on the delay and the firing frequency. **D** Current injection ramps with maxima of 150 and 300 pA. The ramp shown in A-C is marked in red.

For comparison of the normalized data of the delays to the first AP of the ramp pulse protocols, a Friedman-Test was performed to test for significant differences between the three runs, before TA (n. median = 1.00; n = 21), with TA (n. median = 1.20; n = 21), and after the washing-out of TA (n. median = 1.01; n = 21). The Friedman-Test revealed a significant difference between the runs with $p < 0.001$ (n = 21). Pairwise follow-up comparisons of the three runs showed that the 20 % increase of the delay upon application of TA was significant ($p < 0.001$; n = 21). Also, the delay was significantly decreased by 19 % after TA was washed out ($p < 0.001$; n = 21). The first run, before TA, and the third run, after removal of TA, were not significantly different ($p = 1.000$; n = 21) (Figure 16 A). Like in square pulse protocols, the data of the firing frequencies in RPPs were normally distributed in all runs and could be tested by a one-way ANOVA with repeated measures.

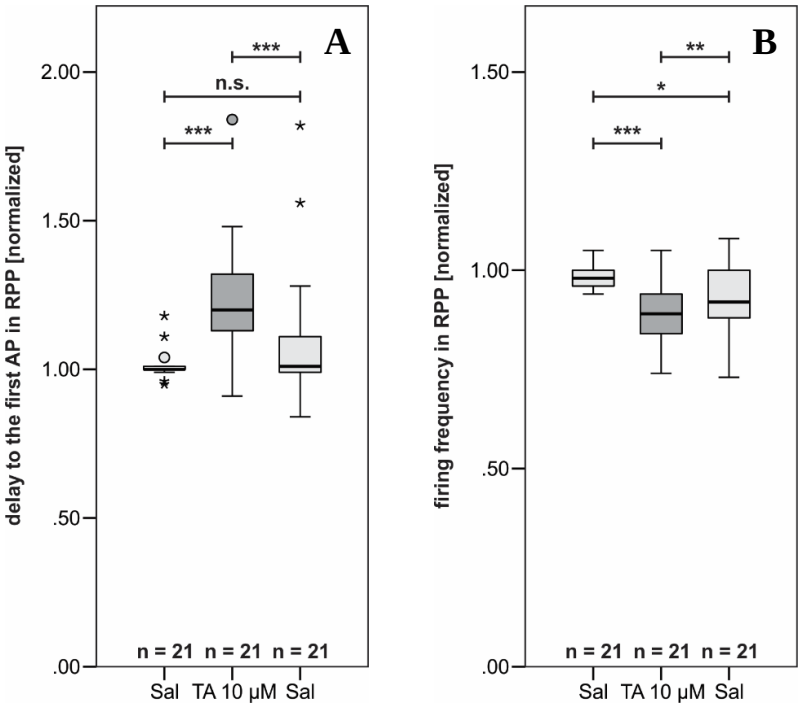

Figure 16: Statistical analysis of the delay to the first AP and the firing frequency in ramp pulse protocols.
A Analysis of the delay to the first AP (F.-T., $p = 0.001$; $n = 21$). Upon application of 10 µM TA, the delay to the first AP was significantly increased (pairwise follow-up comparison, $p < 0.001$; $n = 21$), and significantly reduced after the removal of TA (pairwise follow-up comparison, $p \leq 0.001$; $n = 21$). **B** Analysis of the firing frequency (one-way ANOVA w. r. m., $p = 0.001$; $n = 21$). The firing frequency was significantly reduced after application of 10 µM TA (pairwise follow-up comparison, $p < 0.001$; $n = 21$), and significantly increased after washing with standard saline (pairwise follow-up comparison, $p = 0.002$; $n = 21$). The firing frequency after washing TA out was significantly lower than the frequency at run one (pairwise follow-up comparison, $p = 0.035$; $n = 21$).

The ANOVA indicated significant differences between the three runs, before application of TA (median = 0.98; n = 21), after TA application (median = 0.89; n = 21), and after washing TA out (n. median = 0.92; n = 21) ($p < 0.001$; $n = 21$). The pairwise follow-up analysis showed that the firing frequency was significantly decreased after TA was applied to the bath ($p < 0.001$; $n = 21$), and it was significantly increased after TA was washed out with normal saline ($p = 0.002$; $n = 21$). The effect was, in this case, not entirely reversible. The firing frequency was significantly lower in the third run than in the first run (pairwise follow-up comparison, $p = 0.035$; $n = 21$) (Figure 16 B).

In these recordings in control cells, bath-application of tyramine was found to reduce intrinsic MN excitability significantly. In square pulse protocols, application of TA in a concentration of 10 µM led to a decreased depolarization upon somatic current injection and a therefore increased delay to the first AP. Also, the firing frequency was markedly reduced after TA was added. The same thing could be found in ramp pulse protocols, where bath-application of TA decreased the depolarization rate, which caused an increase of the delay to the first AP and a reduction of the firing frequency. Therefore, it could be assumed that tyramine has neuromodulatory effects on MNISN-Is.

3.4 The Modulation of MNISN-Is Excitability is Dose-Dependent

Concentrations of 100 µM, 10 µM, and 1 µM TA in standard saline were utilized to test whether different amounts of TA had dose-dependent effects on motoneuron excitability of control MNISN-Is neurons. The presented measurements with 10 µM TA were from the control group, which was already shown (Figure 17 B, B' results section 3.3). As controls for the other concentrations, Canton S (1 µM TA, n = 7; 100 µM, n = 6) as well as *RN2*-GAL4, UAS-*mCD8::GFP*; UAS-*FLP* crossed to w^{1118} (1 µM TA, n = 6) (Line 11) were used.

In square pulse protocols, bath-application of 1µM TA elicited similarly strong effects as an application of 10 µM TA (Figure 17 C, C'). For statistical analysis, all data were normalized to the corresponding first values of the first respective run. A Friedman-Test was carried out to test for differences between the delays to the first AP of the three runs, which were in standard saline (n. median = 1.13; n = 13), in saline containing 1 µM TA (n. median = 3.85; n = 13), and again in standard saline after washing out TA (n. median = 1.23; n = 13). It showed a significant difference between the three runs ($p < 0.001$; n = 13). In a pairwise follow-up comparison, a significant increase in the delay to the first AP upon application of 1 µM TA ($p < 0.001$; n = 13), and a significant decrease of the delay after washing TA out ($p = 0.010$; n = 12) were found. There was no statistically significant difference between the third and the first run (pairwise follow-up comparison, $p = 0.718$; n = 13) (Figure 17 C). The data of the firing frequencies were also not normally distributed, which is why a Friedman-Test was carried out. The test indicated significant differences between the frequencies of the runs with and without 1 µM TA in standard saline ($p < 0.001$; n = 13). The pairwise follow-up comparison revealed a significant decrease in the firing frequency after 1 µM was bath-applied to the preparation for 2 min ($p < 0.001$; n = 13), and conversely a significant increase in firing frequency after TA was washed out with standard saline ($p = 0.043$; n = 13). Again, there was no significant difference between the first and the last run, before and after application of TA, respectively ($p = 0.187$; n = 13) (Figure 17 C').

The normalized delays to the first AP measured in the test series with 100 µM TA were statistically analyzed by a Friedman-Test, which indicated no significant differences between the runs (n. median, before TA = 1.46; with TA = 1.54; after washing TA out = 1.24) ($p = 0.115$; n = 6) (Figure 17 A).

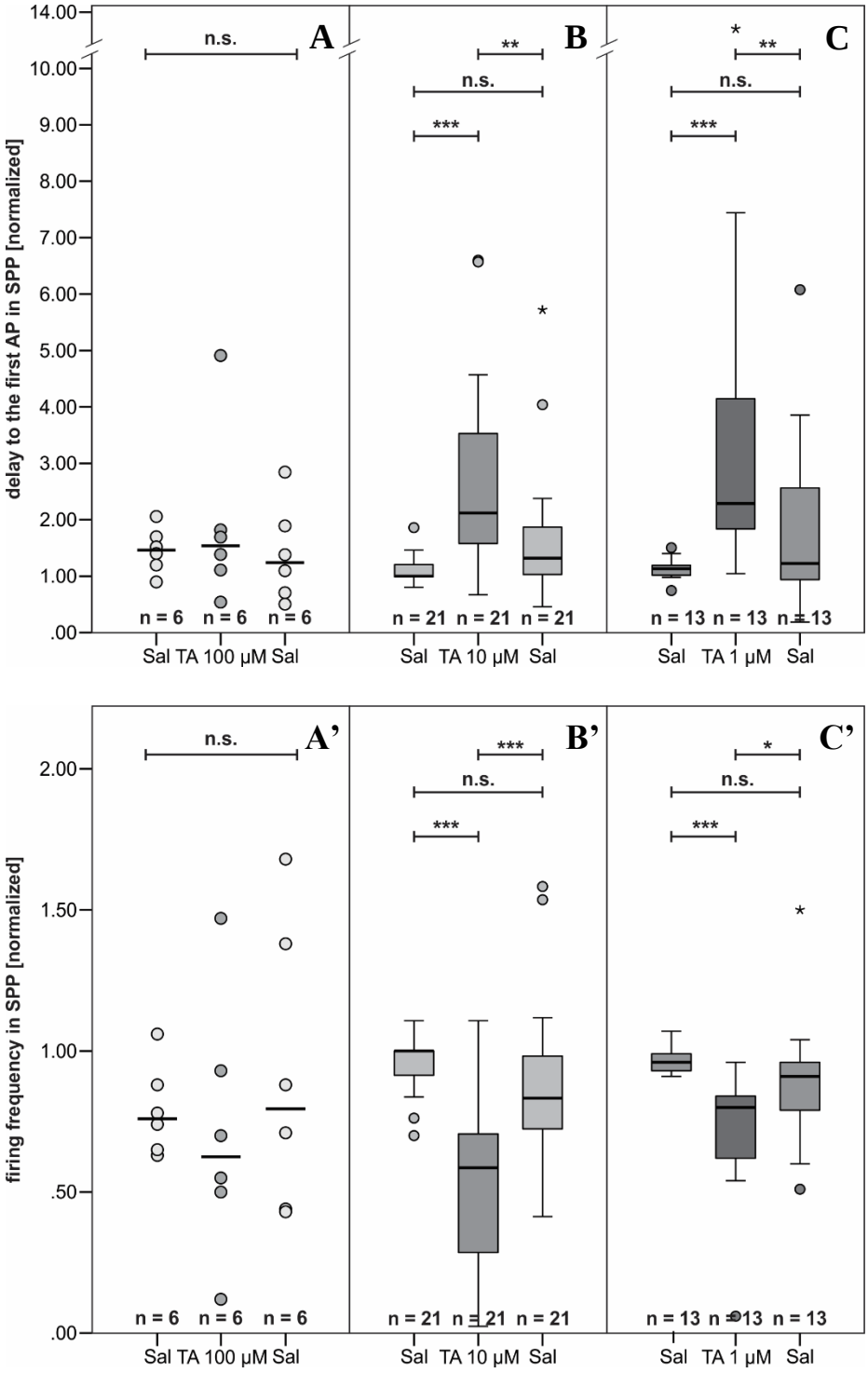

Figure 17: Analysis of TA effectiveness in different concentrations in square pulse protocols.
A-C Analysis of the delay to the first AP in SPPs. **A'-C'** Analysis of the firing frequency in SPPs. **A, A'** Analysis of the effect of 100 µM TA. No significant difference could be found between the runs before TA, with TA, and after washing-out of TA for the delay to the first AP (F.-T., $p = 0.115$; $n = 6$) and for the firing frequency (one-way ANOVA w. r. m., $p = 0.569$; $n = 6$). **B, B'** Analysis of the effect of 10 µM TA. A Friedman-Test showed significant differences between the runs for the delay ($p < 0.001$; $n = 21$). A one-way ANOVA w. r. m. indicated significant differences between the runs for the firing frequency ($p < 0.001$; $n = 21$). Pairwise follow-up analyses showed that the delay was significantly increased ($p < 0.001$; $n = 21$) and the firing frequency was decreased with TA ($p < 0.001$; $n = 21$). After washing TA out, the delay was reduced ($p = 0.002$; $n = 21$), and the firing frequency was increased ($p < 0.001$; $n = 21$). **C, C'** Analysis of 1 µM TA. Friedman-Tests showed significant differences between the runs for both parameters, the delay ($p < 0.001$; $n = 13$), and the firing frequency ($p < 0.001$; $n = 13$). Due to follow-up analyses, the adding of TA increased the delay ($p < 0.001$), and decreased the firing frequency ($p < 0.001$; $n = 13$). Washing TA out decreased the delay ($p = 0.010$; $n = 13$), and increased the firing frequency ($p = 0.043$; $n = 13$).

The same could be found in the analysis of the firing frequencies. A one-way ANOVA with repeated measures showed no significant difference between the runs with (n. median = 0.71; n = 6) and without 100 µM TA (n. median, before TA = 0.79; after washing TA out = 0.80) (p = 0.569; n = 6).

In ramp pulse protocols, similar results could be found. For the experiments with 100 µM TA, one-way ANOVAs with repeated measures were performed to compare the two parameters, delay to the first AP, and the firing frequency of all three runs. In both cases, no differences between the runs were indicated (delay, n. median before TA = 1.03; with TA = 0.93; after washing TA out = 0.95; frequency, n. median before TA = 0.97; with TA = 1.01; after washing TA out = 0.97) (delay p = 0.493; n = 6; frequency p = 0.216; n = 6) (Figure 18 A, A').

For experiments with 10 µM TA, the results have already been presented (results section 3.3).

In the third group, 1 µM TA was tested. Friedman-Tests were performed to compare the normalized delays to the first AP and the firing frequencies of the three runs. For both the delay to the first AP and the firing frequency, significant differences could be found between the runs (delay $p < 0.001$; n = 13; frequency $p < 0.001$; n = 13). Pairwise follow-up comparisons showed that the delay was significantly increased after 1 µM TA was added (n. median before TA = 1.01; with TA = 1.15) (pairwise follow-up comparison, p = 0.001; n = 13), but it was not significantly reduced after TA was washed out (n. median = 1.09) (pairwise follow-up comparison, p = 0.056; n = 13). Nevertheless, a tendency could be seen that the delay was reduced after the washout of TA, since the delay of the third run was not significantly different from the first one, before addition of TA (pairwise follow-up comparison, p = 0.718; n = 13) (Figure 18 C). The firing frequency was significantly reduced after the application of TA (n. median before TA = 0.99; with TA = 0.91) (pairwise follow-up comparison, p = 0.032; n = 13). But it was also not significantly increased after TA was removed (n. median = 1.00) (pairwise follow-up comparison, p = 0.093; n = 13), although a tendency towards an increased frequency upon removal of TA could be seen. The firing frequency measured in the third run, after TA was washed out, was not significantly different from the frequency measured in the first run (pairwise follow-up comparison, p = 1.000; n = 13) (Figure 18 C').

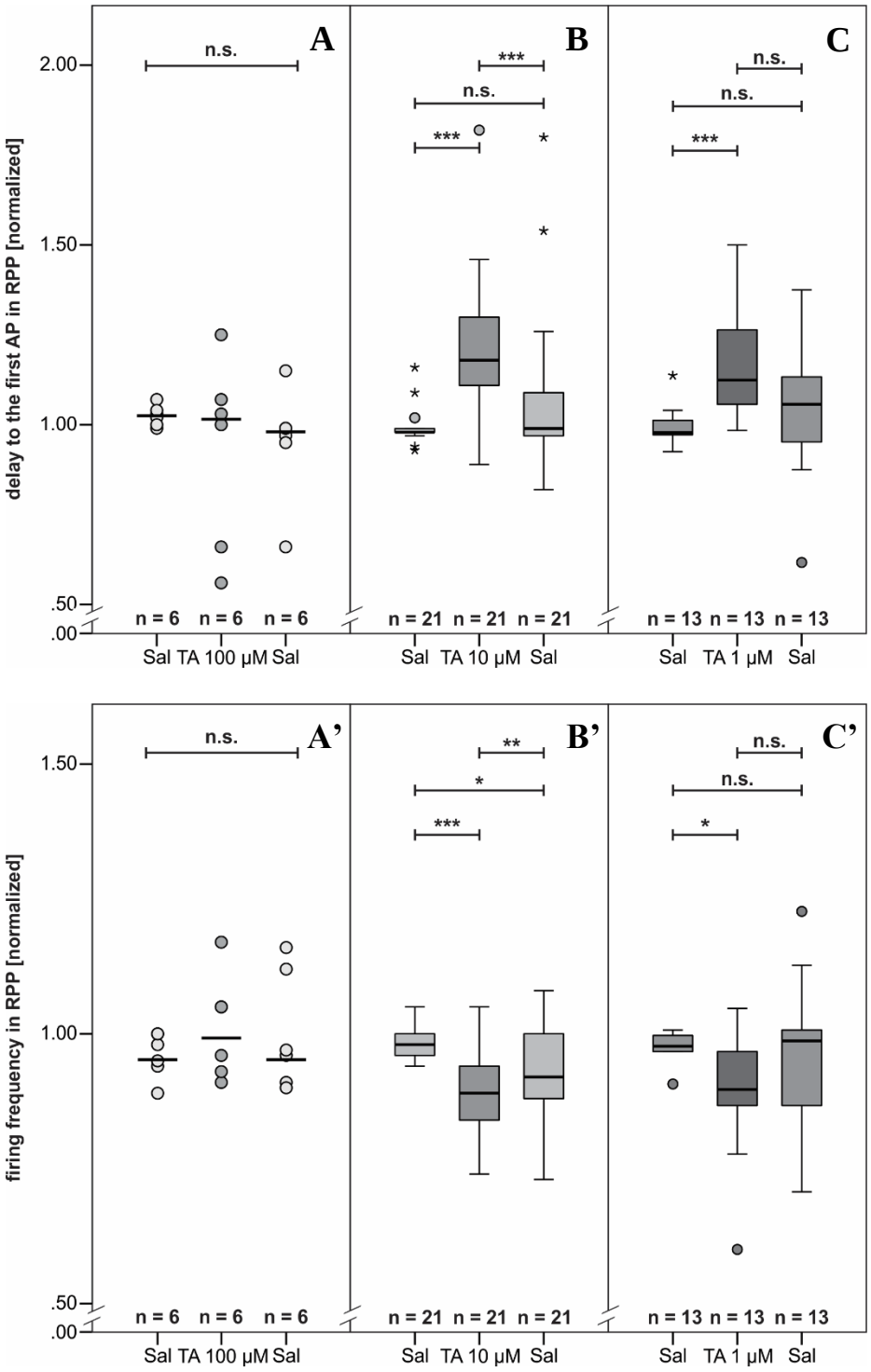

Figure 18: Analysis of TA effectiveness in different concentrations in ramp pulse protocols.
A-**C** Analysis of the delay to the first AP in RPPs. **A'**-**C'** Analysis of the firing frequency in RPPs. **A, A'** Analysis of the effect of 100 µM TA. One-way ANOVAs w. r. m. showed no significant differences between the runs before TA, with TA, and after washing-out of TA for the delay to the first AP ($p = 0.493$; $n = 6$) and for the firing frequency ($p = 0.216$; $n = 6$). **B, B'** Analysis of the effect of 10 µM TA. A Friedman-Test showed significant differences between the runs for the delay ($p < 0.001$; $n = 21$) and a one-way ANOVA w. r. m. indicated significant differences between the runs for the firing frequency ($p < 0.001$; $n = 21$). Follow-up analyses showed that addition of TA significantly increased the delay ($p < 0.001$; $n = 21$) and decreased the firing frequency ($p < 0.001$; $n = 21$). Washing TA out reduced the delay ($p < 0.001$; $n = 21$) and increased the firing frequency ($p = 0.002$; $n = 21$). **C, C'** Analysis of 1 µM TA. Friedman-Tests showed significant differences between the runs for the delay ($p = 0.002$; $n = 13$) and the firing frequency ($p = 0.017$; $n = 13$). Follow-up analyses showed that addition of TA significantly increased the delay ($p = 0.001$; $n = 13$), and reduced the firing frequency ($p = 0.032$; $n = 13$). Washing TA out did not significantly increase the delay ($p = 0.056$; $n = 13$), or reduce the firing frequency ($p = 0.093$; $n = 13$).

Tyramine reduces MNISN-Is intrinsic excitability only at small concentrations. At a concentration of 100 µM, MNISN-Is excitability seemed unaltered. It is likely that MNISN-Is also carries octopamine receptors, since VUM neurons, which were thought to innervate MNISN-Is, also produce and release octopamine (Landgraf et al., 1997; Monastirioti et al., 1995). High concentration of TA might cross-activate these receptors, which could in turn counteract the tyraminergic reduction of intrinsic MNISN-Is excitability.

3.5 Tyramine Modulates MNISN-Is Excitability Directly

MNISN-Is could either be modulated directly by TA if the dendrites of this neuron are equipped with fitting receptors or indirectly through upstream neurons. If indirect modulation was true, a preceding neuron might be modulated by TA and reduce MNISN-Is excitability by, e.g., inhibitory synaptic transmission onto it (Gerschenfeld, 1973). To test that MNISN-Is was not modulated indirectly, the temperature-sensitive dynamin mutant *shibire*[1] was tested. D*rosophila* dynamin is essential for endocytosis, which is why synaptic transmission is fully inhibited in these mutants when they are exposed to non-permissive temperatures (Grigliatti et al., 1973; Kosaka & Ikeda, 1983; Poodry & Edgar, 1979).

The fly strain was reared at 18 °C with a 12 h light-dark cycle to guarantee normal development. For all recordings, the bath temperature was kept at the non-permissive temperature of 30 °C, to only measure in synaptic isolation. Temperature has a huge influence on neuronal firing properties, and 30 °C is above ideal temperatures of *Drosophila*, which is why MNISN-Is firing properties were slightly altered, e.g., AP amplitude was smaller than in control recordings (Figure 19) (Dillon et al., 2009; Janssen, 1992; Montgomery & Macdonald, 1990).

In square pulse protocols, the delay to the first AP could be clearly seen in response to somatic current injections (mean = 94 ms; n = 3). When MNISN-Is neurons were treated with TA at the non-permissive temperature, the delay was on average increased by 223 % (mean = 309 ms; n = 3), which was control-like (Figure 20; results section 3.3).

The firing frequency was control-like in recordings made in standard saline (mean = 31 Hz; n = 3), and was decreased by 48 % (mean = 16 Hz; n = 3) after the application of TA.

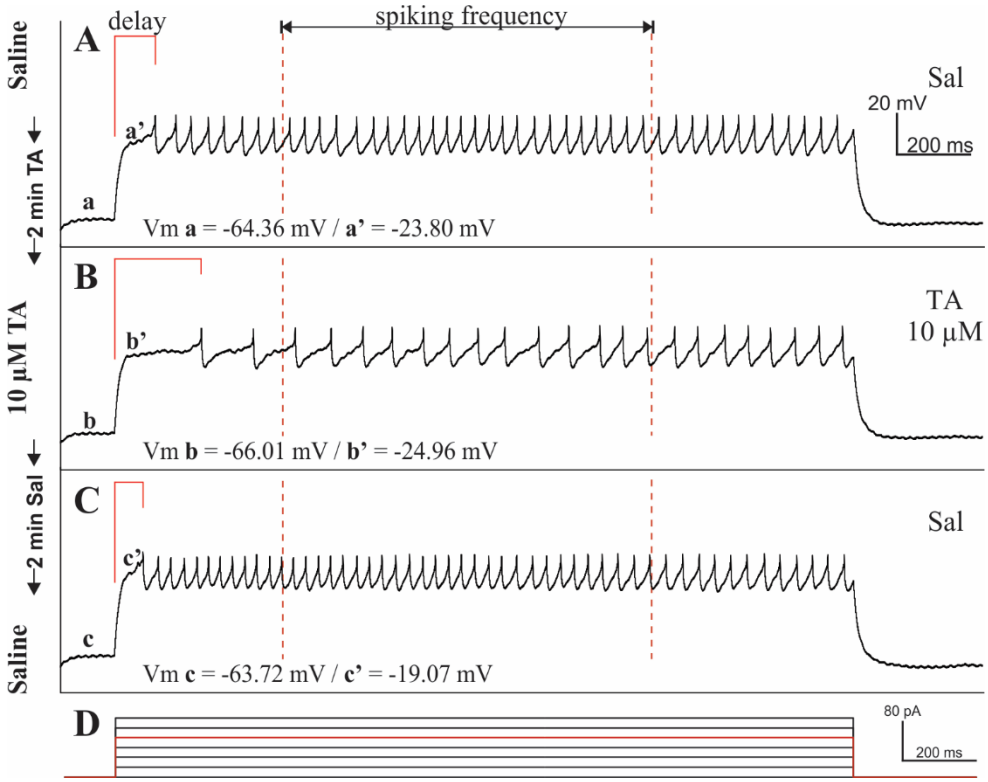

Figure 19: Firing pattern of a temperature sensitive *shibire*[1] MNISN-Is at the non-permissive temperature of 30 °C. A-C In all shown sweeps a current of 80 pA was injected. Besides smaller AP amplitudes, the firing characteristics of MNISN-Is seemed to remain control-like at 30 °C. The delay to the first AP (**A**) was increased, while the firing frequency was reduced after a two-minute application of 10 µM TA (**B**). **C** Just as in controls, the effects were reversed after washing TA out for two minutes. Also, see Figure 20. **D** Current injection steps with 20 pA increments. The sweep shown in A-C is marked in red.

Still at non-permissive temperature, TA was washed out for at least two minutes, which led to a mean decrease in the delay to the first AP of 223 % (mean = 91 ms; n = 3), and to a mean increase in the firing frequency of 43 % (mean = 30 Hz; n = 3) (Figure 20).

In ramp pulse protocols, the delay to the first AP was also control-like when recorded at the non-permissive temperature of 30 °C (mean = 909 ms; n = 3), whereas the firing frequency was slightly higher (mean = 49.60 Hz; n = 3) than control firing frequencies (mean = 34.45 ± 3.75 Hz; n = 21) (results section 3.3). In the second run, two minutes after TA was added to the bath, the delay to the first AP was 23 % longer (mean = 1,117 ms; n = 3), and the firing frequency was on average 12 % slower (mean = 43.69 Hz; n = 3). Both effects were reversible. After TA was washed out for two minutes, the delay to the first AP was reduced by 28 % (mean = 859 ms; n = 3), and the firing frequency was increased by 10 % (mean = 48.41 Hz; n = 3). All effects were comparable to control values (results section 3.3, Figure 21).

MNISN-Is showed a control-like reduction of excitability upon bath-application of 10 µM TA, even with all synaptic transmission being inhibited in *shibire*[1] at the non-permissive temperature. With this result, indirect modulation of MNISN-Is excitability can be ruled out.

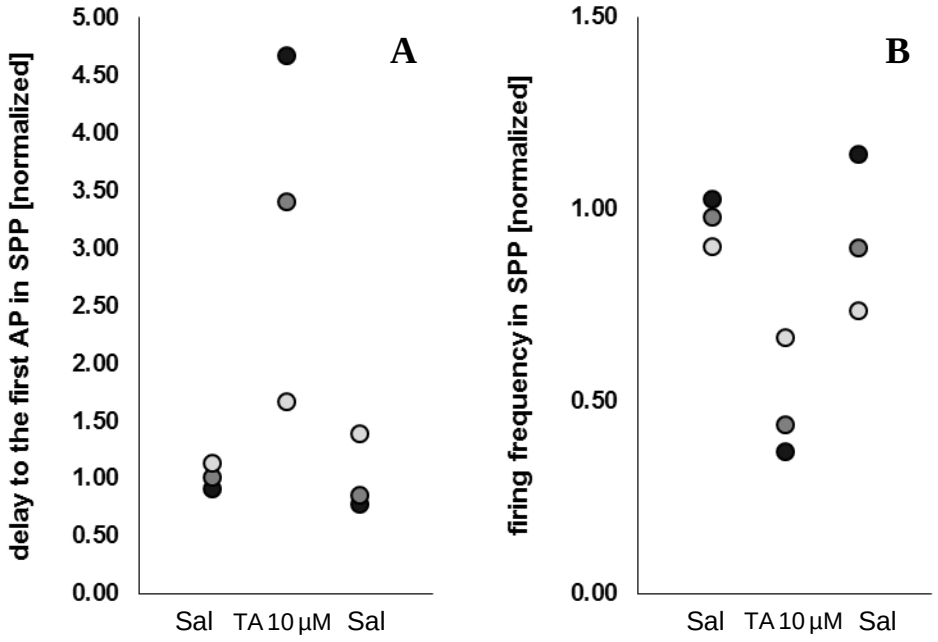

Figure 20: Normalized data points of the delay to the first AP and the firing frequency in square pulse protocols in *shi*[1]. All recordings were carried out at a non-permissive temperature of 30 °C. **A** Normalized data of the delay to the first AP. On average, the delay was increased by 223 % after TA was applied for 2 min. It was decreased by 223 % again after TA was washed out. **B** Normalized data of the firing frequency. Two minutes after TA was applied to the bath, the firing frequency was on average decreased by 48 %. After TA was completely washed out, the firing frequency was 43 % faster. n = 3

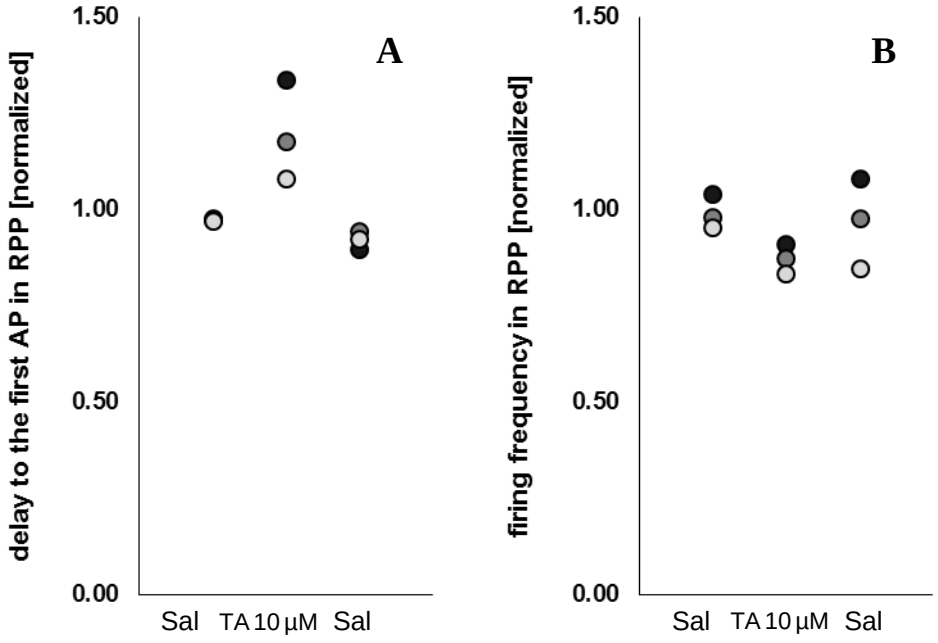

Figure 21: Normalized data points of the delay to the first AP and the firing frequency in ramp pulse protocols in *shi*[1]. All recordings were carried out at a non-permissive temperature of 30 °C. **A** Normalized data of the delay to the first AP. On average, the delay was increased by 23 % after TA could incubate for 2 min. It was decreased by 28 % after TA was washed out. **B** Normalized data of the firing frequency. Two minutes after TA was applied to the bath, the firing frequency was on average decreased by 12 %. After TA was completely washed out, the firing frequency was 10 % faster. n = 3

3.6 Releasing Tyramine Endogenously from Temperature-Sensitive Cells

Since the anatomical prerequisite for a natural TA release onto MN dendrites from tyraminergic cells was given (results section 3.1), a line was created in which tyraminergic cells could be activated by increasing the bath-temperature during recordings. The cross for this line was set up with female virgins from the *Tdc2*-GAL4 strain and male flies carrying the temperature-sensitive ion channel TrpA1 under UAS control, resulting in Line 12 (see also Line 3).

Line 12

$$w^{*}\,;\ \frac{P\{Tdc2-GAL4.C\}2}{UAS-TrpA1}\,;\ \frac{+}{+}\,;\ \frac{+}{+}$$

3.6.1 Temperature Shifts Have an Impact on MNISN-Is Firing Properties

Before the temperature-sensitive line was tested, a pre-test with Canton S (n = 5) and *Tdc2*-GAL4 crossed to w^{1118} (n = 3) was done as a control for effects of temperature shifts on MNISN-Is firing properties. All larvae were dissected in ice-cold saline. The first and last set of recordings were executed at a bath temperature of 20 °C. The second set of recordings was done at 30 °C, which is a suitable temperature to activate TrpA1 (Clapham, 2015; Laursen et al., 2015; Pulver et al., 2009). Heating the bath to 30 °C took about 4 min. Cooling the bath from 30 °C to 20 °C took about 5 min. In square pulse protocols, the delay to the first AP was on average 140 ± 46.16 ms at 20 °C (n = 8), which was not significantly different from the mean delay of control recordings in standard saline at room-temperature (T-Test, p = 0.069; n = 8, 21; results section 3.3) (Figure 28). For statistical analysis, data of all runs in each condition (20 °C, 30 °C, again 20 °C) were normalized to the corresponding first value, which resulted in a normalized median of 1.06 (n = 8) for the delay to the first AP at 20 °C.

The firing frequency was on average 28.07 ± 6.45 Hz in the first run at 20 °C, which was not significantly different from control values measured in standard saline at room-temperature (T-Test, p =0.339; n = 8, 21; results section 3.3). The data of the firing frequency were calculated into a normalized median of 0.96 (n = 8). After the bath temperature was raised to 30 °C, the data of the delay to the first AP, and of the firing frequency spread broader (delay n. median = 1.50; Q1 = 0.98; Q3 = 1.83; frequency n. median = 0.61; Q1 = 0.51; Q3 = 0.94; n = 8) than at 20 °C (delay Q1 = 0.97; Q3 = 1.16; frequency Q1 = 0.90; Q3 = 1.05; n = 8). Also, a tendency towards an increased delay as well as a trend towards a decreased firing frequency were visible (Figure 22). A one-way ANOVA with repeated measures was conducted to statistically compare the delay to the first AP between the three runs. It did not show significant differences between the three runs, at 20 °C, at 30 °C, and again at 20 °C (n. median delay = 0.99; Q1 =

0.63; Q3 = 1.34; n = 8) (p = 0.116; n = 8). To test the firing frequency for significant differences between the runs, a Friedman-Test was conducted, which indicated a significant difference (p = 0.030; n = 8).

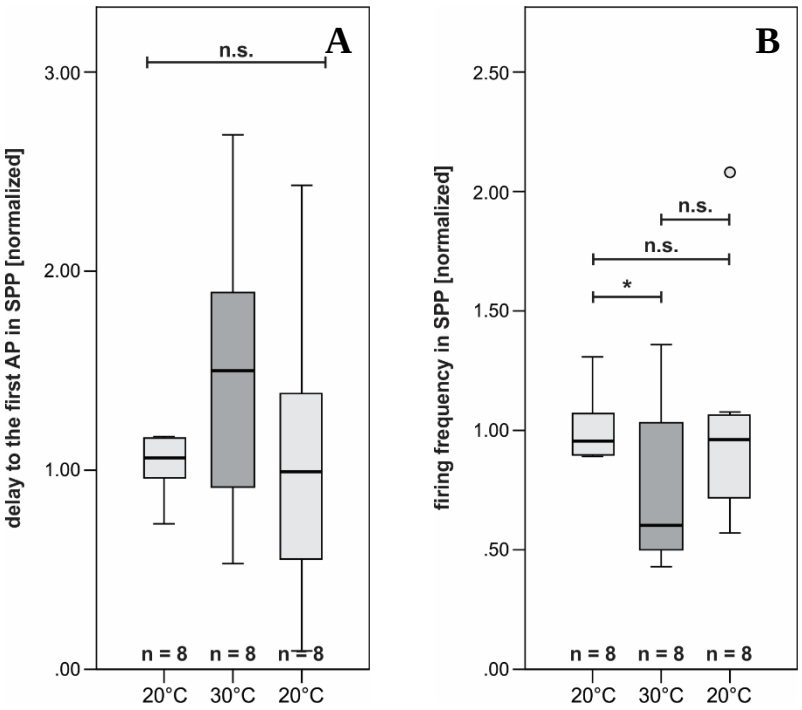

Figure 22: Statistical analysis of changes in the delay to the first AP and the firing frequency upon temperature shifts in square pulse protocols in controls.
A Analysis of the delay to the first AP. The delay was not significantly altered after the bath temperature was raised to 30 °C, or reduced to 20 °C afterward (one-way ANOVA w. r. m., p = 0.501; n = 8). **B** Analysis of the firing frequency (F.-T., p = 0.030; n = 8). The firing frequency was significantly decreased after the bath-temperature was increased to 30 °C (pairwise follow-up comparison, p = 0.037; n = 8), but only slightly and not significantly increased after the temperature was set back to 20 °C (pairwise follow-up comparison, p = 0.137; n = 8).

Due to the pairwise follow-up comparison, the firing frequency was significantly reduced after the temperature was increased to 30 °C (p = 0.037; n = 8), but not significantly increased after the bath was cooled down to 20 °C (n. median = 0.96; Q1 = 0.72; Q3 = 1.06; n = 8) (p = 0.137; n = 8). Also, the first and the third run, at 20 °C each, showed no significantly different firing frequencies (p = 1.000; n = 8).

In the first run of the ramp pulse protocols, the delay to the first AP was on average 810 ± 165 ms, which was not significantly different from the control values measured in standard saline at room-temperature (T-Test, p = 0.611; n = 8, 21; results section 3.3). For analysis, data were normalized to the first value of the first run, which resulted in a normalized median of 1.00 (n = 8) at 20 °C. A one-way ANOVA with repeated measures showed a significant difference between the delays to the first AP of the three runs (p = 0.002; n = 8). As shown by pairwise follow-up comparisons, the delay to the first AP was significantly increased after the bath temperature was raised to 30 °C (n. median = 1.21; p = 0.012; n = 8), and it was significantly

reduced after the temperature was set back to 20 °C again (n. median = 0.98; n = 8) (p = 0.005; n = 8). Therefore, the delay measured in the third run was not significantly different from the delay of the first run (p = 1.000; n = 8), both recorded at a bath temperature of 20 °C (Figure 23 A).

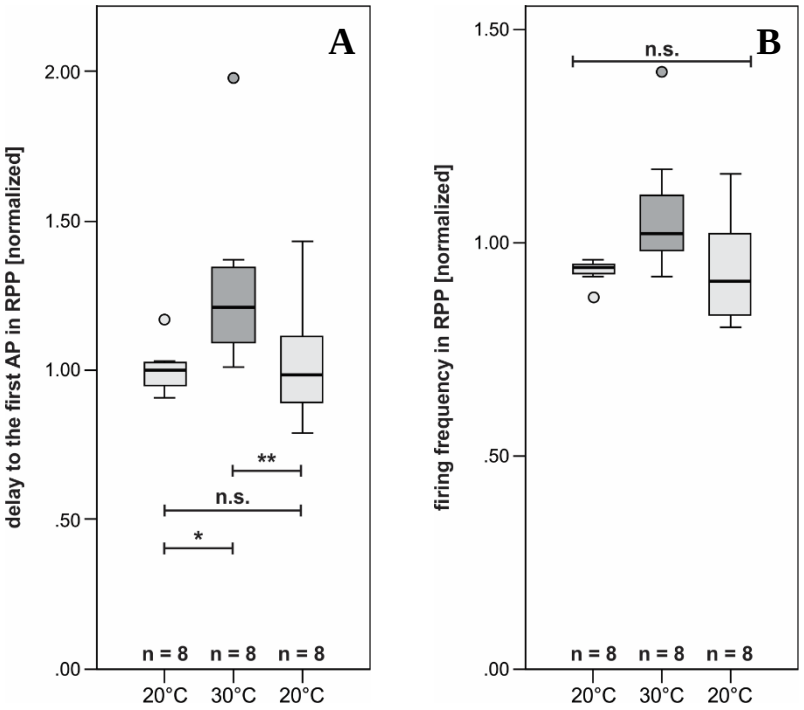

Figure 23: Statistical analysis of changes in the delay to the first AP and the firing frequency upon temperature shifts in ramp pulse protocols in controls.
A Analysis of the delay to the first AP (one-way ANOVA w. r. m., p = 0.002; n = 8). Due to the pairwise follow-up comparisons, the delay was significantly increased after the bath temperature was raised to 30 °C (p = 0.030; n = 8), but not significantly reduced when the bath temperature was reduced to 20 °C afterward (p = 0.124; n = 8). **B** Analysis of the firing frequency. The firing frequency was not significantly altered by any shifts in temperature (one-way ANOVA w. r. m., p = 0.070; n = 8).

The mean firing frequency was 36.37 ± 5.59 Hz in the first run at 20 °C, which was also control-like (T-Test, p = 0.313; n = 8, 21; results section 3.3). It was not significantly altered by raising the temperature to 30 °C (n. median at 20 °C = 0.94; at 30 °C = 1.08; again at 20 °C = 0.97). Although a one-way ANOVA with repeated measured indicated significant differences (p = 0.030; n = 8), this could not be confirmed by pairwise follow-up comparisons between the runs one and two (p = 0.101; n = 8), two and three (p = 0.053; n = 8), and one and three (p = 1.000; n = 8) (Figure 23 B).

Due to the shown data, temperature shifts alone alter the delay to the first AP and the firing frequency of MNISN-Is. Tendencies towards an increased delay to the first AP could be seen in square pulse protocols as well as in ramp pulse protocols upon temperature-shifts to 30 °C. The firing frequency tended to decrease in square pulse protocols whereas it tended to increase in ramp pulse protocols upon increased bath temperature. These alterations should be taken into

account when evaluating the experiments with high-temperature-activated tyraminergic VUM neurons.

3.6.2 Temperature-Sensitive Tyraminergic Neurons Release TA and OA at 30 °C

Following the pre-test with control larvae, Line 12 was tested. The procedure was the same as in pre-tests. Ice-cold saline was used for dissection to prevent the tyraminergic neurons from being activated at room temperature. The first recordings were executed at a bath temperature of 20 °C, then the temperature was raised to 30 °C, and the last recording, again, was done at a bath temperature of 20 °C.

In the first run of the square pulse protocols (20 °C), the delay to the first AP was on average 154 ± 90 ms (n = 9), which was not significantly different from control values measured at room-temperature (T-Test, p = 0.187; n = 9, 21; results section 3.3) (Figure 28). Data were normalized to the first value of the first run at 20 °C for statistical analysis. The normalized delay to the first AP in square pulse protocols was 1.27 (n = 9) at 20 °C. After the bath temperature reached 30 °C in the second run, the delay was increased (n. median = 2.50; n = 9), but the data also spread broader (Q1 = 1.17; Q3 = 3.26) than before at 20 °C (Q1 = 1.05; Q3 = 1.66). However, by comparing the delays of all three runs with a Friedman-Test, no significant differences could be found between the runs (p = 0.459; n = 9; Figure 24 A).

At 20 °C, the firing frequency was on average 32.56 ± 11.95 Hz (n = 9), which was significantly higher than in control recordings in standard saline at room-temperature (mean = 24.14 ± 9.1 Hz; n = 21) (T-Test, p = 0.036; n = 9, 21; results section 3.3). The normalized median was 0.92 (Q1 = 0.75; Q3 = 0.96; n = 9) at 20 °C. The firing frequencies of the three runs were statistically compared by a one-way ANOVA with repeated measures, which showed a significant difference (p = 0.006; n = 9). A pairwise follow-up comparison showed that the reduction of 36 % after the bath temperature reached 30 °C (n. median = 0.56; Q1 = 0.30; Q3 = 0.57; n = 9) was significant (p < 0.001; n = 9). The firing frequency tended to increase after the bath temperature was cooled to 20 °C (n. median = 0.77; Q1 = 0.72; Q3 = 1.16; n = 9), but this increase was not statistically significant (pairwise follow-up comparison, p = 0.112; n = 9). The firing frequency of the third run was not significantly different from the first one, either (pairwise follow-up comparison, p = 1.000; n = 9; Figure 24 B).

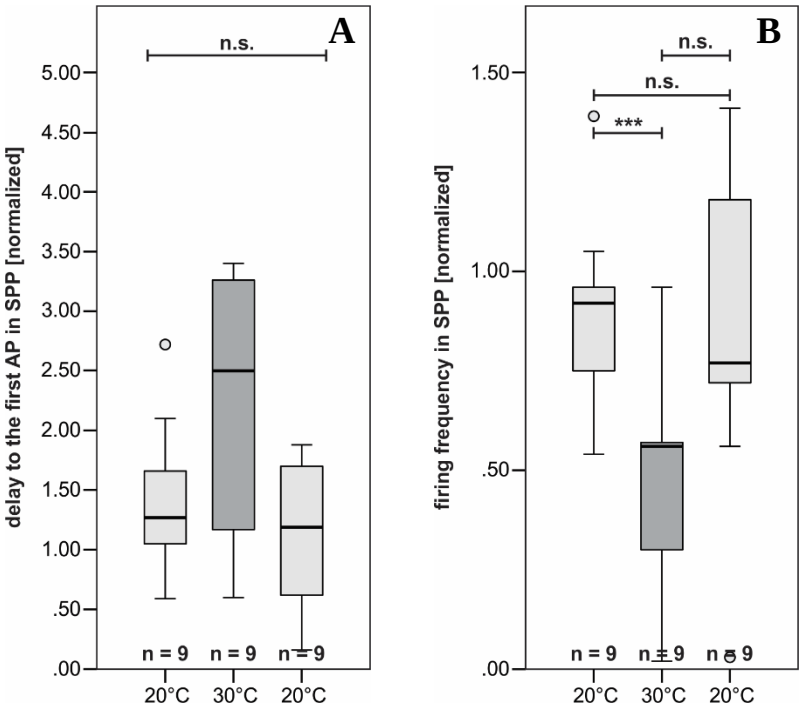

Figure 24: Statistical analysis of changes in the delay to the first AP and the firing frequency upon temperature shifts in square pulse protocols in *Tdc2*-GAL4; UAS-*TrpA1*.
A Analysis of the delay to the first AP. The delay was not significantly altered when the bath temperature was shifted to 30 °C, or back to 20 °C (F.-T., p = 0.459; n = 9). **B** Analysis of the firing frequency (one-way ANOVA w. r. m., p = 0.006; n = 9). The firing frequency was significantly decreased after the bath temperature was raised to 30 °C (pairwise follow-up comparison, p < 0.001; n = 9). It tended to increase after the temperature was switched back to 20 °C, which was not significant (pairwise follow-up comparison, p = 0.112; n = 9).

In ramp pulse protocols, the average delay to the first AP was 855 ± 189 ms (n = 9) at 20 °C, which was like in controls measured at room-temperature (T-Test, p = 0.969; n = 9, 21). The average firing frequency was 41.20 ± 9.18 Hz (n = 9), which was also significantly higher than control values (T-Test, p = 0.001; n = 9, 21; results section 3.3). All data were normalized to the first value of the first run at a bath temperature of 20 °C. The scattering of the data was very broad for the delay to the first AP after the temperature was increased to 30 °C (at 20 °C n. median = 1.000; Q1 = 0.93; Q3 = 1.09; at 30 °C n. median = 1.51; Q1 = 1.05; Q3 = 1.64; at 20 °C again, n. median = 0.94; Q1 = 0.77; Q3 = 0.98). A Friedman-Test, which was carried out to compare the delays of the three runs, revealed significant differences (p = 0.008; n = 9). Further analysis by pairwise follow-up comparisons showed that the increase of the delay following the increase of the bath temperature was not significant (p = 0.716; n = 9), whereas the delay significantly decreased after the temperature was reduced to 20 °C (p = 0.007; n = 9). There was no significant difference between the first and the third run, which both were recorded at 20 °C (pairwise follow-up comparison, p = 0.178; n = 9) (Figure 25 A).

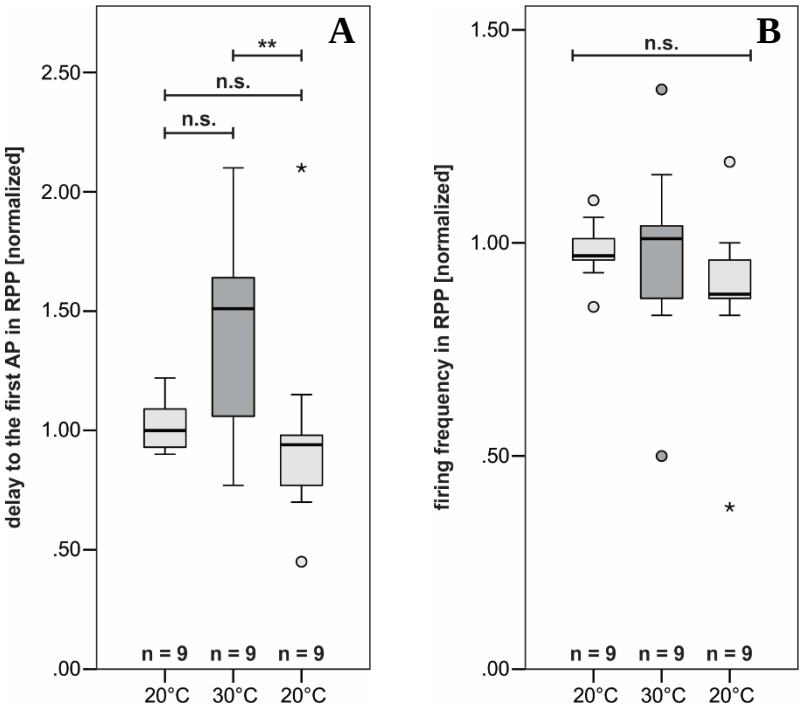

Figure 25: Statistical analysis of changes in the delay to the first AP and the firing frequency upon temperature shifts in ramp pulse protocols in *Tdc2*-GAL4; UAS-*TrpA1*.
A Analysis of the delay to the first AP (F.-T., p = 0.008; n = 9). Pairwise follow-up comparison showed that the delay to the first AP was not significantly increased after the bath temperature was raised to 30 °C (p = 0.716; n = 9), but it significantly decreased after the temperature was reduced to 20 °C afterward (p = 0.007; n = 9). The delay of the third run was not significantly different from the first run (pairwise follow-up comparison, p = 0.178; n = 9). **B** Analysis of the firing frequency. The firing frequency was not significantly altered as the temperature was changed (F.-T., p = 0.147; n = 9).

The firing frequency, which was statistically analyzed by a Friedman-Test, was not significantly altered by shifting the bath temperature to 30 °C, and back to 20 °C afterward (n. median at 20 °C = 0.97; at 30 °C = 1.01; at 20 °C = 0.88) (Friedman-Test, p = 0.147; n = 9) (Figure 25 B). The extensive data spread of the delay to the first AP could simply be caused by the effects of raising the bath-temperature to 30 °C, just as shown in controls (results section 3.6.1). Another reason might be a simultaneous release of TA and OA. Tyraminergic VUM neurons can produce both biogenic amines tyramine and octopamine which might be released unspecifically when the neuron is activated (Lange, 2009). The firing frequency could also be affected by either the mere increase in temperature, or a simultaneous modulation by TA and OA.

3.6.3 Preventing Octopamine from Being Released in a TßH Mutant

As shown, VUM neurons might release both OA and TA if the neuron is activated. In a second attempt, a line with *Tdc2*-GAL4 and UAS-*TrpA1* was crossed, which also carried $TßH^{nM18}$, a mutation of the enzyme TßH, on the first chromosome (Line 13, see also Line 4). Progeny from this cross could not produce any OA, and therefore VUM neurons could only release TA if activated by temperature increase.

Line 13

$$\frac{\text{TßH}^{\text{nM18}}}{\text{w}^{*}} ; \frac{\text{P\{Tdc2} - \text{GAL4.C\}2}}{\text{UAS} - \text{TrpA1}} ; \frac{+}{+} ; \frac{+}{+}$$

Only male L3 larvae were picked for this experiment. The experimental procedure was executed as described above.

In square pulse protocols, the delay to the first AP was on average 181 ± 88 ms (n = 6), and the mean firing frequency was 28.92 ± 6.59 Hz (n = 6) at 20 °C (Figure 28). Both the delay and the firing frequency were not significantly different from the values of control measurements in standard saline at room-temperature (T-Test, delay p = 0.623; frequency p = 0.260; n = 6, 21; results section 3.3). For analysis, all data were normalized to the first value of the first run at 20 °C. A Friedman-Test was used for the statistical comparison of the delays to the first APs of the three runs (Figure 26 A).

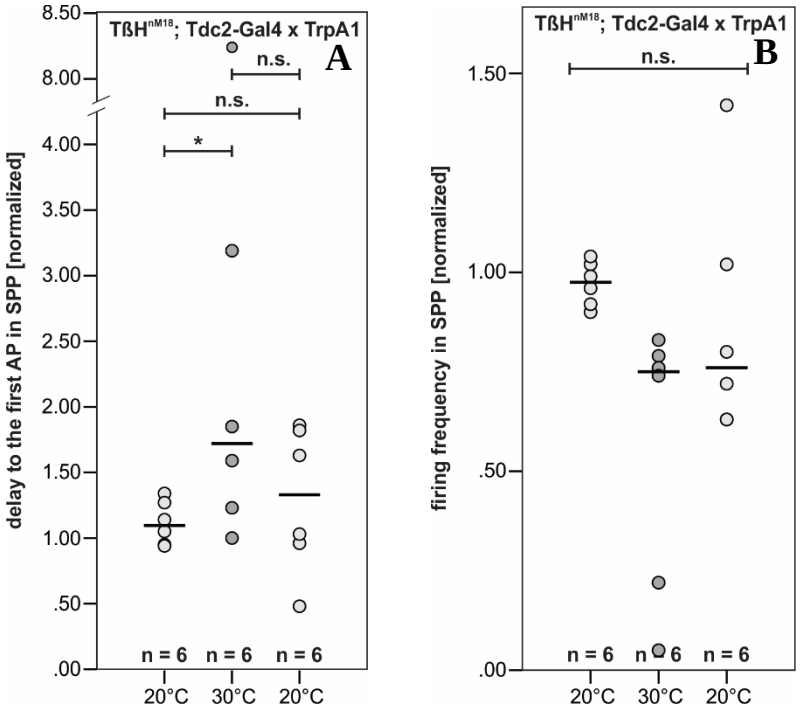

Figure 26: Statistical analysis of changes in the delay to the first AP and the firing frequency upon temperature shifts in square pulse protocols in *TßH*$^{\text{nM18}}$; *Tdc2*-GAL4; UAS-*TrpA1*.

A Analysis of the delay to the first AP (F.-T., p = 0.030; n = 6). Due to pairwise follow-up comparisons, the delay was significantly increased after the bath temperature reached 30 °C (p = 0.028; n = 6). It did not significantly decrease after the temperature was set back to 20 °C (p = 0.250; n = 6). No significant difference was found between the first and the third run (p = 1.000; n = 6). **B** Analysis of the firing frequency. The firing frequency was not significantly altered by changes in temperature (F.-T., p = 0.065; n = 6).

It showed a significant difference with p = 0.030 (n = 6). In the first run, at 20 °C, the normalized median of the delay was 1.10 (Q1 = 0.98; Q3 = 1.24; n = 6). After the temperature of the bath was raised to 30 °C, the delay was significantly increased in the second run (n. median = 1.72)

(pairwise follow-up analysis, p = 0.028; n = 6), and showed a broad spreading tending to higher values (Q1 = 1.32; Q3 = 2.86). With decreasing temperature, the delay tended to also be decreased in the third run (n. median = 1.33; Q1 = 0.98; Q3 = 1.77; n = 6). However, there were neither significant differences between the second and the third run, with bath temperatures of 30 °C and 20 °C, respectively (pairwise follow-up comparison, p = 0.250; n = 6), nor between the first and the third run, both recorded at 20 °C (pairwise follow-up comparison, p = 1.000; n = 6) (Figure 26 A).

The firing frequency, however, was not significantly altered upon changes in bath temperature (Friedman-Test, p = 0.065; n = 6). Still, tendencies could be found, indicating an alteration of the firing frequency upon raising the bath temperature to 30 °C, and upon decreasing it back to 20 °C (run one, n. median = 0.97; Q1 = 0.93; Q3 = 1.01; run two, n. median = 0.75; Q1 = 0.35; Q3 = 0.78; run three, n. median = 0.76; Q1 = 0.65; Q3 = 0.97) (Figure 26 B).

In ramp pulse protocols, the average delay to the first AP was 739 ± 260 ms (n = 6), and the firing frequency was 36.34 ± 6.21 Hz (n = 6). Again, both values were as in control recordings in standard saline at room-temperature (T-Test, delay p = 0.273; frequency p = 0.381; n = 6, 21; results section 3.3). All statistical analyses were conducted with the normalized data. The utilized one-way ANOVA with repeated measures revealed significant differences between the delays of the three runs, first at 20 °C (n. median = 1.01, Q1 = 1.00; Q3 = 1.02), second at 30 °C (n. median = 1.46, Q1 = 1.23; Q3 = 1.75), and third also at 20 °C (n. median = 1.00, Q1 = 0.85; Q3 = 1.10) (p = 0.001; n = 6). As already indicated by the medians, a pairwise follow-up comparison showed that the delay increased significantly after the temperature was raised to 30 °C (p = 0.048; n = 6), and decreased significantly after the bath was cooled down to 20 °C again (p = 0.006; n = 6) (Figure 27 A).

The normalized medians of the firing frequencies of the three runs were 0.96 at 20 °C (Q1 = 0.95; Q3 = 0.97), 0.98 at 30 °C (Q1 = 0.98; Q3 = 1.03), and 0.83 at 20 °C (Q1 = 0.70; Q3 = 0.95). The frequency was not significantly altered by changing the temperature (one-way ANOVA w. r. m., p = 0.426; n = 6) (Figure 27 B).

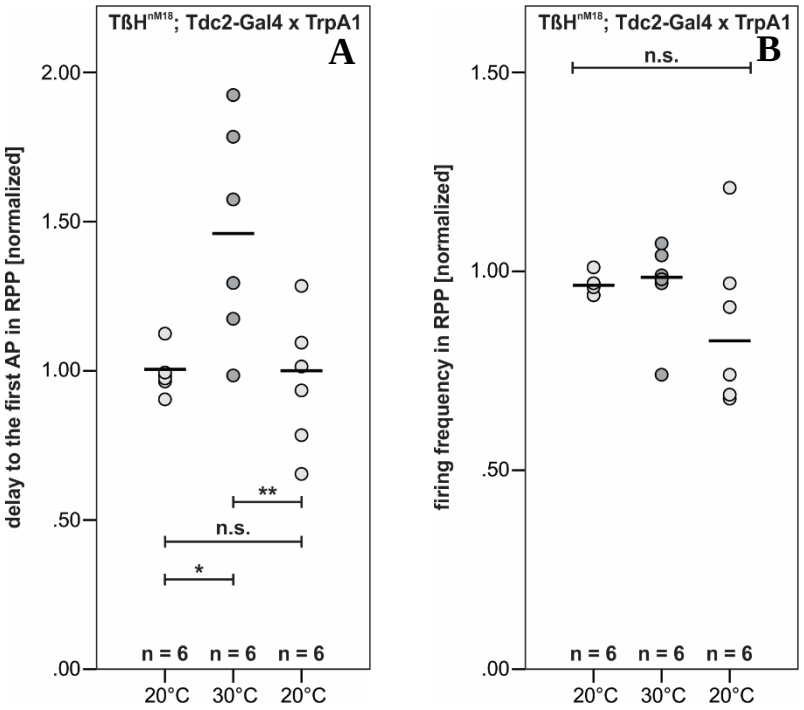

Figure 27: Statistical analysis of changes in the delay to the first AP and the firing frequency upon temperature shifts in ramp pulse protocols in *TßH*^{nM18}; *Td2*-GAL4; UAS-*TrpA1*.
A Analysis of the delay to the first AP (p = 0.001; n = 6). The delay was significantly increased after the bath temperature reached 30 °C (pairwise follow-up comparison, p = 0.048; n = 6). It did also significantly decrease after the temperature was adjusted to 20 °C (pairwise follow-up comparison, p = 0.006; n = 6). **B** Analysis of the firing frequency. The firing frequency was not significantly altered by changes in temperature (one-way ANOVA w. r. m., p = 0.426; n = 6).

The effects on the delay to the first AP upon raising the bath-temperature to 30 °C were more distinct in TßH mutants than in animals with functioning TßH. The data spreading was still extensive, and no clear significant differences could be seen in the firing frequencies (Figure 28). Since OA was not released, the temperature-shifts alone might counteract the tyraminergic effect on the firing frequency in ramp pulse protocols, and induce data spreading. Also, the concentration of the heat-induced released TA was not known, and dose-dependent modulation has already been shown (results section 3.4). Nevertheless, a release of TA from endogenous release sites by targeted activation of VUM neurons could be shown, since the effects were apparently stronger in animals expressing UAS-*TrpA1* than in the controls tested in the temperature pre-tests.

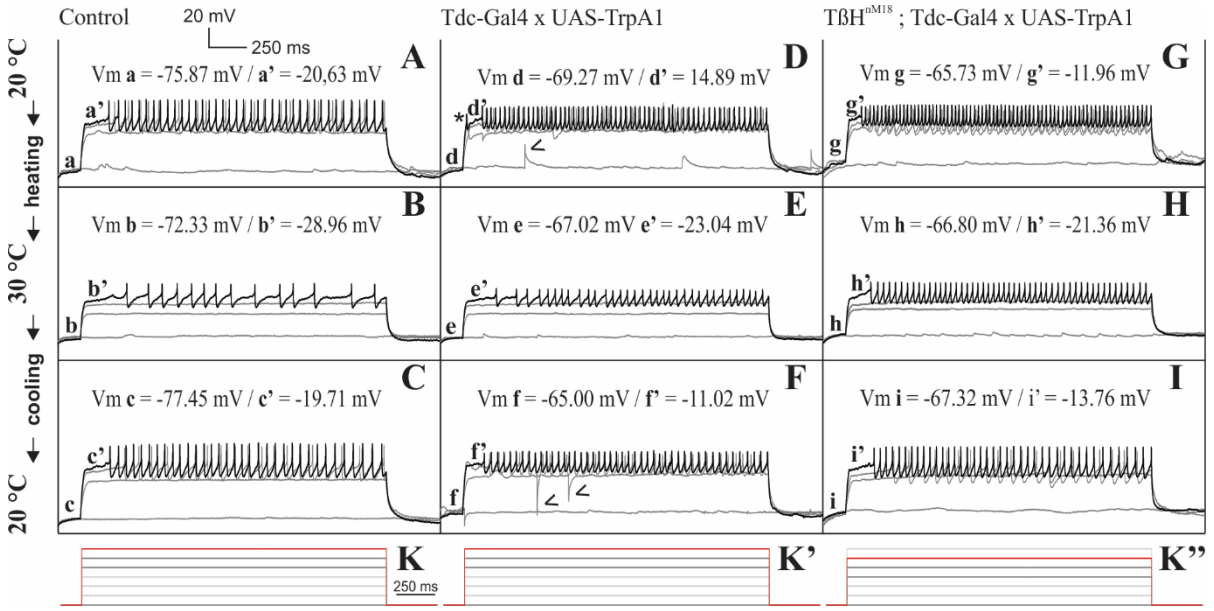

Figure 28: Firing patterns of MNISN-Is with different genetic backgrounds in changing bath-temperatures.
A-C Firing pattern of MNISN-Is from *Tdc2*-GAL4 x w^{1118}. The delay to the first AP was increased, and the firing frequency was reduced by increasing the bath-temperature. The effects were inverted by reducing the temperature. **D-F** Firing pattern of MNISN-Is from *Tdc2*-GAL4 x UAS-*TrpA1*. The delay was increased while the firing frequency decreased upon increased bath-temperature. Both effects were inverted by reducing the temperature. Spontaneous cell activity led to spikes (D, *), and noise of the perfusion led to sharp peaks which are no cell response (F, <). **G-H** Firing pattern of MNISN-Is from *TßH*^{nM18}; *Tdc2*-GAL4 x UAS-*TrpA1*. Intrinsic excitability was reduced after the bath-temperature was increased, and increased after the bath-temperature was reduced, which can be especially seen in the firing of APs in only one sweep at 30 °C. **K-K''** Current injection steps with 20 pA increments. Sweeps shown in A-C, D-F, and G-I are marked in dark grey and red.

3.7 The α_2-Receptor Antagonist Yohimbine Fully Inhibits Tyraminergic Modulation

The reduction of MNISN-Is excitability had to be mediated by specific receptors, i.e., tyramine receptors, which are homolog to mammalian α_2-adrenergic 5-HT receptors (Arakawa et al., 1990; Bayliss et al., 2013; Saudou et al., 1990). The α_2-receptor antagonist yohimbine (YH) was applied together with TA in the next experiment to test whether these receptors truly mediated the modulatory effects. For this series of current-clamp recordings, TA was used in a concentration of 10 µM in standard saline. For YH, concentrations of 10 µM (n = 4), 1 µM (n = 4), and 100 nM (n = 3) were added to standard saline together with TA. The data for these concentrations were pooled for all parameters since no significant differences between the groups could be found in standard saline (Kruskal-Wallis ANOVA, SPP, delay p = 0.160; frequency p = 0.213; RPP, delay p = 0.076; frequency p = 0.385; n = 4, 4, 3). Canton S larvae were used for all experiments. As described above, the first run of recordings was executed in standard saline, the second run was done in saline containing 10 µM TA and YH, and the third run was recorded in standard saline.

The two parameters delay to the first action potential and firing frequency were analyzed in

square and ramp pulse protocols. In square pulse protocols, the mean delays to the first AP were 209 ± 62.90 ms in standard saline, 195 ± 81.15 ms in standard saline with 10 µM TA and YH, and 207 ± 50.62 ms in standard saline after washing TA out.

For analysis, all data were normalized to the first value of the first run for each parameter. A Friedman-Test was carried out to test the data of the delay to the first AP for statistically significant differences between the three runs (n. median before TA & YH = 1.26; with TA & YH = 1.23, after washout = 1.33; n = 11), which showed no significant difference (p = 0.486; n = 11). As shown in the plots, the variance increased with the application of TA and YH, but the median of the delay was not significantly altered in the runs (Figure 29 A).

The average firing frequencies were 22.45 ± 6.23 Hz in standard saline, 24.82 ± 6.31 Hz in TA and YH, and 21.86 ± 2.89 Hz in standard saline after washing TA out. For comparison of the normalized firing frequencies, a one-way ANOVA with repeated measures was chosen.

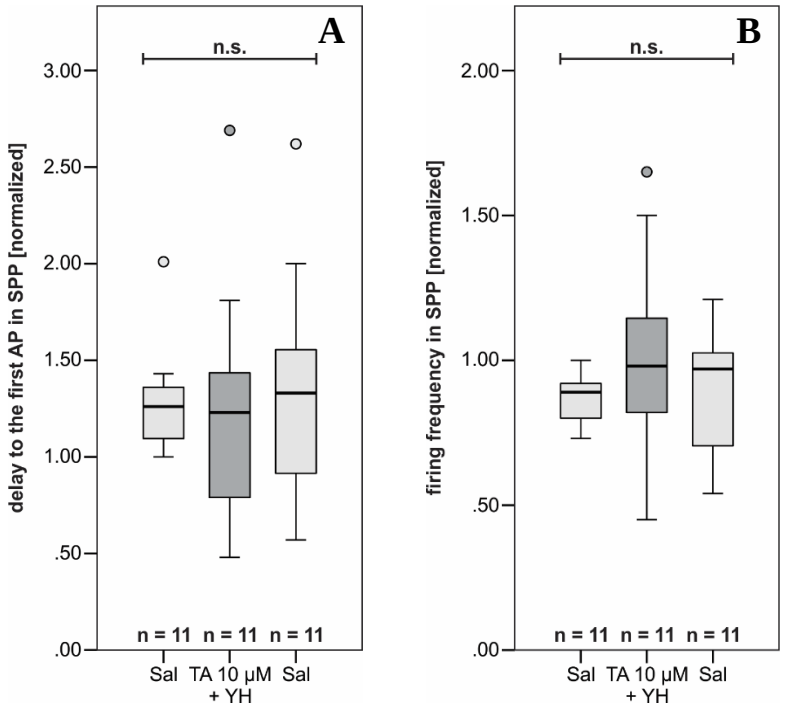

Figure 29: Statistical analysis of changes in the delay to the first AP and the firing frequency upon application of TA and YH in square pulse protocols.

A Analysis of the delay to the first AP. The delay to the first AP was not significantly altered after 10 µM TA and YH were applied, or after TA was washed out (F.-T., p = 0.486; n = 11). **B** Analysis of the firing frequency. The firing frequency was not significantly altered after 10 µM TA and YH were applied, and after TA was washed out (one-way ANOVA w. r. m., p = 0.229; n = 11).

The test did not show any significant differences between the three runs (n. median before TA and YH = 0.89, with TA and YH = 0.98; after washing TA out = 1.00) (p = 0.229; n = 11). The data of the frequency spread more after TA and YH were applied, and the median was slightly but not significantly increased after the application. This finding was contrary to the effects

mediated by TA alone on control MNISN-Is motoneurons (results section 3.3) (Figure 29 B). In ramp pulse protocols, the average delay to the first AP was 1,094 ± 156 ms in standard saline, 980 ± 182 ms after bath-application of 10 µM TA and YH, and 1,055 ± 173 ms after washing TA out in standard saline. The normalized data of the delay to the first AP were analyzed with a one-way ANOVA with repeated measures. In this case, a significant difference between the runs, before application of TA and YH (n. median = 1.03; n = 11), after TA and YH were added (n. median = 0.93; n = 11), and after TA was washed out (n. median = 1.01; n = 11), was indicated (p = 0.001; n = 11) (Figure 30 A). Contrary to the control experiments (results section 3.3), the delay to the first AP was significantly decreased by 10 % after TA and YH were added (pairwise follow-up comparison, p = 0.006; n = 11).

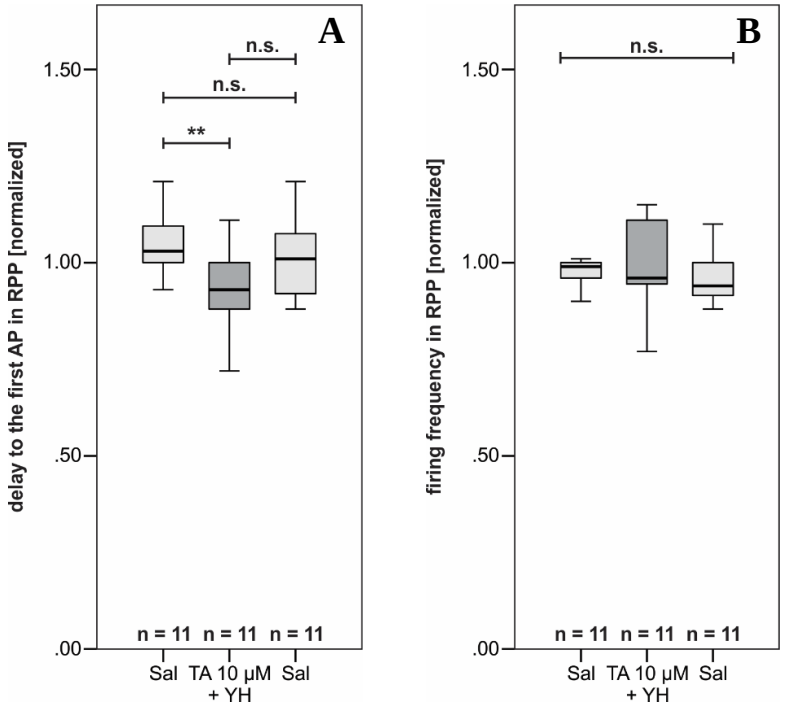

Figure 30: Statistical analysis of changes in the delay to the first AP and the firing frequency upon application of TA and YH in ramp pulse protocols.
A Analysis of the delay to the first AP (one-way ANOVA w. r. m., p = 0.001; n = 11). The delay to the first AP was significantly reduced after 10 µM TA and YH were applied (pairwise follow-up comparison, p = 0.006; n = 11), but not significantly increased after TA was washed out (pairwise follow-up comparison, p = 0.057; n = 11). **B** Analysis of the firing frequency. The firing frequency was not significantly altered after 10 µM TA and YH were applied, and after TA was washed out (F.-T., p = 0.148; n = 11).

However, the delay was neither significantly increased after TA was washed out (p = 0.057; n = 11), although a tendency was visible, nor was the delay of the third run significantly lower than the one of the first run (p = 0.451; n = 11).

The mean firing frequencies were 33.29 ± 3.56 Hz in standard saline, 33.84 ± 3.36 Hz after TA and YH were applied, and 32.55 ± 2.93 Hz after washing TA out with standard saline. The

firing frequency was not significantly altered in any run (n. median before TA & YH = 0.99; with TA and YH = 0.96, after washout = 0.94; n = 11) (Friedman-Test, p = 0.148; n = 11) (Figure 30 B).

Blocking tyramine receptors with yohimbine was sufficient to inhibit all modulatory effects of TA. The delay to the first AP and the firing frequency were not control-like altered after the application of TA. Instead, the delay to the first AP was reduced in ramp pulse protocols, which might indicate a necessity of TA for normal firing properties. However, reversibility of yohimbine or effects of yohimbine alone were not tested.

3.8 Testing Knockdowns of Target Receptors

UAS-RNAi constructs for all three known TA receptors were utilized in further patch-clamp experiments to determine the receptor that was responsible for mediating all above-mentioned tyraminergic effects on MNISN-Is motoneurons. In larvae derived from crosses with an RN2 driver-line and various tyramine receptor RNAi lines (Table 1), mosaic patterns of only a few GFP-labeled motoneurons were created. All neurons expressing GFP also expressed the desired RNAi constructs of tyramine receptors, which is why only MNISN-Is neurons with a clear GFP-expression were used for patch-clamp experiments. Tyramine always affected the delay to the first action potential and the firing frequency in both square pulse protocols and ramp pulse protocols. Since ramp pulse protocols mimic more naturally gradually increasing synaptic input into the MN from the central pattern generator (CPG) (Kadas et al., 2015), only ramp pulse protocols were conducted and analyzed for the screening of possible target receptors.

3.8.1 Knockdowns of TyrR (CG 7431) Show Different Effects on Tyraminergic Modulation

The Tyramine Receptor (TyrR, CG 7431) (Bayliss et al., 2013; Cazzamali et al., 2005) was tested with two different RNAi lines, one was obtained from the Bloomington *Drosophila* Stock Center, and the other one was obtained from the Vienna *Drosophila* Resource Center (Line 5 and Line 6, methods section 2.6).

MNISN-Is motoneurons carrying the *TyrR*-RNAi construct obtained from Bloomington were tested first. The delay to the first AP was 787 ± 115 ms (n = 18), and the firing frequency was 38.62 ± 4.47 Hz in standard saline. The delay was not significantly different from control data (T-Test, p = 0.253; n = 18, 21). The firing frequency was significantly higher in the RNAi than

in controls (T-Test, p = 0.004; n = 18, 21) (results section 3.3).

Data were normalized to the first value of the first run for both parameters. Friedman-Tests were carried out to test for statistically significant differences between the delays to the first AP, and between the firing frequencies of all runs. Both tests indicated significant differences between the three runs, before TA was applied (n. median, delay = 1.03; frequency = 0.98; n = 18), two minutes after TA was applied (n. median, delay = 1.26; frequency = 0.88; n = 18), and two minutes after TA was washed out (n. median, delay = 1.08; frequency = 0.96; n = 18) (delay p = 0.009; frequency p = 0.016; n = 18). Pairwise follow-up comparisons showed that the delay to the first AP was significantly increased upon application of TA (p = 0.008; n = 18). It was not significantly decreased after TA was washed out afterward (pairwise follow-up comparison, p = 0.137; n = 18), although a tendency indicated otherwise. The last run was not significantly different from the first run (pairwise follow-up comparison, p = 0.952; n = 18). The data scattering increased over time, as indicated by the first and third quartiles from each data set (run one Q1 = 1.08; Q3 = 1.05; run two Q1 = 1.13; Q3 = 1.45; run three Q1 = 0.97; Q3 = 1.60; n = 18) (Figure 31 A).

Accordingly, the firing frequency was significantly reduced upon addition of TA (pairwise follow-up comparison p = 0.014; n = 18), but also not significantly increased after TA was washed out (pairwise follow-up comparison, p = 0.470; n = 18). The firing frequency of the third run was not significantly different from the one of the first run (pairwise follow-up comparison, p = 0.470; n = 18). Again, the data scattering increased over time (run one Q1 = 0.96; Q3 = 1.00; run two Q1 = 0.79; Q3 = 0.92; run three Q1 = 0.73; Q3 = 1.03; n = 18) (Figure 31 A').

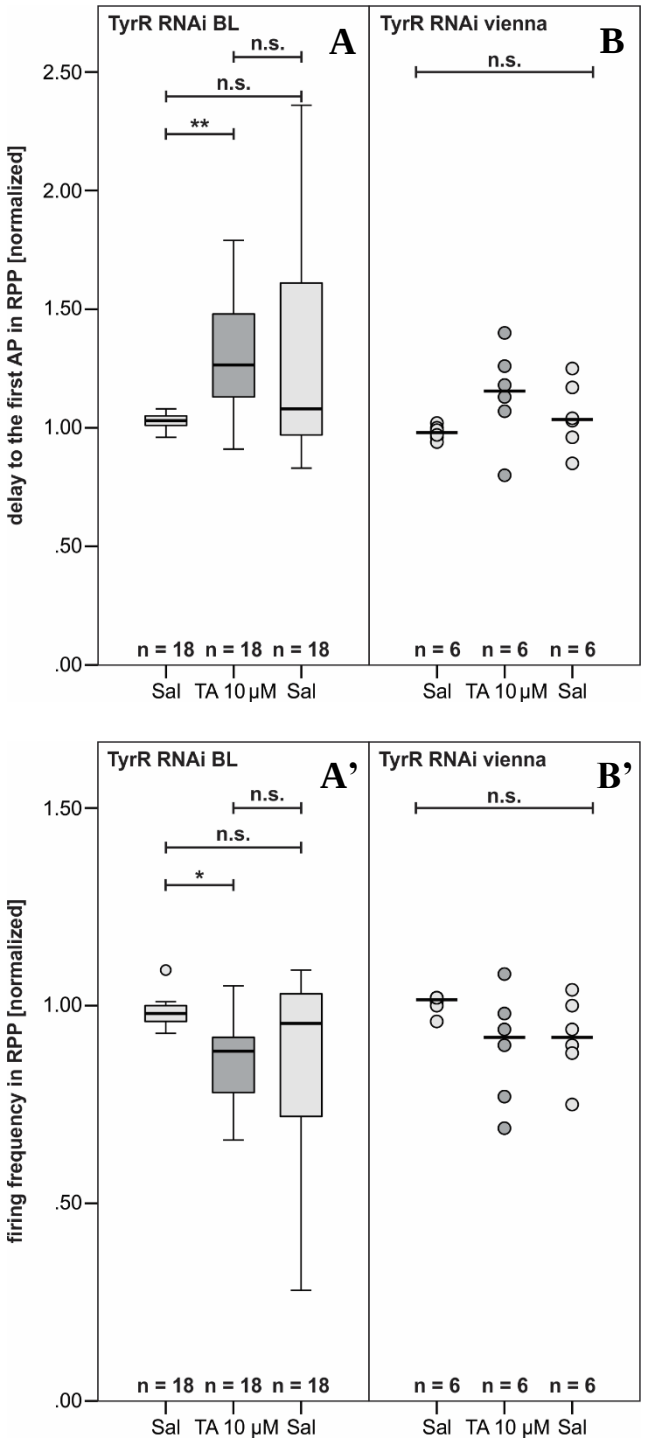

Figure 31: Statistical analysis of the delay to the first AP and the firing frequency in ramp pulse protocols in *TyrR*-RNAi lines from Bloomington and Vienna fly stock centers

A, A' Analysis of the delay to the first AP and the firing frequency in larvae expressing the *TyrR*-RNAi obtained from Bloomington (F.-T., delay p = 0.009; frequency p = 0.016; n = 18). **A** Pairwise follow-up comparison showed that the delay to the first AP was significantly longer after TA was applied (p = 0.008; n = 18). After TA was washed out, the delay was neither significantly shorter than before (p = 0.137; n = 18), nor was it significantly longer than at the beginning of the experiment (p = 0.952; n = 18). **A'** Pairwise follow-up comparison showed that the firing frequency was significantly reduced after TA was added to the bath (p = 0.014; n = 18), but not significantly increased after TA was removed (p = 0.470; n = 18). The firing frequency of the last run was not significantly different from the one of the first run (p = 0.470; n = 18). **B, B'** Analysis of the delay to the first AP and the firing frequency in larvae expressing the *TyrR*-RNAi obtained from Vienna. **B** A one-way ANOVA with repeated measures showed no significant differences in the delay to the first AP between the three runs (p = 0.095; n = 6). **B'** A Friedman-Test showed no significant differences between the firing frequencies of the three runs (p = 0.115; n = 6).

The other *TyrR*-RNAi construct, obtained from Vienna, was tested second. The delay to the first AP was 852 ± 168 ms (n = 6), and the firing frequency was 36.27 ± 6.13 Hz (n = 6). Both values were not significantly different from control values measured in standard saline (T-Test, delay p = 0.923; frequency p = 0.547; n = 6, 21) (results section 3.3).

The normalized data of the delay to the first AP was compared with a one-way ANOVA with repeated measures. It showed no significant differences between the three runs, before application of TA (n. median = 0.98; Q1 = 0.96; Q3 = 1.00; n = 6), after the application of TA (n. median = 1.15; Q1 = 1.09; Q3 = 1.24; n = 6), and after TA was washed out (n. median = 1.04; Q1 = 0.98; Q3 = 1.14; n = 6) (p = 0.095; n = 6). (Figure 31 B).

A Friedman-Test was used to statistically analyze the normalized data of the firing frequency. The test showed no significant differences between the three runs, before application of TA (n. median = 1.01; Q1 = 1.00; Q3 = 1.02; n = 6), after application of TA (n. median = 0.92; Q1 = 0.80; Q3 = 0.97; n = 6), and after TA was washed out (n. median = 0.92; Q1 = 0.89; Q3 = 0.98; n = 6) (p = 0.115; n = 6) (Figure 31 B').

The RNAi line obtained from the Bloomington *Drosophila* Stock Center (BL 25857) showed a control-like alteration of the delay to the first AP, and of the firing frequency. For the Vienna RNAi line (v102643), modulatory effects were not significant. However, the sample size was rather small, and an off-target has been reported for this RNAi line (off-target on CG 17658, http://stockcenter.vdrc.at). Combined with the fact that TyrR mRNA could hardly be detected in larval CNS (http://flyatlas.org/atlas.cgi, Chintapalli et al., 2007), this receptor is unlikely to be mediating tyraminergic modulation on MNISN-Is in *Drosophila* larvae.

3.8.2 Knocking Down TyrR II (CG 16766) Reduces Tyraminergic Modulation

The Tyramine Receptor II (TyrR II, CG 16766) (Bayliss et al., 2013) was tested with one RNAi line obtained from the Vienna *Drosophila* Resource Center (Line 7, chapter 2.6). The delay to the first AP was on average 996 ± 181 ms (n = 10), which was significantly longer than in controls (Mann-Whitney U-Test, p = 0.019; n = 10, 21). For statistical analysis, data were normalized to the first value of the first run in standard saline, which resulted in a normalized median of the delay of 1.00 (n = 10) in standard saline. It showed a tendency to increase upon application of TA to 1.10 (n. median; n = 10). The delay also decreased to a normalized median of 0.95 (n = 10) after TA was washed out. A Friedman-Test was used to statistically compare the delays to the first AP of all runs, which showed a significant difference (p = 0.006; n = 10). The delay did not significantly increase after TA was applied (pairwise follow-up comparison,

p = 0.075; n = 10). However, after TA was washed out, the delay was significantly decreased (pairwise follow-up comparison, p = 0.005; n = 10). The delay of the third run was not significantly different from the delay of the first run (pairwise follow-up comparison, p = 1.000; n = 10) (Figure 32 A).

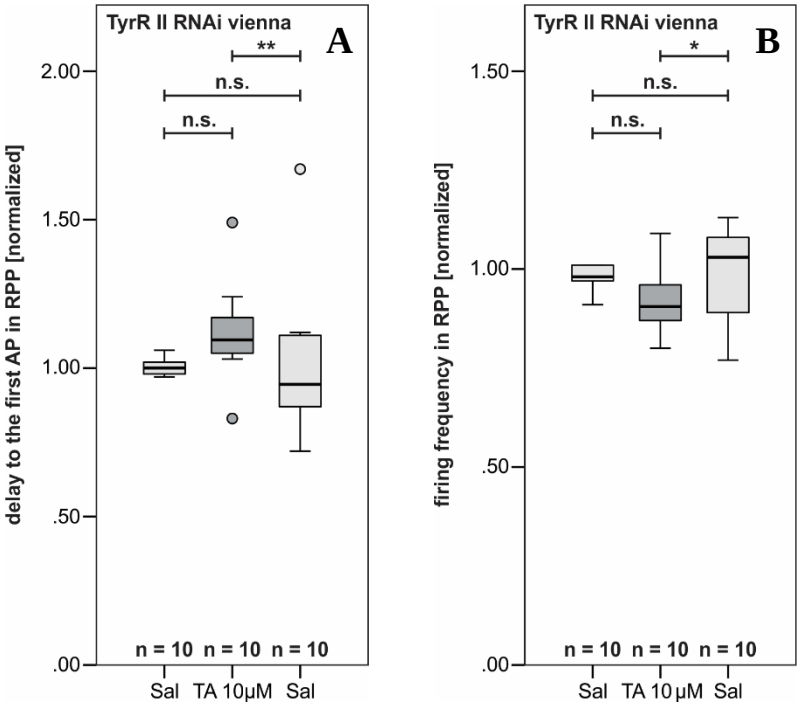

Figure 32: Statistical analysis of the delay to the first AP and the firing frequency in ramp pulse protocols in TyrR *II*-RNAi lines from Vienna fly stock center.
A Statistical analysis of the delay to the first AP (F.-T., p = 0.006; n = 10). Due to the pairwise follow-up comparison, the delay was not significantly altered after TA was applied (p = 0.075; n = 10). After TA was washed out, the delay was significantly decreased (p = 0.005; n = 10), and it was also not significantly longer than at the beginning of the experiment (p = 1.000; n = 10). **B** Statistical analysis of the firing frequency (F.-T., p = 0.020; n = 10). Pairwise follow-up comparisons showed that the firing frequency was not significantly reduced after TA was added to the bath (p = 0.133; n = 10) but significantly increased after TA was removed (p = 0.022; n = 10). The firing frequency of the last run was not significantly different from the one of the first run (p = 1.000; n = 10).

On average, the firing frequency was 37.62 ± 6.43 Hz (n. median = 0.98; n = 10), which was not significantly different from control values (Mann-Whitney U-Test, p = 0.268; n = 10). It tended to get slower after 10 µM TA was bath-applied for 2 min. The normalized frequency decreased from 0.98 (normalized median; n = 10) to 0.91 (n. median; n = 10). After TA was removed by perfusion with standard saline for 2 min, the firing frequency was increased to 1.00 (n. median; n = 10). Just as for the delay to the first AP, a Friedman-Test indicated a significant difference between the three runs (p = 0.020; n = 10). The pairwise follow-up analyses showed that the firing frequency of the second run after TA was added, was not significantly slower than in the first run (p = 0.133; n = 10). But after TA was washed out, the firing frequency was significantly increased (p = 0.022; n = 10). Also, the frequency of the third run was not

significantly different from the frequency of the first run (p = 1.000; n = 10) (Figure 32 B).

The knockdown of TyrR II reduced the modulatory effect of TA on MNISN-Is. For this RNAi construct, no off-targets were reported in the Vienna *Drosophila* Resource Center database. However, only minimal amounts of TyrR II mRNA could be detected in larval CNS (http://flyatlas.org/atlas.cgi, Chintapalli et al., 2007). Although the delay to the first AP and the firing frequency were only slightly but not significantly altered after application of TA, there was a significant effect after TA was washed out. This indicates that TA still had a major effect on MNISN-Is excitability in this knockdown. Therefore, and since the receptor seemed not to be expressed in the larval nervous system, it was also unlikely to mediate tyraminergic modulation in MNISN-Is.

3.8.3 Knockdowns of Oct-TyrR (CG 7485) Have Different Effects on Tyraminergic Modulation

The third known tyramine receptor, the Oct-TyrR (Arakawa et al., 1990; Bayliss et al., 2013; Saudou et al., 1990), was tested with two RNAi lines (Line 8 and Line 9, chapter 2.6).

The data acquired from larvae expressing the *Oct-TyrR*-RNAi from the Bloomington-line were analyzed first. The delay to the first AP was on average 776 ± 129 ms (n = 7), which was not significantly different from the mean delay of control recordings (T-Test, p = 0.364; n = 7, 21). The mean firing frequency was with 41.88 ± 3.33 Hz (n = 7) significantly higher than in control recordings (T-Test, p < 0.001; n = 7, 21) (results section 3.3).

The data were normalized to the first value of the first run in standard saline for statistical analysis. The delay increased from 1.01 (normalized median; n = 7) to 1.17 (n. median; n = 7) after TA was applied. It also tended to decrease after TA was washed out (n. median = 1.09; n = 7). A one-way ANOVA with repeated measures was used to compare the delays of the runs, which showed a significant difference (p = 0.015; n = 7). Pairwise follow-up analyses showed that the only significant change was the increase of the delay after TA was applied (p = 0.048; n = 7). The delay was not significantly decreased by washing TA out (p = 0.090; n = 7), and in the third run, it was not significantly different from the first run (p = 0.511; n = 7) (Figure 33 A).

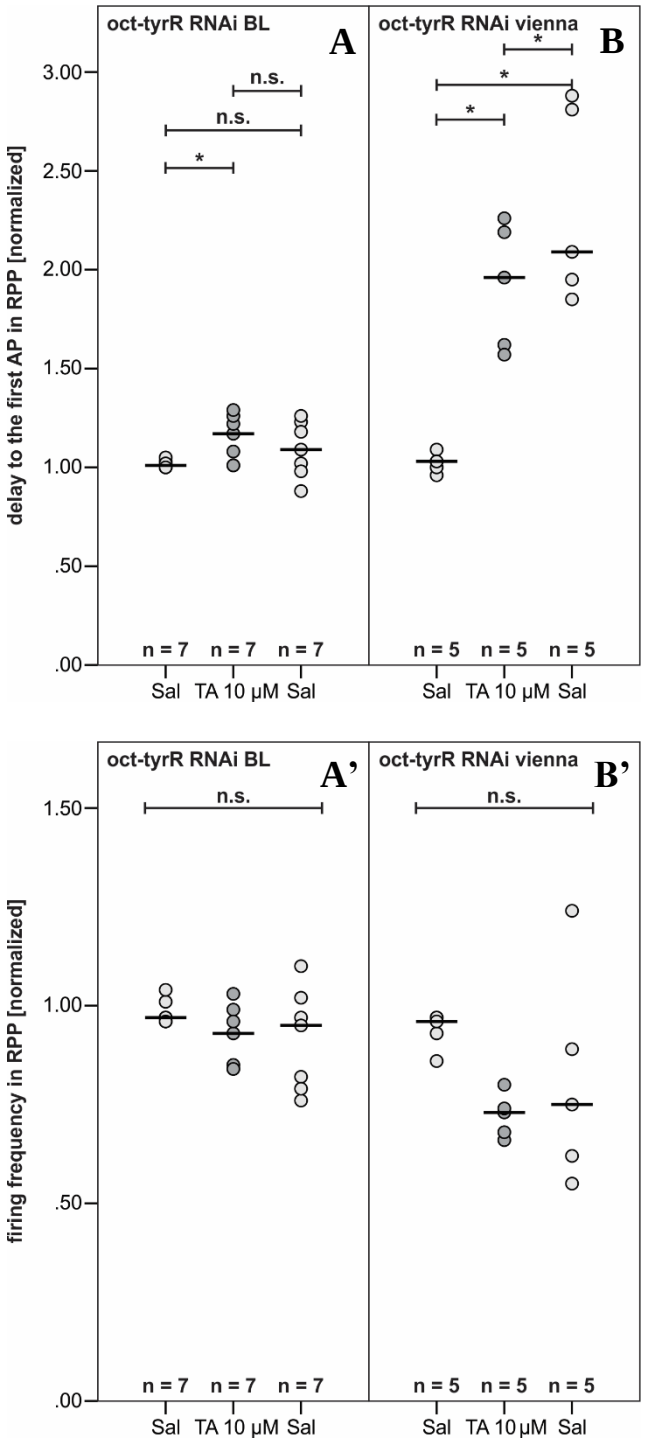

Figure 33: Statistical analysis of the delay to the first AP and the firing frequency in ramp pulse protocols in *Oct-TyrR*-RNAi lines from Bloomington and Vienna fly stock centers

A, A' Analysis of the delay to the first AP and the firing frequency in larvae expressing the *Oct-TyrR*-RNAi obtained from Bloomington (one-way ANOVA w. r. m., delay p = 0.015; frequency p = 0.067; n = 7). **A** The delay to the first AP was significantly increased after TA was applied (pairwise follow-up comparison, p = 0.048; n = 7). After TA was washed out, the delay was neither significantly decreased (follow-up comparison, p = 0.090; n = 7), nor was it significantly different from the first run (follow-up comparison, p = 0.511; n = 7). **A'** Statistical analysis of the firing frequency. The firing frequency was not significantly altered by applying TA or by washing it out (F.-T., p = 0.067; n = 7). **B, B'** Statistical analysis of the delay to the first AP and the firing frequency in larvae expressing the *Oct-TyrR*-RNAi obtained from Vienna (one-way ANOVA w. r. m., delay p < 0.001; frequency p = 0.236; n = 5). **B** Due to pairwise follow-up analyses, the delay to the first AP was significantly increased after application of TA (p = 0.015; n = 5), and significantly further increased after TA was washed out (p = 0.050; n = 5). Also, a significant difference between the delay of the first and the third run was shown (p = 0.017; n = 5). **B'** A one-way ANOVA w. r. m. indicated no significant difference between the firing frequencies of the three runs (p = 0.236; n = 5).

The firing frequency was not significantly altered by applying TA to the bath or by washing TA out (n. median before TA = 0.97; with TA = 0.93; after wash-out = 0.95; n = 7) (Friedman-Test, p = 0.067; n = 7) (Figure 33 A').

The data acquired from larvae expressing the *Oct-TyrR*-RNAi obtained from Vienna showed different results. Here, the delay to the first AP was on average 696 ± 239 ms (n = 5), and the firing frequency was 33.89 ± 7.96 Hz (n = 5) in standard saline. Both were not significantly different from control values (T-Test, delay p = 0.138; frequency p = 0.898; n = 5, 21). A one-way ANOVA with repeated measures, which was carried out to statistically analyze the normalized data of the delay to the first AP, indicated significant differences between the three runs ($p < 0.001$; n = 5). After TA was bath-applied, the delay to the first AP was significantly increased (n. median before TA = 1.03; with TA = 1.92; n = 5) (pairwise follow-up comparison, p = 0.015; n = 5), and began to spread broader (before TA Q1 = 1.00; Q3 = 1.03; with TA Q1 = 1.62; Q3 = 2.19). The delay was significantly further increased after TA was washed out (n. median = 2.09; n = 5) (pairwise follow-up comparison, p = 0.050; n = 5). The data scattering also increased, after TA was washed out (Q1 = 1.95; Q3 = 2.81). In the third run, the delay was significantly longer than in the first (pairwise follow-up comparison, p = 0.017; n = 5) (Figure 33 B).

As shown by a one-way ANOVA with repeated measures, application of TA did not significantly alter the firing frequency (p = 0.236; n = 5). Still, the firing frequency tended to decrease after TA was added to the bath (before TA n. median = 0.96; Q1 = 0.93; Q3 = 0.97; with TA n. median = 0.73; Q1 = 0.68; Q3 = 0.74; n = 5). It seemed not to be altered after TA was washed out, but the data spread broader (n. median = 0.75; Q1 = 0.62; Q3 = 0.89; n = 5) (Figure 33 B').

The two tested RNAi lines showed markedly different results. The RNAi line obtained from the Vienna *Drosophila* Resource Center had no reported off-targets. Nevertheless, the effects after application of TA could not be reversed by washing TA out, which hints to a reduction in MNISN-Is excitability which might not be caused by application of TA. In contrast to the other two RNAi lines obtained from Vienna, the *Oct-TyrR*-RNAi was a GD line, which has been described to be less efficient and less specific in gene disruption than the KK lines (http://stockcenter.vdrc.at/control/library_rnai). In animals carrying the RNAi construct obtained from Bloomington, a weaker increase in the delay to the first AP, and no significant reduction of the firing frequency could be observed. Also, mRNA of this receptor was highly enriched in larval CNS (http://flyatlas.org/atlas.cgi, Chintapalli et al., 2007), which is why this receptor is suggested to mediate tyraminergic modulation in MNISN-Is excitability.

3.9 Knocking Out a Single Receptor Abolishes Tyraminergic Modulation

Knockdowns, like they are generated from UAS-RNAi constructs, do not entirely prevent the synthesis of functioning protein. For the most promising of the three tyramine receptors, the Oct-TyrR, a mutant, *honoka* (also *hono* and *TyrR*^{hono}), could be found (Kutsukake et al., 2000). Animals from this strain do not have a functioning octopamine-tyramine receptor (Kutsukake et al., 2000; Nagaya et al., 2002).

MNISN-Is motoneurons from larvae with the *hono* mutation were patched and treated like control cells. In square pulse protocols, the delay to the first action potential was on average 400 ± 130 ms (n = 7) in standard saline. In controls, the mean delay to the first AP was 201.45 ± 84.76 ms (n = 21) (results section 3.3). In controls, only those sweeps were chosen for analysis, in which cells also fired APs after application of TA, which was very often not the first sweep in which APs were elicited in standard saline. In *TyrR*^{hono}, cells fired AP in the same sweeps in all runs (Figure 34).

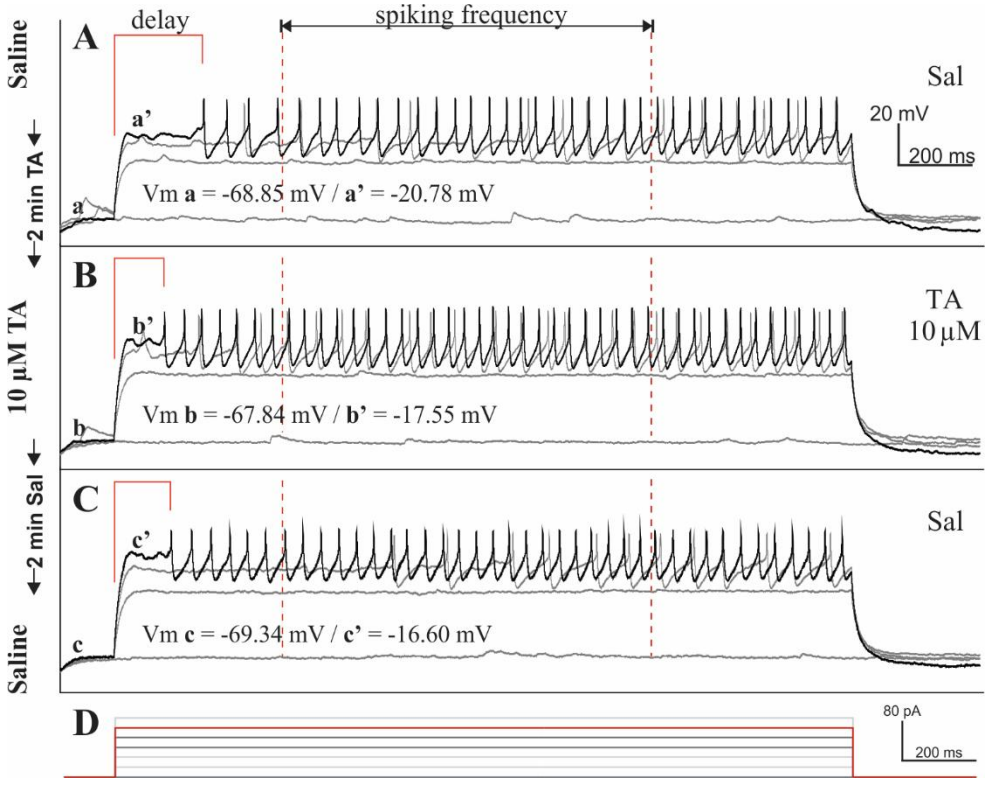

Figure 34: Firing pattern of MNISN-Is in a square pulse protocol in *TyrR*^{hono}.
Firing pattern of MNISN-Is motoneurons upon a two-second somatic square current injection of 80 pA. **A** Response to somatic current injection in standard saline with a characteristic delay to the first AP. **B** Slightly decreased delay to the first AP after 2 min of bath-application of 10 µM TA. **C** Washing in standard saline for 2 min did not alter the delay and the firing frequency. **D** Current injection steps with 20 pA increments. The steps shown in A-C are marked in red and dark grey.

Since later sweeps were chosen for analysis in controls, the mean delay was shorter and should not directly be compared to *TyrR*^{hono}. The *TyrR*^{hono} cells fired action potentials with a frequency

of about 15.00 ± 7.25 Hz (n = 7) (Figure 34 A). The mean firing frequency of control cells was 24.14 ± 9.1 Hz (n = 21) in standard saline (results section 3.3). Again, these values should not directly be compared. Bath-application of standard saline with 10 µM TA for at least two minutes caused the delay to decrease to 320 ± 130 ms (n = 7), and the firing frequency to slightly increase to 17.50 ± 7.75 Hz (n = 7) (Figure 34 B), which both were contrary to control recordings. Washing TA out for at least two minutes led to a further reduction of the delay to an average of 250 ± 100 ms (n = 7). The firing frequency stayed at an average of 17.93 ± 6.56 Hz (n = 7) (Figure 34 C).

For statistical analysis, all data were normalized to the first values of the first runs. Since the data of the three runs were not normally distributed for the delay to the first AP, a Friedman-Test was carried out to test for differences. The test indicated a significant difference between the three runs (p = 0.050; n = 7). Due to a spreading of the raw data, the normalized median of the delay to the first AP was 0.89 (Q1 = 0.84; Q3 = 1.00). After application of TA, the delay was not significantly decreased (n. median = 0.69; Q1 = 0.62; Q3 = 0.86; n = 7) (pairwise follow-up comparison, p = 0.109; n = 7). After TA was washed out, the delay was further, but not significantly decreased (n. median = 0.50; Q1 = 0.44; Q3 = 0.69; n = 7) (pairwise follow-up comparison, p = 0.423; n = 7). Due to its strong decrease, the delay of the third run was significantly shorter than in the first run (pairwise follow-up comparison, p = 0.048; n = 7) (Figure 35 A).

For the firing frequency, the normalized median was 1.10 in standard saline (Q1 = 0.98; Q3 = 1.17; n = 7). After TA was bath-applied for 2 min, the firing frequency was increased to 1.43 (n = 7); the data spreading was also increased (Q1 = 1.22; Q3 = 1.80; n = 7). Washing TA out for at least 2 min increased the firing frequency again (n. median = 1.65; Q1 = 1.17; Q3 = 1.97; n = 7). The firing frequencies of the three normally distributed runs were compared with a one-way ANOVA with repeated measures. No significant difference could be found (p = 0.183; n = 7) (Figure 35 B).

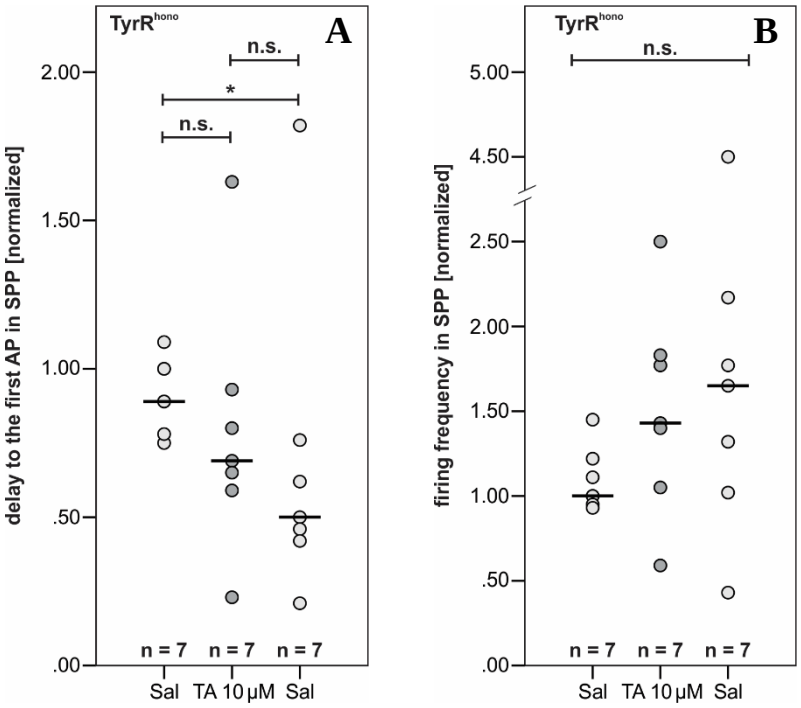

Figure 35: Statistical analysis of the delay to the first AP and the firing frequency in square pulse protocols in *TyrR*^{hono}. **A** Analysis of the delay to the first AP. As shown by a Friedman-Test, significant differences between the runs, before TA, with TA, and after washing TA out could be found (p = 0.050; n = 7). Pairwise follow-up analyses showed that the delay was neither significantly reduced after TA was applied (p = 0.109; n = 7), nor significantly reduced after TA was washed out (p = 0.423; n = 7). The delay was significantly shorter in the third run than in the first one (p = 0.048; n = 7). **B** Analysis of the firing frequency. In a one-way ANOVA with repeated measures, no significant differences could be found between the runs (p = 0.183; n = 7).

Recordings from ramp pulse protocols were also analyzed. In standard saline, the average delay to the first AP was 980 ± 150 ms, while the average firing frequency was found to be 37.71 ± 4.81 Hz (Figure 36 A). Since the first ramp of each recording was analyzed in all experiments just as in control recordings, control values of the delay to the first AP and the firing frequency could be compared with *TyrR*^{hono}. In controls, the mean delay to the first AP was 844.18 ± 172.39 ms (n = 21), and the mean firing frequency was 34.45 ± 3.75 Hz (n = 21), which both were not significantly different from the values of *TyrR*^{hono} (delay Mann-Whitney U-Test, p = 0.113; frequency T-Test p = 0.086; n = 21 / 7)

Applying TA did not visibly alter the delay to the first AP (average = 930 ± 180 ms) or the firing frequency (40.41 ± 5.43 Hz) (Figure 36 B). TA was washed out for at least two minutes, which also did neither affect the delay to the first AP (920 ± 180 ms), nor the firing frequency (40.41 ± 5.91 Hz) (Figure 36 C).

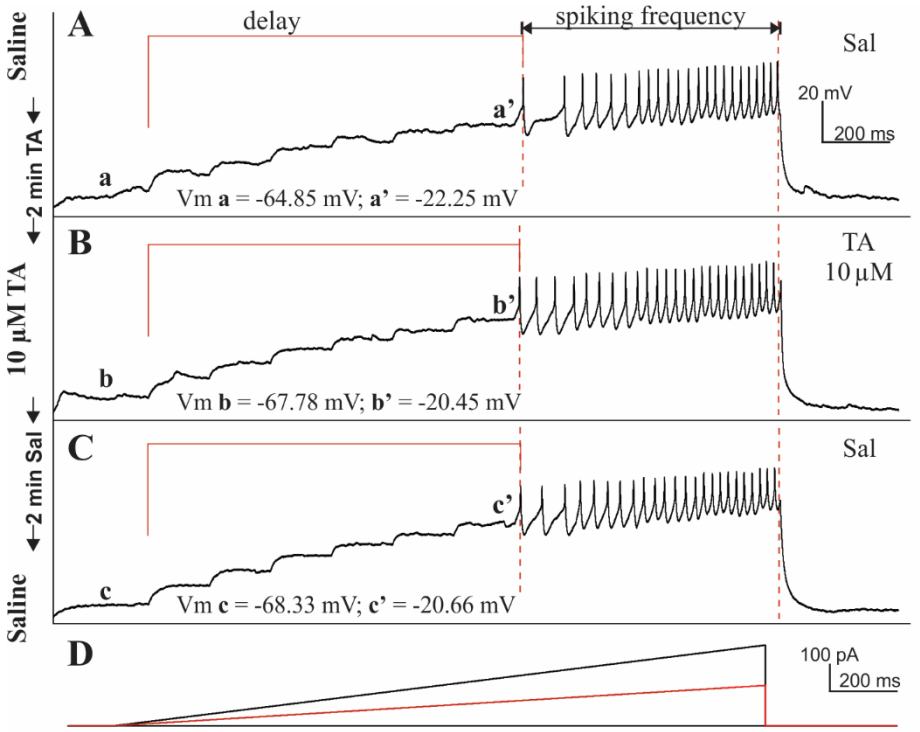

Figure 36: Firing pattern of MNISN-Is in a ramp pulse protocols in *TyrR*^{hono}.
Firing pattern of MNISN-Is upon a somatic two-second ramp current injection up to 150 pA. **A** Response to current injection in standard saline with a characteristic delay to the first AP. **B** Response after 2 min application of 10 µM TA. The delay, as well as the firing frequency, were not visibly altered. **C** Response after washing in standard saline for 2 min. **D** Current injection ramps with maxima of 150 and 300 pA. The ramp shown in A-C is marked in red.

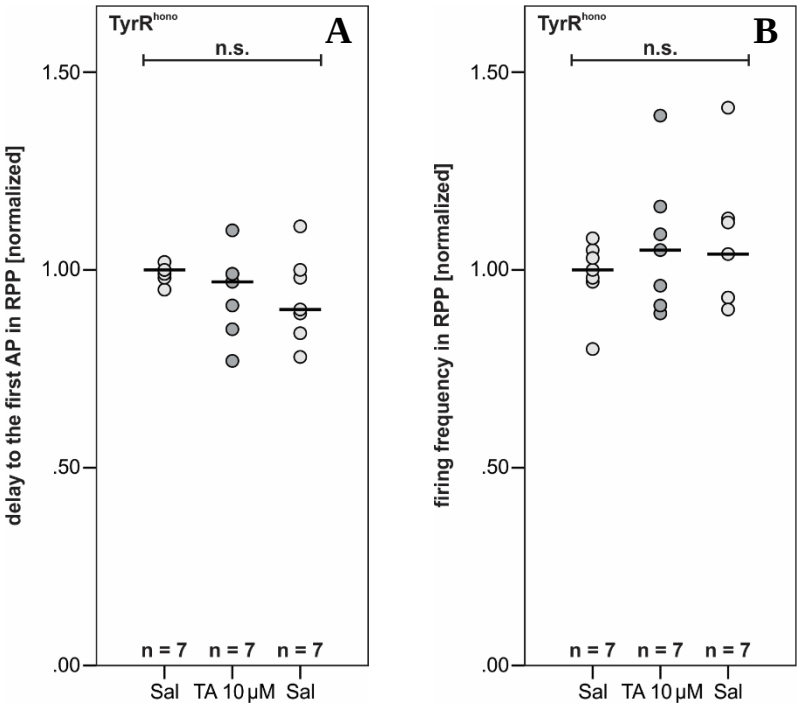

Figure 37: Statistical analysis of the delay to the first AP and the firing frequency in ramp pulse protocols in *TyrR*^{hono}.
A Analysis of the delay to the first AP. As shown by a one-way ANOVA w. r. m., no significant differences between the runs, before TA, with TA, and after washing TA out, could be found ($p = 0.184$; $n = 7$). **B** Analysis of the firing frequency. In a one-way ANOVA w. r. m., no significant differences could be found between the groups ($p = 0.186$; $n = 7$).

The statistical analysis of the normalized data proved, that there were no significant differences between the three runs for the delay to the first AP and the firing frequency in ramp pulse protocols (one-way ANOVA with repeated measures; delay p = 0.184; frequency p = 0.186; n = 7). Over time, the delay was slightly reduced, while the data also spread broader in later runs (run one n. median = 1.00; Q1 = 0.99; Q3 = 1.00; run two n. median = 0.97; Q1 = 0.88; Q3 = 0.99; run three n. median = 0.90; Q1 = 0.86; Q3 = 0.99). The same was true for the firing frequency, over time it slightly increased while the data spread broader (run one n. median = 1.00; Q1 = 0.97; Q3 = 1.04; run two n. median = 1.05; Q1 = 0.93; Q3 = 1.12; run three n. median = 1.04; Q1 = 0.93; Q3 = 1.12) (Figure 37).

The octopamine-tyramine receptor is solely responsible for tyraminergic modulation in MNISN-Is. As shown by current-clamp experiments in controls, bath-application of TA reduces MNISN-Is excitability (Figure 10, chapter 3.3). In *honoka* mutants, the modulatory effects of TA on MNISN-Is were entirely inhibited. This shows that no other receptor compensates for the loss of Oct-TyrR function and that Oct-TyrR is the only tyramine receptor in MN dendrites mediating tyraminergic effects on MN excitability.

3.10 Calcium Imaging

To test if synaptic integration was impaired after bath-application of TA, calcium imaging experiments were conducted. Here, dendrites of MNISN-Is were imaged while nicotine was focally applied, which activated nicotinic acetylcholine receptors (nAChR) and depolarized the cell membrane. Overall Ca^{2+} influx through both nAChRs and voltage-gated Ca^{2+} channels (VGCC) could be measured via changes in the intensity of GCaMP6 fluorescence (methods section 2.4).

3.10.1 TA Reduces Ca^{2+} Influx into MNISN-Is Dendrites

As calcium imaging controls, the *OK37-1*-GAL4 line was utilized to drive expression of GCaMP6m in all MN1-Ib (aCC) and MNISN-Is (RP2) motoneurons in larval nervous systems (Line 2, methods section 2.4.2).

Larvae were dissected as described, and the ganglionic sheath was carefully removed as described in the methods section (chapter 2.4.2). Due to the base fluorescence of GCaMP, MNISN-Is motoneurons could easily be identified. All voltage-activated Na^{+} channels were blocked by application of TTX. Thus, cell-to-cell communication via presynaptic input was

inhibited. Each puff of nicotine activated nAChRs (Dani, 2015), which led to an immediate Ca^{2+} influx, activation of VGCCs, and subsequently a rapid increase in fluorescence due to the binding of Ca^{2+} to GCaMP6 (Figure 38). For a detailed description of the experimental procedure, see methods section (chapter 2.4.2).

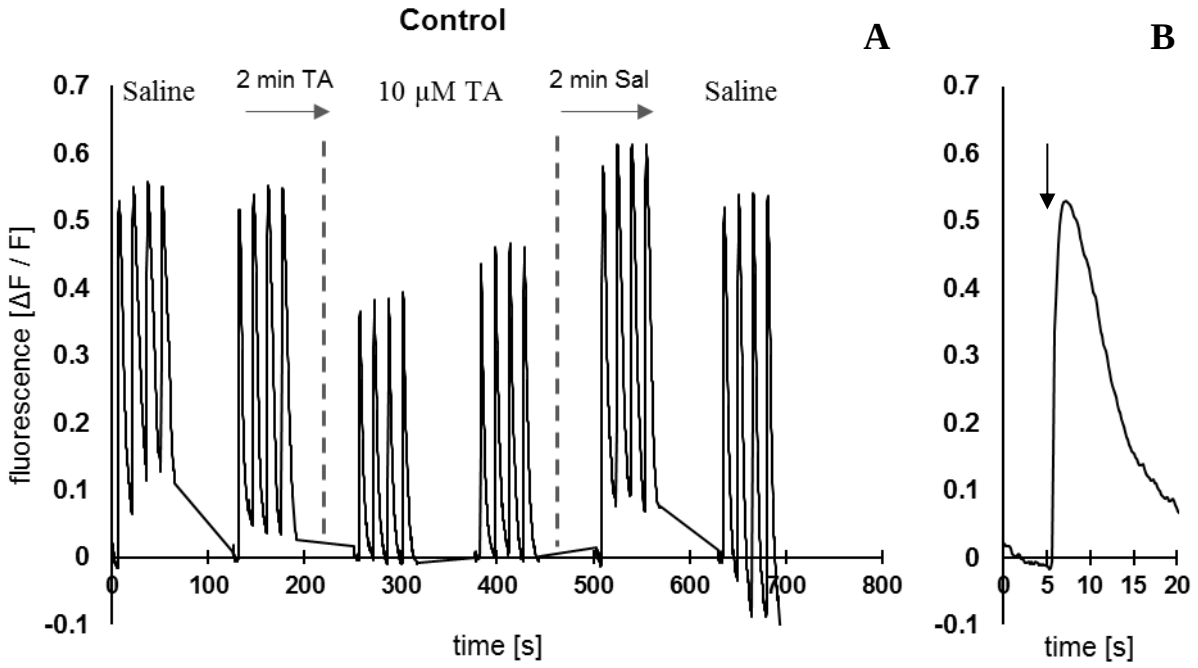

Figure 38: Raw data of the changes in fluorescence (ΔF/F) in control cells.
A One Ca^{2+} imaging analysis with a set of six separate consecutive recordings is shown. Two sets of recordings were carried out in standard saline, 10 µM TA, and in standard saline after washing TA out. Each set was one minute apart. For the graphical representation, the data has been merged, and one-minute pauses were inserted manually. TA was applied for 2 min and washed out for 2 min (dashed lines). Each peak is the rapid increase in fluorescence due to Ca^{2+} influx initiated by a nicotine puff. Puffs were given in intervals of 15 s. The increase in fluorescence is smaller after application of 10 µM TA. **B** Example response to one nicotine puff. First peak of the first recording of A in standard saline. The nicotine puff was given at 5 s (arrow).

The mean increase in fluorescence, ΔF/F, was 0.51 ± 0.11 (n = 16) in standard saline. After application of TA, the mean increase was reduced to 0.40 ± 0.15 (n = 16). TA was washed out for 2 min, which reversed the effect. The mean increase in fluorescence initiated by single nicotine puffs was 0.53 ± 0.10 (n = 16) after the washing-out (Figure 38).

For analysis, all calcium responses were normalized to the first value of the first run in standard saline. The two runs in saline (paired T-Test, p = 0.031; n = 16, 16), the two runs in 10 µM TA (paired T-Test, p = 0.067; n = 16, 16), and the two runs in saline after washing TA out (paired T-Test, p = 0.076; n = 16, 16), were pooled to get three runs, one in each condition (see also Figure 70, appendix section 6.4). The normalized median was therefore 1.06 (n = 16) in standard saline (Figure 39). After the two-minute bath-application of TA, the fluorescence

evoked by nicotine puffs was significantly reduced (n. median = 0.89; Friedman-Test, p = 0.009; pairwise follow-up comparison, p = 0.040; n = 16) (Figure 39 A, row three, B).

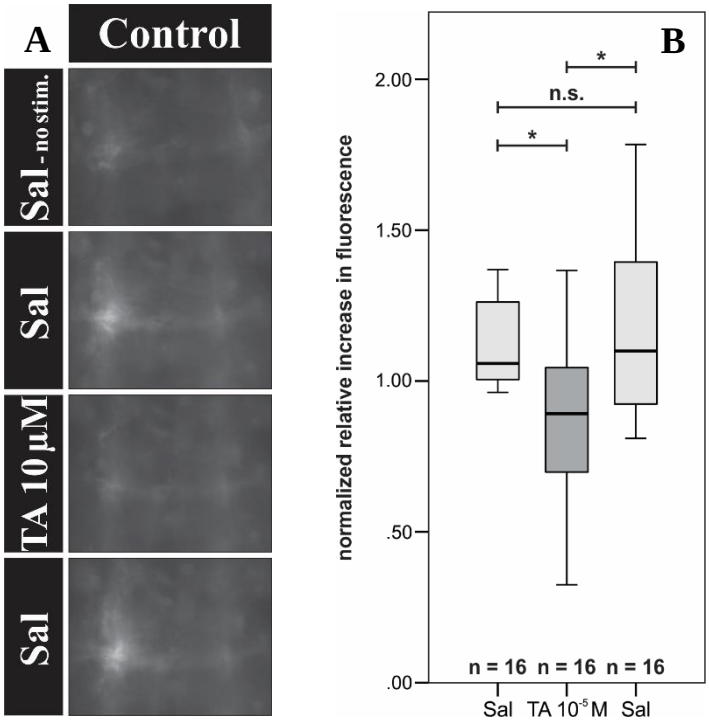

Figure 39: Intensity of fluorescence upon nicotine puffs in control larvae.
A Example of the intensity of fluorescence in single video frames. Each picture except for the first was taken directly after a nicotine puff. **B** Statistical analysis of the intensity of fluorescence. A Friedman-Test indicated a significant difference between the three runs (p = 0.009; n = 16). Pairwise follow-up analyses showed that the intensity of fluorescence was significantly reduced after TA was applied (p = 0.040; n = 16). The intensity also increased significantly again after TA was washed out (pairwise follow-up comparison, p = 0.014; n = 16). In the third run, it was as bright as in the first run (pairwise follow-up comparison, p = 1.000; n = 16).

After TA was washed out for 2 min, the fluorescence was significantly increased again (n. median = 1.10; n = 16) (pairwise follow-up comparison, p = 0.014; n = 16), and therefore as intense as in the beginning (pairwise follow-up comparison, p = 1.000; n = 16) (Figure 39 A, row four; B).

These experiments indicate that synaptic integration is profoundly affected by tyramine. After bath-application of TA, a smaller net Ca^{2+} influx could be estimated from the change in fluorescence intensity of the Ca^{2+} indicator GCaMP6m. The nicotine puffs activated nAChRs, which depolarized the membrane through Ca^{2+} influx. This, in turn, activated VGCCs, like DmCa1D, which further increased the Ca^{2+} influx. TA could either target nAChRs or VGCCs. However, modulation of nAChRs is unlikely, since MNISN-Is excitability was also reduced in synaptic isolation (results section 3.5).

3.10.2 Knocking Out the Oct-TyrR Inhibits Reduction of Ca^{2+} Influx

Oct-TyrR was shown to mediate tyraminergic effects on MNISN-Is excitability (results section 3.9). By repeating the previous calcium imaging experiments in *TyrR*^{hono}, the mutant of the octopamine-tyramine receptor, the role of Oct-TyrR in the tyraminergic modulation of postsynaptic dendritic Ca^{2+} responses upon nAChR activation should be demonstrated.

To conduct these experiments, the line to test was a combination of the *OK37-1*-GAL4 driver-line with GCaMP6m and the *TyrR*^{hono} mutant (Line 16). Two lines had to be recombined first to keep the mutation of the Oct-TyrR homozygous. One of them carried the GAL4 driver-line combined with *TyrR*^{hono} (Line 14), and the second one contained the necessary GCaMP6m, also together with *TyrR*^{hono} (Line 15). Both lines were balanced with the balancer-chromosomes CyO and CxD, with the dominant markers *Curly* (*Cy*) and *Dicheate* (*D*), to keep the lines stable. Progeny of a cross from both lines carried the desired genotype (Line 16).

Line 14

$$w^{*}\,;\,\frac{OK37-1-GAL4}{CyO}\,;\,\frac{P\{lwB\}Oct-TyrR^{hono}}{CxD}\,;\,+$$

Line 15

$$w^{*}\,;\,\frac{P\{20XUAS-IVS-GCaMP6m\}attP40}{CyO}\,;\,\frac{P\{lwB\}Oct-TyrR^{hono}}{CxD}\,;\,+$$

Line 16

$$w^{*}\,;\,\frac{OK37-1-GAL4}{P\{20XUAS-IVS-GCaMP6m\}attP40}\,;\,\frac{P\{lwB\}Oct-TyrR^{hono}}{P\{lwB\}Oct-TyrR^{hono}}\,;\,+$$

MNISN-Is neurons could easily be identified by the base fluorescence of GCaMP6m. A single puff of nicotine evoked a quick Ca^{2+} influx and a rapid increase in fluorescence, just as in control cells (Figures 40, 41 C). In standard saline, the mean increase in fluorescence ($\Delta F/F$) was 0.58 ± 0.10 (n = 7), which was not significantly different from control values in standard saline (T-Test, p = 0.191; n = 16, 7). After 2 min of bath-application of 10 µM TA, the average increase in fluorescence was still 0.57 ± 0.10 (n = 7). The mean increase in fluorescence was also 0.56 ± 0.10 (n = 7) after washing TA out for two minutes (Figure 40).

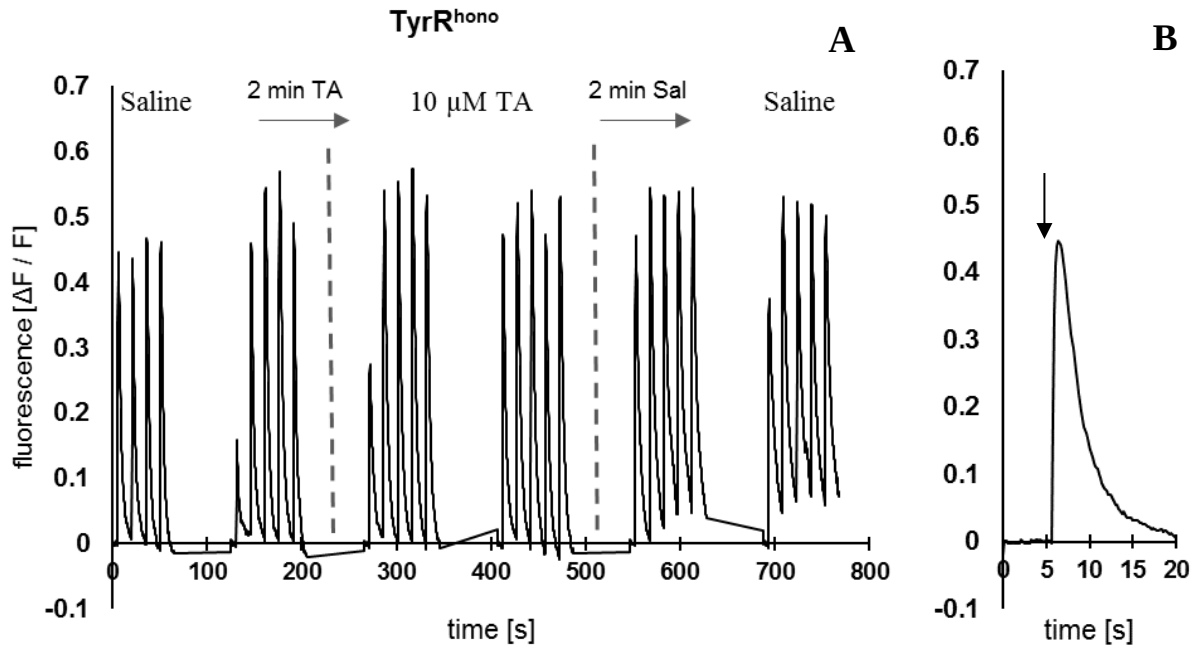

Figure 40: Raw data of the changes in fluorescence (ΔF/F) in *TyrR*^{hono} cells.
A One Ca^{2+} imaging analysis with a set of six separate consecutive recordings is shown. Two sets of recordings were carried out in standard saline, 10 µM TA, and in standard saline after washing TA out. Each set was one minute apart. For the graphical representation, the data has been merged, and one-minute pauses were inserted manually. TA was applied for 2 min and washed out for 2 min (dashed lines). Each peak is the rapid increase in fluorescence due to Ca^{2+} influx initiated by a nicotine puff. Puffs were given in intervals of 15 s. The increase in fluorescence is not altered after application of 10 µM TA. Only the last four intensity peaks of each set were included in the analysis. **B** Example response to one nicotine puff. First peak of the first recording of A in standard saline. The nicotine puff was given at 5 s (arrow).

For statistical analysis, all calcium responses were, again, normalized to the first value of the first run, and the data of runs from the same conditions (in standard saline (paired T-Test, p = 0.717; n = 7, 7), in 10 µM TA (paired T-Test, p = 0.947; n = 7, 7), in standard saline after washing TA out (paired T-Test, p = 7, 7)) were pooled (see also Figure 71, appendix section 6.5). A one-way ANOVA with repeated measures was carried out to test for changes in the maximum fluorescence upon application or removal of TA, which showed no significant difference between the runs (p = 0.798; n = 7). The normalized median of the increase in fluorescence upon nicotine puffs was 1.04 (n = 7) in standard saline. Bath-application of 10 µM TA for 2 min did not reduce the brightness of the fluorescence (n. median = 1.05; n = 7) (Figure 41 A, row three; B). It was also not altered by washing TA out with standard saline for two minutes (n. median = 0.98; n = 7) (Figure 41 A, row four; B).

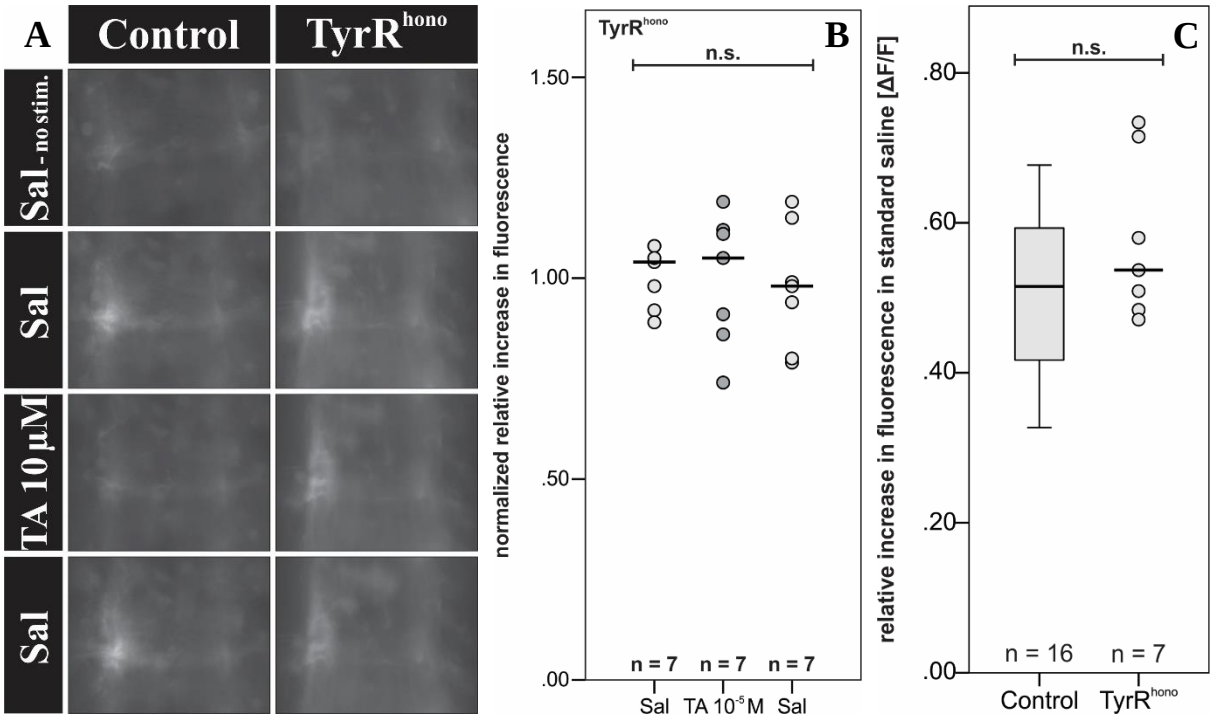

Figure 41: Intensity of fluorescence upon nicotine puffs in Oct-TyrR mutant larvae
A Example of fluorescence in single video frames. Each picture except for the first one was taken directly after a nicotine puff. The first column represents examples of the control; the second column contains pictures of Oct-TyrR mutant cells. **B** Statistical analysis of the intensity of fluorescence. A one-way ANOVA with repeated measures showed no significant differences between the three runs ($p = 0.798$; $n = 7$). **C** Comparison of the mean intensity of fluorescence of control and *TyrR*^{hono} in standard saline. A T-Test showed no significant difference between the genotypes ($p = 0.191$; $n = 16, 7$).

Again, the Oct-TyrR solely mediated the tyraminergic modulation, in this case, of postsynaptic dendritic Ca^{2+} responses upon activation of nAChRs. Since no difference could be found in the increase in fluorescence with and without TA, there seemed to be no other tyramine receptor that compensated for the loss of Oct-TyrR function in synaptic integration.

3.11 Knocking Down Shal K^+ Channels Does Not Fully Inhibit Tyraminergic Modulation of MNISN-Is

Current-clamp recordings of control MNISN-Is motoneurons revealed that TA reduces MN excitability. This could be seen in a significant increase of the delay to the first AP, and a significant reduction of the firing frequency, as well as a significantly reduced Ca^{2+} influx after bath-application of TA (results sections 3.3 and 3.10.1). The receptor which mediated these effects had been identified as the Oct-TyrR (results section 3.9). In the next step, the still unknown ion channel, which was the target of the tyraminergic modulation, should be identified.

Shal K^+ channels are thought to underlie the delay to the first action potential in MNISN-Is motoneurons. Electrophysiological studies with a dominant negative K_v4 subunit, and with a Shal knockdown showed that the delay was completely abolished if Shal channels were not functional (Ping et al., 2011; Schaefer et al., 2010). Since the delay to the first AP was severely affected by tyraminergic modulation, a motoneuron-specific knockdown of the transient K^+ channel Shal was tested in current-clamp experiments. For this purpose, a fly line was created which carried the UAS-s*hal*-RNAi construct and a UAS-*dcr2* construct for increased knockdown strength (Dietzl et al., 2007; Hutchinson et al., 2014). This line was then crossed to the *RN2*-GAL4, UAS-*mCD8::GFP*; UAS-*FLP* line (Line 17), to express both constructs motoneuron-specific.

Line 17

$$w^*\,;\ \frac{RN2-GAL4, mCD8::GFP}{UAS-Shal-RNAi}\ ;\ \frac{Act<Stop>GAL4, UAS-FLP}{UAS-dcr2}\ ;\ \frac{+}{+}$$

Current-clamp experiments were executed as in control larvae (methods section 2.2.2). Only cells which were GFP-labeled were chosen for experiments since only these also expressed the Shal knockdown.

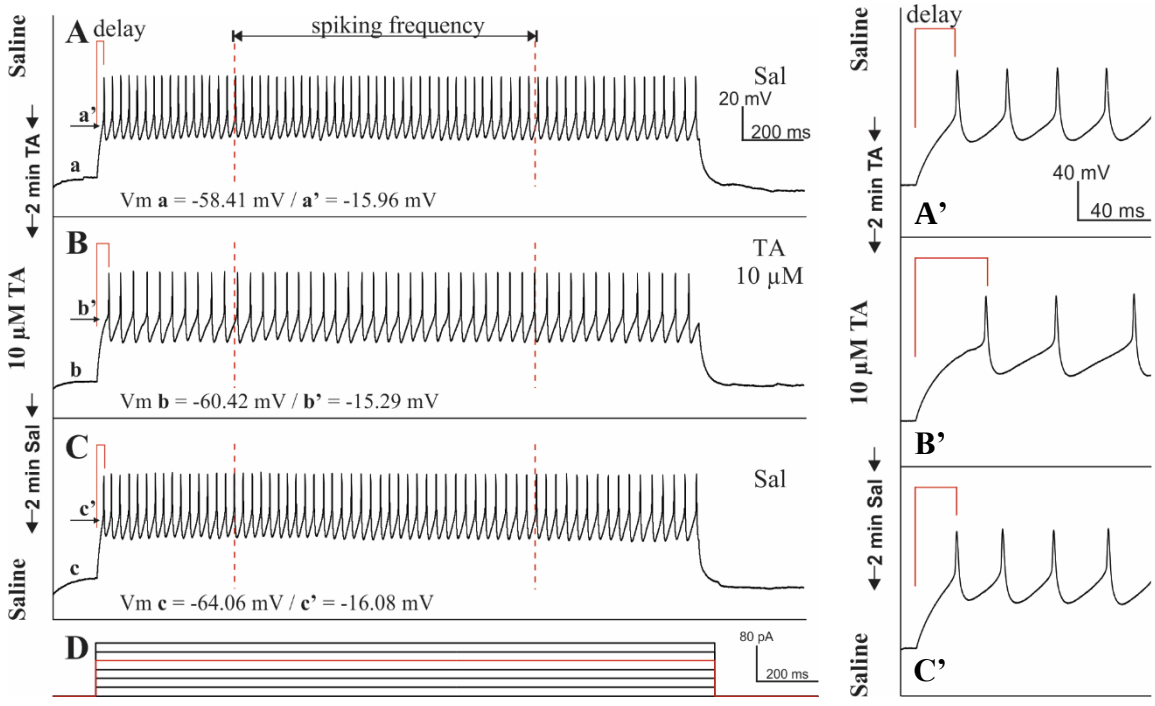

Figure 42: Firing pattern of MNISN-Is with a Shal knockdown in a square pulse protocol.
Firing pattern of MNISN-Is upon a two-second 80 pA square pulse current injection in larvae carrying the *shal*-RNAi. **A** Response to somatic current injection in standard saline with a nearly abolished delay to the first AP. **A'** Magnification of the first 130 ms of A. **B** 10 µM TA was applied for 2 min. The delay slightly increased while the firing frequency slightly decreased. **B'** Magnification of the first 130 ms of B. Both an increased delay to the first AP and a decreased firing frequency are visible. **C** Washing in standard saline for 2 min removed the effects of TA on the delay and the firing frequency. **C'** Magnification of the first 130 ms of C. **D** Current injection steps with 20 pA increments. The step shown in A-C is marked in red.

As expected, in square pulse protocols, the delay to the first AP was nearly abolished in MNISN-Is motoneurons expressing the *Shal*-RNAi (mean = 35.5 ± 10.58 ms; n = 6) (Figure 42 A). The delay to the first AP was significantly shorter than in control neurons (T-Test, p < 0.001; n = 6, 21). The average firing frequency was 31.50 ± 8.46 Hz (mean; n = 6), which was control-like (T-Test, p = 0.125; n = 6, 21) (results section 3.3) (Figure 42 A, A'). 10 µM TA was bath-applied for 2 min before new recordings were made. In these recordings of the second run, a slightly longer delay was visible, as well as a slightly decreased firing frequency (mean, delay = 47.45 ± 11.09 ms; frequency = 21.75 ± 3.73 Hz; n = 6) (Figure 42 B, B'). After TA was washed out for 2 min, the average delay to the first AP was 27.00 ± 44.27 ms (n = 6), and the mean firing frequency was 28.1 ± 5.29 Hz (n = 6) (Figure 42 C, C').

The data were normalized to the first values of the first recordings for each parameter. Only one recording instead of two was carried out in the first run, in standard saline, which is why all normalized medians and quartiles were 1 for the first run.

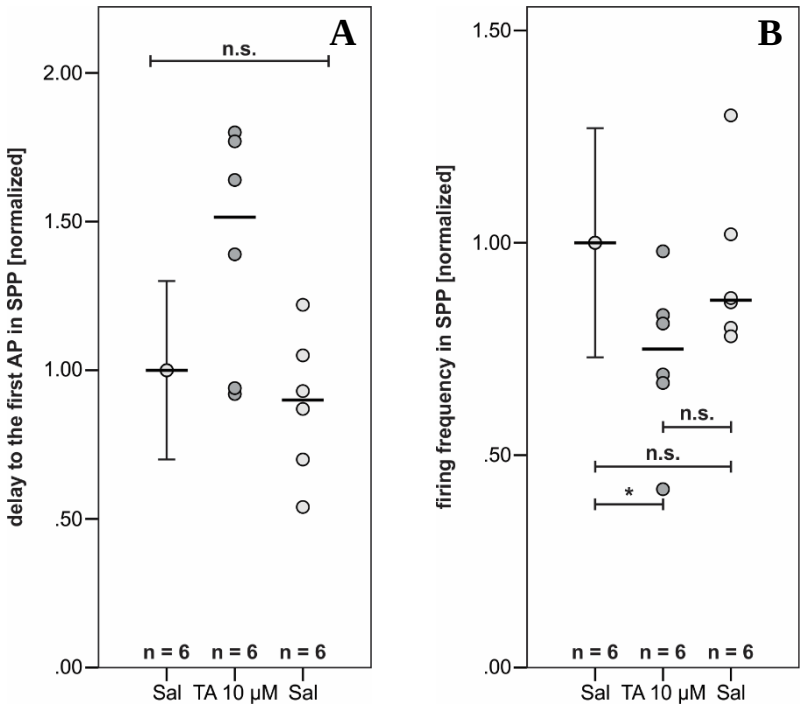

Figure 43: Statistical analysis of the delay to the first AP and the firing frequency upon TA treatment in square pulse protocols in *RN2*-GAL4 / UAS-*Shal*-RNAi; UAS-*FLP* / UAS-*dcr2*

The first run is shown as normalized median with indicated normalized standard deviation of the raw data. **A** Analysis of the delay to the first AP. The delay was not significantly altered upon application or washing-out of TA (F.-T., p = 0.069; n = 6). **B** Statistical analysis of the firing frequency (F.-T., p = 0.030; n = 6). The firing frequency was significantly decreased after TA was added (follow-up comparison, p = 0.028; n = 6). It did not significantly increase after TA was washed out (follow-up comparison, p = 0.250; n = 6). No significant difference was found between the first and the third run (follow-up comparison, p = 1.000; n = 6).

A Friedman-Test was used to test for significant differences between the runs, which indicated no significant differences, although tendencies were visible (p = 0.069; n = 6) (Figure 43 A).

After the bath-application of TA, the delay to the first AP increased to 1.51 (n. median; Q1 = 1.05; Q3 = 1.74; n = 6). In the third run, after TA was washed out, the delay was reduced to 0.90 (n. median; Q1 = 0.74; Q3 = 1.02; n = 6). Data spreading was markedly increased after TA was bath-applied.

The normalized median of the firing frequency was also 1.00 (n = 6) in standard saline because the first run contained only one recording from each cell. In the statistical analysis, significant differences could be found between the runs (Friedman-Test, p = 0.030; n = 6). After the preparation was washed with 10 µM TA for 2 min, the frequency was significantly reduced (n. median = 0.75; Q1 = 0.67; Q3 = 0.82) (pairwise follow-up analysis, p = 0.028; n = 6). However, the firing frequency was not significantly increased after TA was washed out (n. median = 0.87; Q1 = 0.81; Q3 = 0.99) (pairwise follow-up comparison, p = 0.250; n = 6). But also, the firing frequency of the third run was not significantly different from the frequency of the first run (pairwise follow-up comparison, p = 1.000; n = 6) (Figure 43 B).

For recordings acquired in ramp pulse protocols, similar results could be found. The delay to the first AP was on average 651 ± 93ms (n = 6), and the firing frequency was 43.04 ± 7.49 Hz (n = 6). Both parameters were significantly different from control values. The delay was significantly shorter (Mann-Whitney U-Test, p = 0.026; n = 21, 6), and the firing frequency was significantly higher than in controls (T-Test, p = 0.050; n = 21, 6) (results section 3.3). Just as in square pulse protocols, the data were normalized to the first value of the first recording. In standard saline the normalized median for both the delay and the firing frequency were 1.00 (n = 6). After application of TA, the delay to the first AP tended to increase (n. median = 1.16; Q1 = 1.07; Q3 = 1.32), and after washing TA out, it tended to decrease again (n. median = 1.00; Q1 = 0.95; Q3 = 1.00). As shown by a Friedman-Test, which was carried out to test for significant differences between the runs, these changes were not significant (p = 0.094; n = 6) (Figure 44 A). The firing frequency decreased significantly after TA was bath-applied for 2 min (n. median = 0.85; Q1 = 0.87; Q3 = 0.84; n = 6) (Friedman-Test, p = 0.006; pairwise follow-up comparison, p = 0.007; n = 6). It did not significantly increase after TA was washed out (n. median = 0.90; Q1 = 0.86; Q3 = 0.91; n = 6) (pairwise follow-up comparison, p = 1.000; n = 6)

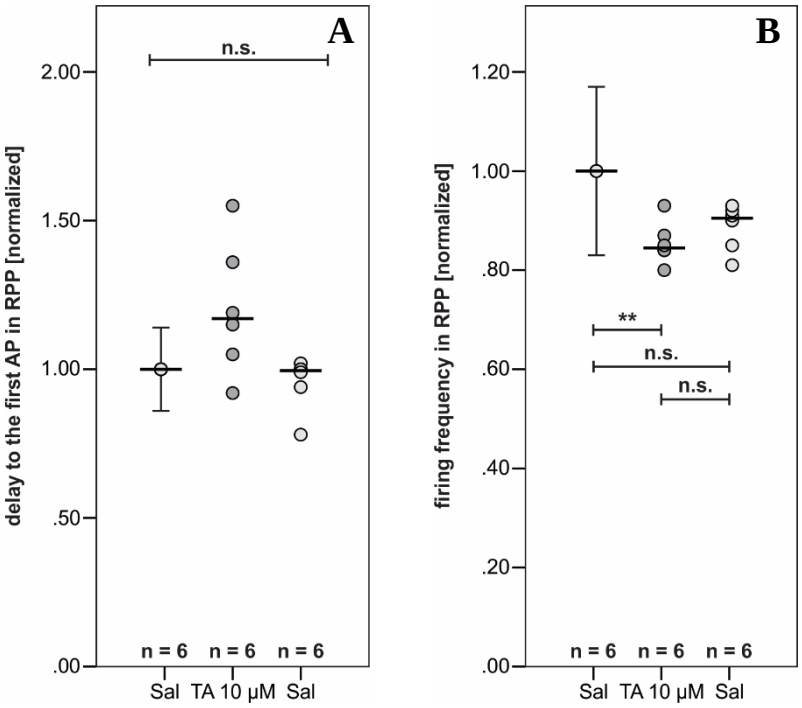

Figure 44: Statistical analysis of the delay to the first AP and the firing frequency upon TA treatment in ramp pulse protocols in *RN2*-Gal4 / UAS-*Shal*-RNAi; UAS-*FLP* / UAS-*dcr2*
A Analysis of the delay to the first AP. The delay was not significantly altered after treatment with TA (F.-T., p = 0.094; n = 6). **B** Statistical analysis of the firing frequency (F.-T., p = 0.006; n = 6). The firing frequency was significantly decreased after application of TA (follow-up comparison, p = 0.007; n = 6). It did not significantly increase after TA was washed out (follow-up comparison, p = 1.000; n = 6). No significant difference was found between the frequency of the first and the third run (follow-up comparison, p = 0.091; n = 6).

The firing frequency of the third run was also not significantly different from the one of the first run (pairwise follow-up comparison, p = 0.091; n = 6) (Figure 44 B).

Although not significant, the delay to the first AP tended to increase after the application of TA in both square pulse protocols and ramp pulse protocols. Simultaneously, the firing frequency was significantly reduced. This means that the effects of TA were reduced, but nevertheless, they were apparently present. Shal K^+ channels were obviously underlying the delay to the first AP, but they were either no or not the only target of tyraminergic modulation.

3.12 VGCCs as Possible Targets of Tyraminergic Modulation

3.12.1 Knocking Down DmCa1D Reduces Tyraminergic Modulation of MNISN-Is Excitability

Calcium imaging experiments revealed the tyraminergic modulation of Ca^{2+} influx upon nAChR activation (results section 3.10.1). As shown in synaptic isolation, the motoneuron intrinsic excitability was modulated directly, which is why nAChRs were ruled out as targets for tyraminergic modulation (results section 3.5). Further patch-clamp experiments were

carried out in larvae with a knockdown of DmCa1D to test for its role. UAS-*DmCa1D*-RNAi expression was targeted to MNs by a cross with our *RN2*-GAL4 driver-line containing GFP (Line 18) (n = 4), or with the *OK37-1*-GAL4 driver-line (Line 19) (n = 5).

Line 18

$$w^{*}\ y^{*}\ v^{*}\ ;\ \frac{RN2-GAL4,UAS-mCD8::GFP}{+}\ ;\ \frac{Act<Stop>GAL4,UAS-FLP}{P\{TRiP.HMS00294\}attP2}\ ;\ +$$

Line 19

$$w^{*}\ ;\ \frac{OK37-1-GAL4}{+}\ ;\ \frac{P\{TRiP.HMS00294\}attP2}{+}\ ;\ +$$

For all experiments, wandering L3 larvae were randomly picked from both lines. MNISN-Is motoneurons were thoroughly identified and used for patch-clamp experiments. The neurons showed similar firing properties as control cells (Figure 45). In current-clamp recordings made in square pulse protocols, the delay to the first AP was on average 238 ± 109 ms (n = 9), and the firing frequency was 18.94 ± 5.52 Hz (n = 9). It was expected, that the firing frequency was higher, and the delay was shorter in the knockdown than in controls (Worrell & Levine, 2008).

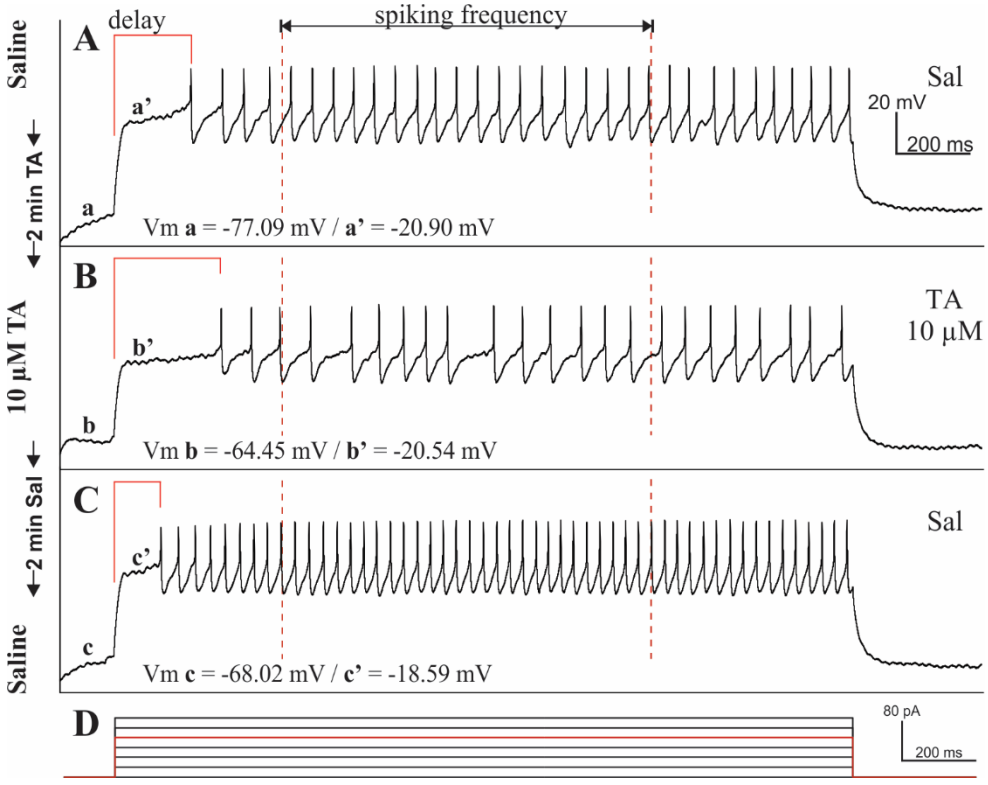

Figure 45: Firing pattern of MNISN-Is with a DmCa1D knockdown in a square pulse protocol.
Firing pattern of MNISN-Is upon a two-second 80 pA square pulse current injection in larvae carrying a DmCa1D knockdown. **A** Response to somatic current injection in standard saline with a well-described delay to the first AP. **B** 10 µM TA was applied for 2 min. The delay increased while the firing frequency decreased. **C** Washing in standard saline for 2 min entirely removed the effects of TA on the delay and the firing frequency. **D** Current injection steps. The step shown in A-C is marked in red.

Maybe due to the method of choosing the sweeps for analysis (results section 3.3), the average delay to the first AP and the average firing frequency were not significantly different from control values in the analyzed sweeps (delay: Mann-Whitney U-Test, p = 0.563; frequency: T-Test, p = 0.135; n = 9 / 21) (Figure 46). After bath application of TA for two minutes, the delay to the first AP was increased to 465 ± 372 ms (n = 9), and the firing frequency was reduced to 13.11 ± 5.10 Hz (n = 9). The effects were fully reversible. Two minutes after TA was washed out with standard saline, the delay to the first AP was reduced (347 ± 281 ms; n = 9), and the firing frequency was increased (17.22 ± 8.07 Hz; n = 9) (Figure 45).

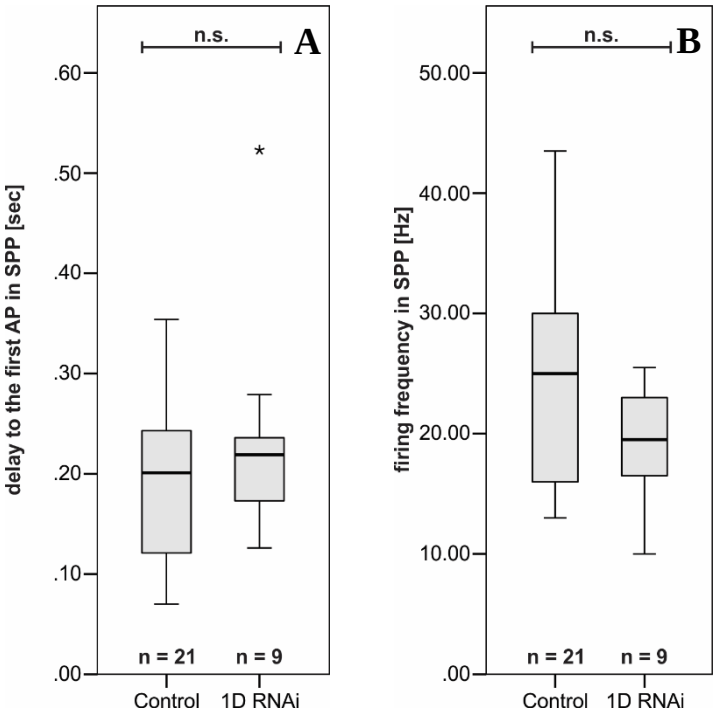

Figure 46: Statistical comparison between the delay to the first AP and the firing frequency of DmCa1D knockdowns and controls in square pulse protocols.

A The mean delay to the first AP of control cells in standard saline (201.45 ± 84.76 ms) was statistically compared to the mean delay of DmCa1D knockdown cells in standard saline (238 ± 109 ms; n = 9). A Mann-Whitney U-Test was carried out, which showed no significant difference between the genotypes (p = 0.563; n = 21, 9). **B** Statistical comparison between the average firing frequencies of control cells (24.14 ± 9.1 Hz) and DmCa1D knockdown cells (18.94 ± 5.52 Hz) in standard saline. A T-Test did not show a significant difference between the genotypes (p = 0.135; n = 9, 21).

For statistical analysis, data were normalized to the first value of the first run for each parameter. The normalized median for the delay to the first AP was 1.03 (Q1 = 0.89; Q3 = 1.04; n = 9) in standard saline, 1.87 (Q1 = 0.98; Q3 = 2.06; n = 9) in 10 µM TA, and 1.20 (Q1 = 0.66; Q3 = 1.64; n = 9) after TA has been washed out (Figure 47). The delay to the first AP tended to increase after TA was applied. Data also spread broader after bath-application of TA. Still, a Friedman-Test for the comparison of the delay to the first AP between all runs indicated no

significant differences (p = 0.070; n = 9) (Figure 47 A).

The normalized median of the firing frequency was 1.05 (Q1 = 1.02; Q3 = 1.10; n = 9) in standard saline, 0.75 (Q1 = 0.48; Q3 = 1.03; n = 9) in 10 µM TA, and 1.08 (Q1 = 0.59; Q3 = 1.56; n = 6) after TA was washed out for 2 min (Figure 47 B). Again, a tendency towards a reduced firing frequency and a broad spreading of the data could be seen after the application of TA. A one-way ANOVA with repeated measures was carried out to test for differences between the firing frequencies of the runs, which indicated no significant differences (p = 0.189; n = 9) (Figure 47 B).

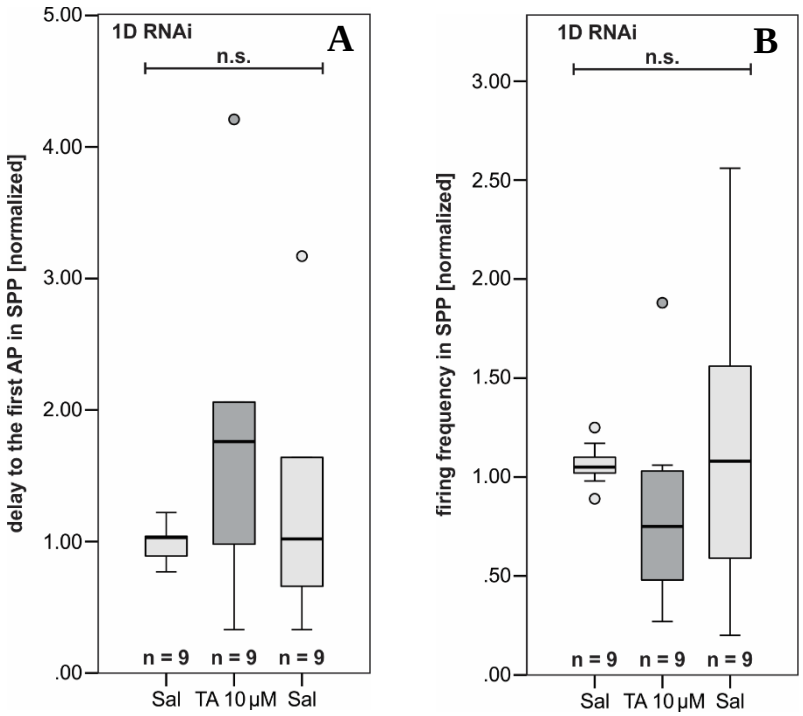

Figure 47: Statistical analysis of the delay to the first AP and the firing frequency in square pulse protocols in DmCa1D knockdowns.

A Analysis of the delay to the first AP. Although tendencies could be seen, a Friedman-Test showed no significant differences between the three runs before TA, with TA, and after TA was washed out (p = 0.070; n = 9). **B** Analysis of the firing frequency. The firing frequency was not significantly altered by TA, although tendencies were present (one-way ANOVA w. r. m., p = 0.189; n = 9).

In ramp pulse protocols, DmCa1D knockdowns also showed control-like firing properties (Figure 48). In standard saline, the delay to the first AP was on average 972 ± 169 ms (n = 9), and the firing frequency was on average 33.71 ± 4.13 Hz (n = 9). These values were not significantly different from the average control delay and firing frequency in standard saline (T-Test, delay p = 0.091; frequency p = 0.648; n = 9, 21) (Figure 49). Upon application of 10 µM TA, the delay to the first AP was only slightly increased to 1,043 ± 130 ms (n = 9), and the firing frequency was slightly decreased to 31.61 ± 4.51 Hz (n = 9).

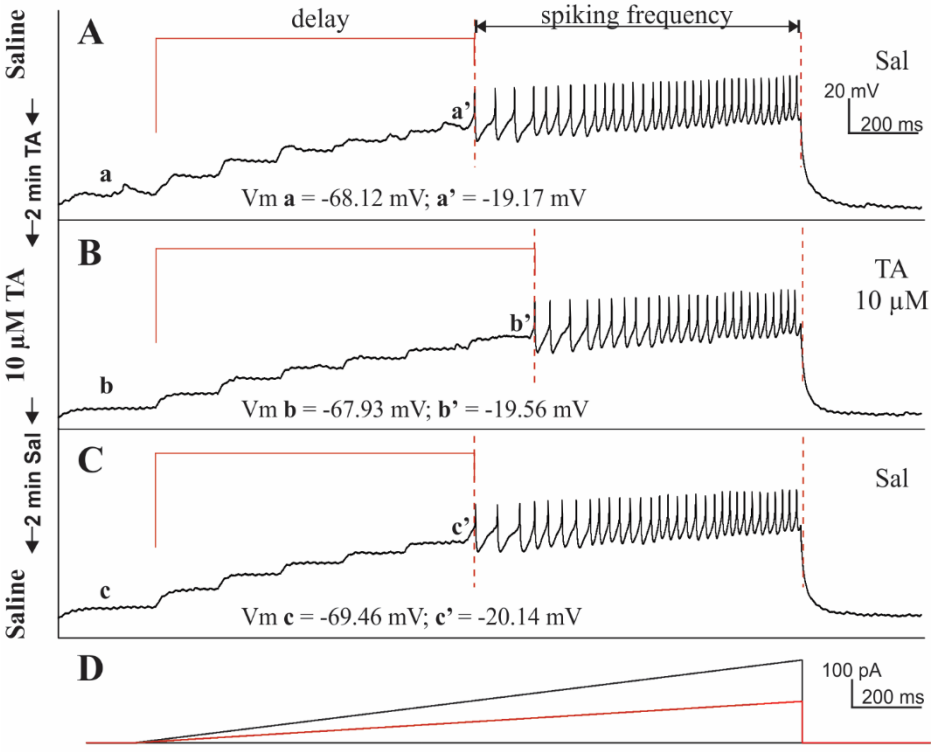

Figure 48: Firing pattern of MNISN-Is with a DmCa1D knockdown in a ramp pulse protocol.
Firing pattern of MNISN-Is upon a two-second ramp pulse current injection with a maximum of 150 pA in larvae carrying a DmCa1D knockdown. The delay was measured from the beginning of the current injection to the onset of the first AP. The firing frequency was measured from all spikes. **A** Response to current injection in standard saline. **B** 10 µM TA was applied for 2 min. The delay increased while the firing frequency decreased. **C** Washing in standard saline for 2 min entirely removed the effects of TA on the delay and the firing frequency. **D** Current injection ramps. The ramp shown in A-C is marked in red.

After washing TA out for two minutes, the mean delay to the first AP was 997 ± 146 ms (n = 9), and the firing frequency was 32.95 ± 5.55 Hz (n = 9) (Figure 48). For statistical analysis, data were normalized to the first value in the first run. For the statistical comparison of the normalized data of the parameters delay to the first AP and firing frequency, one-way ANOVAs with repeated measures were carried out. For both parameters, no significant differences were indicated between the three runs (delay p = 0.401; frequency p = 0.253; n = 9). The normalized median of the delay to the first AP was 1.00 (Q1 = 0.99; Q3 = 1.00; n = 9) in standard saline. It slightly increased upon application of TA (n. median = 1.14; Q1 = 1.00; Q3 = 1.19; n = 9), and it also slightly decreased after TA was washed out (n. median = 1.09; Q1 = 0.87; Q3 = 1.20; n = 9) (Figure 50 A).

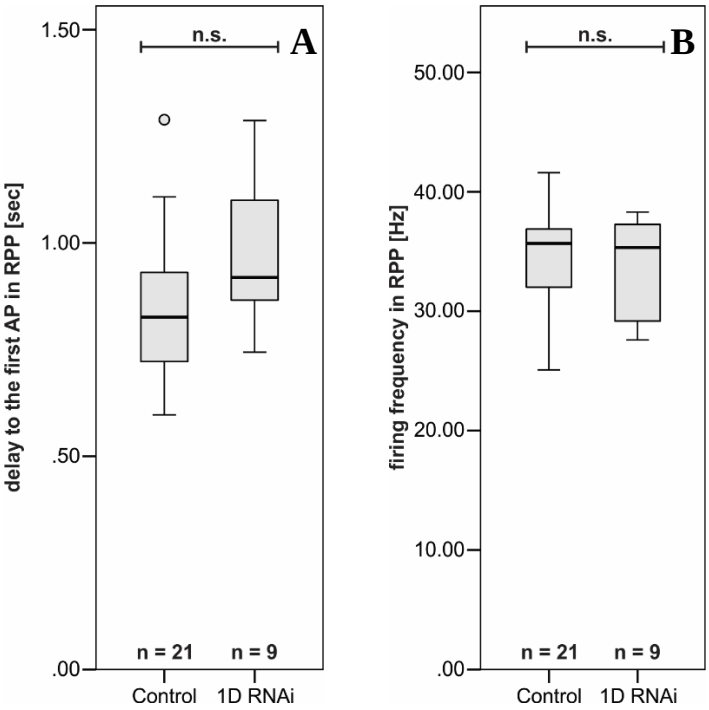

Figure 49: Statistical comparison between the delay to the first AP and the firing frequency of DmCa1D knockdowns and controls in ramp pulse protocols.

A Statistical comparison between the mean delays to the first AP of control cells (844.18 ± 172.3 ms) and DmCa1D knockdown cells (972 ± 169 ms; n = 9) in standard saline. A T-Test showed no significant difference between the genotypes (p = 0.091; n = 21, 9). **B** Statistical comparison between the mean firing frequencies of control cells (34.45 ± 3.75 Hz) and DmCa1D knockdown cells (33.71 ± 4.13 Hz) in standard saline. A T-Test did not show a significant difference between the genotypes (p = 0.648; n = 9, 21).

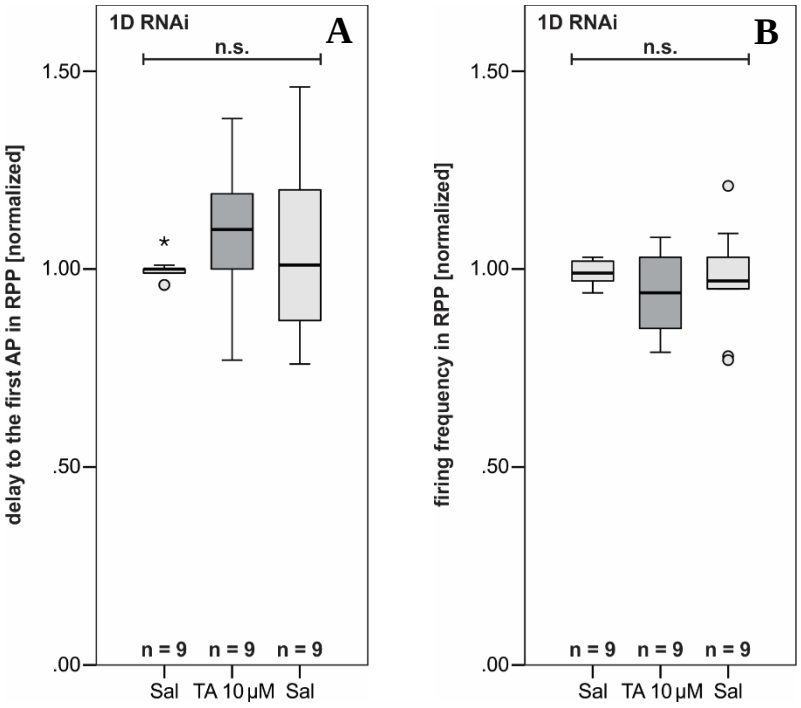

Figure 50: Statistical analysis of the delay to the first AP and the firing frequency in ramp pulse protocols in DmCa1D knockdowns.

A Analysis of the delay to the first AP. A one-way ANOVA w. r. m. did not indicate any significant differences between the three runs (p = 0.401; n = 9). **B** Analysis of the firing frequency. The firing frequency was not significantly altered by application or washing-out of 10 µM TA (one-way ANOVA w. r. m., p = 0.253; n = 9).

The firing frequency tended to be slightly reduced after TA was added to the bath (before TA n. median = 0.99; Q1 = 0.97; Q3 = 1.02; with TA n. median = 0.94; Q1 = 0.85; Q3 = 1.03; n = 9). It tended to increase again, after TA was washed out for two minutes (n. median = 0.97; Q1 = 0.95; Q3 = 1.03; n = 9) (Figure 50 B).

In comparison to control cells (results section 3.3), the reduction of intrinsic excitability was weaker in MNISN-Is motoneurons with a DmCa1D knockdown. Therefore, and together with the results acquired in calcium imaging experiments (results section 3.10.1), dendritically localized DmCa1D Ca^{2+} channels could clearly be suggested as targets for tyraminergic modulation (Heckman et al., 2008; Klein, 2016; Worrell & Levine, 2008).

3.12.2 Pharmacologically Blocking DmCa1D with La^{3+} Reduces Tyraminergic Modulation of MNISN-Is Excitability

Calcium imaging experiments (results section 3.10.1) and patch-clamp recordings (results section 3.12.1) indicated a role of the voltage-gated Ca^{2+} channel DmCa1D in the tyraminergic modulation of MNISN-Is excitability. In current-clamp experiments with cells carrying an RNAi knockdown of *DmCa1D*, developmental effects, like compensation for the lost channel or altered gene expression (Flavell & Greenberg, 2008; Marder & Goaillard, 2006), could neither be excluded nor detected. Therefore, an acute blocking of the channel was necessary to rule out any developmental side-effects. Lanthanum, La^{3+}, is suggested to be a specific blocker of DmCa1D channels (Klein, 2016), and was therefore used in further patch-clamp experiments. For all solutions with lanthanum, $LaCl_3$ was used. Canton S larvae were used in their L3 wandering stage for experiments. The first recordings were made in standard saline, followed by recordings in 1 µM La^{3+}, recordings in 1 µM La^{3+} together with 10 µM TA, and at last in standard saline again, which made up a total of four runs. Between the first and the second run, at least 3 min were given for incubation of La^{3+}. TA was incubated for 2 min, just as in control experiments.

In square pulse protocols, the delay to the first AP was on average 383 ± 95 ms (n = 10), and the firing frequency was 10.25 ± 3.58 Hz (n = 10) in standard saline (Figure 51). After bath-application and incubation of La^{3+} for 3 min, the mean delay decreased to 234 ± 106 ms (n = 10), whereas the firing frequency increased to 14.20 ± 2.95 Hz (n = 10). Additional bath-application of 10 µM TA slightly increased the delay (238 ± 142 ms; n = 10), and decreased the firing frequency (11.05 ± 2.51 Hz; n = 10). Washing TA out with standard saline for 2 min reversed the effect of TA, but not of La^{3+}. The delay to the first AP was 211 ± 150 ms (n = 10),

and the firing frequency was 16 ± 3.66 Hz (n = 10) (Figure 51).

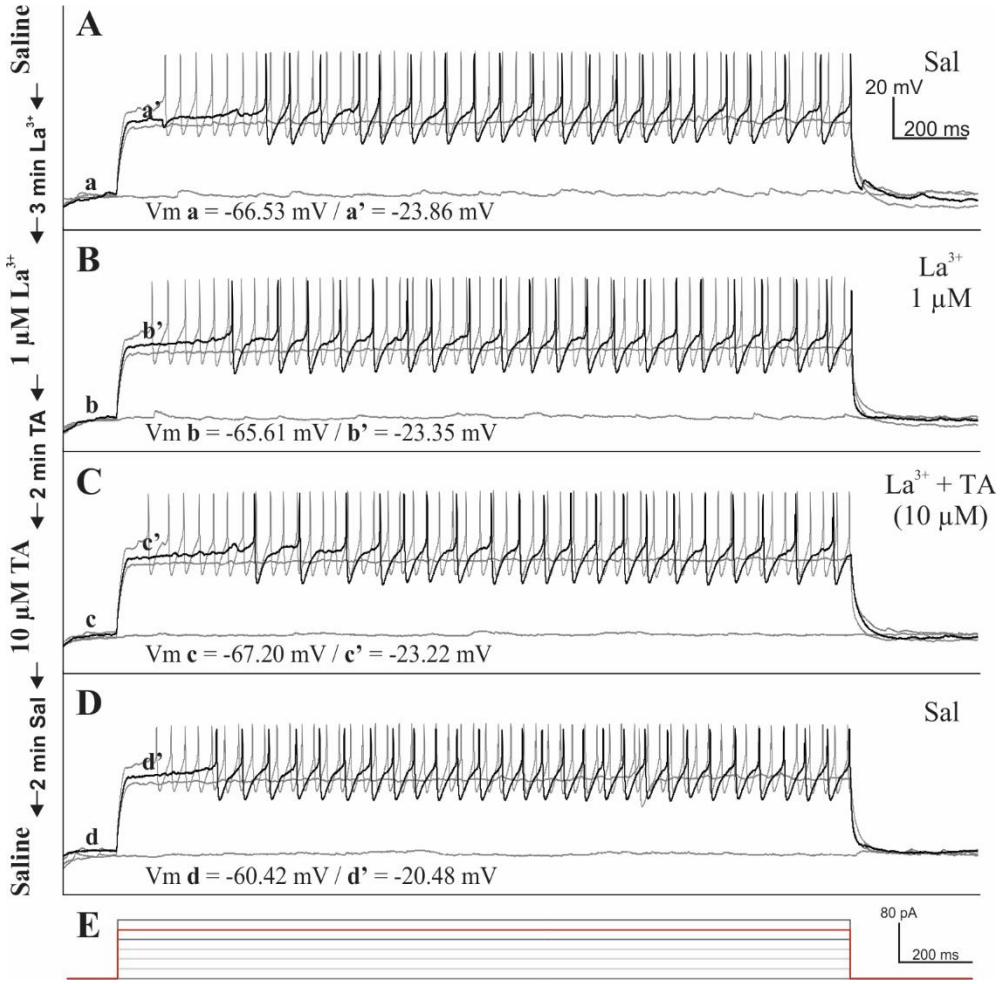

Figure 51: Firing pattern of MNISN-Is with the pharmacological blocking of DmCa1D during recording in a square pulse protocol.
Firing pattern of MNISN-Is upon a two-second somatic square pulse current injection. Sweeps with 0, 80, 100, and 120 pA current injection are shown. **A** Response to current injection in standard saline. **B** 1 µM La^{3+} was bath-applied for 3 min. The delay to the first AP was decreased. **C** La^{3+} and 10 µM TA were applied for 2 min. The delay slightly increased while the firing frequency slightly decreased. **D** Washing in standard saline for 2 min fully removed the effects of TA but not of La^{3+} on the delay and the firing frequency. **E** Current injection steps with 20 pA increments. The steps shown in A-D are marked in dark grey and red.

Again, for statistical analysis, all data were normalized to the first value of the first run for each parameter. Friedman-Tests were carried out to compare the delays to the first AP and the firing frequencies of all four runs. The tests indicated significant differences between the runs for the delay to the first AP (p = 0.009; n = 10), and for the firing frequency (p = 0.002; n = 10) (Figure 52). Pairwise follow-up comparisons between the single runs were conducted to locate the differences. The normalized delay to the first AP was 1.08 (Q1 = 0.91; Q3 = 1.63; n = 10), and the normalized firing frequency was 0.94 (Q1 = 0.83; Q3 = 1.03; n = 10) in standard saline. After the bath-application of 1 µM La^{3+}, the delay was slightly but not significantly decreased (n. median = 0.61; Q1 = 0.52; Q3 = 0.92; n = 10) (pairwise follow-up comparison, p = 0.146;

n = 10), while the firing frequency was slightly but not significantly increased (n. median = 1.25; Q1 = 1.09; Q3 = 1.56; n = 10) (pairwise follow-up comparison, p = 0.116; n = 10). The delay to the first AP was slightly but not significantly increased upon switching the perfusion to 1µM La^{3+} together with 10 µM TA (n. median = 0.72; Q1 = 0.65; Q3 = 1.61; n = 10) (pairwise follow-up comparison, p = 0.995; n = 10), while the firing frequency was slightly but not significantly decreased (n. median = 1.02; Q1 = 0.84; Q3 = 1.22; n = 10) (pairwise follow-up comparison, p = 0.278; n = 10). To remove TA, the preparations were washed with standard saline for 2 min, which resulted in a not significant decrease of the delay to the first AP (n. median = 0.60; Q1 = 0.21; Q3 = 1.09; n = 10) (pairwise follow-up comparison, p = 0.146; n = 10), and a significant increase in the firing frequency (n. median = 1.34; Q1 = 1.11; Q3 = 2.21; n = 10) (pairwise follow-up comparison, p = 0.026; n = 10). The delay to the first AP was significantly shorter in the last run than in the first (pairwise follow-up comparison, p = 0.011; n = 10). The firing frequency was also significantly higher in the last run compared to the first (pairwise follow-up comparison, p = 0.008; n = 10) (Figure 52).

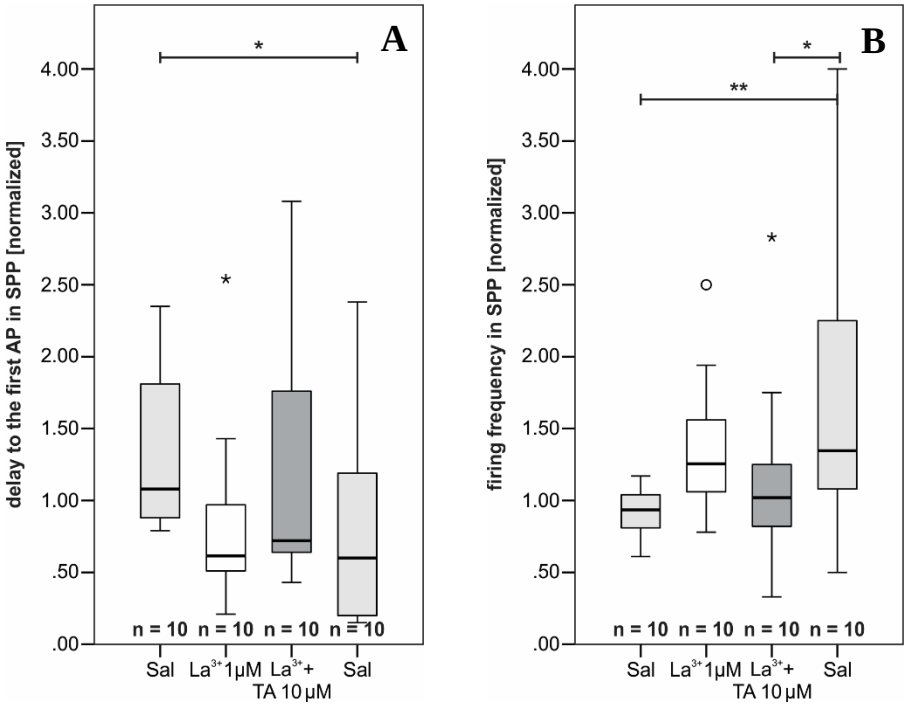

Figure 52: Statistical analysis of the delay to the first AP and the firing frequency in square pulse protocols in Canton S with pharmacologically blocked DmCa1D channels.

A Analysis of the delay to the first AP (F.-T., p = 0.009; n = 10). Pairwise follow-up comparisons showed that the delay decreased slightly but not significantly upon application of La^{3+} (p = 0.146; n = 10), and it increased slightly but not significantly after TA was additionally added (p = 0.995; n = 10). After TA was washed out by standard saline, the delay tended to decrease again, which was also not significant (follow-up, p = 0.146; n = 10). The delay was significantly shorter in the last run than in the first run before La^{3+} was applied (follow-up, p = 0.011; n = 10). **B** Analysis of the firing frequency (F.-T., p 0.002; n = 10). Pairwise follow-up comparisons showed that after La^{3+} was applied to the bath, the firing frequency was slightly but not significantly increased (p = 0.116; n = 10). Upon application of La^{3+} together with TA, the firing frequency decreased slightly but not significantly (follow-up, p = 0.278; n = 10). It significantly increased after TA was washed out (follow-up, p = 0.026), and was therefore significantly higher than in the first run (follow-up, p = 0.008; n = 10).

In ramp pulse protocols, the delay to the first AP was on average 1,017 ± 122 ms (n = 10), and the mean firing frequency was 31.74 ± 2.55 Hz (n = 10) (Figure 53). Like in square pulse protocols, the delay to the first AP was reduced to 956 ± 131 ms (n = 10) after bath-application of La^{3+}. The firing frequency was hardly altered (31.83 ± 2.00 Hz; n = 10). Application of 10 µM TA had only little effect on the delay and the firing frequency. The mean delay was 982 ± 152 ms (n = 10), and the firing frequency was 31.06 ± 2.21 Hz (n = 10) after addition of TA. However, washing TA out slightly reduced the mean delay to the first AP (915 ± 168 ms; n = 10), and it slightly increased the firing frequency (32.18 ± 3.31 Hz; n = 10) (Figure 53).

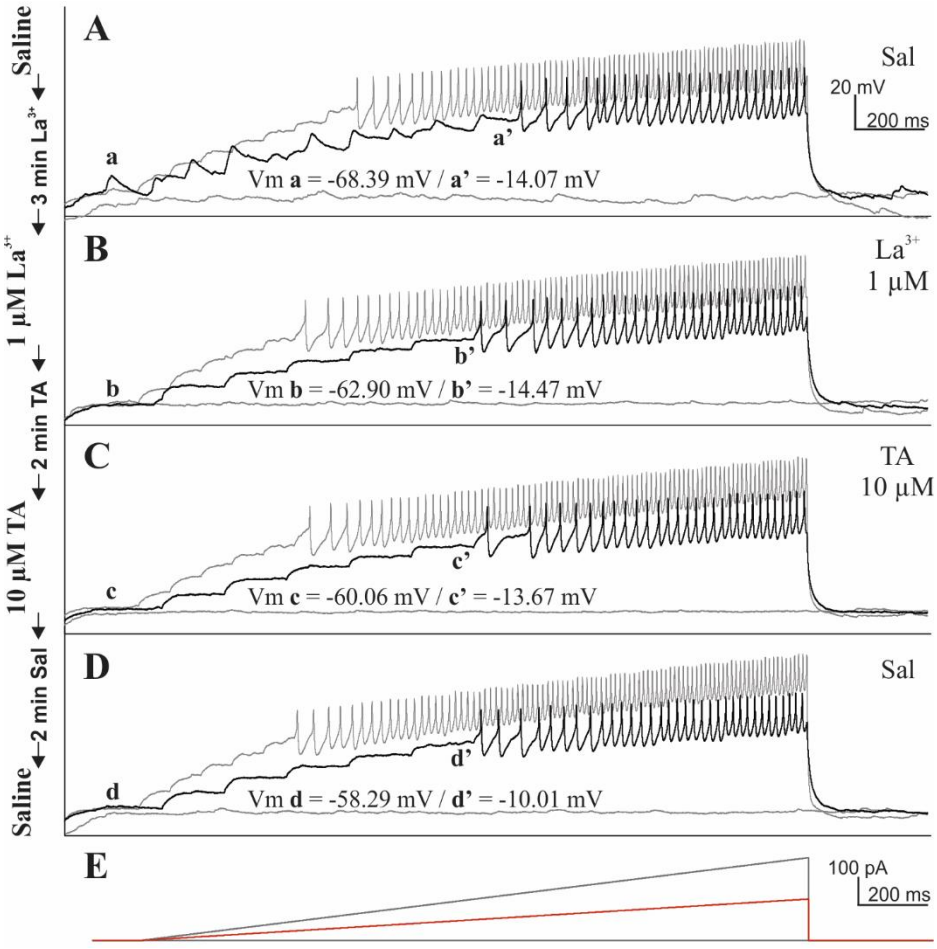

Figure 53: Firing pattern of MNISN-Is with the pharmacological blocking of DmCa1D during recordings in a ramp pulse protocol.
Firing pattern of MNISN-Is upon a two-second somatic ramp pulse current injection. Sweeps with no current injection, and with maxima of 150, and 300 pA are shown. **A** Response to current injection in standard saline. **B** 1 µM La^{3+} was bath-applied for 3 min. The delay to the first AP was decreased. **C** La^{3+} and 10 µM TA were applied for 2 min. The delay and the firing frequency were hardly altered. **D** Washing in standard saline for 2 min had only little effect on the delay and the firing frequency. **E** Current injection ramps. The ramps shown in A-D are marked in dark grey and red.

For statistical analysis, all data were normalized to the first value of the first run for both parameters. Accordingly, the normalized median of the delay to the first AP was 0.99 (Q1 = 0.98; Q3 = 1.00; n = 10), and the normalized median of the firing frequency was 1.00 (Q1 = 0.97; Q3 = 1.01; n = 10). One-way ANOVAs with repeated measures were conducted to test for differences between the four runs. They indicated a significant difference for the delay to the first AP (p = 0.028; n = 10), but not for the firing frequency (p = 0.321; n = 10) (Figure 54). As shown by a pairwise follow-up comparison, the delay was significantly reduced after La^{3+} was applied (n. median = 0.94; Q1 = 0.90; Q3 = 0.98; n = 10) (pairwise follow-up comparison, p = 0.026; n = 10), but it was neither significantly altered by additional application of TA (n. median = 0.95; Q1 = 0.92; Q3 = 1.00; n = 10) (pairwise follow-up comparison, p = 1.000; n = 10), nor by the washout of TA afterward (n. median = 0.91; Q1 = 0.82; Q3 = 0.99; n = 10) (pairwise follow-up comparison, p = 0.315; n =10).

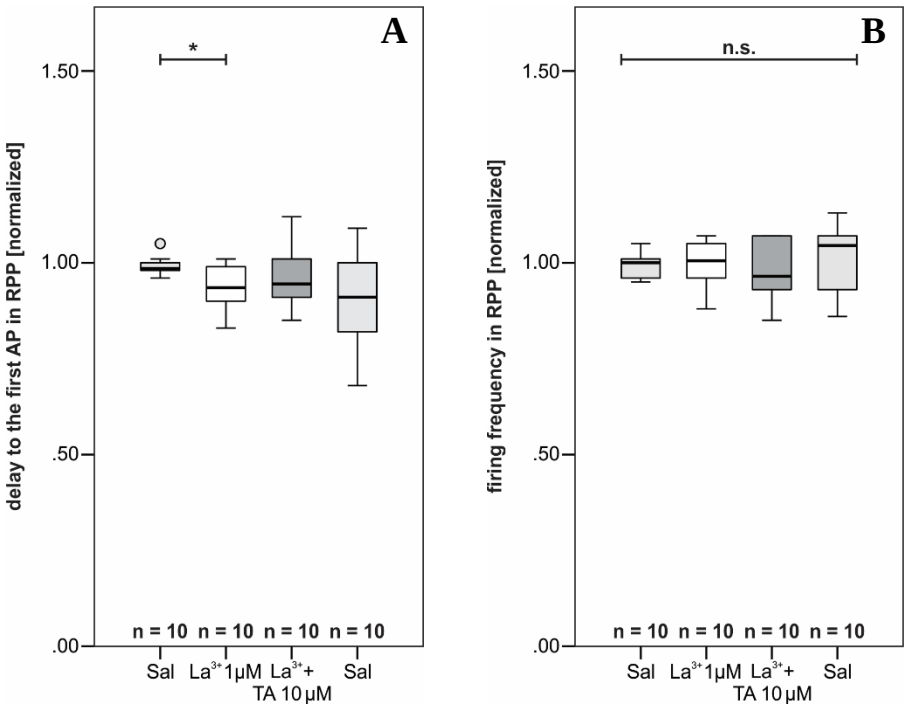

Figure 54: Statistical analysis of the delay to the first AP and the firing frequency in ramp pulse protocols in Canton S with the pharmacological blockade of DmCa1D channels.
A Analysis of the delay to the first AP (one-way ANOVA w. r. m., p = 0.028; n = 10). Due to the pairwise follow-up comparison, the delay was significantly shorter after La^{3+} was applied (p = 0.026; n = 10). Other than that, it was not significantly altered in any run. **B** Analysis of the firing frequency. The firing frequency was not significantly altered by application of either La^{3+} or La^{3+} and TA (one-way ANOVA w. r. m., p = 0.321; n = 10).

The firing frequency hardly showed any tendency to be altered in any of the four runs, which were before La^{3+}, with 1 µM La^{3+} (n. median = 1.00; Q1 = 0.97; Q3 = 1.04; n = 10); with La^{3+} and 10 µM TA (n. median = 0.97; Q1 = 0.94; Q3 = 1.05; n = 10), and after washing TA out (n.

median = 1.04; Q1 = 0.95; Q3 = 1.07; n = 10) (Figure 54).

Not only knocking down *DmCa1D* encoded Ca^{2+} channels, but also the acute blocking of those channels with La^{3+} reduced tyraminergic effects. Bath-application of TA did not reduce intrinsic MNISN-Is excitability after DmCa1D channels were blocked. These results reinforce the suggestion of DmCa1D being a target of tyraminergic modulation.

3.12.3 Knocking Down DmCa1A Reduces Tyraminergic Modulation of MNISN-Is in Ramp Pulse Protocols

DmCa1A, also called cacophony, is a VGCC which is known to be localized to neuromuscular presynapses (Kawasaki et al., 2004; Klein, 2016), as well as for mediating somatodendritic HVA and LVA Ca^{2+} currents in adult flight motoneurons (Ryglewski et al., 2012). In larval motoneurons, DmCa1A might play a role in shaping cellular firing properties, which is why a dendritically localization was suggested (Worrell & Levine, 2008). The knockdown of DmCa1A was therefore tested to confirm whether tyramine also modulated this Ca^{2+} channel. A fly strain carrying the UAS-*cac*-RNAi was crossed to both our *RN2*-GAL4 driver-line with GFP (Line 20) (n = 4) and the *OK37-1*-GAL4 driver-line (Line 21) (n = 7).

Line 20

$$w^{*}\,;\ \frac{\mathrm{RN2-GAL4,UAS-mCD8::GFP}}{\mathrm{P\{KK101478\}VIE-260B}}\ ;\ \frac{\mathrm{Act<Stop>GAL4,UAS-FLP}}{+}\ ;\ +$$

Line 21

$$w^{*}\,;\ \frac{\mathrm{OK37-1-GAL4}}{\mathrm{P\{KK101478\}VIE-260B}}\ ;\ +\ ;\ +$$

Wandering L3 larvae of both lines were randomly picked for experiments. For all recordings, MNISN-Is motoneurons were thoroughly identified and picked for patch-clamp experiments. The mean delay to the first AP was 187 ± 59 ms (n = 11), and the mean firing frequency was 20.32 ± 4.78 Hz (n = 11) in standard saline (Figure 55). Both parameters were not significantly different from control values (T-Test, delay p = 0.625; frequency p = 0.142; n = 11, 21). After TA was bath-applied for two minutes, the mean delay to the first AP increased to 287 ± 122 ms (n = 11), and the mean firing frequency decreased to 15.09 ± 5.64 Hz (n = 11). TA could be washed out with standard saline.

After two minutes, the delay to the first AP was reduced to 189 ± 61 ms (n = 11), and the firing frequency was increased to 20.36 ± 5.07 Hz (n = 11) (Figure 55).

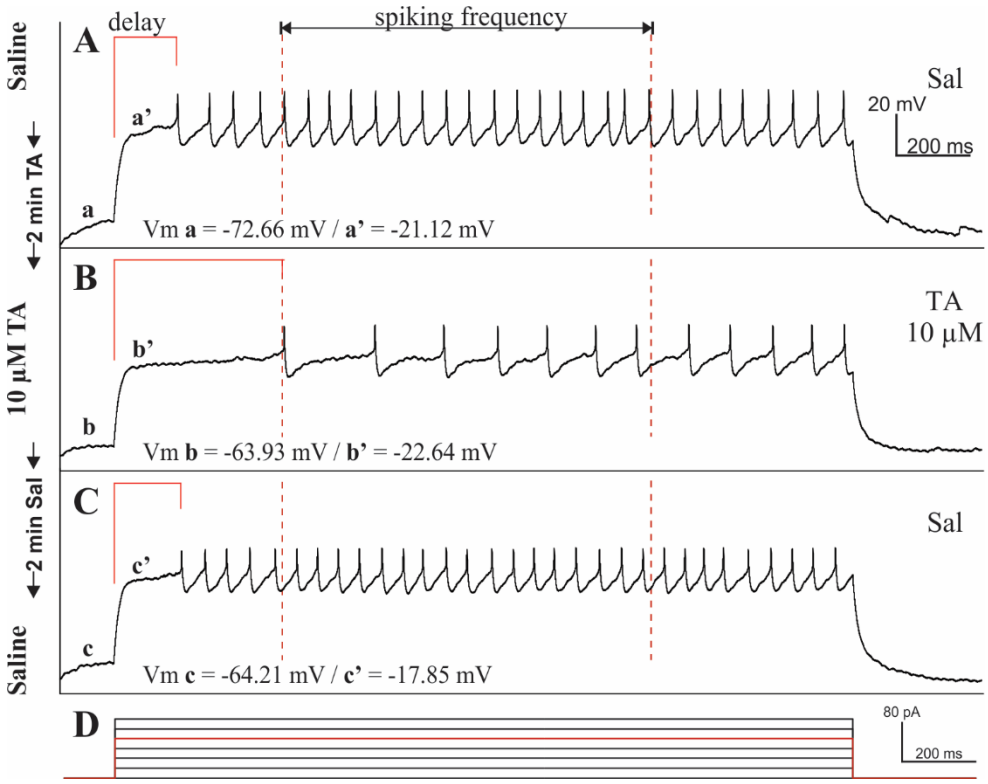

Figure 55: Firing pattern of MNISN-Is with a DmCa1A knockdown in a square pulse protocol.
Firing pattern of MNISN-Is upon a two-second 80 pA square pulse current injection in larvae carrying a DmCa1A knockdown. The delay was measured from the beginning of the depolarization to the onset of the first AP (red lines). The firing frequency was measured from one second of the response (red dashed lines) **A** Response to somatic current injection in standard saline. **B** 10 µM TA was applied for 2 min. The delay increased while the firing frequency decreased. **C** Washing in standard saline for 2 min entirely removed the effects of TA on the delay and the firing frequency. **D** Current injection steps with 20 pA increments. The step shown in A-C is marked in red.

For statistical analysis, all data were normalized to the first respective value of the first run. The delay to the first AP had a normalized median of 1.00 (Q1 = 1.00; Q3 = 1.35; n = 11). After TA was bath-applied, the delay increased to 2.14 (n. median; Q1 = 1.30; Q3 = 2.35; n = 11). Washing TA out with standard saline for two minutes led to a decrease of the delay to the first AP (n. median = 0.97; Q1 = 0.87; Q3 = 1.68; n = 11). For comparison of the delays of the three runs, a Friedman-Test was carried out. Due to this test, none of the changes in the delay to the first AP between the runs were significant (p = 0.060; n = 11) (Figure 56 A).

These findings were reflected in the firing frequencies measured in square pulse recordings. For comparison, all data were normalized, which resulted in a normalized median of 1.00 in standard saline (Q1 = 0.90; Q3 = 1.00; n = 11). A one-way ANOVA with repeated measures indicated a significant difference between the three runs (p = 0.020; n = 11).

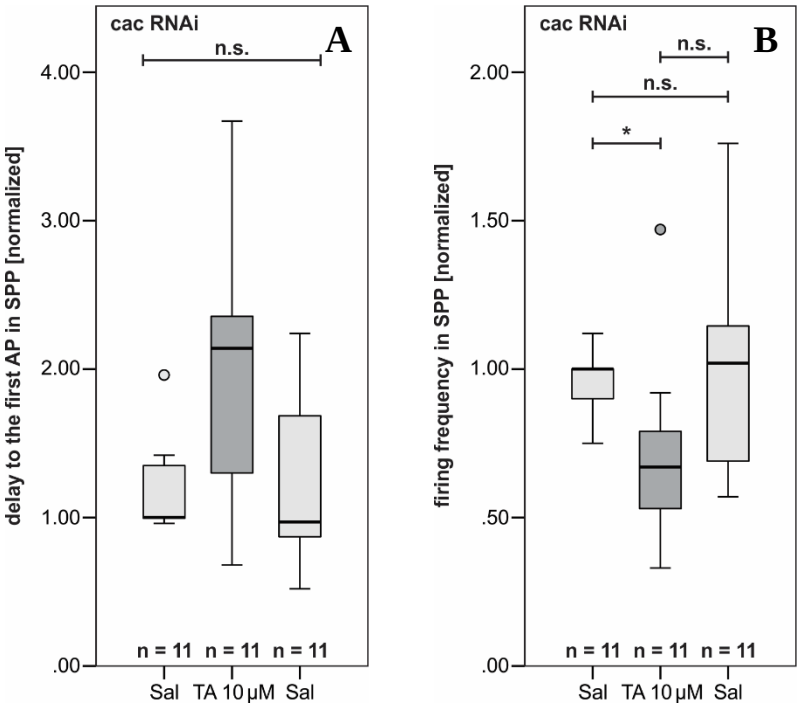

Figure 56: Statistical analysis of the delay to the first AP and the firing frequency in square pulse protocols in DmCa1A knockdowns.
A Analysis of the delay to the first AP. Although clear tendencies could be seen, a Friedman-Test did not indicate any significant changes in the delay between the three runs (p = 0.060; n = 11). **B** Analysis of the firing frequency. A one-way ANOVA w. r. m. indicated a significant difference in the firing frequency between the three runs (p = 0.020; n = 11). It significantly decreased after TA was applied (pairwise follow-up comparison, p = 0.043; n = 11), but it did not significantly increase after TA was washed out (pairwise follow-up comparison, p = 0.099; n = 11). The frequency of the third run was not significantly different from the first run (pairwise follow-up comparison, p = 1.000; n = 11).

Pairwise follow-up comparisons showed that the firing frequency was significantly reduced upon application of TA (n. median = 0.67; Q1 = 0.53; Q3 = 0.79; n = 11) (p = 0.043; n = 11), but not significantly increased after TA was washed out (n. median = 1.02; Q1 = 0.69; Q3 = 1.14; n = 11) (p = 0.099; n = 11). The firing frequency of the third run, after the removal of TA, was not significantly different from the first one, before the application of TA (p = 1.000; n = 11) (Figure 56 B).

In ramp pulse protocols, the average delay to the first AP was 944 ± 153 ms (n = 11), and the average firing frequency was 36.06 ± 5.00 Hz (n = 11) in standard saline (Figure 57). Both mean values were not significantly different from control values (T-Test, delay p = 0.128; frequency p = 0.329; n = 11, 21). After bath-application of TA, the delay was only slightly increased (1,029 ± 186 ms; n = 11), while the firing frequency was slightly decreased (34.13 ± 5.87 Hz; n = 11). After washing TA out with standard saline for 2 min, the delay to the first AP was 953 ± 192 ms (n = 11), and the firing frequency was 35.68 ± 6.38 Hz (n = 11) (Figure 57).

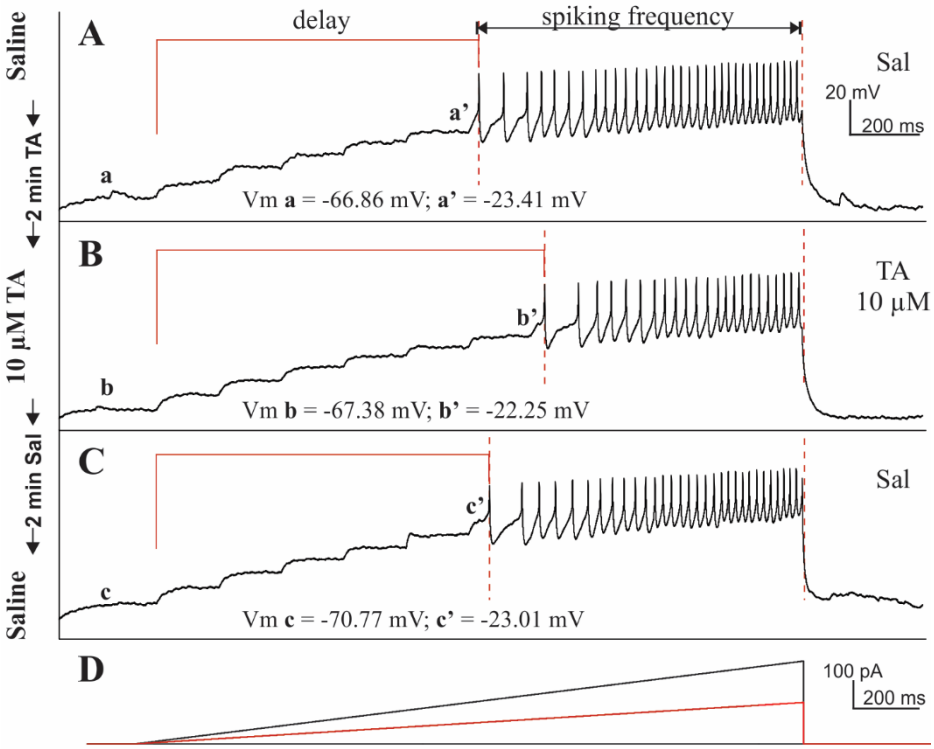

Figure 57: Firing pattern of MNISN-Is with a DmCa1A knockdown in a ramp pulse protocol.
Firing pattern of MNISN-Is upon a two-second somatic ramp current injection with a maximum of 150 pA in larvae carrying a DmCa1A knockdown. The delay was measured from the beginning of the depolarization to the onset of the first AP (red lines). The firing frequency was measured from all spikes (red dashed lines) **A** Response to current injection in standard saline. **B** 10 µM TA was applied for 2 min. The delay slightly increased while the firing frequency slightly decreased. **C** Washing in standard saline for 2 min entirely removed the effects of TA on the delay and the firing frequency. **D** Current injection ramps. The ramp shown in A-C is marked in red.

The normalized median of the delay to the first AP was 1.00 (Q1 = 0.99; Q3 = 1.00; n = 11) in standard saline. It was hardly increased after TA was applied (n. median = 1.01; Q1 = 0.97; Q3 = 1.21; n = 11), or decreased after TA was washed out (p = 1.01; Q1 = 0.92; Q3 = 1.04; n = 11). A one-way ANOVA with repeated measures was carried out to statistically compare the delays, which showed no significant difference between the three runs (p = 0.082; n = 11) (Figure 58 A).

To compare the firing frequencies of the ramps, a Friedman-Test was carried out, which showed no significant differences between the three runs (p = 0.148; n = 11) (Figure 58 B). The normalized median of the firing frequency was 1.00 (n. median; Q1 = 0.99; Q3 = 1.00; n = 11) in standard saline. It was slightly reduced upon application of TA (n. median = 0.94; Q1 = 0.90; Q3 = 1.02; n = 11), and similarly little increased after TA was washed out (n. median = 1.02; Q1 = 0.90; Q3 = 1.05; n = 11).

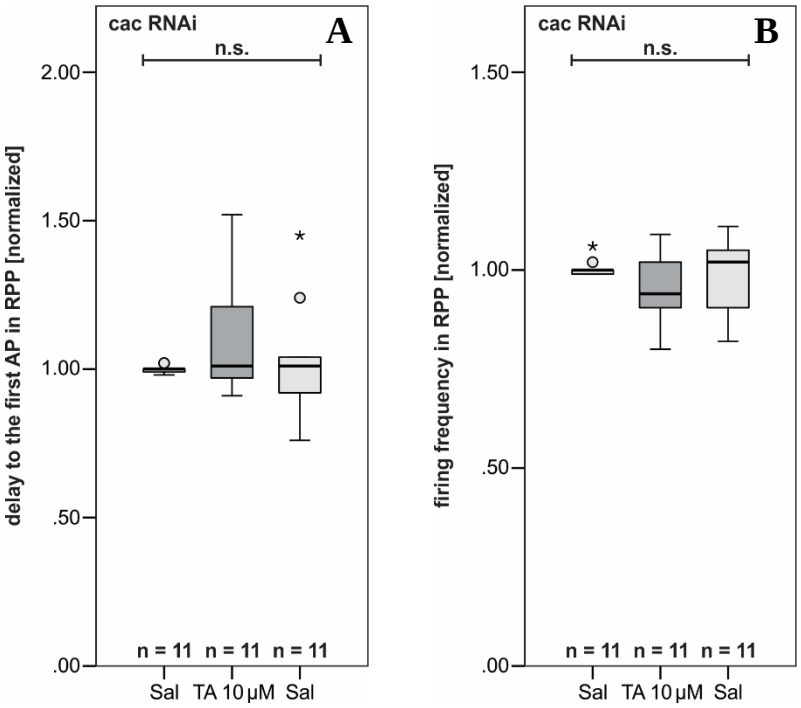

Figure 58: Statistical analysis of the delay to the first AP and the firing frequency in ramp pulse protocols in DmCa1A knockdowns.
A Analysis of the delay to the first AP. For the delay, no significant difference could be found between the three runs (one-way ANOVA w. r. m., p = 0.082; n = 11). **B** Analysis of the firing frequency. For the firing frequency, no significant difference could be found between the three runs (F.-T., p = 1.000; n = 11).

DmCa1A seemed to contribute to intrinsic excitability since modulatory effects of TA were inhibited in ramp current injections in DmCa1A knockdowns. However, in square pulse current injections, TA still showed modulatory effects.

3.13 Calcium Imaging in Larvae Lacking DmCa1D

3.13.1 Knocking Down DmCa1D Reduces the Downregulation of Ca^{2+} Influx into MNISN-Is Dendrites

To further investigate the contribution of DmCa1D to tyraminergic modulation, calcium imaging experiments were repeated with a DmCa1D knockdown. Since a GAL4 driver, as well as a UAS-*GCaMP6* construct and the UAS-*DmCa1D*-RNAi were necessary, a different *RN2*-GAL4 driver-line without GFP was used. This line was recombined to also carry UAS-*GCaMP6s* on the second chromosome and could directly be crossed to the previously used UAS-*DmCa1D*-RNAi (Line 22).

Line 22

$$w^{*}\ y^{*}\ sc^{*}\ v^{*};\ \frac{RN2-GAL4,UAS-GCaMP6s}{+};\ \frac{Act<Stop>GAL4,UAS-FLP}{P\{TRiP.HMS00294\}attP2};\ +$$

In all larvae, a mosaic pattern of single GCaMP6s-positive MN1-Ib (aCC) and MNISN-Is (RP2) motoneurons expressing the *DmCa1D*-RNAi could be found. The base fluorescence of GCaMP was used to identify MNISN-Is motoneurons. The experimental procedure was done as described (methods section 2.4.2). Upon single puffs of nicotine onto the dendrites, an instant increase of fluorescence could be seen. The fluorescence was rather weak in the dendrites and could be mainly seen in the somata and the primary neurites (Figure 60 A, column three). The fluorescence was measured from the dendrites and statistically analyzed afterward.

In standard saline, the mean increase in fluorescence, ΔF/F, was 0.58 ± 0.10 (n = 16) (Figure 59), which was not significantly different from the control value (T-Test, p = 0.078; n = 16, 16). Bath-application of 10 µM TA reduced the mean increase in fluorescence to 0.49 ± 0.13 (n = 16). After TA was washed out for two minutes, the mean increase in fluorescence was further reduced to 0.46 ± 0.10 (n = 16).

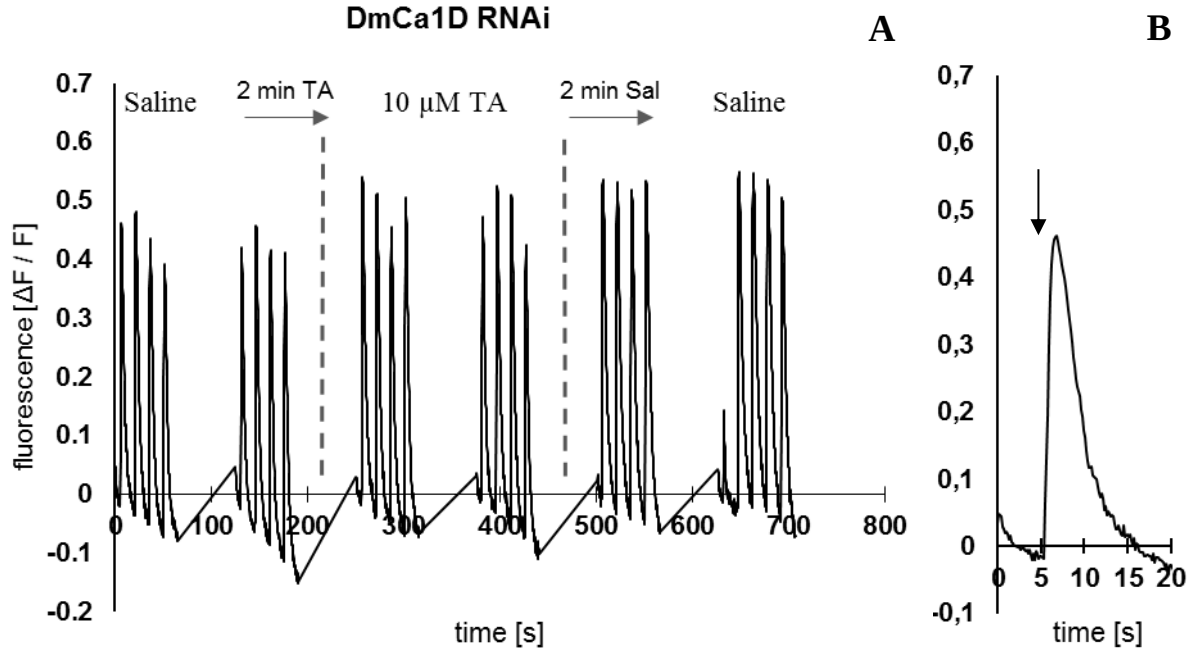

Figure 59: Raw data of the changes in fluorescence (ΔF/F) in DmCa1D knockdown cells.
A One Ca^{2+} imaging analysis with a set of six separate consecutive recordings is shown, which had no run-down. Two sets of recordings were carried out in standard saline, 10 µM TA, and in standard saline after washing TA out. Each set was one minute apart. For the graphical representation, the data has been merged, and one-minute pauses were inserted manually. TA was applied for 2 min and washed out for 2 min (dashed lines). Each peak is the rapid increase in fluorescence due to Ca^{2+} influx initiated by a nicotine puff. Puffs were given in intervals of 15 s. The increase in fluorescence is not altered after application of 10 µM TA. Only the last four intensity peaks of each set were included in the analysis. **B** Example response to one nicotine puff. First peak of the first recording of A in standard saline. The nicotine puff was given at 5 s (arrow).

For statistical analysis, all data were normalized to the first value of the first run in standard saline. A one-way ANOVA with repeated measures was conducted to test for significant differences between the normalized increases in fluorescence of the three runs. The ANOVA showed a significant difference between the runs, which were before TA (n. median = 0.97; n = 16), with TA (n. median = 0.84; n = 16), and after washing TA out (n. median = 0.75; n = 16) (p = 0.001; n = 16). Pairwise follow-up comparisons showed that the increase in fluorescence upon stimulation was significantly weaker after TA was applied (pairwise follow-up comparison, p = 0.003; n = 16). The value was not significantly altered after TA was washed out (pairwise follow-up comparison, p = 1.000; n = 16). Yet, after TA was washed out (third run), the increase in fluorescence was significantly weaker than before the application of TA (first run) (pairwise follow-up comparison, p = 0.010; n = 16) (Figure 60).

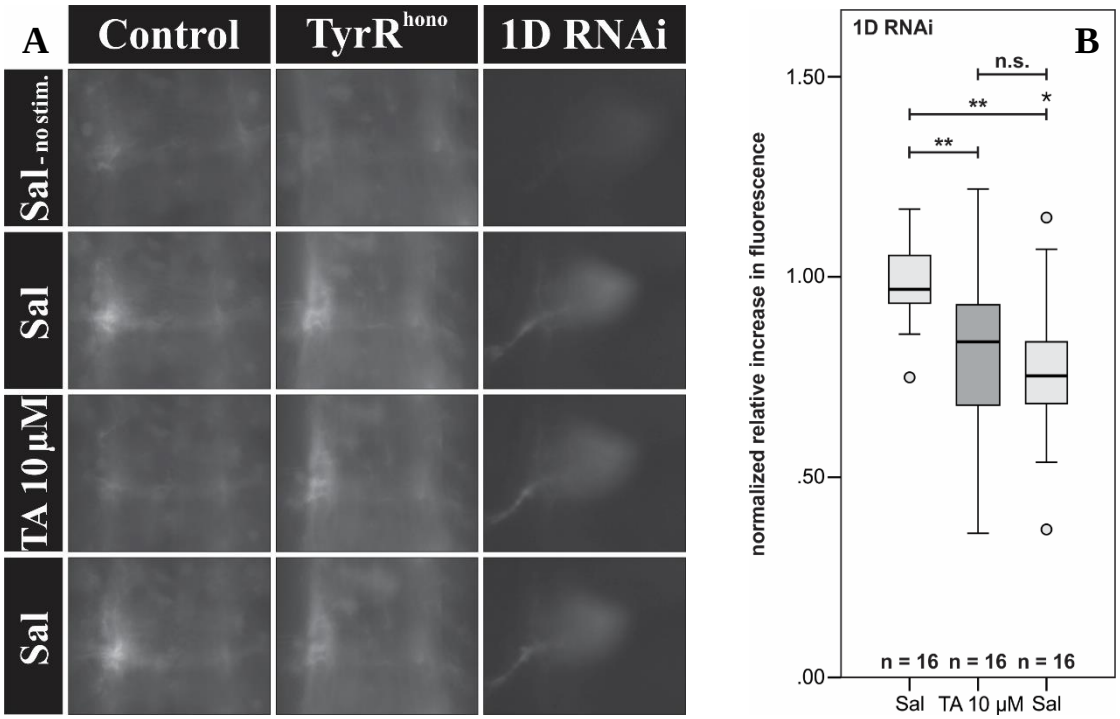

Figure 60: Intensity of fluorescence upon nicotine puffs in DmCa1D knockdowns.
A Example of the intensity of fluorescence in single video frames. Each picture except for the first of each column was taken directly after a nicotine puff. The third column shows a high magnification of a single MNISN-Is. **B** Statistical analysis of the intensity of fluorescence. A one-way ANOVA w. r. m. indicated a significant difference between the three runs (p = 0.001; n = 16). The fluorescence was significantly weaker after TA was applied (pairwise follow-up comparison, p = 0.003; n = 16). The fluorescence was not significantly weaker after TA was washed out (pairwise follow-up comparison, p = 1.000; n = 16). The fluorescence was significantly lower in the third run than in the first (pairwise follow-up comparison, p = 0.010; n = 16).

In control experiments, no run-down could be seen (results section 3.10.1). Therefore, data were reduced to include only those values, in which the mean increase in fluorescence of the third run was at least 75 % of the first run. By doing so, the mean increase in fluorescence was 0.56 ± 0.09 (n = 8) in standard saline, 0.50 ± 0.11 (n = 8) after bath-application of TA, and 0.52 ±

0.09 (n = 8) after washing TA out (Figure 59). For a second statistical analysis, also only the normalized data of this reduced group were used. The normalized median of the first run was 1.00 (n = 8). A Friedman-Test did not indicate any significant differences between the runs (p = 0.223; n = 8). The fluorescence was still slightly but not significantly decreased after TA was applied for 2 min (n. median = 0.90; n = 8), and it decreased further but also not significantly after TA was washed out (n. median = 0.84; n = 8) (Figure 61).

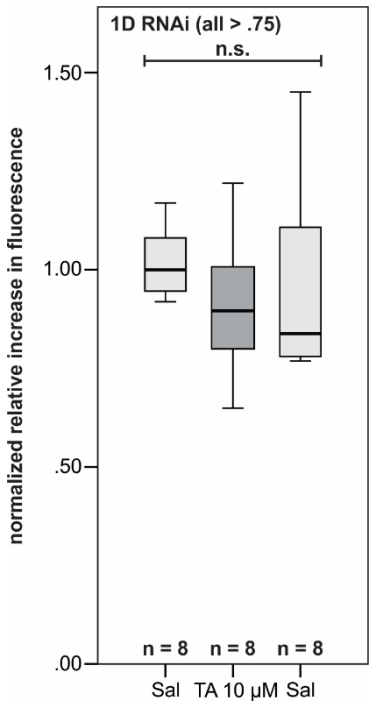

Figure 61: Statistical analysis of the fluorescence in DmCa1D knockdowns.
Only such cells were chosen for this analysis, in which the fluorescence of the last run was not further decreased than 75 % of the first run. A Friedman-Test did not indicate any significant differences between the three runs (p = 0.223; n = 8).

Due to the knockdown of DmCa1D, the dendritic Ca^{2+} influx was disturbed, which resulted in a run-down of the signal over time. Nevertheless, the dendritic Ca^{2+} influx seemed not to be significantly downregulated by TA.

3.13.2 Blocking DmCa1D with La^{3+} Reduces the Downregulation of Dendritic Ca^{2+} Influx upon Application of TA

Again, to rule out any developmental effects upon knocking-down DmCa1D genetically, La^{3+} was utilized as an acute DmCa1D blocker during the experiments. As controls, an *RN2*-GAL4 driver-line without GFP was crossed to UAS-*GCaMP6m* for better comparability with the previous control experiments (Line 23, results section 3.10).

Line 23

$$w^{*}\,;\,\frac{RN2-GAL4}{P\{20XUAS-IVS-GCaMP6m\}attP40}\,;\,\frac{Act<Stop>GAL4,UAS-FLP}{+}\,;\,+$$

The first video recordings were carried out in standard saline. After that, 1 µM La^{3+} was applied to the bath and incubated for 3 min. Subsequently, 10 µM TA was applied together with 1 µM La^{3+} for 2 min, followed by the washout of TA with standard saline.

In standard saline, the mean increase in fluorescence, ΔF/F, was 0.51 ± 0.09 (n = 13). After 3 min of bath-application of La^{3+}, the mean increase in fluorescence was reduced to 0.46 ± 0.10 (n = 13). It was further decreased to 0.42 ± 0.08 (n = 13) after TA was additionally added. After washing the preparation for 2 min with standard saline, the mean increase in fluorescence was only 0.34 ± 0.10 (n = 13).

Data were normalized to the first value of the first run in standard saline for statistical analysis. A one-way ANOVA with repeated measures indicated a significant difference between the four runs ($p < 0.001$; n = 13). As seen in the previous experiments with DmCa1D knockdowns (results section 3.13.1), a run-down of fluorescence could be seen over time (Figure 62 A). The normalized increase in fluorescence of the first recording was 1.01 (n = 13), which dropped not significantly to 0.93 (n = 13) after the application of La^{3+} (pairwise follow-up analysis, p = 0.653; n = 13). The intensity of fluorescence upon nicotine puffs was significantly further decreased after the application of TA together with La^{3+} (n. median = 0.84) (pairwise follow-up comparison, p = 0.020; p = 13) as well as after washing TA out (n. median = 0.71) (pairwise follow-up comparison, p = 0.044; n = 13) (Figure 62 A).

The same could be seen in a different statistical analysis, in which all changes in fluorescence were normalized to the first value of the run in 1 µM La^{3+}. In this case, a one-way ANOVA with repeated measures also indicated significant differences between the three runs (p = 0.002; n = 13) (Figure 62 B). The increase in fluorescence (n. median = 0.95; n = 13) was significantly reduced after 10 µM TA was added to the bath (n. median = 0.87) (pairwise follow-up comparison, p = 0.025; n = 13). An even significantly weaker fluorescence upon single nicotine puffs could be seen, after TA was washed out with standard saline (n. median = 0.77) (pairwise follow-up comparison, p = 0.022; n = 13) (Figure 62 B).

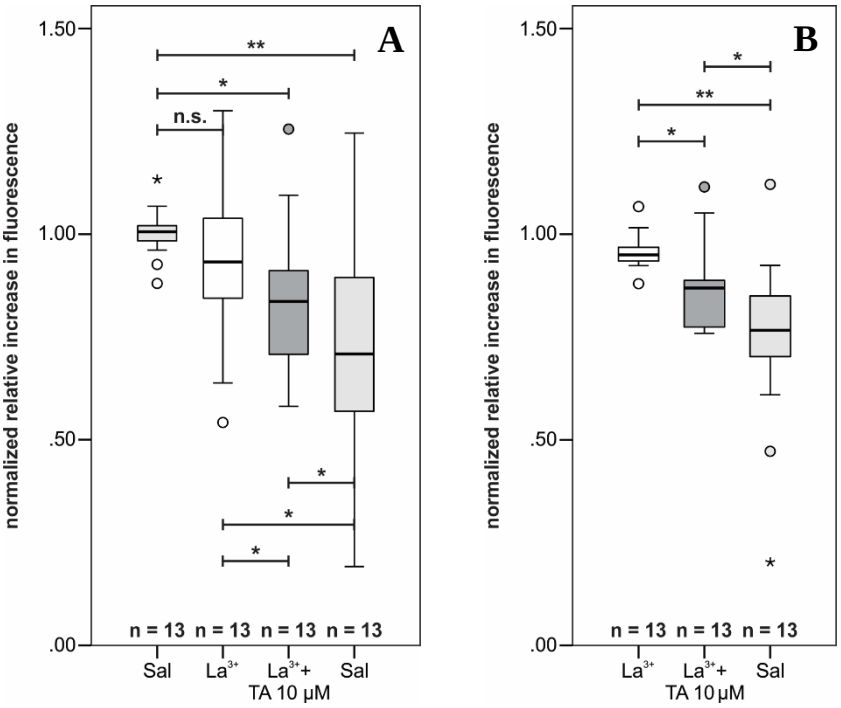

Figure 62: Statistical analysis of the increase in fluorescence in control cells treated with La^{3+}.
A Statistical analysis of the fluorescence (one-way ANOVA w. r. m., $p < 0.001$; $n = 13$). Pairwise follow-up comparisons showed that the fluorescence upon nicotine puffs was slightly but not significantly decreased after 1µM La^{3+} was applied to the bath ($p = 0.653$; $n = 13$). It was significantly weaker after 10 µM TA was applied together with 1 µM La^{3+} (pairwise follow-up comparison, $p = 0.020$; $n = 13$), and also significantly weaker after TA was washed out with standard saline (pairwise follow-up comparison, $p = 0.044$; $n = 13$). **B** Comparison of the increase in fluorescence of only the three runs, which were carried out in La^{3+}, in La^{3+} and TA, and in standard saline after washing-out of TA (one-way ANOVA w. r. m., $p = 0.002$; $n = 13$). Due to pairwise follow-up comparisons, the fluorescence upon nicotine puffs was significantly decreased after 1µM La^{3+} was applied together with 10 µM TA ($p = 0.025$; $n = 13$), and significantly further decreased after the preparations were washed in standard saline ($p = 0.022$; $n = 13$).

Just as in DmCa1D knockdowns, a massive run-down could be seen. For a second evaluation, only those measurements were used, in which the increase in fluorescence of the last run was, in comparison to the second run, in La^{3+}, not further decreased than 75 %. Accordingly, the mean increase in fluorescence was 0.50 ± 0.06 (n = 8) in standard saline, 0.44 ± 0.09 (n = 8) in 1 µM La^{3+}, 0.42 ± 0.08 (n = 8) in La^{3+} and 10 µM TA, and 0.39 ± 0.09 (n = 8) in standard saline after washing TA out. For the statistical analysis of these values, also only normalized data were used. The conducted one-way ANOVA with repeated measures still indicated a significant difference between the four runs, which were in standard saline (n. median = 1.00; n = 8), with La^{3+} (n. median = 0.92; n = 8), with La^{3+} and TA (n. median = 0.86; n = 8), and in standard saline after the washing-out of TA (n. median = 0.79) (ANOVA w. r. m., $p = 0.047$; $n = 8$). Despite this finding, no significant differences between the groups could be found in pairwise follow-up comparisons, possibly due to the decision to use only corrected p-values (Figure 63 A).

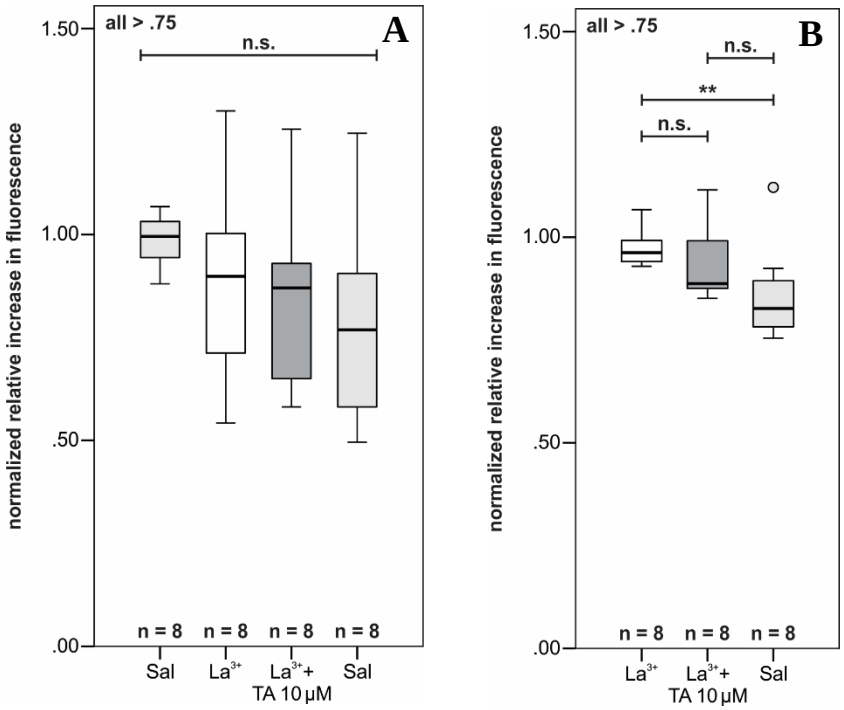

Figure 63: Statistical analysis of the increase in fluorescence in control cells with pharmacologically blocked DmCa1D channels.

Analysis of the fluorescence in all cells with the fluorescence of the last run, in comparison to the run in La^{3+}, not further decreased than 75 %. **A** The fluorescence decreased from run to run over time. Although a one-way ANOVA w. r. m. indicated a significant difference between the four runs (p = 0.047; n = 8), no significant differences could be found in pairwise follow-up comparisons of the runs. **B** Comparison of the increase in fluorescence of only the three runs, which were carried out in La^{3+}, in La^{3+} and TA, and in standard saline after washing TA out (F.-T., p = 0.021; n = 8). Pairwise follow-up comparisons showed that the fluorescence was slightly but not significantly weaker after 10 µM TA was applied together with La^{3+} (p = 0.952; n = 8). After TA was washed out with standard saline, the fluorescence upon nicotine puffs was slightly but not significantly weaker than before (pairwise follow-up comparison, p = 0.240; n = 8). The increase in fluorescence upon puffs of nicotine of the last run was significantly weaker than the one of the first run, in La^{3+} (pairwise follow-up comparison, p = 0.018; n = 8).

The same analysis was done for only the three groups, which were with La^{3+} (n. median = 0.95; n = 8), with La^{3+} and TA (n. median = 0.87; n = 8), and in standard saline after washing TA out (n. median = 0.77; n = 8). With all data normalized to the first recording in 1 µM La^{3+}, the values were not normally distributed, and a Friedman-Test was utilized, which indicated a significant difference between the runs (p = 0.021; n = 8). The only significance found was the strongly reduced increase in fluorescence of the last run in comparison with the increase in fluorescence of the first run in La^{3+} (p = 0.018; n = 8) (Figure 63 B).

Bath-application of La^{3+} reduced the postsynaptic dendritic Ca^{2+} response upon nAChR activation. After the application of La^{3+}, tyraminergic effects were shown to be similarly weak as in MNISN-Is motoneurons with a DmCa1D knockdown.

3.14 Feeding TA to *Drosophila* Larvae Reduces Crawling Behavior, Which is Mediated by the Oct-TyrR in Motoneurons

To prove that tyraminergic modulation of MNISN-Is excitability explains altered crawling behavior in *Drosophila* L3 larvae, behavioral studies were conducted in the course of a bachelor thesis (methods section 2.8) (Girwert, 2017). Mid-L3 larvae were fed with 30 mg/ml TA (in instant food containing brilliant blue) for 2 h to show tyraminergic modulation of crawling behavior. Canton S served as control. To show that modulatory effects were mediated by the octopamine-tyramine receptor Oct-TyrR, the *honoka* mutant *TyrR*^{hono} was utilized. To further prove, that the modulatory effects were solely mediated by the reduction of motoneuron excitability, a motoneuron-specific knockdown of Oct-TyrR was crossed and tested. The knockdown strength was improved by expression of UAS-*dcr2* (Line 10) (Dietzl et al., 2007; Hutchinson et al., 2014).

For each genotype, two groups were randomly generated. One group of larvae was fed with pure instant food, the other group of larvae was fed with instant food containing 30 mg/mg TA. The first group is referred to as control, the second as test group in each genotype.

It could be shown, that larval crawling behavior could be significantly reduced by feeding TA to the larvae. The mean total track length was 92.61 ± 22.32 mm (n = 70) and the mean crawling speed was 0.78 ± 0.19 mm/s (n = 70) in Canton S controls (Figure 64).

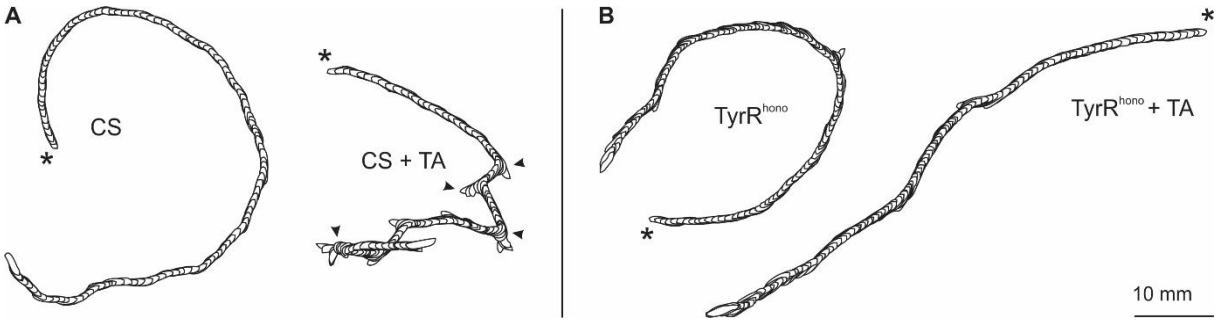

Figure 64: Example crawling tracks of Canton S and *TyrR*^{hono} larvae with and without feeding of TA.
Crawling tracks of four different larvae. Asterisks indicate the starting point. **A** Canton S larvae which were fed with 30 mg/ml TA showed a disturbed crawling behavior. They crawled less far and slower than their respective controls. Also, they showed more often immediate changes in their direction of crawling (arrowheads). **B** *TyrR*^{hono} larvae which were fed with TA did not show altered crawling behavior in comparison to their control group.

Both parameters were significantly reduced after the larvae were fed with 30 mg/ml TA (mean total track length = 78.81 ± 22.94 mm; mean crawling speed = 0.66 ± 0.19 mm/s; n = 33) (T-Test, p = 0.005; n = 70, 33) (Figure 65). It was further observed, that larvae of the test group turned their heads very often. Also, they changed their direction of crawling rather often and very instantaneous. Control larvae were crawling straighter (Figure 64).

The total track length and the crawling speed of larvae of both the *TyrR*^{hono} (n = 67) and the *Oct-TyrR*-RNAi (n = 80) control groups were statistically compared to the Canton S control group. A one-way ANOVA indicated a significant difference between the genotypes for both parameters (total track length $p < 0.001$; crawling speed $p < 0.001$; n = 70, 67, 80). Pairwise follow-up analyses showed that larvae with a *TyrR*^{hono} background were crawling significantly less far ($p = 0.001$; n = 70, 67) and significantly slower ($p = 0.001$; n = 70, 67) than Canton S larvae.

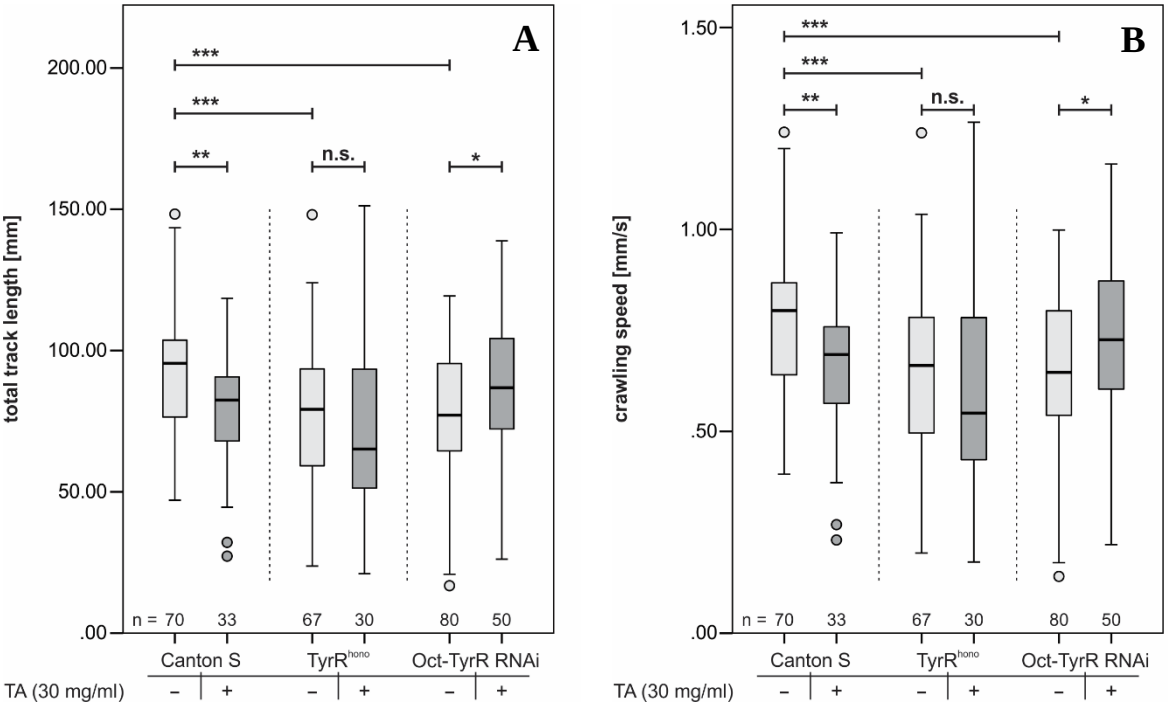

Figure 65: Statistical comparison of the total track length (TTL) and the crawling speed (CS).
Statistical comparison between the control and test groups within the genotypes, and between the control groups of the different genotypes. Larval crawling was filmed for 2 min. **A** Comparison of the total track length. **B** Comparison of the crawling speed. Larvae of the Canton S control group crawled significantly longer tracks, and significantly faster than the respective test group, which was fed with TA (T-Test, TTL $p = 0.005$; CS $p = 0.005$; n = 70, 33). Canton S control larvae crawled significantly longer and faster than the control larvae of *TyrR*^{hono} (ANOVA pairwise follow-up comparison, TTL $p < 0.001$; CS $p < 0.001$; n = 70, 67) and of *Oct-TyrR*-RNAi (ANOVA pairwise follow-up comparison, TTL $p < 0.001$; CS $p < 0.001$; n = 70, 80). In comparison to their control group, larvae of the *TyrR*^{hono} test group did not show altered crawling behavior when they were fed with TA (T-Test, TTL $p = 0.566$; CS $p = 0.566$; n = 67, 30). Larvae of the *Oct-TyrR*-RNAi test group showed a significantly elevated crawling behavior in comparison to their control group (T-Test, TTL $p = 0.037$; CS $p = 0.038$; n = 80, 50).

Larvae with a motoneuron-specific knockdown of the Oct-TyrR were also crawling significantly less far ($p = 0.001$; n = 70, 80) and significantly slower ($p = 0.001$; n = 70, 80) than Canton S larvae. No statistically significant difference could be found in the total track length ($p = 1.000$; n = 67, 80) and the crawling speed ($p = 1.000$; n = 67, 80) between the knockout and the knockdown of Oct-TyrR.

In control larvae of *TyrR*^{hono}, the mean total track length was 76.64 ± 26.47 mm (n = 67), and

the mean crawling speed was 0.64 ± 0.22 mm/s (n = 67). A T-Test showed that the crawling behavior was not significantly reduced in the test group of *TyrR*^{hono}, in which larvae were fed with TA (mean total track length = 73.11 ± 30.86 mm; mean crawling speed = 0.61 ± 0.26 mm/s; n = 30) (p = 0.566; n = 67, 30).

Larvae with the Oct-TyrR knockdown had a mean total track length of 77.13 ± 25.17 mm (n = 80). Their mean crawling speed was 0.65 ± 0.21 mm/s (n = 80). When these larvae, in which the *Oct-TyrR*-RNAi was targeted to only motoneurons, were fed with TA their mean total track length (86.73 ± 25.57 mm; n = 50) and their mean crawling speed (0.73 ± 0.21 mm/s; n = 50) were significantly increased instead of reduced (T-Test, total track length p = 0.037; crawling speed p = 0.038; n = 80, 50).

These behavioral studies show that tyraminergic modulation, i.e., reduction of MN excitability is sufficient to modulate larval crawling behavior. However, tyramine might contribute to wild-type like crawling speed and distance, which is why larvae in which the Oct-TyrR is knocked out or knocked down crawled slower and less far than larvae of the Canton S strain.

4 Discussion

It was the aim of this thesis to test for a potential direct modulation of motoneuron firing properties by tyramine, based on the hypothesis of a highly conserved mechanism of regulating motor output via aminergic modulation of motoneurons, which are the output elements of motor circuitry, from insects to vertebrates. In vertebrates, motor output is strongly modulated by descending aminergic input to spinal motoneurons from brainstem (Heckman et al., 2008; Heckman et al., 2003; Jay et al., 2015). Accordingly, I predicted that motoneurons are directly innervated by tyraminergic ventral unpaired median neurons (prediction one), which are the source of octopamine and tyramine in the ventral nerve cord of insects (Kononenko et al., 2009; Monastirioti et al., 1995; Roeder, 2005; Roeder et al., 2003; Selcho et al., 2012). Moreover, I predicted that the release of tyramine would directly affect motoneuron intrinsic membrane properties (prediction two), and aimed to uncover part of the underlying molecular mechanisms by testing specific predictions on the octopamine-tyramine receptor (prediction three) and the affected downstream ion channels (prediction four). Finally, if the predictions one and two held, I aimed to employ a combination of targeted genetic manipulation and behavioral tests to dissect the contribution of tyraminergic modulation of motoneurons to the known effects of tyramine on locomotor behavior of *Drosophila* larvae (prediction five) (Fox et al., 2006; Saraswati et al., 2004).

4.1 Immunohistochemistry with High Resolution CLSM Indicates Synaptic Release of TA and / or OA from VUM Neurons onto Motoneurons

In vertebrates, spinal motoneurons are densely innervated by aminergic neurons, which modulate the motoneuron firing properties and the motor output (Heckman et al., 2008; Heckman et al., 2003; Jay et al., 2015; McDearmid et al., 1997; Wallén et al., 1989). In *Drosophila*, motor behavior, such as flight in adult flies and crawling in larvae is modulated by a coordinated interplay of the biogenic amines octopamine and tyramine (Brembs et al., 2007; Saraswati et al., 2004). My first prediction that motoneurons are innervated by the aminergic ventral median unpaired neurons (VUM) was supported by immunohistochemical stainings, which showed a co-localization of the tyramine synthesizing enzyme tyrosine-decarboxylase with the synaptic marker Bruchpilot in VUM neurons, and these labels were directly adjacent to mCD8::GFP-positive motoneuron dendrites. The substantial overlap of Bruchpilot and Tdc2 indicates synaptic vesicle release sites in central processes of the tyraminergic VUM neurons.

The proximity to motoneuron dendrites indicated a possible synaptic release of biogenic amines from the VUM neurons onto targets in the dendritic motoneuron membrane. Due to a lack of antibodies with a satisfactory quality against the octopamine-tyramine receptor, it could not be tested for a specific localization of this receptor in the motoneuron. In addition, Bruchpilot was also co-localized with Tdc2 in tyraminergic axons close to motoneuron axons, both passing through larval nerves. It is not clear whether the Bruchpilot protein is integrated in active zones along the VUM axons or if it is just transported to the neuromuscular synapses. However, at least on the level of light microscopy, the anatomical prerequisite for a direct neuromodulation of the larval motoneurons is given.

Aminergic modulation of either motoneuron dendrites, or axons, or both might cause distinctly different changes in motoneuron firing properties. For example, dendritic L-type Ca^{2+} channels amplify excitatory synaptic input to motoneuron dendrites (Kadas et al., 2017), whereas axonal L-type Ca^{2+} currents speed up the de-inactivation of voltage-gated Na^{+} channels by a fast afterhyperpolarization that is caused by Ca^{2+} activation of *slo* encoded BK K^{+} channels. This in turn increases the maximum firing rate of the motoneuron (Kadas et al., 2017; Kadas et al., 2015). Given that L-type Ca^{2+} channels expressed in motoneurons are target of tyraminergic modulation (see below, section 4.3.2), axonal and dendritic tyramine receptor activation in motoneurons will have different electrophysiological consequences.

However, based on my neuroanatomical findings I concluded that tyramine is likely released from the VUM neurons onto motoneuron dendrites and potentially onto motoneuron axons. To test more direct for synaptic connections between the adjacent compartments, a double-labeling with GRASP (GFP reconstitution across synaptic partners) could be utilized (Feinberg et al., 2008; Gordon & Scott, 2009). However, a final proof for synaptic release sites of VUM neurons in direct vicinity to either motoneuron dendrites or axons, or both would require dual label electron microscopy, which was beyond the scope of this study. However, the light microscopy data indicated potential direct aminergic synaptic contacts between *Drosophila* VUM neurons and motoneurons. Therefore, I next tested the hypothesis that motoneuron intrinsic excitability is affected by tyramine.

4.2 Direct Aminergic Modulation of Motoneuron Intrinsic Excitability is Conserved from Flies to Humans

To test the second prediction that tyramine reduces the motoneuron excitability, I carried out somatic patch-clamp recordings from control motoneurons in current-clamp mode with and

without bath-application of tyramine. In addition, in a second set of experiments I replaced the bath-application of tyramine by thermogenetic activation of tyraminergic neurons. The results of these experiments strongly indicate that tyramine reduces motoneuron intrinsic excitability. First, bath-application of tyramine reduced MNISN-Is firing-frequencies in response to somatic current injections significantly within two minutes. Second, the effect was reversible. Third, this effect could also be evoked by endogenous release of tyramine from VUM neurons upon thermogenetic activation. However, the increase of temperature affected the firing properties of MNISN-Is also in the absence of tyramine. Although temperature effects were significantly less pronounced than tyraminergic effects, it remained difficult to fully distinguish between the two. To circumvent this issue, I suggest a genetically encoded light-induced activation mechanism, such as Channelrhodopsin, to specifically activate tyraminergic neurons (Dawydow et al., 2014; Nagel et al., 2003).

Modulation of *Drosophila* larval crawling motoneurons by presynaptic aminergic neurons is in accord with findings in vertebrates. In zebrafish, dopaminergic input into motoneurons mediates swimming behavior (Jay et al., 2015), the firing properties of spinal motoneurons in lamprey are modulated by serotonergic input (Wallén et al., 1989), and the swimming behavior of tadpoles can be accelerated or attenuated by serotonin and norepinephrine (McDearmid et al., 1997). In chronic spinal cats, treatment with the norepinephrine-agonist clonidine induces rhythmic stepping movements, whereas serotonergic and noradrenergic modulation alters consisting locomotor patterns (Barbeau & Rossignol, 1991). In turtles, serotonin has been shown to facilitate plateau potentials, which are generated by L-type Ca^{2+}, and K^{+} currents, in motoneuron dendritic fields. In addition, serotonin was demonstrated to suppress glutamate-evoked spinal motoneuron firing in turtles (Skydsgaard & Hounsgaard, 1996), and to facilitate it in rats (Jackson & White, 1990). In humans, excitatory synaptic input is amplified in the spinal motoneuron dendrites by persistent inward currents, which are generated by L-type Ca^{2+} currents, and voltage-activated Na^{+} currents. Serotonergic and noradrenergic input from the brainstem can strongly modulate these currents to further amplify synaptic inputs (Heckman et al., 2008; Heckman et al., 2003), which primes the neurons for generating a maximum output in, e.g., fight or flight responses. Also, altered firing rates of motoneurons could directly be translated into altered locomotion behavior, i.e., high bursting frequencies mediate more vivid motor output and vice versa (Jay et al., 2015; McDearmid et al., 1997). In parallel, several studies showed the relevance of tyramine as a modulator of motor output in behavioral experiments in *Drosophila* (Brembs et al., 2007; Ormerod et al., 2013; Roeder et al., 2003; Saraswati et al., 2004). For example, an excess of tyramine, induced by a mutation of the

tyramine-ß-hydroxylase, reduces larval crawling behavior significantly (Fox et al., 2006; Saraswati et al., 2004). But in none of these studies, cellular and molecular targets of tyramine were investigated, except some reports of tyraminergic action on larval neuromuscular transmission (Fox et al., 2006; Nagaya et al., 2002). However, the reported effects of tyraminergic modulation of neuromuscular transmission are unlikely to explain the observed effects on locomotor behavior.

As for the cellular targets of tyramine in the CNS, my electrophysiological and anatomical findings indicated a direct tyraminergic modulation of MNISN-Is. However, to rule out the possibility that the observed effects of tyramine were caused by tyraminergic action on the properties of upstream neurons, which in turn affected the motoneuron by synaptic release of yet another modulator (Gerschenfeld, 1973; Marder, 2012), I repeated experiments with bath-application of tyramine in synaptic isolation. Current-clamp recordings in the temperature-sensitive dynamin null mutant *shi*^{1}, which results in synaptic isolation at non-permissive temperatures (Grigliatti et al., 1973; Kosaka & Ikeda, 1983; Poodry & Edgar, 1979), supported the prediction that motoneurons are modulated directly by tyramine, since the reduction of motoneuron excitability was clearly apparent at non-permissive temperature. Therefore, no other neuron of the nervous system was involved in the modulation of motoneurons and an intrinsic regulation mechanism must be present within the motoneuron.

Based on these results, I concluded that the firing properties of a motoneuron in *Drosophila* are directly modulated by the biogenic amine tyramine. In the next step, I tested the hypothesis that the modulation of motoneuron excitability is mediated by a single tyramine-specific receptor, and that tyramine targets ion channels in the motoneuron.

4.3 Molecular Mechanisms of Tyraminergic Modulation of Motoneurons

4.3.1 The Oct-TyrR Alone is Necessary to Mediate the Tyraminergic Modulation of MNISN-Is Excitability

Insect octopamine and tyramine receptors are structurally and pharmacologically homolog to vertebrate adrenergic receptors (Arakawa et al., 1990; Blenau & Baumann, 2001; Saudou et al., 1990). In my experiments, I found that pharmacological blockade of tyramine receptors with yohimbine abolished the tyraminergic effects on MNISN-Is. Due to this finding, it was likely that tyramine binds to a specific G protein-coupled receptor in the motoneuron membrane to mediate modulatory effects. In *Drosophila*, three tyramine-specific receptors have been identified, cloned, and expressed in various heterologous expression systems, such as *Xenopus*

oocytes or CHO cells to analyze the pharmacological profiles of the receptors (Bayliss et al., 2013; Cazzamali et al., 2005; Saudou et al., 1990). One of them is the octopamine-tyramine receptor, which displays the highest similarities to human $5HT_{1A}$-receptors, human α_2A- and B adrenergic receptors, and to *Drosophila* serotonin receptors (Fargin et al., 1988; Kobilka et al., 1987; Regan et al., 1988; Saudou et al., 1990; Witz et al., 1990). Species homologs of this receptor could be found in several other insects, like locusts (*Locusta migratoria*) (Vanden Broeck et al., 1995), honey bees (*Apis mellifera*) (Blenau et al., 2000), or moths (*Heliothis virescens*) (Von Nickisch-Rosenegk et al., 1996). In all named species, the receptor has been shown to be preferentially activated by tyramine and to inhibit adenylyl cyclase activity upon activation (Blenau & Baumann, 2001; Robb et al., 1994; Saudou et al., 1990). In addition, high levels of octopamine-tyramine receptor RNA have been detected in the larval CNS (Chintapalli et al., 2007). Based on these findings, I predicted that the octopamine-tyramine receptor is necessary to mediate the tyraminergic modulation of MNISN-Is. I tested RNAi knockdowns of TyrR, TyrR II, and Oct-TyrR. One knockdown of the octopamine-tyramine receptor was very effective in reducing the tyraminergic action on MNISN-Is. Mixed results could be found for the other knockdowns. Different RNAi constructs are known to cause knockdowns of different strengths (Dietzl et al., 2007; Yamamoto-Hino & Goto, 2013), which can explain the variability in the results. Therefore, the RNAi experiments were further supplemented by recordings from octopamine-tyramine receptor mutants. Tyramine showed no effects on motoneuron excitability in animals carrying a mutation of *honoka* (Kutsukake et al., 2000), the gene encoding the octopamine-tyramine receptor.

These findings underline that the octopamine-tyramine receptor is required for the modulatory effects of tyramine, and support the role of tyramine as a neuromodulator in the *Drosophila* nervous systems. In the absence of *hono*, the activation of other tyramine receptors has no effect on motoneuron excitability. This is in accord with the finding that TyrR and TyrR II are generally not expressed in the larval central nervous system as opposed to Oct-TyrR (Chintapalli et al., 2007). However, I cannot exclude that other receptors add to the effects of octopamine-tyramine receptor activation.

4.3.2 Tyramine Reduces Calcium Influx Through the Voltage-Gated L-type Calcium Channel DmCa1D

Tyraminergic modulation of motoneuron excitability must function by a modification of electrical properties downstream of octopamine-tyramine receptor activation. The first prediction was that tyramine affected *Shal* encoded K^+ channels, which was not supported by somatic current-clamp recordings in *Shal*-RNAi knockdowns. Although this A-type K^+ current underlies the delay to the first action potential in MNISN-Is (Ping et al., 2011; Schaefer et al., 2010), it did not seem to be a primary target of the modulatory action of tyramine. The second prediction was that tyramine affected dendritic Ca^{2+} channels. Calcium imaging experiments of MNISN-Is dendrites supported this prediction, since bath-application of tyramine reduced the relative increase in indicator fluorescence intensity upon nAChR activation by 20 %. This effect was not present in *honoka* mutants.

These data indicate a highly conserved feature of aminergic modulation of motoneuron properties, similar to vertebrate spinal motoneurons, where dendritic L-type Ca^{2+} channels (Ca_v1) amplify excitatory synaptic input. The rate of amplification is coupled to the amount of neuromodulatory input from serotonergic innervation (Heckman et al., 2008). In *Drosophila*, dendritically localized L-type calcium channels have also been demonstrated to amplify synaptic input by prolonging excitatory postsynaptic responses (Kadas et al., 2017; Worrell & Levine, 2008). I predicted that the reduction of Ca^{2+} influx into MNISN-Is dendrites upon application of tyramine was due to a tyraminergic effect on DmCa1D channels, which are the *Drosophila* homolog to vertebrate L-type Ca^{2+} channels. Two lines of evidence supported the prediction that the voltage-gated calcium channel DmCa1D is modulated. First, tyraminergic modulation was reduced in an RNAi knockdown of DmCa1D channels in motoneurons in both calcium imaging experiments and somatic current-clamp recordings. However, this was only an indirect proof for the role of dendritic DmCa1D channels. Calcium fulfills a variety of tasks, like acting as a charge carrier which is necessary for membrane depolarization, or as a second messenger which induces synaptic vesicle release or muscle contraction, and it regulates gene expression (Clapham, 1995; Tsien & Tsien, 1990). Since the RNAi knockdown expressed throughout development, other genes or cell properties might be affected (Flavell & Greenberg, 2008; Marder & Goaillard, 2006). Therefore, in a second approach, the DmCa1D channel was acutely blocked in wild-type larvae with lanthanum, La^{3+}, which blocks DmCa1D with high specificity at a concentration of 1 µM (Kadas et al., 2017; Klein, 2016). Bath-application of La^{3+} during both calcium imaging experiments and current-clamp recordings had the same effect as knocking the channel down by expression of a motoneuron-specific *DmCa1D*-RNAi.

Therefore, I concluded that dendritic DmCa1D calcium currents are downregulated by tyraminergic activation of dendritically localized octopamine-tyramine receptors.

These findings of the tyraminergic action on DmCa1D channels seem to contradict the published effects of a genetic knockdown or pharmacological blockade of DmCa1D on motoneuron firing properties (Kadas et al., 2017). RNAi knockdown and pharmacological blockade of DmCa1D both reduce the amplitude of L-type calcium current, which in turn increases the firing frequency of *Drosophila* larval motoneurons, likely via reduced activation of Ca^{2+} activated K^+ channels (Kadas et al., 2017; Worrell & Levine, 2008). Accordingly, calcium imaging experiments showed reduced Ca^{2+} influx following genetic knockdown and pharmacological blockade of the DmCa1D channel (Kadas et al., 2017). My data clearly showed that tyramine also reduces Ca^{2+} influx into motoneuron dendrites, but it acts in the opposite way on the firing responses of MNISN-Is to somatic current injections as compared to genetic and pharmacological blockade of DmCa1D. Reducing DmCa1D current genetically or pharmacologically increased MNISN-Is firing rates (Kadas et al., 2017; Worrell & Levine, 2008), whereas reducing DmCa1D current by tyraminergic modulation decreases MNISN-Is firing rates.

There are multiple possible explanations to resolve this contradiction. First, localization of octopamine-tyramine receptors and tyraminergic effects on motoneurons could play a role. Dendritic and axonal Dmca1D channels have distinctly different functions in larval motoneurons (Kadas et al., 2017). Although, I found putative contacts with amine releasing processes on motoneuron dendrites and motoneuron axons, it remains unclear whether tyramine is released onto both motoneuron compartments, and whether bath-application of tyramine affected both dendrites and axons. I know from calcium imaging experiments that bath-application of tyramine reduces dendritic Ca^{2+} influx upon focal activation of nAChRs. Preliminary calcium imaging experiments from motoneuron axons indicated that bath-application of TA did not affect axonal DmCa1D channels. Although it remains unclear whether tyramine release from endogenous sources would also be selective for either motoneuron dendrites or axons, it could well be that a selective reduction of dendritic DmCa1D current decreases MN firing rates in response to somatic current injections. Meanwhile, their axonal function, which is the activation of axonal Ca^{2+} activated BK K^+ channels and therefore the increase of maximum firing rates of the neuron (Kadas et al., 2017; Kadas et al., 2015), would remain unaltered. By contrast, both pharmacological and genetic blockade of DmCa1D affects both axonal and dendritic Ca^{2+} channels. However, neither axonal tyramine release from VUM neurons onto motoneuron axons nor the localization of the octopamine-tyramine receptor has

been shown yet, while DmCa1D was found in all compartments of MNISN-Is (Klein, 2016). Therefore, at present the possibility of selective tyramine release on different motoneuron compartments remains somewhat speculative.

A second possibility is that tyramine might not exclusively act on DmCa1D channels, but also on other ion channels. The activation of the octopamine-tyramine receptor inhibits adenylyl cyclase activity, cAMP synthesis, and cAMP dependent protein phosphorylation through PKA (Blenau & Baumann, 2003; Reale et al., 1997; Robb et al., 1994). L-type Ca^{2+} channels show elevated Ca^{2+} conduction properties upon PKA-dependent phosphorylation (Ismailov & Benos, 1995; H. Wang & Sieburth, 2013), which fits the finding that Ca^{2+} influx is reduced in MNISN-Is upon application of tyramine, which reduces phosphorylation. Since PKA has numerous phosphorylation targets, other channels, such as K^+ channels, might also be affected. An increased K^+ efflux due to less K^+ channel phosphorylation (Hoffman & Johnston, 1998; Ismailov & Benos, 1995) could further delay the firing of action potentials. I suggest a combined effect through the reduction of Ca^{2+} influx, which leads to a slower depolarization, and a faster K^+ efflux. The result would be a reduced motoneuron excitability upon exposure to tyramine, since firing thresholds cannot be reached by the same given input. Although my voltage-clamp experiments revealed no clear differences in A-type like K^+ currents upon tyramine application, this possibility cannot entirely be ruled out. In the widely branching motoneurons, the site of modulation might be distal and thus hidden to somatic voltage-clamp recordings due to space-clamp problems. I did also not test for a potential modulation of other potassium currents, such as Shab (K_v2), Shaw (K_v3), or EAG channels, but at least some of them are expressed in larval *Drosophila* motoneurons (Hodge et al., 2005; Srinivasan et al., 2012a; Tsunoda & Salkoff, 1995).

However, even if K^+ currents or other currents are targets of tyraminergic action on motoneurons, none of these alone can be sufficient to mediate tyraminergic effects on motoneurons, because blockade of only DmCa1D suffices to inhibit tyraminergic modulation of motoneuron excitability.

These findings are in accord with the aminergic modulation of vertebrate L-type Ca^{2+} channels in spinal motoneuron dendrites (Heckman et al., 2008; Heckman et al., 2003). In response to a given synaptic input, spinal motoneuron firing output is profoundly increased by descending serotonergic and noradrenergic modulatory input, to a degree that suggests that aminergic modulation controls motoneuron firing output more effectively than sensory feedback (Heckman et al., 2003). During electrical stimulation of human muscles, a significant hysteresis in the frequency force relationship has been attributed to central mechanisms (Collins et al.,

2002), which possibly is aminergic modulation of spinal motoneuron dendritic PICs (Heckman et al., 2003). I employed *Drosophila* genetics to dissect the relative contribution of direct modulation of motoneuron firing properties to the effects of tyramine on larval locomotion.

4.4 Tyraminergic Modulation of Motoneuron Excitability is Sufficient to Explain Known Tyraminergic Effects on Locomotion

In several studies it has been shown that tyramine decreases larval crawling activity (Fox et al., 2006; Saraswati et al., 2004). But both the cellular targets and molecular basis of tyraminergic action on larval locomotion remained unknown. In principle, biogenic amines may modulate brain circuitry upstream of the motoneurons and affect the motivation (Bromberg-Martin et al., 2010), and / or the decision to crawl (Crisp & Mesce, 2006), and / or general arousal (Adamo et al., 1995). Moreover, it is known that tyramine affects neuromuscular transmission in *Drosophila* larvae (Nagaya et al., 2002). This thesis has demonstrated for the first time that motoneuron intrinsic membrane properties are also modulated by tyramine in an insect.

Based on my finding that tyramine modulates motoneuron Dmca1D Ca^{2+} channels via octopamine-tyramine receptor activation, I next supervised a bachelor thesis (Girwert, 2017) to design a genetic manipulation to uncover the relative contribution of tyraminergic effects on motoneurons to the known effects of tyramine on larval locomotion. By employing *Drosophila* genetics, we targeted a *hono*-RNAi selectively to motoneurons. As in *hono* mutants, the motoneuron-specific *hono* knockdown completely abolished the effects of tyramine on larval locomotion that were significant when feeding tyramine to control animals.

At least at the resolution of our behavioral assay the reduction in locomotion speed and distances that appear upon feeding tyramine can be entirely explained by tyraminergic action on the octopamine-tyramine receptor localized to motoneurons. Therefore, tyraminergic modulation of *Drosophila* larval locomotion can be fully explained by modulatory effects on the input/output computations of motoneurons, the final output relay from central motor circuitry to the muscle.

On the other hand, it is well known that food deprivation (states of hunger) induce increased locomotor activity in *Drosophila* larvae (Koon et al., 2011). Moreover, this effect requires the synthesis product and counter-player of tyramine, namely octopamine (Brembs et al., 2007; Fox et al., 2006; Nagaya et al., 2002; Saraswati et al., 2004). Upon starvation, octopamine release from neuromuscular terminals of VUM neurons induces the formation of new neuromuscular varicosities in larval type I and II motor terminals (Koon et al., 2011). This

indicates that starvation also stimulates the final relay neurons to the muscles to increase locomotion and thus aid food seeking behavior. It will be interesting to test whether tyramine also elicits structural changes at the neuromuscular junction, which along with a reduction of motoneuron excitability would decrease locomotor activity in satiated animals after feeding. However, the investigation of structural neuromuscular changes upon peripheral tyramine release were beyond the scope of this study. As stated above, tyramine and octopamine elicit opposite effects on motor behavior. On the other hand, it is not yet clear how tyramine and octopamine can act independently from each other, since both amines are produced in, and released from VUM neurons (Monastirioti et al., 1995; Selcho et al., 2012). One possibility is that the biogenic amines do not share the same release sites. Octopamine is for sure released at the neuromuscular junction (Koon et al., 2011), while tyramine is clearly acting centrally and is released within the central nervous system onto motoneurons (this study). One possibility is that peripheral release of octopamine increases locomotion during starvation, but central release of tyramine reduces locomotion during satiation. However, the underlying mechanism for such a potential regulation remains unclear. It is also not clear yet, whether octopamine elicits central effects on motoneurons, which would contradict a muscle-specific action, or if it elicits no or the same effect as tyramine, which would suggest a cross-activation of tyramine receptors and support a site-specific action. To test this, current-clamp recordings from control cells are required during which octopamine must be bath-applied. Alternatively, tyramine and octopamine might both act centrally and peripherally, but not simultaneously and in opposite directions. To adjust amine release to different states of hunger, VUM neurons might modify the conversion rate from tyramine to octopamine depending on the state of feeding. This theory could in principle be tested by measuring the amount of TßH, which synthesizes octopamine from tyramine in well fed versus starved animals. Several methods could be utilized for this purpose. It could either be tested with a TßH-specific antibody staining (Monastirioti et al., 1996), or by quantitative Western blotting. With the former method, it could also be seen whether a state of hunger-related alteration in TßH levels is located to different cell compartments, e.g. elevated TßH signal in motoneuron axons after starvation. Another possibility is the measurement of TßH activity with a radiometric assay (Reinhard et al., 1986), by which the enzyme activity in nervous systems of animals with different states of hunger could be estimated. Furthermore, it could be feasible to measure the concentrations of tyramine and octopamine in the nervous systems of well-fed and starved *Drosophila* larvae by mass spectrometry (Macfarlane et al., 1990).

However, my findings indicated that the modulation of motoneurons alone is sufficient, to alter

Drosophila larval crawling behavior, which is in accord with the known profound actions of biogenic amines on locomotor behavior in vertebrates (Jay et al., 2015; McDearmid et al., 1997; Wallén et al., 1989). My results further underscore the notion that motoneurons are not simply passive output elements from central circuitry to the muscle, but by contrast, are equipped with active and conditional membrane properties that adjust motor output to different behavioral demands.

5 Literature

Adamo, S. A. (2010). Why should an immune response activate the stress response? Insights from the insects (the cricket Gryllus texensis). *Brain, Behavior, and Immunity*, *24*(2), 194–200. https://doi.org/10.1016/j.bbi.2009.08.003

Adamo, S. A., Linn, C. E., & Hoy, R. R. (1995). The role of neurohormonal octopamine during "fight or flight" behaviour in the field cricket Gryllus bimaculatus. *Journal of Experimental Biology*, *198*(8), 1691–1700. https://doi.org/10.1.1.300.1325

Akerboom, J., Chen, T.-W., Wardill, T. J., Tian, L., Marvin, J. S., Mutlu, S., … Looger, L. L. (2012). Optimization of a GCaMP Calcium Indicator for Neural Activity Imaging. *The Journal of Neuroscience*, *32*(40), 13819–13840. https://doi.org/10.1523/JNEUROSCI.2601-12.2012

Akerboom, J., Rivera, J. D. V., Rodríguez Guilbe, M. M., Malavé, E. C. A., Hernandez, H. H., Tian, L., … Schreiter, E. R. (2009). Crystal structures of the GCaMP calcium sensor reveal the mechanism of fluorescence signal change and aid rational design. *Journal of Biological Chemistry*, *284*(10), 6455–6464. https://doi.org/10.1074/jbc.M807657200

Alkema, M. J., Hunter-Ensor, M., Ringstad, N., & Horvitz, H. R. (2005). Tyramine functions independently of octopamine in the Caenorhabditis elegans nervous system. *Neuron*, *46*(2), 247–260. https://doi.org/10.1016/j.neuron.2005.02.024

Alvarez, F. J., Pearson, J. C., Harrington, D., Dewey, D., Torbeck, L., & Fyffe, R. E. (1998). Distribution of 5-hydroxytryptamine-immunoreactive boutons on alpha-motoneurons in the lumbar spinal cord of adult cats. *The Journal of Comparative Neurology*, *393*(1), 69–83. Retrieved from http://www.ncbi.nlm.nih.gov/pubmed/9520102

Andretic, R., Van Swinderen, B., & Greenspan, R. J. (2005). Dopaminergic modulation of arousal in Drosophila. *Current Biology*, *15*(13), 1165–1175. https://doi.org/10.1016/j.cub.2005.05.025

Arakawa, S., Gocayne, J. D., McCombie, W. R., Urquhart, D. A., Hall, L. M., Fraser, C. M., & Venter, J. C. (1990). Cloning, localization, and permanent expression of a Drosophila octopamine receptor. *Neuron*, *4*(3), 343–354. https://doi.org/10.1016/0896-6273(90)90047-J

Baird, G. S., Zacharias, D. A., & Tsien, R. Y. (1999). Circular permutation and receptor insertion within green fluorescent proteins. *Proceedings of the National Academy of Sciences of the United States of America*, *96*(20), 11241–11246. https://doi.org/10.1073/pnas.96.20.11241

Baldwin, J. M. (1994). Structure and function of receptors coupled to G proteins. *Current Opinion in Cell Biology*, *6*(2), 180–190. https://doi.org/10.1016/0955-0674(94)90134-1

Barbeau, H., & Rossignol, S. (1991). Initiation and modulation of the locomotor pattern in the adult chronic spinal cat by noradrenergic, serotonergic and dopaminergic drugs. *Brain Research*, *546*(2), 250–260. https://doi.org/10.1016/0006-8993(91)91489-N

Bate, M. (1990). The embryonic development of larval muscles in Drosophila. *Development*, *110*, 791–804. https://doi.org/10.1016/S0960-9822(02)00757-1

Bayliss, A., Roselli, G., & Evans, P. D. (2013). A comparison of the signalling properties of two tyramine receptors from Drosophila. *Journal of Neurochemistry*, *125*(1), 37–48. https://doi.org/10.1111/jnc.12158

Bear, M. F., Connors, Barry, W., & Paradiso, M. A. (2007). *Neuroscience - Exploring the Brain*. (E. Lupash, E. Connolly, B. Dilernia, & P. C. Williams, Eds.) (Third). Baltimore: Lippincott Williams & Wilkins.

Bender, K. J., Ford, C. P., & Trussell, L. O. (2010). Dopaminergic Modulation of Axon Initial Segment

Calcium Channels Regulates Action Potential Initiation. *Neuron*, *68*(3), 500–511. https://doi.org/10.1016/j.neuron.2010.09.026

Blenau, W., Balfanz, S., & Baumann, A. (2000). Amtyr1: characterization of a gene from honeybee (Apis mellifera) brain encoding a functional tyramine receptor. *Journal of Neurochemistry*, *74*(3), 900–8. Retrieved from http://www.ncbi.nlm.nih.gov/pubmed/10693920

Blenau, W., & Baumann, A. (2001). Molecular and pharmacological properties of insect biogenic amine receptors: Lessons from Drosophila melanogaster and Apis mellifera. *Archives of Insect Biochemistry and Physiology*, *48*(1), 13–38. https://doi.org/10.1002/arch.1055

Blenau, W., & Baumann, A. (2003). Aminergic signal transduction ininvertebrates: focus on tyramine and octopamine receptors. *Recent Research Developments in Neurochemistry*, *6*, 225–240. Retrieved from https://publishup.uni-potsdam.de/opus4-ubp/frontdoor/deliver/index/docId/4179/file/pmnf107.pdf

Brembs, B., Christiansen, F., Pflüger, H. J., Duch, C., Pfluger, H. J., & Duch, C. (2007). Flight Initiation and Maintenance Deficits in Flies with Genetically Altered Biogenic Amine Levels. *Journal of Neuroscience*, *27*(41), 11122–11131. https://doi.org/10.1523/JNEUROSCI.2704-07.2007

Broadie, K., Sink, H., Van Vactor, D., Fambrough, D., Whitington, P. M., Bate, M., & Goodman, C. S. (1993). From growth cone to synapse: the life history of the RP3 motor neuron. *Development (Cambridge, England). Supplement*, *Supplement*, 227–38. Retrieved from http://www.ncbi.nlm.nih.gov/pubmed/8049478

Bromberg-Martin, E. S., Matsumoto, M., & Hikosaka, O. (2010). Dopamine in Motivational Control: Rewarding, Aversive, and Alerting. *Neuron*, *68*(5), 815–834. https://doi.org/10.1016/j.neuron.2010.11.022

Byrne, J. H., Shapiro, E., Dieringer, N., & Koester, J. (1979). Biophysical mechanisms contributing to inking behavior in Aplysia. *Journal of Neurophysiology*, *42*(5), 1233–50. Retrieved from http://www.ncbi.nlm.nih.gov/pubmed/573783

Catterall, W. A. (1980). Neurotoxins that Act on Voltage-Sensitive Sodium Channels in Excitable Membranes. *Annual Review of Pharmacology and Toxicology*, *20*(1), 15–43. https://doi.org/10.1146/annurev.pa.20.040180.000311

Cazzamali, G., Klaerke, D. A., & Grimmelikhuijzen, C. J. P. (2005). A new family of insect tyramine receptors. *Biochemical and Biophysical Research Communications*, *338*(2), 1189–1196. https://doi.org/10.1016/j.bbrc.2005.10.058

Chen, T.-W., Wardill, T. J., Sun, Y., Pulver, S. R., Renninger, S. L., Baohan, A., … Kim, D. S. (2013). Ultrasensitive fluorescent proteins for imaging neuronal activity. *Nature*, *499*(7458), 295–300. https://doi.org/10.1038/nature12354

Chintapalli, V. R., Wang, J., & Dow, J. A. T. (2007). Using FlyAtlas to identify better Drosophila melanogaster models of human disease. *Nature Genetics*, *39*(6), 715–720. https://doi.org/10.1038/ng2049

Choi, J. C., Park, D., Griffith, L. C., Zwart, M. F., Randlett, O., Evers, J. F., … Sanyal, S. (2004). Electrophysiological and Morphological Characterization of Identified Motor Neurons in the Drosophila Third Instar Larva Central Nervous System. *Journal of Neurobiology*, *91*(December 2003), 2353–2365. https://doi.org/10.1152/jn.01115.2003

Clapham, D. E. (1995). Calcium signaling. *Cell*, *80*(2), 259–268. https://doi.org/10.1016/0092-8674(95)90408-5

Clapham, D. E. (2015). Pain-sensing TRPA1 channel resolved. *Nature*, *520*(April), 439–441.

Clapham, D. E., Montell, C., Schultz, G., & Julius, D. (2003). International Union of Pharmacology. XLIII. Compendium of Voltage-Gated Ion Channels: Transient Receptor Potential Channels.

Pharmacological Reviews, *55*(4), 591–596. https://doi.org/10.1124/pr.55.4.6.2

Clements, J. D., Nelson, P. G., & Redman, S. J. (1986). Intracellular Tetraethylammonium Ions Enhance Group Ia Excitatory Post-Synaptic Potentials Evoked in Cat Motoneurons. *Journal of Physiology*, *377*, 267–282. Retrieved from https://www.ncbi.nlm.nih.gov/pmc/articles/PMC1182832/

Cole, S. H., Carney, G. E., McClung, C. A., Willard, S. S., Taylor, B. J., & Hirsh, J. (2005). Two functional but noncomplementing Drosophila tyrosine decarboxylase genes: Distinct roles for neural tyramine and octopamine in female fertility. *Journal of Biological Chemistry*, *280*(15), 14948–14955. https://doi.org/10.1074/jbc.M414197200

Collins, D. F., Burke, D., & Gandevia, S. C. (2002). Sustained contractions produced by plateau-like behaviour in human motoneurones. *The Journal of Physiology*, *538*(Pt 1), 289–301. https://doi.org/10.1013/jphysiol.2001.012825

Crisp, K. M., & Mesce, K. A. (2006). Beyond the central pattern generator: amine modulation of decision-making neural pathways descending from the brain of the medicinal leech. *The Journal of Experimental Biology*, *209*(Pt 9), 1746–1756. https://doi.org/10.1242/jeb.02204

Crivici, A., & Ikura, M. (1995). Molecular and structural basis of target recognition by calmodulin. *Annu Rev Biophys Biomol Struct*, *24*, 85–116. https://doi.org/10.1146/annurev.bb.24.060195.000505

Dani, J. A. (2015). Neuronal Nicotinic Acetylcholine Receptor Structure and Function and Response to Nicotine. *Int Rev NeuroBiol*, *124*, 3–19. https://doi.org/10.1016/bs.irn.2015.07.001.Neuronal

Dawydow, A., Gueta, R., Ljaschenko, D., Ullrich, S., Hermann, M., Ehmann, N., … Kittel, R. J. (2014). Channelrhodopsin-2-XXL, a powerful optogenetic tool for low-light applications. *Proceedings of the National Academy of Sciences of the United States of America*, *111*(38), 13972–7. https://doi.org/10.1073/pnas.1408269111

de Visser, A. (2016). *Eine zellspezifische Hypothese zum Tyramin-Abbau im Nervensystem von Drosophila melanogaster*. Johannes Gutenberg-University Mainz.

Dietzl, G., Chen, D., Schnorrer, F., Su, K.-C., Barinova, Y., Fellner, M., … Dickson, B. J. (2007). A genome-wide transgenic RNAi library for conditional gene inactivation in Drosophila. *Nature*, *448*(7150), 151–156. https://doi.org/10.1038/nature05954

Dillon, M. E., Wang, G., Garrity, P. A., & Huey, R. B. (2009). Thermal preference in Drosophila. *Journal of Thermal Biology*, *34*(3), 109–119. https://doi.org/10.1016/j.jtherbio.2008.11.007

Downer, R. G. H., Hiripi, L., & Juhos, S. (1993). Characterization of the tyraminergic system in the central nervous system of the locust, Locusta migratoria migratoides. *Neurochemical Research*, *18*(12), 1245–1248. https://doi.org/10.1007/BF00975042

Duffy, J. B. (2002). GAL4 system in Drosophila: a fly geneticist's Swiss army knife. *Genesis (New York, N.Y. : 2000)*, *34*(1–2), 1–15. https://doi.org/10.1002/gene.10150

El-Kholy, S., Stephano, F., Li, Y., Bhandari, A., Fink, C., & Roeder, T. (2015). Expression analysis of octopamine and tyramine receptors in Drosophila. *Cell and Tissue Research*, *361*(3), 669–684. https://doi.org/10.1007/s00441-015-2137-4

Evans, P. D., & Siegler, M. V. (1982). Octopamine mediated relaxation of maintained and catch tension in locust skeletal muscle. *The Journal of Physiology*, *324*, 93–112. https://doi.org/10.1113/jphysiol.1982.sp014102

Fargin, A., Raymond, J. R., Lohse, M. J., Kobilka, B. K., Caron, M. G., & Lefkowitz, R. J. (1988). The genomic clone G-21 which resembles a β-adrenergic receptor sequence encodes the 5-HT1A receptor. *Nature*, *335*(6188), 358–360. https://doi.org/10.1038/335358a0

Feinberg, E. H., VanHoven, M. K., Bendesky, A., Wang, G., Fetter, R. D., Shen, K., & Bargmann, C. I. (2008). GFP Reconstitution Across Synaptic Partners (GRASP) Defines Cell Contacts and Synapses in Living Nervous Systems. *Neuron*, *57*(3), 353–363.

https://doi.org/10.1016/j.neuron.2007.11.030

Field, A. (2013). *Discovering Statistics using IBM SPSS Statistics* (4th ed.). SAGE Publications Ltd.

Flavell, S. W., & Greenberg, M. E. (2008). Signaling Mechanisms Linking Neuronal Activity to Gene Expression and Plasticity of the Nervous System. *Annual Review of Neuroscience*, *31*(1), 563–590. https://doi.org/10.1146/annurev.neuro.31.060407.125631

Florey, E. (1967). Neurotransmitters and modulators in the animal kingdom. *Federation Proceedings*, *26*(4), 1164–78. Retrieved from http://www.ncbi.nlm.nih.gov/pubmed/5339262

Fox, L. E., Soll, D. R., & Wu, C.-F. (2006). Coordination and Modulation of Locomotion Pattern Generators in Drosophila Larvae: Effects of Altered Biogenic Amine Levels by the Tyramine beta Hydroxlyase Mutation. *Journal of Neuroscience*, *26*(5), 1486–1498. https://doi.org/10.1523/JNEUROSCI.4749-05.2006

Fujioka, M., Lear, B. C., Landgraf, M., Yusibova, G. L., Zhou, J., Riley, K. M., … Jaynes, J. B. (2003). Even-skipped, acting as a repressor, regulates axonal projections in Drosophila. *Development*, *130*(22), 5385–5400. https://doi.org/10.1242/dev.00770

Gerschenfeld, H. M. (1973). Chemical transmission in invertebrate central nervous systems and neuromuscular junctions. *Physiological Reviews*, *53*(1), 1–119. Retrieved from http://www.ncbi.nlm.nih.gov/pubmed/4405559

Gether, U., & Kobilka, B. K. (1998). G Protein-coupled Receptors. *The Journal of Biological Chemistry*, *273*, 17979–17982. https://doi.org/10.1074/jbc.273.29.17979

Girwert, C. (2017). *The Action of Tyramine on Drosophila melanogaster Larval Locomotion*. Johannes Gutenberg-University Mainz.

Golic, K. G., & Lindquist, S. (1989). The FLP recombinase of yeast catalyzes site-specific recombination in the drosophila genome. *Cell*, *59*(3), 499–509. https://doi.org/10.1016/0092-8674(89)90033-0

Goodman, C. S., Bastiani, M. J., Doe, C. Q., du Lac, S., Helfand, S. L., Kuwada, J. Y., & Thomas, J. B. (1984). Cell recognition during neuronal development. *Science*, *225*(4668), 1271–1279. https://doi.org/10.1126/science.6474176

Gorczyca, M., Augart, C., & Budnik, V. (1993). Insulin-like receptor and insulin-like peptide are localized at neuromuscular junctions in Drosophila. *The Journal of Neuroscience : The Official Journal of the Society for Neuroscience*, *13*(9), 3692–704. Retrieved from http://www.ncbi.nlm.nih.gov/pubmed/8366341

Gordon, M. D., & Scott, K. (2009). Motor Control in a Drosophila Taste Circuit. *Neuron*, *61*(3), 373–384. https://doi.org/10.1016/j.neuron.2008.12.033

Green, C. H., Burnet, B., & Connolly, K. J. (1983). Organization and patterns of inter- and intraspecific variation in the behaviour of Drosophila larvae. *Animal Behaviour*, *31*(1), 282–291. https://doi.org/10.1016/S0003-3472(83)80198-5

Green, E. W., Fedele, G., Giorgini, F., & Kyriacou, C. P. (2014). A Drosophila RNAi collection is subject to dominant phenotypic effects. *Nature Methods*, *11*(3), 222–223. https://doi.org/10.1038/nmeth.2856

Grigliatti, T. A., Hall, L., Rosenbluth, R., & Suzuki, D. T. (1973). Temperature-sensitive mutations in Drosophila melanogaster. *MGG Molecular & General Genetics*, *120*(2), 107–114. https://doi.org/10.1007/BF00267238

Guan, B., Hartmann, B., Kho, Y. H., Gorczyca, M., & Budnik, V. (1996). The Drosophila tumor suppressor gene, dlg, is involved in structural plasticity at a glutamatergic synapse. *Current Biology : CB*, *6*(6), 695–706. Retrieved from http://www.ncbi.nlm.nih.gov/pubmed/8793296

Hamill, O. P., Marty, A., Neher, E., Sakmann, B., & Sigworth, F. J. (1981). Improved patch-clamp techniques for high-resolution current recording from cells and cell-free membrane patches. *Pflügers Archiv European Journal of Physiology*, *391*(2), 85–100. https://doi.org/10.1007/BF00656997

Hammer, M., & Menzel, R. (1998). Multiple sites of associative odor learning as revealed by local brain microinjections of octopamine in honeybees. *Learning & Memory (Cold Spring Harbor, N.Y.)*, *5*(1–2), 146–56. https://doi.org/10.1101/lm.5.1.146

Han, K. A., Millar, N. S., & Davis, R. L. (1998). A novel octopamine receptor with preferential expression in Drosophila mushroom bodies. *The Journal of Neuroscience : The Official Journal of the Society for Neuroscience*, *18*(10), 3650–8. Retrieved from http://www.ncbi.nlm.nih.gov/pubmed/9570796

Harris-Warrick, R. M., & Marder, E. (1991). Modulation of Neural Networks for Behavior. *Annual Review of Neuroscience*, *14*(1), 39–57. https://doi.org/10.1146/annurev.ne.14.030191.000351

Hartwig, C. L., Worrell, J., Levine, R. B., Ramaswami, M., & Sanyal, S. (2008). Normal dendrite growth in Drosophila motor neurons requires the AP-1 transcription factor. *Developmental Neurobiology*, *68*(10), 1225–1242. https://doi.org/10.1002/dneu.20655

Harvey, J., Brunger, H., Middleton, C. A., Hill, J. A., Sevdali, M., Sweeney, S. T., … Elliott, C. J. H. (2008). Neuromuscular control of a single twitch muscle in wild type and mutant Drosophila, measured with an ergometer. *Invertebrate Neuroscience*, *8*(2), 63–70. https://doi.org/10.1007/s10158-008-0070-x

Heckman, C. J., Johnson, M., Mottram, C., & Schuster, J. (2008). Persistent Inward Currents in Spinal Motoneurons and Their Influence on Human Motoneuron Firing Patterns. *The Neuroscientist*, *14*(3), 264–75. https://doi.org/10.1177/1073858408314986

Heckman, C. J., Lee, R. H., & Brownstone, R. M. (2003). Hyperexcitable dendrites in motoneurons and their neuromodulatory control during motor behavior. *Trends in Neurosciences*, *26*(12), 688–695. https://doi.org/10.1016/j.tins.2003.10.002

Heckscher, E. S., Lockery, S. R., & Doe, C. Q. (2012). Characterization of Drosophila Larval Crawling at the Level of Organism, Segment, and Somatic Body Wall Musculature. *Journal of Neuroscience*, *32*(36), 12460–12471. https://doi.org/10.1523/JNEUROSCI.0222-12.2012

Heinemann, U. (1995). Circular permutation of polypeptide chains: Implications for protein folding and stability. *Progress in Biophysics and Molecular Biology*, *64*(2–3), 121–143. https://doi.org/10.1016/0079-6107(95)00013-5

Hoang, B., & Chiba. (2001). Single-cell analysis of Drosophila larval neuromuscular synapses. *Developmental Biology*, *229*(1), 55–70. https://doi.org/10.1006/dbio.2000.9983

Hodge, J. J. L., Choi, J. C., O'Kane, C. J., & Griffith, L. C. (2005). Shaw potassium channel genes in Drosophila. *Journal of Neurobiology*, *63*(3), 235–254. https://doi.org/10.1002/neu.20126

Hoffman, D. A., & Johnston, D. (1998). Downregulation of transient K+ channels in dendrites of hippocampal CA1 pyramidal neurons by activation of PKA and PKC. *The Journal of Neuroscience : The Official Journal of the Society for Neuroscience*, *18*(10), 3521–3528. https://doi.org/10.1523/jneurosci.0430-09.2009

Hooper, J. E. (1986). Homeotic gene function in the muscles of Drosophila larvae. *The EMBO Journal*, *5*(9), 2321–2329. Retrieved from http://www.pubmedcentral.nih.gov/articlerender.fcgi?artid=1167116&tool=pmcentrez&rendertype=abstract

Hubbard, R., & Armstrong, J. S. (2006). Why we don't really know what "statistical significance" means: A major educational failure. *Journal of Marketing Education*, *28*(2), 114–120. https://doi.org/10.1177/0273475306288399

Hutchinson, K. M., Vonhoff, F., & Duch, C. (2014). Dscam1 Is Required for Normal Dendrite Growth and Branching But Not for Dendritic Spacing in Drosophila Motoneurons. *Journal of Neuroscience*, *34*(5), 1924–1931. https://doi.org/10.1523/JNEUROSCI.3448-13.2014

Iiri, T., Farfel, Z., & Bourne, H. R. (1998). G-protein diseases furnish a model for the turn-on switch. *Nature*, *394*(6688), 35–8. https://doi.org/10.1038/27831

Ismailov, I. I., & Benos, D. J. (1995). Effects of phosphorylation on ion channel function. *Kidney International*, *48*(4), 1167–1179. https://doi.org/10.1038/ki.1995.400

Jackson, D. A., & White, S. R. (1990). Receptor subtypes mediating facilitation by serotonin of excitability of spinal motoneurons. *Neuropharmacology*, *29*(9), 787–797. https://doi.org/10.1016/0028-3908(90)90151-G

Jan, L. Y., & Jan, Y. N. (1976). Properties of the Larval Neuromuscular Junction in Drosophila melanogaster. *Journal of Physiology*, *262*, 189–214.

Janssen, R. (1992). Thermal influences on nervous system function. *Neuroscience and Biobehavioral Reviews*, *16*(3), 399–413. https://doi.org/10.1016/S0149-7634(05)80209-X

Jaquemar, D., Schenker, T., & Trueb, B. (1999). An Ankyrin-like Protein with Transmembrane Domains Is Specifically Lost after Oncogenic Transformation of Human Fibroblasts. *Biochemistry*, *274*(11), 7325–7333. https://doi.org/10.1074/jbc.274.11.7325

Jay, M., De Faveri, F., & McDearmid, J. R. (2015). Firing dynamics and modulatory actions of supraspinal dopaminergic neurons during zebrafish locomotor behavior. *Current Biology*, *25*(4), 435–444. https://doi.org/10.1016/j.cub.2014.12.033

Ji, T. H., Grossmann, M., & Ji, I. (1998). G protein-coupled receptors. I. Diversity of receptor-ligand interactions. *The Journal of Biological Chemistry*, *273*(28), 17299–302. Retrieved from http://www.ncbi.nlm.nih.gov/pubmed/9651309

Johansen, J., Halpern, M. E., Johansen, K. M., & Keshishian, H. (1989). Stereotypic morphology of glutamatergic synapses on identified muscle cells of Drosophila larvae. *The Journal of Neuroscience*, *9*(2), 710–25. Retrieved from http://www.ncbi.nlm.nih.gov/pubmed/2563766

Johansen, J., Halpern, M. E., & Keshishian, H. (1989). Axonal guidance and the development of muscle fiber-specific innervation in Drosophila embryos. *The Journal of Neuroscience*, *9*(12), 4318–32. Retrieved from http://www.ncbi.nlm.nih.gov/pubmed/2512376

Kadas, D., Klein, A., Worrell, J. W., Ryglewski, S., & Duch, C. (2017). Dendritic and Axonal L-Type Calcium Channels Enhance Motoneuron Firing Output during Drosophila Larval Locomotion. *The Journal of Neuroscience*. https://doi.org/10.1523/JNEUROSCI.1064-17.2017

Kadas, D., Ryglewski, S., & Duch, C. (2015). Transient BK outward current enhances motoneurone firing rates during *Drosophila* larval locomotion. *The Journal of Physiology*, *593*(22), 4871–4888. https://doi.org/10.1113/JP271323

Katz, P. (Ed.). (1999). *Beyond Neurotransmission: Neuromodulation and Its Importance for Information Processing*. New York: Oxford Univ. Press.

Kawasaki, F., Zou, B., Xu, X., & Ordway, W. (2004). Active Zone Localization of Presynaptic Calcium Channels Encoded by the cacophony Locus of Drosophila. *Journal of Neuroscience*, *24*(1), 282–285. https://doi.org/10.1523/JNEUROSCI.3553-03.2004

Khan, M. Z., & Nawaz, W. (2016). The emerging roles of human trace amines and human trace amine-associated receptors (hTAARs) in central nervous system. *Biomedicine and Pharmacotherapy*, *83*(24), 439–449. https://doi.org/10.1016/j.biopha.2016.07.002

Kim, M. D., Wen, Y., & Jan, Y. N. (2009). Patterning and organization of motor neuron dendrites in the Drosophila larva. *Developmental Biology*, *336*(2), 213–221. https://doi.org/10.1016/j.ydbio.2009.09.041

Kittel, R. J., Wichmann, C., Rasse, T. M., Fouquet, W., Schmidt, M., Schmid, A., … Sigrist, S. J. (2006). Bruchpilot Promotes Active Zone Assembly, Ca2+ Channel Clustering, and Vesicle Release. *Science*, *312*(5776), 1051–1054. https://doi.org/10.1126/science.1126308

Klein, A. (2016). *Presynaptic function of the voltage-gated calcium channel DmCa1D in Drosophila larval motoneurons*. Johannes Gutenberg-University Mainz.

Kobilka, B. K., Matsui, H., Kobilka, T. S., Yang-Feng, T. L., Francke, U., Caron, M. G., … Regan, J. W. (1987). Cloning, sequencing, and expression of the gene coding for the human platelet alpha 2-adrenergic receptor. *Science*, *238*(4827), 650–656. https://doi.org/10.1126/science.2823383

Kononenko, N. L., Wolfenberg, H., & Pflüger, H. J. (2009). Tyramine as an independent transmitter and a precursor of octopamine in the locust central nervous system: An immunocytochemical study. *Journal of Comparative Neurology*, *512*(4), 433–452. https://doi.org/10.1002/cne.21911

Koon, A. C., Ashley, J., Barria, R., DasGupta, S., Brain, R., Waddell, S., … Budnik, V. (2011). Autoregulatory and paracrine control of synaptic and behavioral plasticity by octopaminergic signaling. *Nature Neuroscience*, *14*(2), 190–199. https://doi.org/10.1038/nn.2716

Kosaka, T., & Ikeda, K. (1983). Possible Temperature-Dependent Blockage of Synaptic Vesicle Recycling Induced by a Single Gene Mutation in Drosophila. *Journal of Neurobiology*, *14*(3), 207–225. https://doi.org/10.1002/neu.480140305

Kupfermann, I. (1979). Modulatory Actions of Neurotransmitters. *Annual Review of Neuroscience*, *2*(1), 447–465. https://doi.org/10.1146/annurev.ne.02.030179.002311

Kutsukake, M., Komatsu, A, Yamamoto, D., & Ishiwa-Chigusa, S. (2000). A tyramine receptor gene mutation causes a defective olfactory behavior in Drosophila melanogaster. *Gene*, *245*(1), 31–42. https://doi.org/10.1016/S0378-1119(99)00569-7

Landgraf, M., Bossing, T., Technau, G. M., & Bate, M. (1997). The origin, location, and projections of the embryonic abdominal motorneurons of Drosophila. *The Journal of Neuroscience : The Official Journal of the Society for Neuroscience*, *17*(24), 9642–55. Retrieved from http://www.ncbi.nlm.nih.gov/pubmed/9391019

Lange, A. B. (2009). Tyramine: From octopamine precursor to neuroactive chemical in insects. *General and Comparative Endocrinology*, *162*(1), 18–26. https://doi.org/10.1016/j.ygcen.2008.05.021

Laursen, W. J., Anderson, E. O., Hoffstaetter, L. J., Bagriantsev, S. N., & Gracheva, E. O. (2015). Species-specific temperature sensitivity of TRPA1. *Temperature (Austin)*, *2*(2), 214–226. https://doi.org/10.1080/23328940.2014.1000702

Lee, R. H., & Heckman, C. J. (1999). Paradoxical effect of QX-314 on persistent inward currents and bistable behavior in spinal motoneurons in vivo. *Journal of Neurophysiology*, *82*(5), 2518–27. Retrieved from http://www.ncbi.nlm.nih.gov/pubmed/10561423

Lee, T., & Luo, L. (1999). Mosaic analysis with a repressible cell marker for studies of gene function in neuronal morphogenesis. *Neuron*, *22*(3), 451–61. https://doi.org/10.1016/S0896-6273(00)80701-1

Leroy, F., Lamotte, B., Zytnicki, D., Leroy, X. F., Lamotte, X. B., & Zytnicki, X. D. (2015). Potassium currents dynamically set the recruitment and firing properties of F-type motoneurons in neonatal mice. *J Neurophysiology*, *114*(August 2015), 1963–1973. https://doi.org/10.1152/jn.00193.2015

Li, Y., Bennett, D. J., Zijdewind, I., Gant, K., Bakels, R., Thomas, C. K., … Cope, T. C. (2003). Persistent Sodium and Calcium Currents Cause Plateau Potentials in Motoneurons of Chronic Spinal Rats Persistent Sodium and Calcium Currents Cause Plateau Potentials in Motoneurons of Chronic Spinal Rats. *Journal of Neurophysiology*, *90*(2), 857–869. https://doi.org/10.1152/jn.00236.2003

Li, Y., Gorassini, M. a, & Bennett, D. J. (2004). Role of persistent sodium and calcium currents in

motoneuron firing and spasticity in chronic spinal rats. *Journal of Neurophysiology*, *91*(2), 767–783. https://doi.org/10.1152/jn.00788.2003

Livingstone, M. S., & Tempel, B. L. (1983). Genetic dissection of monoamine neurotransmitter synthesis in Drosophila. *Nature*, *303*(5912), 67–70. https://doi.org/10.1038/303067a0

Macfarlane, R. G., Midgley, J. M., Watson, D. G., & Evans, P. D. (1990). The analysis of biogenic amines in the thoracic nervous system of the locust, Schistocerca gregaria, by gas-chromatography negative ion chemical ionization mass spectrometry (GC-NICIMS). *Insect Biochemistry*, *20*(3), 305–311. https://doi.org/10.1016/0020-1790(90)90048-Y

Malutan, T., McLean, H., Caveney, S., & Donly, C. (2002). A high-affinity octopamine transporter cloned from the central nervous system of cabbage looper Trichoplusia ni. *Insect Biochemistry and Molecular Biology*, *32*(3), 343–357. https://doi.org/10.1016/S0965-1748(01)00114-X

Marder, E. (2012). Neuromodulation of Neuronal Circuits: Back to the Future. *Neuron*, *76*(1), 1–11. https://doi.org/10.1016/j.neuron.2012.09.010

Marder, E., & Goaillard, J.-M. (2006). Variability, compensation and homeostasis in neuron and network function. *Nature Reviews Neuroscience*, *7*(7), 563–574. https://doi.org/10.1038/nrn1949

Marder, E., & Thirumalai, V. (2002). Cellular, synaptic and network effects of neuromodulation. *Neural Networks*, *15*(4–6), 479–493. https://doi.org/10.1016/S0893-6080(02)00043-6

Marella, S., Mann, K., & Scott, K. (2012). Dopaminergic Modulation of Sucrose Acceptance Behavior in Drosophila. *Neuron*, *73*(5), 941–950. https://doi.org/10.1016/j.neuron.2011.12.032

McDearmid, J. R., Scrymgeour-Wedderburn, J. F., & Sillar, K. T. (1997). Aminergic modulation of glycine release in a spinal network controlling swimming in Xenopus laevis. *Journal of Physiology*, *503*(1), 111–117. https://doi.org/10.1111/j.1469-7793.1997.111bi.x

Mentel, T., Duch, C., Stypa, H., Wegener, G., Müller, U., & Pflüger, H.-J. (2003). Central modulatory neurons control fuel selection in flight muscle of migratory locust. *The Journal of Neuroscience : The Official Journal of the Society for Neuroscience*, *23*(4), 1109–1113. https://doi.org/23/4/1109 [pii]

Miyawaki, A., Llopis, J., Heim, R., & McCaffery, J. (1997). Fluorescent indicators for Ca2+ based on green fluorescent proteins and calmodulin. *Nature*, *388*, 882–887. Retrieved from http://www.tsienlab.ucsd.edu/Publications/Miyawaki 1997 Nature - Fluorescent indicators.pdf

Mollemann, A. (2003). *Patch Clamping - An Introductory Guide to Patch Clamp Electrophysiology*. John Wiley & Sons, LTD.

Monastirioti, M., Gorczyca, M., Rapus, J., Eckert, M., White, K., & Budnik, V. (1995). Octopamine immunoreactivity in the fruit fly Drosophila melanogaster. *The Journal of Comparative Neurology*, *356*(2), 275–287. https://doi.org/10.1002/cne.903560210

Monastirioti, M., Linn, C. E., & White, K. (1996). Characterization of Drosophila tyramine beta-hydroxylase gene and isolation of mutant flies lacking octopamine. *The Journal of Neuroscience : The Official Journal of the Society for Neuroscience*, *16*(12), 3900–3911. https://doi.org/10.1111/J.1471-4159.1976.TB04449.X

Montell, C., Birnbaumer, L., Flockerzi, V., Bindels, R. J., Bruford, E. A., Caterina, M. J., … Zhu, M. X. (2002). A unified nomenclature for the superfamily of TRP cation channels. *Molecular Cell*, *9*(2), 229–231. https://doi.org/10.1016/S1097-2765(02)00448-3

Montgomery, J. C., & Macdonald, J. A. (1990). Effects of temperature on nervous system: implications for behavioral performance. *The American Journal of Physiology*, *259*(2 Pt 2), R191-6. Retrieved from http://www.ncbi.nlm.nih.gov/pubmed/2201212

Moqrich, A. (2005). Impaired Thermosensation in Mice Lacking TRPV3, a Heat and Camphor Sensor in the Skin. *Science*, *307*(5714), 1468–1472. https://doi.org/10.1126/science.1108609

Nagaya, Y., Kutsukake, M., Chigusa, S. I., & Komatsu, A. (2002). A trace amine, tyramine, functions as a neuromodulator in Drosophila melanogaster. *Neuroscience Letters*, *329*(3), 324–328. https://doi.org/10.1016/S0304-3940(02)00596-7

Nagel, G., Szellas, T., Huhn, W., Kateriya, S., Adeishvili, N., Berthold, P., … Bamberg, E. (2003). Channelrhodopsin-2, a directly light-gated cation-selective membrane channel. *Proceedings of the National Academy of Sciences of the United States of America*, *100*(24), 13940–5. https://doi.org/10.1073/pnas.1936192100

Neckameyer, W. S., & White, K. (1993). Drosophila tyrosine hydroxylase is encoded by the pale locus. *Journal of Neurogenetics*, *8*(4), 189–99. https://doi.org/10.3109/01677069309083448

Oldham, W. M., & Hamm, H. E. (2008). Heterotrimeric G protein activation by G-protein-coupled receptors. *Nature Reviews Molecular Cell Biology*, *9*(1), 60–71. https://doi.org/10.1038/nrm2299

Orchard, I., & Lange, A. B. (1985). Evidence for octopaminergic modulation of an insect visceral muscle. *Journal of Neurobiology*, *16*(3), 171–181. https://doi.org/10.1002/neu.480160303

Ormerod, K. G., Hadden, J. K., Deady, L. D., Mercier, A. J., & Krans, J. L. (2013). Action of octopamine and tyramine on muscles of Drosophila melanogaster larvae. *Journal of Neurophysiology*, *110*(8), 1984–96. https://doi.org/10.1152/jn.00431.2013

Palczewski, K., Kumasaka, T., Hori, T., Behnke, C. A., Motoshima, H., Fox, B. A., … Miyano, M. (2000). Crystal structure of rhodopsin: A G protein-coupled receptor. *Science (New York, N.Y.)*, *289*(5480), 739–45. Retrieved from http://www.ncbi.nlm.nih.gov/pubmed/10926528

Perkins, L. A., Holderbaum, L., Tao, R., Hu, Y., Sopko, R., McCall, K., … Perrimon, N. (2015). The transgenic RNAi project at Harvard medical school: Resources and validation. *Genetics*, *201*(3), 843–852. https://doi.org/10.1534/genetics.115.180208

Ping, Y., Waro, G., Licursi, A., Smith, S., Vo-Ba, D. A., & Tsunoda, S. (2011). Shal/Kv4 channels are required for maintaining excitability during repetitive firing and normal locomotion in Drosophila. *PLoS ONE*, *6*(1), 15–20. https://doi.org/10.1371/journal.pone.0016043

Poodry, C. A., & Edgar, L. (1979). Reversible Alterations in the Neuromuscular Junctions of Drosophila melanogaster Bearing a Temperature-Sensitive Mutation, shibire. *J. Cell Biology*, *81*(June), 520–527. Retrieved from http://jcb.rupress.org/content/jcb/81/3/520.full.pdf

Pulver, S. R., Pashkovski, S. L., Hornstein, N. J., Garrity, P. a, & Griffith, L. C. (2009). Temporal dynamics of neuronal activation by Channelrhodopsin-2 and TRPA1 determine behavioral output in Drosophila larvae. *Journal of Neurophysiology*, *101*(6), 3075–88. https://doi.org/10.1152/jn.00071.2009

Ramsey, I. S., Delling, M., & Clapham, D. E. (2006). AN INTRODUCTION TO TRP CHANNELS. *Annual Review of Physiology*, *68*(1), 619–647. https://doi.org/10.1146/annurev.physiol.68.040204.100431

Rasch, B., Friese, M., Hofmann, W., & Naumann, E. (2010). SPSS Ergänzungen zu Kapitel 7: Varianzanalyse mit Messwiederholung. *Quantitative Methoden 2. Einführung in Die Statistik Für Psychologen Und Sozialwissenschaftler.*, *2*, 1–23. Retrieved from http://quantitative-methoden.de/Dateien/Auflage3/Band_II/Kapitel_7_SPSS_Ergaenzungen_A3.pdf

Reale, V., Hannan, F., Midgley, J. M., & Evans, P. D. (1997). The expression of a cloned Drosophila octopamine/tyramine receptor in Xenopus oocytes. *Brain Research*, *769*(2), 309–320. https://doi.org/10.1016/S0006-8993(97)00723-3

Regan, J. W., Kobilka, T. S., Yang-Feng, T. L., Caron, M. G., Lefkowitz, R. J., & Kobilka, B. K. (1988). Cloning and expression of a human kidney cDNA for an alpha 2-adrenergic receptor subtype. *Proceedings of the National Academy of Sciences of the United States of America*, *85*(17), 6301–5. Retrieved from http://www.pubmedcentral.nih.gov/articlerender.fcgi?artid=281957&tool=pmcentrez&rendertyp

e=abstract

Reinhard, J. F., Smith, G. K., & Nichol, C. A. (1986). A rapid and sensitive assay for tyrosine-3-monooxygenase based upon the release of 3H2O and adsorption of [3H]-tyrosine by charcoal. *Life Sciences*, *39*(23), 2185–9.

Reuter, H. (1983). Calcium channel modulation by neurotransmitters, enzymes and drugs. *Nature*, *301*(5901), 569–574. https://doi.org/10.1038/301569a0

Ries, A.-S., Hermanns, T., Poeck, B., & Strauss, R. (2017). Serotonin modulates a depression-like state in Drosophila responsive to lithium treatment. *Nature Communications*, *8*. https://doi.org/10.1038/ncomms15738

Robb, S., Cheek, T. R., Hannan, F. L., Hall, L. M., Midgley, J. M., & Evans, P. D. (1994). Agonist-specific coupling of a cloned Drosophila octopamine/tyramine receptor to multiple second messenger systems. *The EMBO Journal*, *1*(1), 325–1330. https://doi.org/10.1111/j.1476-5381.2011.01749.x

Roeder, T. (1999). Octopamine in invertebrates. *Progress in Neurobiology*, *59*(5), 533–561. https://doi.org/10.1016/S0301-0082(99)00016-7

Roeder, T. (2005). Tyramine and Octopamine: Ruling Behavior and Metabolism. *Annu. Rev. Entomol.*, *50*(20), 447–477. https://doi.org/10.1146/annurev.ento.50.071803.130404

Roeder, T., Seifert, M., Kähler, C., & Gewecke, M. (2003). Tyramine and octopamine: Antagonistic modulators of behavior and metabolism. *Archives of Insect Biochemistry and Physiology*, *54*(1), 1–13. https://doi.org/10.1002/arch.10102

Ryglewski, S., & Duch, C. (2009). Shaker and Shal Mediate Transient Calcium-Independent Potassium Current in a Drosophila Flight Motoneuron. *Journal of Neurophysiology*, *102*(6), 3673–3688. https://doi.org/10.1152/jn.00693.2009

Ryglewski, S., Duch, C., & Altenhein, B. (2017). Tyramine Actions on Drosophila Flight Behavior Are Affected by a Glial Dehydrogenase/Reductase. *Frontiers in Systems Neuroscience*, *11*(September), 1–8. https://doi.org/10.3389/fnsys.2017.00068

Ryglewski, S., Lance, K., Levine, R. B., & Duch, C. (2012). Ca(v)2 channels mediate low and high voltage-activated calcium currents in Drosophila motoneurons. *The Journal of Physiology*, *590*(Pt 4), 809–25. https://doi.org/10.1113/jphysiol.2011.222836

Saraswati, S., Fox, L. E., Soll, D. R., & Wu, C. F. (2004). Tyramine and Octopamine Have Opposite Effects on the Locomotion of Drosophila Larvae. *Journal of Neurobiology*, *58*(4), 425–441. https://doi.org/10.1002/neu.10298

Sasaki, T., Matsuki, N., & Ikegaya, Y. (2011). Action-Potential Modulation During Axonal Conduction. *Science*, *331*(6017), 599–601. https://doi.org/10.1126/science.1197598

Saudou, F., Amlaiky, N., Plassat, J. L., Borrelli, E., & Hen, R. (1990). Cloning and characterization of a Drosophila tyramine receptor. *The EMBO Journal*, *9*(11), 3611–7. Retrieved from http://www.pubmedcentral.nih.gov/articlerender.fcgi?artid=1326448&tool=pmcentrez&rendertype=abstract

Schaefer, J. E., Worrell, J. W., & Levine, R. B. (2010). Role of intrinsic properties in Drosophila motoneuron recruitment during fictive crawling. *Journal of Neurophysiology*, *104*(3), 1257–1266. https://doi.org/10.1152/jn.00298.2010

Scheiner, R., Baumann, A., & Blenau, W. (2006). Aminergic control and modulation of honeybee behaviour. *Current Neuropharmacology*, *4*, 259–76. https://doi.org/10.2174/157015906778520791

Schmid, A., Chiba, A., & Doe, C. Q. (1999). Clonal analysis of Drosophila embryonic neuroblasts: neural cell types, axon projections and muscle targets. *Development (Cambridge, England)*,

126(21), 4653–89. Retrieved from http://www.ncbi.nlm.nih.gov/pubmed/10518486

Schwaerzel, M., Monastirioti, M., Scholz, H., Friggi-Grelin, F., Birman, S., & Heisenberg, M. (2003). Dopamine and octopamine differentiate between aversive and appetitive olfactory memories in Drosophila. *The Journal of Neuroscience*, *23*(33), 10495–502. https://doi.org/Copyright © 2012 by the Society for Neuroscience

Selcho, M., Pauls, D., el Jundi, B., Stocker, R. F., & Thum, A. S. (2012). The Role of octopamine and tyramine in Drosophila larval locomotion. *Journal of Comparative Neurology*, *520*(16), 3764–3785. https://doi.org/10.1002/cne.23152

Simon, M. I., Strathmann, M. P., & Gautam, N. (1991). Diversity of G Proteins in Signal Transduction. *Science*, *252*(1971), 802–808. https://doi.org/10.1126/science.1902986

Sink, H., & Whitington, P. M. (1991). Location and connectivity of abdominal motoneurons in the embryo and larva of Drosophila melanogaster. *Journal of Neurobiology*, *22*(3), 298–311. https://doi.org/10.1002/neu.480220309

Skydsgaard, M., & Hounsgaard, J. (1996). Multiple actions of iontophoretically applied serotonin on motorneurones in the turtle spinal cord in vitro. *Acta Physiologica Scandinavica*, *158*(4), 301–310. https://doi.org/10.1046/j.1365-201X.1996.558326000.x

Srinivasan, S., Lance, K., & Levine, R. B. (2012a). Contribution of EAG to excitability and potassium currents in Drosophila larval motoneurons. *Journal of Neurophysiology*, *107*(10), 2660–2671. https://doi.org/10.1152/jn.00201.2011

Srinivasan, S., Lance, K., & Levine, R. B. (2012b). Segmental differences in firing properties and potassium currents in Drosophila larval motoneurons. *Journal of Neurophysiology*, *107*(5), 1356–1365. https://doi.org/10.1152/jn.00200.2011

Stevenson, P. A., Dyakonova, V., Rillich, J., & Schildberger, K. (2005). Octopamine and Experience-Dependent Modulation of Aggression in Crickets. *Journal of Neuroscience*, *25*(6), 1431–1441. https://doi.org/10.1523/JNEUROSCI.4258-04.2005

Story, G. M., Peier, A. M., Reeve, A. J., Eid, S. R., Mosbacher, J., Hricik, T. R., … Patapoutian, A. (2003). ANKTM1, a TRP-like channel expressed in nociceptive neurons, is activated by cold temperatures. *Cell*, *112*(6), 819–829. https://doi.org/10.1016/S0092-8674(03)00158-2

Suzuki, N., Hajicek, N., & Kozasa, T. (2009). Regulation and physiological functions of G12/13-mediated signaling pathways. *NeuroSignals*, *17*(1), 55–70. https://doi.org/10.1159/000186690

Tian, L., Hires, S. A., Mao, T., Huber, D., Chiappe, M. E., Chalasani, S. H., … Looger, L. L. (2009). Imaging neural activity in worms, flies and mice with improved GCaMP calcium indicators. *Nature Methods*, *6*(12), 875–881. https://doi.org/10.1038/nmeth.1398

Todaka, H., Taniguchi, J., Satoh, J., Mizuno, A., & Suzuki, M. (2004). Warm temperature-sensitive transient receptor potential vanilloid 4 (TRPV4) plays an essential role in thermal hyperalgesia. *The Journal of Biological Chemistry*, *279*(34), 35133–8. https://doi.org/10.1074/jbc.M406260200

Tsien, R. W., & Tsien, R. Y. (1990). Calcium channels, stores, and oscillations. *Annu Rev Cell Biol*, *6*, 715–760. https://doi.org/10.1146/annurev.cb.06.110190.003435

Tsunoda, S., & Salkoff, L. (1995). The major delayed rectifier in both Drosophila neurons and muscle is encoded by Shab. *The Journal of Neuroscience*, *15*(July), 5209–5221.

van Swinderen, B., Nitz, D. A., & Greenspan, R. J. (2004). Uncoupling of Brain Activity from Movement Defines Arousal States in Drosophila. *Current Biology*, *14*(2), 81–87. https://doi.org/10.1016/j.cub.2003.12.057

Vanden Broeck, J., Vulsteke, V., Huybrechts, R., & De Loof, A. (1995). Characterization of a Cloned Locust Tyramine Receptor cDNA by Functional Expression in Permanently Transformed Drosophila S2 Cells. *Journal of Neurochemistry*, *64*(6), 2387–2395.

https://doi.org/10.1046/j.1471-4159.1995.64062387.x

Viswanath, V., Story, G. M., Peier, A. M., Petrus, M. J., Lee, V. M., Hwang, S. W., … Jegla, T. (2003). Opposite thermosensor in fruitfly and mouse. *Nature*, *423*(6942), 822–3. https://doi.org/10.1038/423822a

Vömel, M., & Wegener, C. (2008). Neuroarchitecture of aminergic systems in the larval ventral ganglion of Drosophila melanogaster. *PLoS ONE*, *3*(3). https://doi.org/10.1371/journal.pone.0001848

Von Nickisch-Rosenegk, E., Krieger, J., Kubick, S., Laage, R., Strobel, J., Strotmann, J., & Breer, H. (1996). Cloning of biogenic amine receptors from moths (Bombyx mori and Heliothis virescens). *Insect Biochemistry and Molecular Biology*, *26*(8–9), 817–827. https://doi.org/10.1016/S0965-1748(96)00031-8

Wagh, D. A., Rasse, T. M., Asan, E., Hofbauer, A., Schwenkert, I., Dürrbeck, H., … Buchner, E. (2006). Bruchpilot, a protein with homology to ELKS/CAST, is required for structural integrity and function of synaptic active zones in Drosophila. *Neuron*, *49*(6), 833–844. https://doi.org/10.1016/j.neuron.2006.02.008

Wallén, P., Buchanan, J. T., Grillner, S., Hill, R. H., Christenson, J., & Hokfelt, T. (1989). Effects of 5-hydroxytryptamine on the afterhyperpolarization, spike frequency regulation, and oscillatory membrane properties in lamprey spinal cord neurons. *Journal of Neurophysiology*, *61*(4), 759–768. Retrieved from http://jn.physiology.org/content/61/4/759.short%5Cnpapers3://publication/uuid/885D6D8A-CADF-4F6C-8C9E-72F39A1D7295

Wang, H., & Sieburth, D. (2013). PKA Controls Calcium Influx into Motor Neurons during a Rhythmic Behavior. *PLoS Genetics*, *9*(9). https://doi.org/10.1371/journal.pgen.1003831

Wang, J. W., Sylwester, A. W., Reed, D., Wu, D. A., Soll, D. R., & Wu, C. F. (1997). Morphometric description of the wandering behavior in Drosophila larvae: aberrant locomotion in Na+ and K+ channel mutants revealed by computer-assisted motion analysis. *Journal of Neurogenetics*, *11*(3–4), 231–254. https://doi.org/10.3109/01677069709115098

Witz, P., Amlaiky, N., Plassat, J. L., Maroteaux, L., Borrelli, E., & Hen, R. (1990). Cloning and characterization of a Drosophila serotonin receptor that activates adenylate cyclase. *Proceedings of the National Academy of Sciences of the United States of America*, *87*(22), 8940–8944. https://doi.org/10.1073/pnas.87.22.8940

Worrell, J. W., & Levine, R. B. (2008). Characterization of voltage-dependent Ca2+ currents in identified Drosophila motoneurons in situ. *Journal of Neurophysiology*, *100*(2), 868–878. https://doi.org/10.1152/jn.90464.2008

Yamamoto-Hino, M., & Goto, S. (2013). In Vivo RNAi-based screens: Studies in model organisms. *Genes*, *4*(4), 646–665. https://doi.org/10.3390/genes4040646

Zheng, W., Feng, G., Ren, D., Eberl, D. F., Hannan, F., Dubald, M., & Hall, L. M. (1995). Cloning and characterization of a calcium channel alpha 1 subunit from Drosophila melanogaster with similarity to the rat brain type D isoform. *The Journal of Neuroscience : The Official Journal of the Society for Neuroscience*, *15*(2), 1132–43. Retrieved from http://www.ncbi.nlm.nih.gov/pubmed/7869089

Zumstein, N., Forman, O., Nongthomba, U., Sparrow, J. C., & Elliott, C. J. H. (2004). Distance and force production during jumping in wild-type and mutant Drosophila melanogaster. *The Journal of Experimental Biology*, *207*, 3515–3522. https://doi.org/10.1242/jeb.01181

6 Appendix

6.1 List of Chemicals

Chemical	Origin	Ordering # / Search ID
α-brp (mouse)	Developmental Studies Hybridoma Bank	nc82
α-chicken (goat)	Thermo Fisher Scientific	A11039
α-GFP (chicken)	Thermo Fisher Scientific	A10262
α-mouse (goat)	Jackson Immuno Research	115-175-003
α-rabbit (donkey)	Thermo Fisher Scientific	A10042
α-Tdc2 (rabbit)	Covalab	pab0822-P
Agarose	Carl Roth	5210.5
Ascorbic acid	Carl Roth	3525.3
Cornmeal	Rapunzel – Bio Fachhandel	
$CaCl_2$	Sigma Aldrich	C5670
EGTA	Carl Roth	3054.1
Glucose	Carl Roth	HN06.4
HEPES	Sigma Aldrich	H3375
Immersion Oil, Type F	Fisher Scientific	11944399
KCl	Sigma Aldrich	P5405
KGluc	Sigma Aldrich	P1847
KOH	Carl Roth	K017.1
$LaCl_3$	Sigma Aldrich	449830
Methyl salicylate	Sigma Aldrich	M6752
MgATP	Sigma Aldrich	A9187
$MgCl_2$	Sigma Aldrich	M2670
NaCl	Carl Roth	0962.1
NaOH	Carl Roth	K021.1
Nicotine	Sigma Aldrich	
Paraformaldehyde	Sigma Aldrich	P6148
PBS	Sigma Aldrich	P4417
Protease	Sigma Aldrich	P5147
Sucrose	Carl Roth	4621.1
Sylgard	Dow Corning	Sylgard® 184 Silicone Elastomer Kit
Tyramine	Sigma Aldrich	T2879
Triton X 100	Carl Roth	3051.3
TTX	Carl Roth	6973.1
Tegosept	Apex BioResearch Products	
Yeast	Huber Mühle	49192
YH	Sigma Aldrich	Y3125

6.2 Comparison of Tyramine Effect in Canton S and RN2 Controls

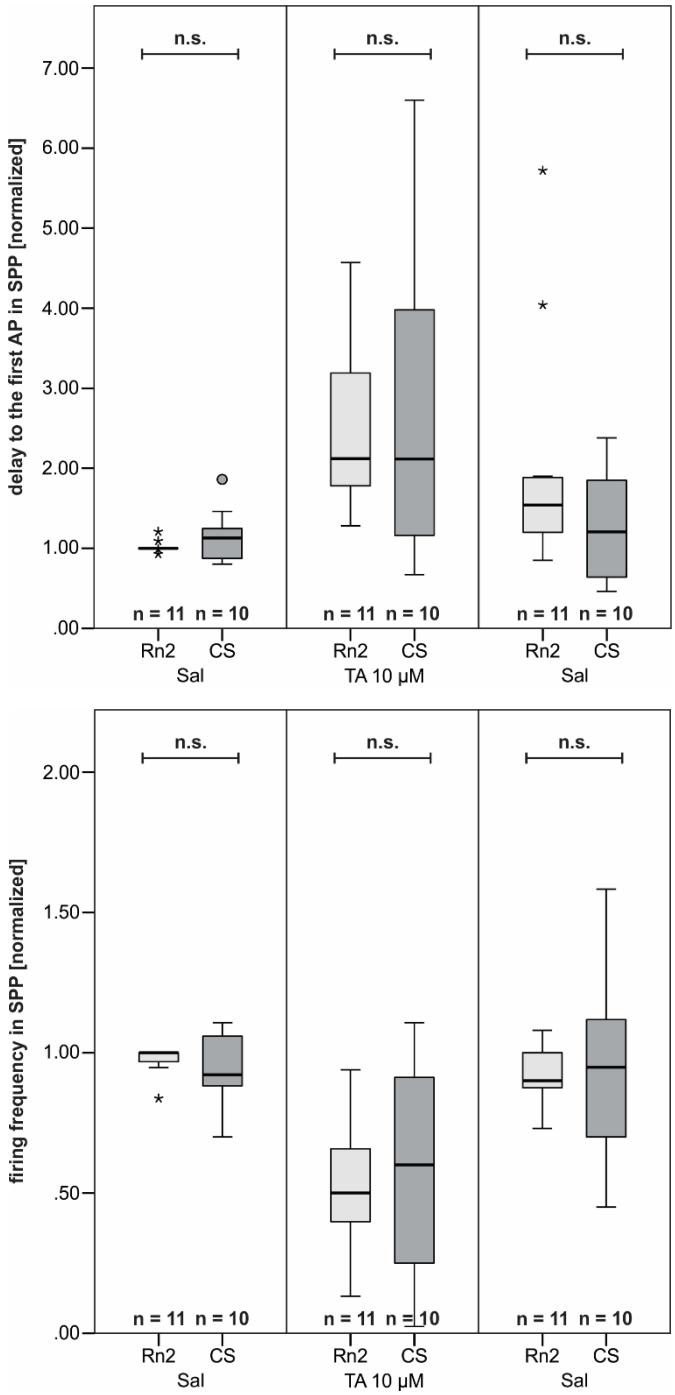

Figure 66: Effect of tyramine on MNISN-Is in Canton S and RN2-GAL4 Control groups in square pulse protocols. The elicited effect of tyramine is equally strong in CS and in RN2 control groups. The mean delay to the first AP was 151 ± 56 ms in RN2 (n = 11) and 257 ± 76 ms in CS (n = 10), which was significantly different (M.-W. U-Test, p = 0.006; n = 11, 10). The mean firing frequency was 29.14 ± 8.76 Hz in RN2 (n = 11) and 18.65 ± 5.64 Hz in CS (n = 10), which was also significantly different (M.-W. U-Test, p = 0.016; n = 11, 10). All values were normalized to the first value of the first recording, and then compared pairwise in the three runs. The normalized medians were not significantly different in standard saline for both the delay and the firing frequency (M.-W. U-Test, delay p = 0.512; frequency p = 0.654; n = 11, 10). The delay was increased by 112 % (RN2) and by 99 % (CS) upon application of TA, which was not significantly different (M.-W. U-Test, p = 0.705; n = 11, 10). The firing frequency was similarly reduced by 50 % (RN2) and 32 % (CS), which was not significantly different (M.-W. U-Test, p = 0.918; n = 11, 10). Washing TA out reduced the delay by 58 % (RN2) and 92 % (CS), which was not significantly different (M.-W. U-Test, p = 0.197; n = 11, 10). The firing frequency was increased by 26 % (RN2) and 35 % (CS) upon washing TA out, which was not significantly different (M.-W. U-Test, p = 0.918; n = 11, 10). Since the effects were similarly strong in the two genotypes, they were pooled and used as one control group.

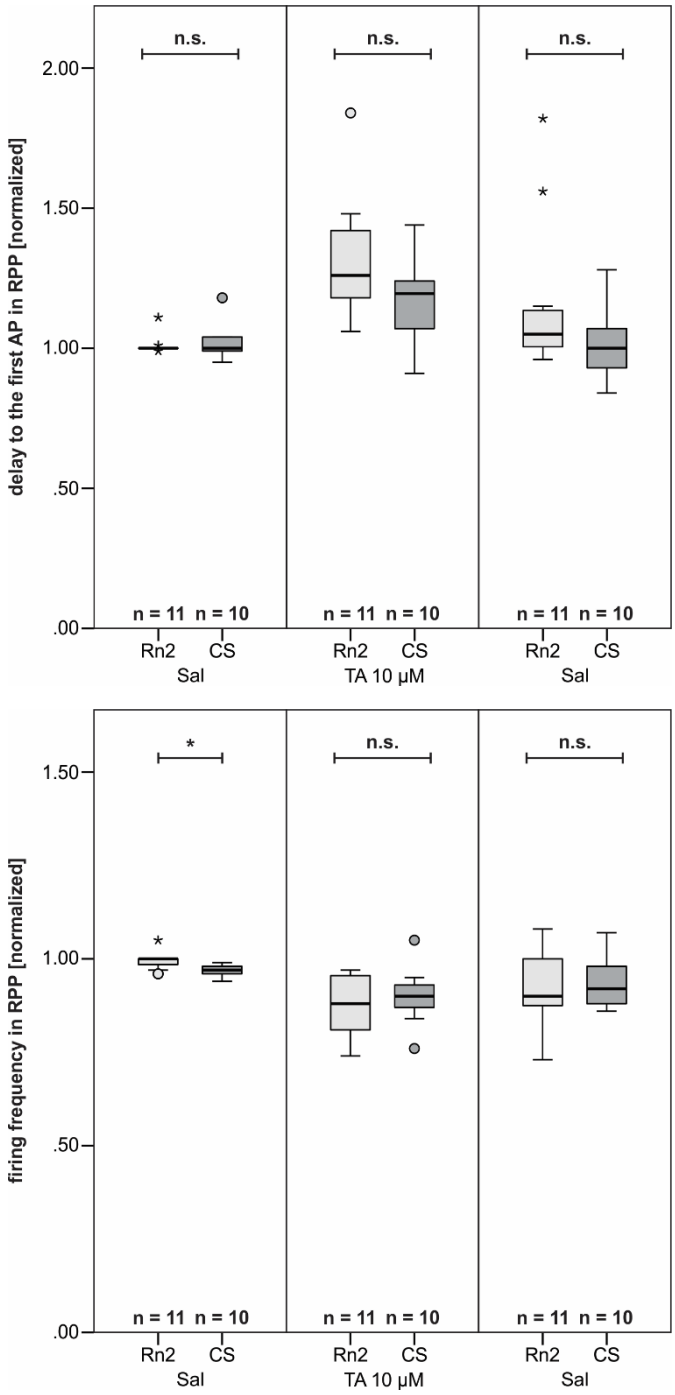

Figure 67: Effect of tyramine on MNISN-Is in Canton S and *RN2*-GAL4 Control groups in ramp pulse protocols. The elicited effect of tyramine is equally strong in CS and in RN2 control groups. The mean delay to the first AP was 773 ± 98 ms in RN2 (n = 11) and 923 ± 200 ms in CS (n = 10), which was significantly different (T-Test, p = 0.049; n = 11, 10). The mean firing frequency was 36.08 ± 2.68 Hz in RN2 (n = 11) and 32.65 ± 3.93 Hz in CS (n = 10), which was not significantly different (M.-W. U-Test, p = 0.085; n = 11, 10). All values were normalized to the first value of the first recording, and then pairwise compared in the three runs. The normalized medians were significantly different in standard saline for the firing frequency, but not for the delay (M.-W. U-Test, delay p = 0.973; frequency p = 0.010; n = 11, 10). The delay was increased by 26 % (RN2) and by 20 % (CS) upon application of TA, which was not significantly different (p = 0.099; n = 11, 10). The firing frequency was similarly reduced by 12 % (RN2) and 7 % (CS), which was not significantly different (M.-W. U-Test, p = 0.654; n = 11, 10). Washing TA out reduced the delay by 21 % (RN2) and 20 % (CS), which was not significantly different (M.-W. U-Test, p = 0.197; n = 11, 10). The firing frequency was increased by 2 % (RN2) and 2 % (CS) upon washing TA out, which was not significantly different (M.-W. U-Test, p = 0.863; n = 11, 10). Since the effects were similarly strong in the two genotypes, they were pooled and used as one control group.

6.3 Single Data Points for the Measurements in Yohimbine

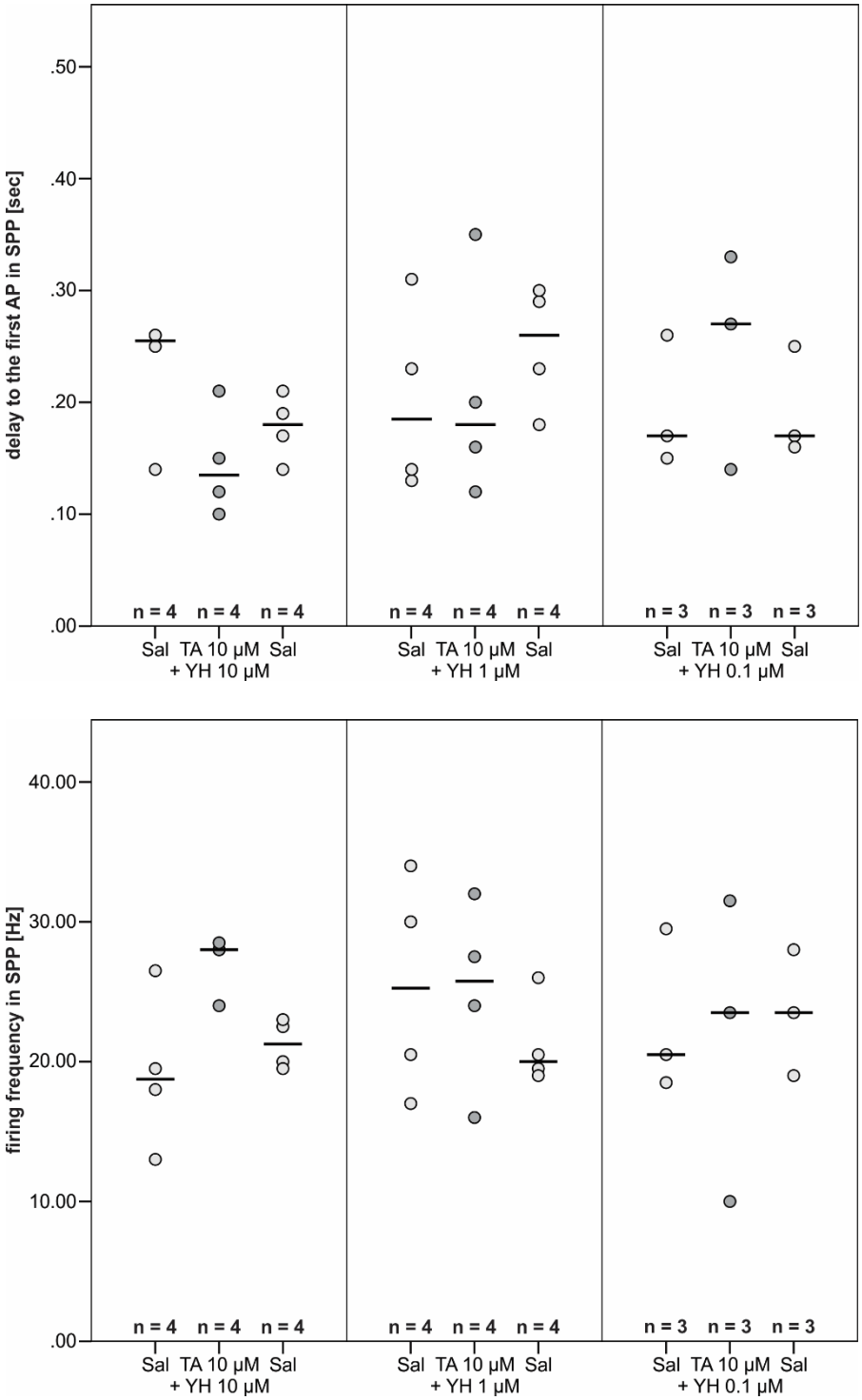

Figure 68: Single data points of recordings in saline containing tyramine and yohimbine in square pulse protocols. The single groups are very small, which is why no statistical analysis was conducted. The data points of the three groups spread in a comparable manner, which is why the data were pooled for analysis. In no case did tyramine induce a clear reduction in MNISN-Is excitability when applied together with the α_2-adrnergic receptor antagonist yohimbine.

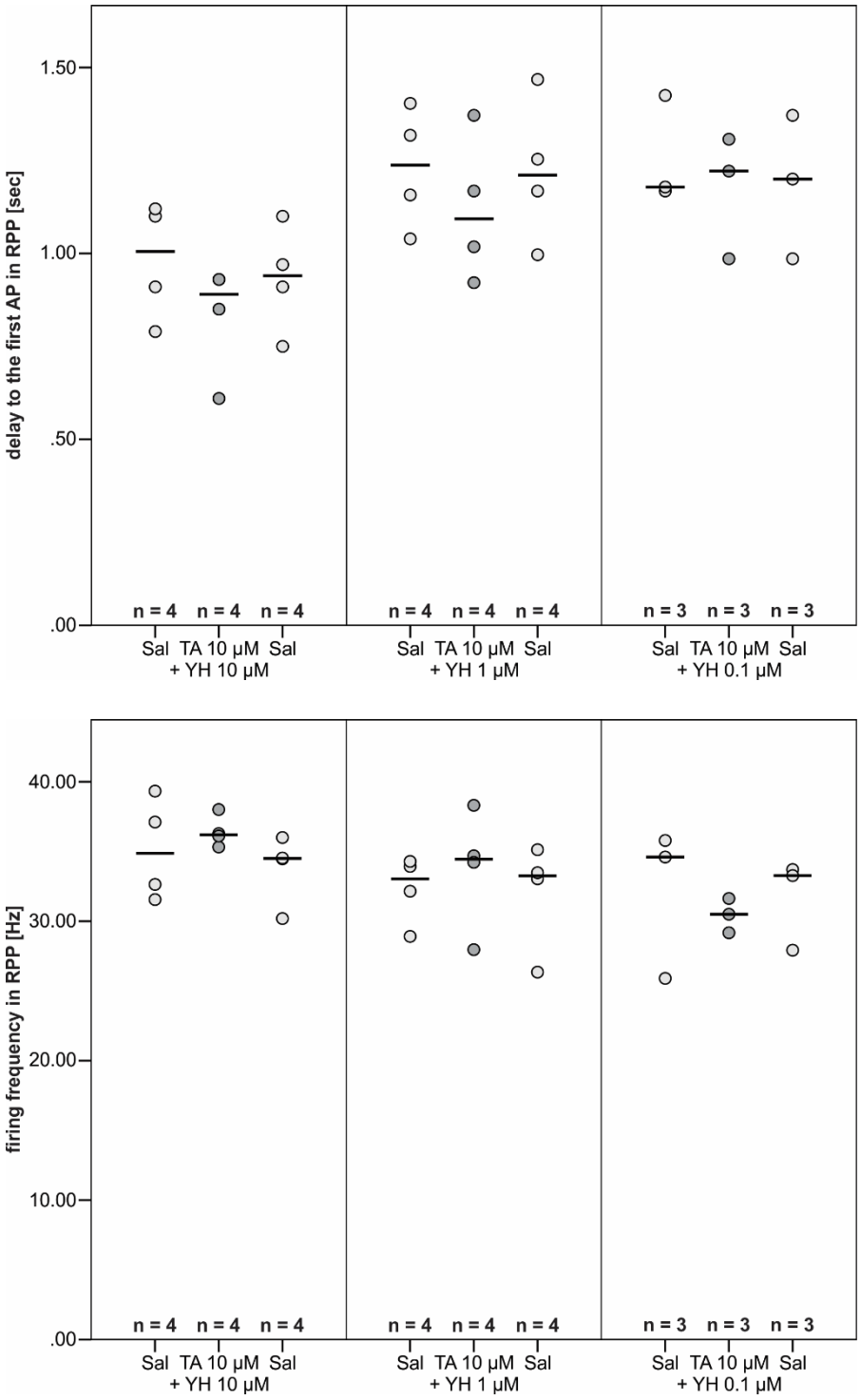

Figure 69: Single data points of recordings in saline containing tyramine and yohimbine in ramp pulse protocols. The single groups are very small, which is why no statistical analysis was conducted. The data points of the three groups spread in a comparable manner, which is why the data were pooled for analysis. In no case did tyramine induce a clear reduction in MNISN-Is excitability when applied together with the α_2-adrnergic receptor antagonist yohimbine.

6.4 Comparison of Single Runs in Calcium Imaging Experiments with Controls

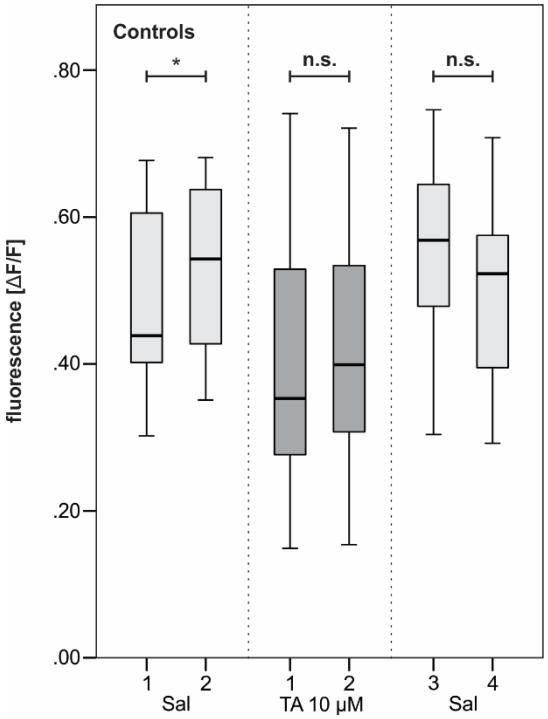

Figure 70: Single runs of the calcium imaging experiments with control MNISN-Is motoneurons.
In the first run in standard saline, the mean increase in fluorescence (ΔF/F) was 0.49 ± 0.12, which slightly increased to 0.53 ± 0.12 in the second run in standard saline. After TA was bath-applied, the mean increase in fluorescence was 0.39 ± 0.15 in the first run in 10 µM TA, and 0.41 ± 0.15 in the second run in TA. After TA was washed out, the mean increase in fluorescence was 0.56 ± 0.12, and 0.50 ± 0.12 in the two runs in standard saline after TA was washed out. All data were normally distributed, which is why a paired T-Test was conducted to test for differences between each two runs in the same conditions. The two runs in standard saline were significantly different ($p = 0.031$; $n = 16, 16$), but for the two runs in TA ($p = 0.067$; $n = 16, 16$), and for the two runs in standard saline after the washout ($p = 0.076$; $n = 16, 16$), no significant differences could be found. Since the increase in fluorescence did not run down in the second run, data were pooled.

6.5 Comparison of Single Runs in Calcium Imaging Experiments with *TyrR*^{hono}

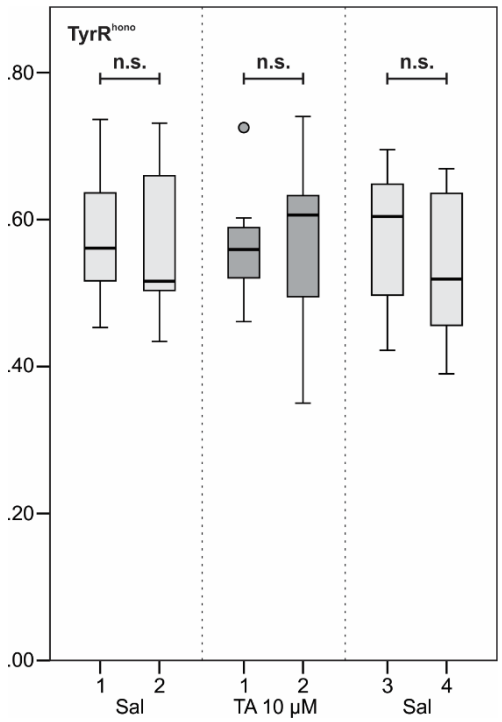

Figure 71 Single runs of the calcium imaging experiments with *TyrR*^{hono} MNISN-Is motoneurons.
In the first run in standard saline, the mean increase in fluorescence (ΔF/F) was 0.58 ± 0.10, which slightly increased to 0.57 ± 0.11 in the second run in standard saline. After TA was bath-applied, the mean increase in fluorescence was 0.57 ± 0.08 in the first run in 10 µM TA, and 0.57 ± 0.12 in the second run in TA. After TA was washed out, the mean increase in fluorescence was 0.57 ± 0.10, and 0.54 ± 0.10 in the two runs in standard saline after TA was washed out. All data were normally distributed, which is why a paired T-Test was conducted to test for differences between each two runs in the same conditions. No significant differences could be found between the two runs in standard saline ($p = 0.717$; $n = 7, 7$), the two runs in TA ($p = 0.947$; $n = 7, 7$), or the two runs in standard saline after the washout ($p = 0.121$; $n = 7, 7$). Thus, every two runs in the same conditions were pooled.

6.6 Eidesstattliche Versicherung

Versicherung gemäß § 11, Abs. 3d der Promotionsordnung vom 22.12.2003

1. Ich habe die als Dissertation vorgelegte Arbeit selbst angefertigt und alle benutzten Hilfsmittel (Literatur, Apparaturen, Material) in der Arbeit angegeben.

2. Ich habe und hatte die als Dissertation vorgelegte Arbeit nicht als Prüfungsarbeit für eine staatliche oder andere wissenschaftliche Prüfung eingereicht.

3. Ich hatte weder die jetzt als Dissertation vorgelegte Arbeit noch Teile einer Abhandlung bei einer anderen Fakultät bzw. einem anderen Fachbereich als Dissertation eingereicht.

Mainz, den 20.12.2017 Natalie Schützler